

UC Santa Barbara

UC Santa Barbara Electronic Theses and Dissertations

Title

Developing Novel Synthetic Methods for Tailored Sensors and Functional Materials

Permalink

<https://escholarship.org/uc/item/0r74d807>

Author

Diaz, Yvonne

Publication Date

2019

Peer reviewed|Thesis/dissertation

UNIVERSITY OF CALIFORNIA

Santa Barbara

Developing Novel Synthetic Methods for Tailored Sensors and Functional Materials

A dissertation submitted in partial satisfaction of the
requirements for the degree Doctor of Philosophy
in Chemistry

by

Yvonne Jeannine Diaz

Committee in charge:

Professor Craig J. Hawker, Co-Chair

Professor Javier Read de Alaniz, Co-Chair

Professor Gabriel Ménard

Professor Ram Seshadri

Joseph M. Mabry, Ph.D.

December 2019

The dissertation of Yvonne Jeannine Diaz is approved.

Joseph M. Mabry

Ram Seshadri

Gabriel Ménard

Javier Read de Alaniz, Co-Chair

Craig J. Hawker, Co-Chair

December 2019

Developing Novel Synthetic Methods for Tailored Sensors and Functional Materials

Copyright © 2019

by

Yvonne Jeannine Diaz

This dissertation is dedicated to my wonderful family.

Thank you for all of your love and support!

Esta tesis está dedicada a mi amada familia.

¡Gracias por todo el amor y apoyo!

Acknowledgements

As I reach this tremendous milestone in my life, I realize that none of it could have been possible without the support of many remarkable mentors, friends, and family.

First, to my two brilliant advisors Javier and Craig. Throughout these years you have pushed me more than I ever thought possible and have helped me to become not only a better scientist, but a stronger person as well. Thank you for all of the doors you have opened for me and all the support you have given me both in the lab and out.

I would also like to thank my awesome team of mentors from Edwards AFRL who first introduced me to the wonderful world of polymers and who encouraged me to continue toward my PhD. Joe, words cannot express how grateful I am to have had the opportunity to work in your lab in my undergrad years and to continue to learn from you since. Sean, thank you for showing me the true beauty of science and for never getting tired of my constant stream of questions even long after you left the lab! Thank you also to Ray, Jeff, and Tim, who have some of the most brilliant minds I have had the honor to work with and learn from.

Throughout my time in the Hawker and Read lab, I have had the privilege to work alongside many amazing and talented people. From the beginning, my fellow CSUN alum Saemi served as a tremendous mentor for me and also introduced me to the world of country dancing for which I am incredibly grateful. To my “Team ZANY”- Zac, Abby, and Nic: We might have made the lab smell like dead fish, but working on the sensor project with you was some of the most fun times I had in the lab. Thanks for helping me to navigate the crazy rollercoaster that is grad school! I would also like to deeply thank Reggie and Zhishuai (Frank) for their advice, assistance, and support in getting through many late nights and long weeks.

I truly started at UCSB with one of the best cohorts I could have asked for including Kyle, Jaime, Meghan, Tim, Maša, and Jake: we started this wild ride together and you have made the journey so much more fun! I am grateful for all the crazy times spent in Dow lab

with Manny, Jeff, and Emre that made it exciting to come to work every day and to Serena who helped me navigate traveling desk situations with ocean visits and puppy playtime. I would also like to thank my awesome MRL office mates Joya and Emily for putting up with all my random questions and providing a super fun work environment. And a huge thanks to all the other members of the Read, Hawker, Seshadri, and Ménard groups past and present who have helped contribute to my incredible experience at Santa Barbara.

Jessi and Belinda, no matter how far apart we are I know I can always count on you guys. Thank you for always being there for me through all of the best and worst times.

Kevin, you are my best friend, and I'm not sure I could have made it through any of this without you. You have helped me to be strong and brave, served as my personal escape from all the madness, AND read through endless drafts of my papers & presentations. All I can say is thank you for everything and I can't wait to see what our next adventure brings.

And above all I would like to thank my family who never let me forget what truly matters in life. To all of my grandparents, whose incredible journey, strength, and sacrifice are the reason I have these opportunities today. Thank you for always being an inspiration for me. To my ninos, thank you for always giving me a home away from home. Roxy and Luis, I am so proud of you both and can easily say that I have the best siblings in the world. Mami and Papi, I did it! And it couldn't have happened without you! Thank you for always believing in me, pushing me to reach for the stars and being there to catch me when I fall. I love you!

Y sobre todo, me gustaría agradecer a mi familia que nunca me dejó olvidar lo que realmente importa en la vida. Para todos mis abuelitos: Su esfuerzo y sacrificio son las razones por las que tengo estas oportunidades hoy. Gracias por ser siempre una inspiración para mí. A mis padrinos, gracias por darme siempre un hogar lejos de casa. Roxy y Luis, no saben lo orgullosa que estoy de ustedes y son los mejores hermanos del mundo. ¡Mami y Papi, lo hice! ¡Y no podría haber sucedido sin ti! Gracias por siempre creer en mí, por empujarme a alcanzar las estrellas y por ayudarme cuando caigo. ¡Los quiero mucho!

Yvonne Jeannine Diaz

Curriculum Vitae

SUMMARY OF QUALIFICATIONS

Research Chemist fluent in Spanish and English offering versatile lab work experience from academic and government laboratories in synthesis/characterization of organic and inorganic monomers and polymers. Strong planner and problem solver with capabilities in navigating communication between campus staff, students, and departments along with collaborations in industry.

EDUCATION

Ph. D. in Materials Chemistry

Expected Dec 2019

University of California, Santa Barbara (UCSB)

B.S. in Chemistry

Dec 2014

California State University Northridge (CSUN) | *cum laude*

RESEARCH EXPERIENCES

• **Ph.D. Student | UCSB**

2015 - Present

Co-Advisors: Craig J. Hawker and Javier Read de Alaniz

- Synthesized and characterized a range of organic small molecules and polymers for targeted application in colorimetric sensors, stimuli responsive materials, and dispersants.
- Developed synthetic methods for tailoring polymer architectures and investigated their structure/property relationship.
- Led an interdisciplinary team of scientists in collaboration project with **Dow Chemical** to design and synthesize novel water-soluble dispersants.
- Co-authored 1 patent and 3 manuscripts for peer-reviewed journals, drafted 5 quarterly research reports for industrial collaborators, and presented at 7 conferences.
- Mentored 4 junior researchers through instrument training, synthetic methods development, and characterization techniques and ensured safe execution.

• **Co-Op | Edwards Air Force Research Laboratory**

2010 - 2015

Group Lead: Joseph M. Mabry | Applied Materials Group

- Synthesized and characterized siloxane-containing small molecules and polymers to produce both superhydrophobic and superoleophobic surface coatings for aerospace applications.
- Collaborated with a diverse team of engineers, material scientists, and chemists to co-author 2 peer-reviewed manuscripts, 1 book chapter, and 2 presentations.
- Mentored 2 undergraduate students resulting in a publication in *Polymer Chemistry*.

- **Undergraduate Researcher | CSUN** **2013 - 2014**
 Advisor: Yann Schrodi
 - Investigated the ring-opening metathesis polymerization of dicylopentadiene in collaboration with the CSUN engineering department toward the recycling of end-of-life tire rubber.

HONORS AND AWARDS

National Science Foundation Graduate Research Fellow	2016-2019
Outstanding Service to the Department: For exceptional leadership	2019
Outstanding K-12 Volunteer	2018
Chosen as Dow BEST Symposium Participant	2018
Doctoral Scholars Fellowship	2015
UCSB Summer Research Fellowship	2015
Hotchkiss Scholarship	2010-2014
ACS Scholars Program Scholarship	2012-2014
Northridge University Scholarship	2012-2013
Hispanic Scholarship Fund Award	2010-2011
Robert C. Byrd Honors Scholarship	2010-2011
Emblem Club Scholarship Award	2010

SELECT LEADERSHIP AND OUTREACH EXPERIENCE

- **Outreach Director | Graduate Students for Diversity in Science** **2017-Present**
 - Managed team of 5-6 Ph.D. students to host bi-annual outreach events – exposing undergraduates from minority backgrounds to graduate school experiences.
 - Reduced spending over 50% for outreach event by implementing new student host program.
 - Co-planned and presided over bi-annual Dow Foundation Lecture Series to promote research excellence and diversity at UCSB.

- **Materials Science Ambassador | K-12 Education Program** **2016-Present**
 - Led volunteer groups in conducting materials science workshops (“It’s a Material World!”) at local K-12 schools and at UCSB in order to engage students through hands-on activities.
 - Participated in various workshops to help students learn about the structure-property relationship of molecules through building their own Buckminsterfullerene (Buckyball) molecular model.

PATENT

- "Colorimetric Sensors and Methods of Using Colorimetric Sensors," **Diaz, Y.J.**; Page, Z.A.; Knight, A.S.; Hemmer, J.R.; Treat, N.J.; Margalith, T.; Hawker, C.J.; and Read de Alaniz, J.; U.S. Patent 62/410,650, filed October 20, 2015.

BOOK CHAPTER

- "Functionalization of Fluoroalkyl Polyhedral Oligomeric Silsesquioxanes (F-POSS)," In *Advances in Fluorine-Containing Polymers*; Ramirez, S.M.; **Diaz, Y.J.**; Campos, R.; Haddad, T.S.; Mabry, J.M.; ACS Symposium Series 1106. (2012), 95-109.

PUBLICATIONS

- "Stable Activated Furan and Donor – Acceptor Stenhouse Adduct Polymer Conjugates as Chemical and Thermal Sensors," Chen, Q.*; **Diaz, Y.J.***; Hawker, M.C.; Martinez, M.R.; Page, Z.A.; Zhang, S.X.A.; Hawker, C.J.; Read de Alaniz, J.; *Macromolecules* (2019), 52 (11), 4370-4375.
*These authors contributed equally to this work.
- "A Versatile and Highly Selective Colorimetric Sensor for the Detection of Amines," **Diaz, Y.J.**; Page, Z.A.; Knight, A.S.; Treat, N.J.; Hemmer, J.R.; Hawker, C.J.; Read de Alaniz, J.; *Chemistry, A European Journal* (2017), 23 (15), 3562-3566.
- "Tunable Visible and Near Infrared Photoswitches," Hemmer, J.R.; Poelma, S.O.; Treat, N.; Page, Z.A.; Dolinski, N.D.; **Diaz, Y.J.**; Tomlinson, W.; Clark, K.D.; Hooper, J.P.; Hawker, C.; Read de Alaniz, J.; *Journal of the American Chemical Society* (2016), 138 (42), 13960-13966.
- "Reversible Addition-Fragmentation Chain Transfer (RAFT) Copolymerization of Fluoroalkyl Polyhedral Oligomeric Silsesquioxane (F-POSS) Macromers," Ramirez, S.M.; **Diaz, Y.J.**; Sahagun, C.M.; Duff, M.W.; Lawal, O.B.; Iacono, S.T.; Mabry, J.M.; *Polymer Chemistry* (2013), 4 (7), 2230-2234.
- "Incompletely Condensed Fluoroalkyl Silsesquioxanes and Derivatives: Precursors for Low Surface Energy Materials," Ramirez, S.M.; **Diaz, Y.J.**; Campos, R.; Stone, R.L.; Haddad, T.S.; Mabry, J.M.; *Journal of the American Chemical Society* (2011), 133 (50), 20084-20087.

INVITED LECTURES AND PRESENTATIONS

- "Development of new activated furan and DASA polymer conjugates: Expanding the utility of DASAs, a new sensing platform." **Diaz, Y.J.**; Chen, Q.; Hawker, M.C.; Martinez, M.R.; et.al.; Gordon Research Polymer Symposium, South Hadley, MA, United States, June 8-17 (2019).
- "One Fish, Two Fish, Red Fish? Dead Fish! : Combating food spoilage with color." **Diaz, Y.J.**; Page, Z.A.; Knight, A.S.; Treat, N.J.; et.al.; UCSB 7th Annual Grad Slam Competition, Santa Barbara, CA, United States, April 8-19 (2019).
- "Probing the utility of Donor-Acceptor Stenhouse Adducts (DASAs) as sensors." **Diaz, Y.J.**; Hawker, C.J.; Read de Alaniz, J.; Presented at Jackson State University – University of California, Santa Barbara (JSU UCSB) Mentoring Partnership Workshop, Santa Barbara, CA, United States, March 8 (2019).

-
- "One Fish, Two Fish, Red Fish? Dead Fish!" **Diaz, Y.J.**; Page, Z.A.; Knight, A.S.; Treat, N.J.; et.al.; Dow BEST Symposium, Midland, MI, United States, Sep 4-6 (2018).
 - "Scalable Colorimetric Sensor for Selective and Sensitive Amine Detection." **Diaz, Y.J.**; Page, Z.A.; Knight, A.S.; Treat, N.J.; Hemmer, J.R.; Hawker, C.J.; Read de Alaniz, J.; Presented at the Materials Research Outreach Program Symposium, Santa Barbara, CA, United States, February 1-2, (2017).
 - "Visible Light as a Stimulus for Organic Catalyst Recycling." **Diaz, Y.J.**; Helmy, S.; Leibfarth, F.A.; Poelma, S.O.; Hawker, C.J.; Read de Alaniz, J.; Presented at the Partnership for Research and Education in Materials Conference, El Paso, TX, United States, June 26-28, (2016).

CONFERENCE CONTRIBUTIONS

- "Development of Selective and Affordable Small Molecule Sensors for an Array of Applications." **Diaz, Y.J.**; Page, Z.A.; Knight, A.S.; Treat, N.J.; Hemmer, J.R.; Hawker, C.J.; Read de Alaniz, J.; Presented at the 253rd ACS National Meeting and Exposition, San Francisco, CA, United States, April 2-6 (2016).
 - "Copolymerization of Fluoroalkyl-Substituted Polyhedral Oligomeric Silsesquioxane (FluoroPOSS) Macromers via Ring-Opening Metathesis Polymerization (ROMP)." Ramirez, S.M.; **Diaz, Y.J.**; Campos, R.; Haddad, T.S.; Mabry, J.M.; Presented at the 250th ACS National Meeting and Exposition, Boston, MA, United States, August 16-20, (2015), POLY-345.
 - "Incompletely-Condensed Fluorinated Silsesquioxane: Synthesis and Crystal Structure." Ramirez, S.M.; **Diaz, Y.J.**; Haddad, T.S.; Mabry, J.M.; Presented at the 243rd ACS National Meeting and Exposition, San Diego, CA, United States, March 25-29 (2012), POLY-331.
-

Abstract

Developing Novel Synthetic Methods for Tailored Sensors and Functional Materials

by

Yvonne Jeannine Diaz

The ability to access functional materials through affordable and facile synthetic methods has long been sought after for various research and commercial applications. Many innovative academic syntheses, although fundamentally interesting, cannot be adopted by industry due to complexity, cost, or incompatibility for scale-up. Therefore, this dissertation highlights the development of novel avenues to produce materials tailored for either colorimetric sensing or dispersion with an emphasis on developing accessible and inexpensive methods such that they can be readily adapted to industrial processes.

A colorimetric sensor for amines is presented based on the facile reaction of activated furans with amines to form highly colored donor-acceptor Stenhouse adducts (DASAs). This synthetic method gives non-experts access to a more sensitive and selective detector from an inexpensive biomass precursor. Although the small molecule version of this detector was prone to leeching and was thus incompatible with most applications, incorporation into an oxanorbornene polymer backbone enhanced the stability of this sensor and expanded its potential uses, particularly in aqueous media. The utility of this system for commercial applications including food spoilage detection and chemical reaction monitoring is explored.

Another area of industrial interest is the tailorability of poly(acrylic acid)s (PAA) for a number of applications including dispersants, coatings, and mineralization control where microstructure changes to these materials have been shown to produce dramatically different macroscopic properties. A universal method to prepare well-defined PAAs with readily

interchangeable chain end chemistries is described. This new platform provides easier access to targeted PAA structures and facilitates future studies into the structure-property relationship of these versatile compounds. Additionally, this process may enable the creation of novel dispersants for improved paint formulations or other related fields.

Industrial innovations often arise from developments in academic laboratories. However, translation of these developments into modern technology can be hindered by inaccessible chemistries or overly complex syntheses. This dissertation presents two synthetic strategies to access functional materials for a range of targeted applications, each with methods that can be readily applied in an industrial setting thus helping to expand the utility of novel academic syntheses for industrial use.

Table of Contents

CHAPTER 1: INTRODUCTION	1
1.1 Materials Science	1
1.2 Colorimetric Sensors	2
1.2.1 Introduction to colorimetric sensors	2
1.2.2 Popular methods for amine detection	3
1.2.3 The use of colorimetric sensors for the detection of amines	4
1.2.4 Donor-Acceptor Stenhouse Adducts (DASA): creating new materials for improved detectors	6
1.3 Poly(acrylic acid) (PAA) : A Versatile Water Soluble Polymer	8
1.3.1 Exploring the structure-property relationship of PAA	8
1.3.2 Common methods for polymerization	10
1.3.3 Overview of chain-end functionalization	11
1.4 References	15
CHAPTER 2: A VERSATILE AND HIGHLY SELECTIVE COLORIMETRIC SENSOR FOR DETECTION OF AMINES	19
2.1 Abstract	19
2.2 Introduction	20
2.3 Colorimetric Detection in Solution	22
2.4 Colorimetric Detection on Solid Supports	25
2.5 Colorimetric Detection in Vapor Phase.....	29
2.6 Conclusion.....	31
2.7 Experimental	31

2.7.1 Materials and equipment	31
2.7.2 Activated furan synthesis	32
2.7.3 Amine sensing in solution	32
2.7.4 Quantifying Color: International Commission on Illumination (CIE) Guidelines.....	33
2.8 Supplemental Results	34
2.8.1 Stability of sensor solution	34
2.8.2 Optical properties and reactivity of activated furan solution	35
2.8.3 Amine sensing on solid supports.....	40
2.8.4 Set up for food spoilage detection monitoring	43
2.9 References	44

CHAPTER 3: STABLE ACTIVATED FURAN AND DASA POLYMER CONJUGATES AS CHEMICAL AND THERMAL SENSORS49

3.1 Abstract	49
3.2 Introduction	50
3.3 Synthesis of Functional Meldrum’s Acid Activated Furan.....	53
3.4 Early Studies – Activated Furan Polymerization Compatibility	54
3.5 Creating a Highly Tunable Sensor <i>via</i> Ring Opening Metathesis Polymerization.....	55
3.6 Facilitating Use of DASA Dyes for Sensors in Aqueous Media	56
3.7 Sensitivity of Polymeric Activated Furan for Amine Detection	58
3.8 Influence of Glass Transition Temperature (T_g).....	59
3.9 Polymeric Activated Furan as a Thermal Sensor	61
3.10 Conclusion.....	63

3.11 Experimental	64
3.11.1 Materials and equipment	64
3.11.2 Quantification of color from images	65
3.11.3 Synthesis and characterization of monomers and polymers	65
3.12 Supplemental Results	75
3.12.1 Polymer thin film preparation	75
3.12.2 Stability of small molecule activated furan and DASA in aqueous environment.....	76
3.12.3 Leaching studies for small molecule DASA and AF versus polymeric activated furan	77
3.12.4 Glass transition temperatures for co-polymers 6-12	80
3.12.5 Temperature effect on amine detection	81
3.12.6 Amine detection scope of polymeric activated furan	82
3.12.7 Limit of detection for various amines with activated furan polymer film	83
3.12.8 Stability of thermal sensor.....	88
3.12.9 Stability of carboxylic acid activated furan 3 over time.....	89
3.12.10 Stability of oxa-norbornene Meldrum’s activated furan (NF-AF) over time.....	90
3.13 References	91

CHAPTER 4: A UNIVERSAL AND SCALABLE SYNTHESIS OF WELL-DEFINED POLY(ACRYLIC ACID)S WITH TAILORED CHAIN END CHEMISTRIES98

4.1 Abstract	98
4.2 Introduction	99
4.3 Synthesis of Bromine-Terminated PtBA.....	101

4.4 Synthesis of Acrylate-Terminated PtBA	102
4.5 Synthesis of Charged Chain End Modified PtBAs	107
4.6 Synthesis of Dodecyl-Terminated PtBA	108
4.7 Synthesis of Chain End Modified PAA: From Hydrophobic to Charged Species	109
4.8 Conclusion.....	110
4.9 Experimental	111
4.9.1 Materials and equipment	111
4.10 Supplemental Results	112
4.10.1 Bromine-terminated PtBA: synthesis and characterization.....	112
4.10.2 Acrylate-terminated PtBA: synthesis and characterization.....	117
4.10.3 Dodecyl-terminated PAA: synthesis and characterization	121
4.10.4 Sulfonate-terminated PAA: synthesis and characterization	125
4.10.5 Phosphonic acid-terminated PAA: synthesis and characterization	130
4.10.6 Carboxylic acid-terminated PAA: synthesis and characterization	135
4.10.7 Dicarboxylic acid-terminated PAA: synthesis and characterization ...	140
4.10.8 Comparison of ¹ H NMR analysis with and without d-TFA treatment	144
4.10.9 Control NMR of d-MeOH with d-TFA.....	146
4.10.10 Comparing synthesis of acrylate-terminated PtBA product under acidic and basic conditions.	147
4.10.11 Characterization for synthesis of dodecyl-terminated PtBA via S _N 2 substitution	148
4.11 References	150

APPENDIX

A: INVESTIGATING THE INFLUENCE OF CHAIN END ON DISPERSANT AND BIO-MINERALIZATION CONTROL	152
A1 Introduction	152
A2 The Influence of PAA Chain End on Dispersant Performance	153
A3 The Effect of PAA Chain End on the Morphology and Size of Hydroxyapatite Crystals	154
B: TUNABLE VISIBLE AND NEAR INFRARED PHOTOSWITCHES	158

Abbreviations

1°	primary
2°	secondary
3°	tertiary
a*	red/green
a.u.	absorbance unit
AF	activated furan
ATRP	atom transfer radical polymerization
b*	yellow/blue
BAF	1,3-dimethyl barbituric acid activated furan
bbp	parts per billion (bbp)
CDCl ₃	deuterated chloroform
CF ₃ COOH	trifluoroacetic acid
CIE	International Commission on Illumination
CRP	controlled radical polymerization
CuBr ₂	copper (II) bromide
Da	Dalton
DASA	donor-acceptor Stenhouse adduct
DBU	1, 8- diazobicyclo [5.4.0]undec-7-ene
DCM	dichloromethane
DEA	diethylamine
DI	deionized (water)
DMA	dimethylamine
DMAP	dimethylaminopyridine
DMF	dimethylformamide
DMSO	dimethyl sulfoxide
DP	degree of polymerization
DSC	differential scanning calorimetry
Đ	dispersity
EDC	1-ethyl-3-(3-dimethylaminopropyl) carbodiimide
Et ₃ SiH	triethylsilane
EtOAc	ethyl acetate
Equiv.	equivalence
FT-IR	Fourier Transform Infrared
g	gram(s)
h	hour(s)

Abbreviations (cont.)

HCl	hydrochloric acid
HTPB	hydroxyl-terminated polybutadiene
K ₂ CO ₃	potassium carbonate
L*	lightness from black to white
LAH	lithium aluminum hydride
LOD	limit of detection
M	molar
MAF	Meldrum's activated furan
MALDI-ToF-MS	matrix-assisted laser desorption ionization time of flight mass spectrometry
Me ₆ -Tren	tris[2 (dimethylamino)ethyl]amine
MeCN	acetonitrile
mg	milligram(s)
MHz	megahertz
min	minute(s)
mL	milliliter(s)
mM	millimolar
mol	mole
<i>n</i>	<i>normal</i>
NaOH	sodium hydroxide
NB-AF	oxa-norbornene Meldrum's activated furan monomer
nm	nanometer(s)
NMP	nitroxide mediated polymerization
NMR	nuclear magnetic resonance
<i>o</i>	<i>ortho</i>
<i>p</i>	<i>para</i>
PAA	poly(acrylic acid)
ppm	parts per million
PS	polystyrene
<i>pt</i> BA	poly(<i>tert</i> -butyl acrylate)
RAFT	reversible addition fragmentation chain transfer
RI	refractive index
ROMP	ring-opening metathesis polymerization
RPM	revolutions per minute
SEC	size exclusion chromatography

Abbreviations (cont.)

<i>t</i> BA	<i>tert</i> -butyl acrylate
<i>t</i> B-BiB	<i>tert</i> -butyl α -bromoisobutyrate
TEA	triethylamine
TFA	trifluoroacetic acid
TFE	2,2,2- trifluoroethanol
T_g	glass transition temperature
THF	tetrahydrofuran
TiO ₂	titanium dioxide
TLC	thin layer chromatography
TMS	tetramethylsilane
UV-NIR	ultraviolet-near IR
UV-vis	ultraviolet-visible
ΔE	Delta E
ϵ	molar absorptivity
μg	microgram(s)
μL	microliter(s)
μM	micromolar
μm	micrometer(s)

CHAPTER 1

INTRODUCTION

1.1 Materials Science

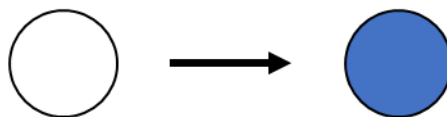
The field of materials science combines the expertise from various scientific disciplines including chemistry, engineering, and physics to explore how the microstructures of materials translate to their overall macromolecular properties.¹ This area brings together a vast variety of knowledge from these fields in order to provide a deeper understanding on how the structure and composition of a material can influence its properties and utility toward specific applications. This insight can then be leveraged to either modify the properties of materials or to create new materials with the goal of enhancing their effectiveness. Due to the interdisciplinary nature of this field, materials science can be useful for anything from the development of new paint formulations to the design of prosthetics and implants that are more compatible with the human body. In particular, this thesis will touch on how the study of materials chemistry can be leveraged to **a)** develop new materials for novel colorimetric sensors and **b)** provide increased functionality to existing poly(acrylic acid)s in order to tailor their use toward specific applications and provide a more thorough understanding into their structure-property relationship.

1.2 Colorimetric Sensors

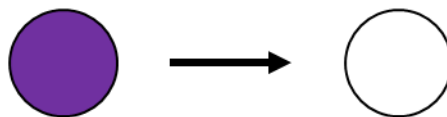
1.2.1 Introduction to colorimetric sensors

One application which has benefited from investigating the structure-property relationship of materials is the creation of colorimetric sensors. These detectors are coveted for their ability to quickly and efficiently respond to an outside stimulus with a change in color visible to the naked eye.² This change can be either a “turn ON” detection, where a change from a colorless to a colored state is observed, or a “turn OFF” detection, which can consist of either a colored to colorless transition or colored to colored transformation (**Figure 1.1**). Common examples of colorimetric sensors include pH indicators,³ dyes for fingerprint

a) “Turn ON” detection (colorless to colored state)



b) “Turn OFF” detection (colored to colorless state)



c) “Turn OFF” detection (colored to colored state)



Figure 1.1 Schematic representation of different types of colorimetric detection. **a)** “Turn ON” detection where an outside stimulus will trigger the transformation of a colorless state to one that is colored, **b)** “turn OFF” detection where a change from a colored to a colorless state is observed, or **c)** “turn OFF” detection in which one color is lost in favor of a second color.

analysis,⁴ and early pregnancy tests.⁵ These types of sensors provide a cheap and easy-to-use alternative to expert analytical techniques such as mass spectrometers or ultrasounds. However, most current colorimetric detectors sacrifice much of the sensitivity in exchange for affordability and ease of use. As such, there is a need to develop new colorimetric sensors that are readily available to non-experts while maintaining a high sensitivity.

1.2.2 Popular methods for amine detection

Amine detectors are desired for their versatile use in a wide variety of applications spanning chemical synthesis⁶, drug detection,^{7,8} and environmental monitoring for example.⁹⁻¹⁷ Among the most popular methods of detection for amines are those that track changes in resistivity and luminescence due to their increased sensitivity and selectivity over alternative methods. In early 2000, Grubbs, Lewis, and co-workers presented the construction of an “electronic nose” capable of a million-fold greater detection limits for amines than that of the human nose by utilizing an array of organic and inorganic conductors.¹⁸ More recent advancements to chemiresistive detectors have included Swager’s carbon nanotube and metalloporphyrin composites which were shown to provide sub-parts per million (ppm) sensitivities toward biogenic amines such as putrescine and cadaverine along with good stability of the detector when exposed to air or moisture.¹⁷ Analogous advancements to fluorescence-sensors, which have sought to access quicker and more sensitive detection, include the use of fluorescent nanotubes which lose their high fluorescence in the presence of amines down to parts per billion levels.¹² However, while these methods have proven capable

of significantly increasing the detection limits for amine sensors, they often require complex synthetic methods and are limited to the recognition of only volatile and primary amines.¹⁹

1.2.3 The use of colorimetric sensors for the detection of amines

In order to address the limitations to these classic detectors, there has been a growing interest into the use of colorimetric amine sensors due to their easier and more rapid detection capabilities in various media. Additionally, advances to colorimetric sensors have provided competitive sensitivities (<1 ppm) to chemiresistors and fluorescence-sensors. For example, the use of polyacrylonitrile nanofibers were utilized to create porous paper which responded to low ppm levels of ammonia vapor with a change in color from yellow to blue within minutes.²⁰ One of the most notable illustrations to the capabilities of colorimetric sensors includes a colorimetric array introduced by Suslick and co-workers in 2005 that provided selective discrimination of amines within larger amine families, giving vast improvements to the selectivity of colorimetric sensors. This was achieved by utilizing a combination of modern digital imaging with pattern recognition techniques to obtain < 1 ppm detection limits.²¹ With these methods, quick identification and even quantification of specific analytes was possible (**Figure 1.2**);⁹ however, the need for specialized equipment in these methods and the restriction to the type of amine detection possible (volatile amines only), leaves room for improvement. Specifically, the creation of a sensor easily available to non-experts that also allows for the detection of amines beyond those in the vapor phase would greatly expand the utility of colorimetric amine detectors.

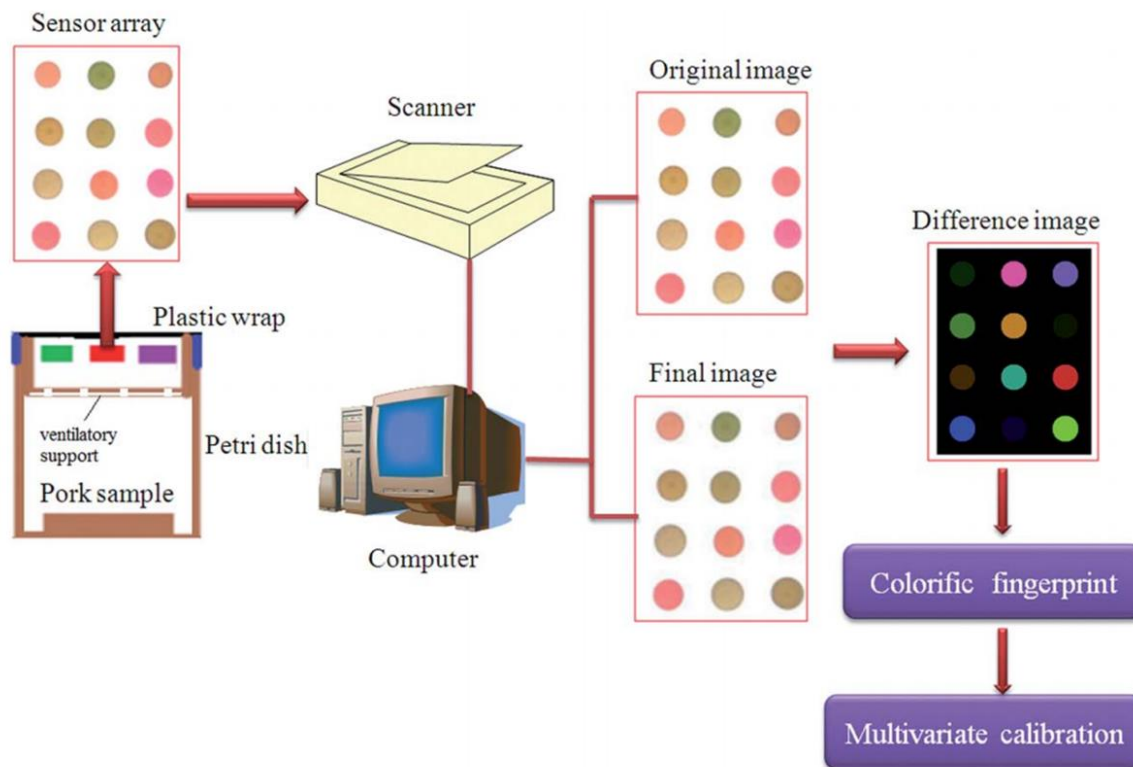


Figure 1.2 Some notable examples of improvements to colorimetric detectors include the use of colorimetric sensor arrays as demonstrated in this schematic diagram of an electronic-nose system. This figure was reproduced from *Anal. Methods*, **2014**, *6*, 6271-6277 (Reference #9) by permission of The Royal Society of Chemistry. CCC License Number 1000679-1.

1.2.4 Donor-Acceptor Stenhouse Adducts (DASA): creating new materials for improved detectors

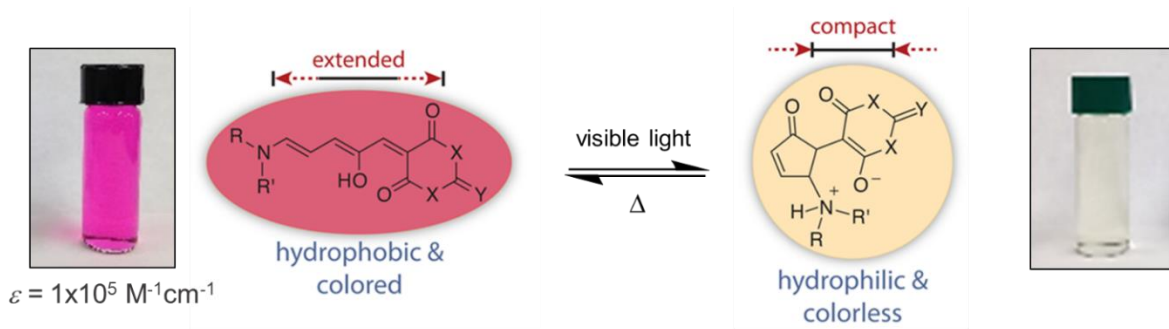


Figure 1.3 DASAs are a new class of organic photochromic molecules that can reversibly transform from a brightly colored “extended” isomer with a high extinction coefficient ($\epsilon = 1 \times 10^5 \text{ M}^{-1} \text{ cm}^{-1}$) to a “compact” and colorless isomer. Figure adapted with permission from *J. Am. Chem. Soc.*, **2014**, *136*, 8169–8172 (Reference #22) © 2014 American Chemical Society.

Donor-Acceptor Stenhouse Adducts are a new class of photochromic molecules, capable of reversible transformation between two isomers with different absorption spectra when triggered by light, that were first introduced by Read de Alaniz and co-workers in 2014 (**Figure 1.3**).^{22,23} Since their discovery, heavy investigation into the structure-property relationship of these compounds has resulted in a plethora of materials with applications spanning drug delivery and catalyst recycling to photopatterning of surfaces. Due to the favorable properties of these compounds, including their ease of preparation, high molar absorptivity, and tailored response to heat or chemical stimuli, DASAs have also grown in popularity for use in colorimetric sensors²⁴ (a complete description into the current uses of DASAs as sensors is described in **Chapters 2** and **3**). In particular, it was discovered that the DASA photochromes would provide molar absorptivity values ($\epsilon = 1 \times 10^5 \text{ M}^{-1} \text{ cm}^{-1}$) that exceeded those of commonly used dyes such as Magic Blue (tris(4-bromophenyl)ammoniumyl

hexachloroantimonate, $\epsilon = 1 \times 10^4 \text{ M}^{-1} \text{ cm}^{-1}$) or Methylene Blue (methylthioninium chloride, $\epsilon = 7 \times 10^4 \text{ M}^{-1} \text{ cm}^{-1}$) (**Figure 1.4**). This revealed an avenue to increase the selectivity and sensitivity of current detectors. **Chapter 2** will explore the development of improved colorimetric amine detectors *via* the facile reaction of activated furans with amines to form the DASA with high extinction coefficients. **Chapter 3** will then introduce the synthesis of novel activated furan and DASA polymer conjugates and discuss how these new materials were exploited to reveal methods of controlling the reactivity and stability of activated furans and DASAs in aqueous media. Furthermore, **Chapter 3** will also explore the subsequent performance of these new materials as sensors.

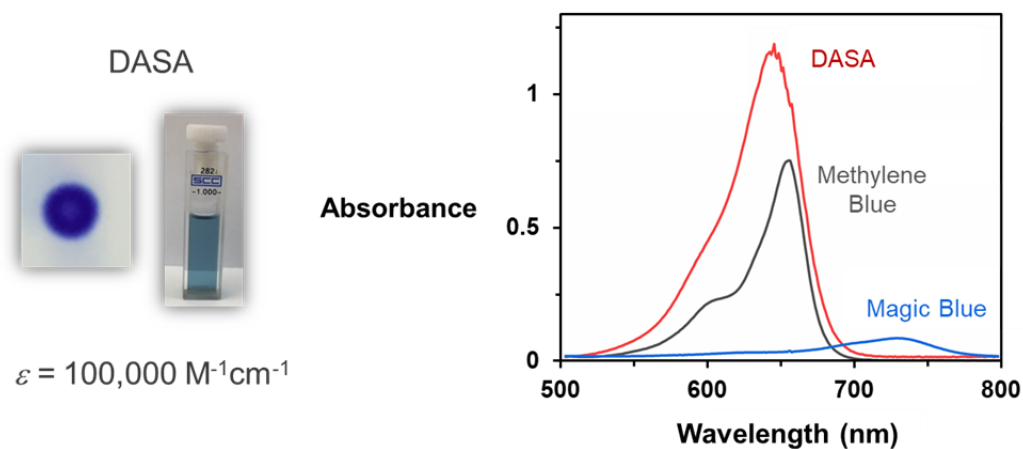


Figure 1.4 Comparing the absorbance of commonly used dyes such as Methylene Blue and Magic Blue to that of DASA at the same concentration, reveals a stronger absorbance in the visible range for the DASA. This demonstrates the capabilities of DASA to be used as a stronger dye in solution and on solid supports than popular examples. Credit for absorbance spectra: Ms. Serena Seshadri.

1.3 Poly(acrylic acid) (PAA) : A Versatile Water Soluble Polymer

1.3.1 Exploring the structure-property relationship of PAA

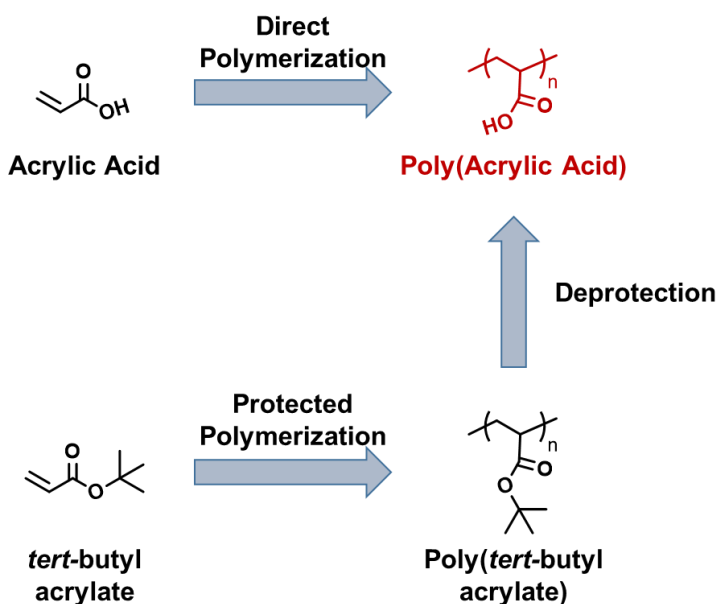


Figure 1.5 Synthesis of poly(acrylic acid) via two common routes **a**) direct polymerization of acrylic acid and **b**) polymerization of a protected acid followed by subsequent deprotection. Protected synthesis can allow for easier incorporation of functional groups.

Research in materials science not only seeks to develop new materials but also contributes improvements to current technologies by providing a deeper understanding into the structure-property relationship of existing materials. The functionalization of PAA is one such example. PAA is a synthetic polymer of acrylic acid that is soluble in aqueous media due to the ionization of the carboxyl side chains (**Figure 1.5**). Various homopolymer and copolymer derivatives of PAA have resulted in materials useful in a wide variety of industrially relevant applications including coatings,²⁵ dispersants,²⁶ and mineralization control.^{27,28} For example, the ability of PAA to absorb and retain water allows the polymer to swell several times its own

weight thus increasing its utility as a superabsorbent polymer.²⁹ Alternatively, PAA derivatives have been used to modify the properties of inorganic pigments, such as titanium dioxide, to achieve uniform dispersions in paint formulations (**Figure 1.6**).^{30,31} This versatility of different poly(acrylic acid) derivatives has resulted in an in-depth analysis of how properties such as polymer architecture, dispersity, and molecular weight will influence the performance of PAA towards these applications.²⁵ One such characteristic of recent interest is the composition of the polymer end groups. Although preliminary investigation has revealed that the end group functionalization of PAA will have a direct effect on the utility of the polymer toward specific applications,^{32–34} a thorough investigation into the effects of end group chemistry would provide a more systematic understanding into the influence of these structural changes to the polymer characteristics.

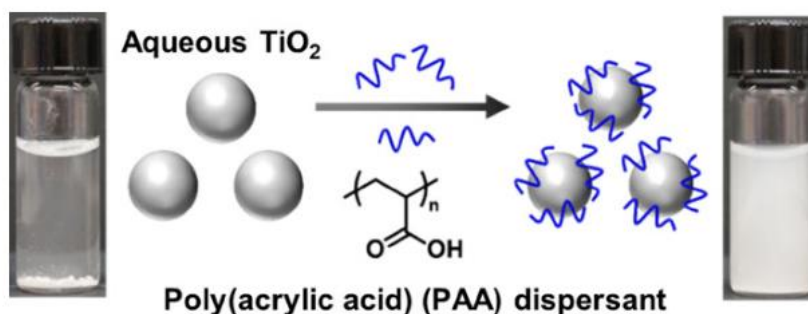


Figure 1.6 Poly(acrylic acid) derivatives can be used toward numerous applications including the dispersant of inorganic pigments such as titanium dioxide (TiO₂). Figure reprinted with permission from *J. Polym. Sci., Part A Polym. Chem*, **2019**, 57, 716–725 (Reference #30) © 2019 John Wiley & Sons, Inc. CCC License Number 4695011434918.

1.3.2 Common methods for polymerization

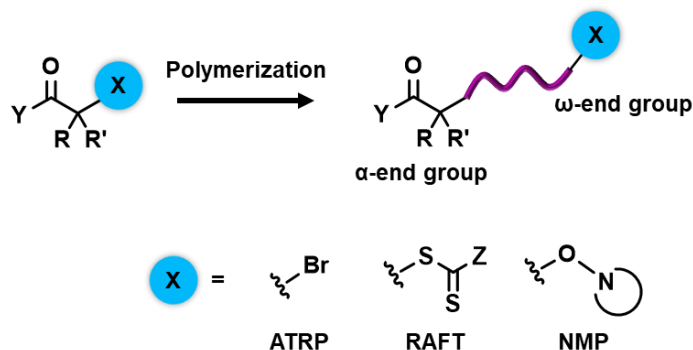


Figure 1.7 Chemical functionality that result from the initiators and chain transfer agents of three main controlled radical polymerization methods. Figure reproduced with permission from J. Polym. Sci., Part A Polym. Chem, **2019**, 57, 716–725 (Reference #30) © 2019 John Wiley & Sons, Inc. CCC License Number 4695020653131.

Controlled chain-growth polymerization is a rapidly expanding field that has facilitated access to low dispersity materials with tailored chain-end functionality.³⁵ As such, the research in this area has uncovered the high influence a polymer chain-end will have on the physical properties of a material. In particular, controlled radical polymerizations (CRP) including atom transfer radical polymerization (ATRP), reversible addition fragmentation chain transfer (RAFT) polymerization, and nitroxide mediated polymerization (NMP) remain the favored choices for polymer synthesis. This preference for CRP stems from the large monomer scope available, the mild reaction conditions, and reaction versatility. More specifically, the functional initiators or residual reactive terminal groups that result from these methods of polymerization, offer a wide selection for tailored functionality (**Figure 1.7**).

1.3.3 Overview of chain-end functionalization

a) Post-polymerization modification



b) Use of functional initiators



c) End capping with reactive terminators

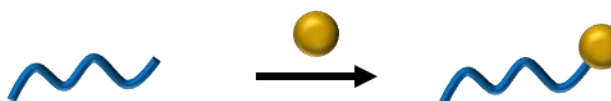


Figure 1.8 Schematic representation of chain-end functionalization strategies available. **a)** modification of an existing chain-end, **b)** use of a functional initiator and **c)** in situ termination of polymer with a reactive terminator. Figure adapted with permission from *J. Polym. Sci., Part A Polym. Chem*, **2019**, *57*, 716–725 (Reference #30) © 2019 John Wiley & Sons, Inc. CCC License Number 4695020653131.

Among the techniques for chain-end modification, the most popular methods include post-polymerization functionalization of pre-existing chain ends, the use of functional initiators, and the use of reactive terminators as caps for growing polymer chains (**Figure 1.8**). In a recent review by Hawker and coworkers, established and emerging chain-end modification strategies for popular chain-growth processes, including ATRP, RAFT, and NMP were highlighted.³⁵ **Figure 1.9** demonstrates just a few of the functionalization possibilities for these techniques with a particular emphasis on ω -chain end modifications. From these controlled radical polymerizations, ATRP is reportedly the most versatile of methods due to the halide terminal group that remains after polymerization which provides an ideal route toward more

tailored functionality. Alternatively, although RAFT is capable of providing a larger monomer scope and greater tolerance to reaction conditions, such as aqueous, suspension, or emulsion synthesis, the chain-transfer agents required often introduce more challenging synthetic techniques or additional odors and color that must be further purified. Finally, NMP strategies also allow for the introduction of various end groups yet do not require the use of additional catalysts or initiators. While current modification techniques have enabled the synthesis of large libraries of polymeric materials with tailored chain-end functionality, further advancements to this area can offer a broader understanding into the influence of chain-end to the overall material properties.

1.3.4 Investigating the effect of chain-end on PAA characteristics

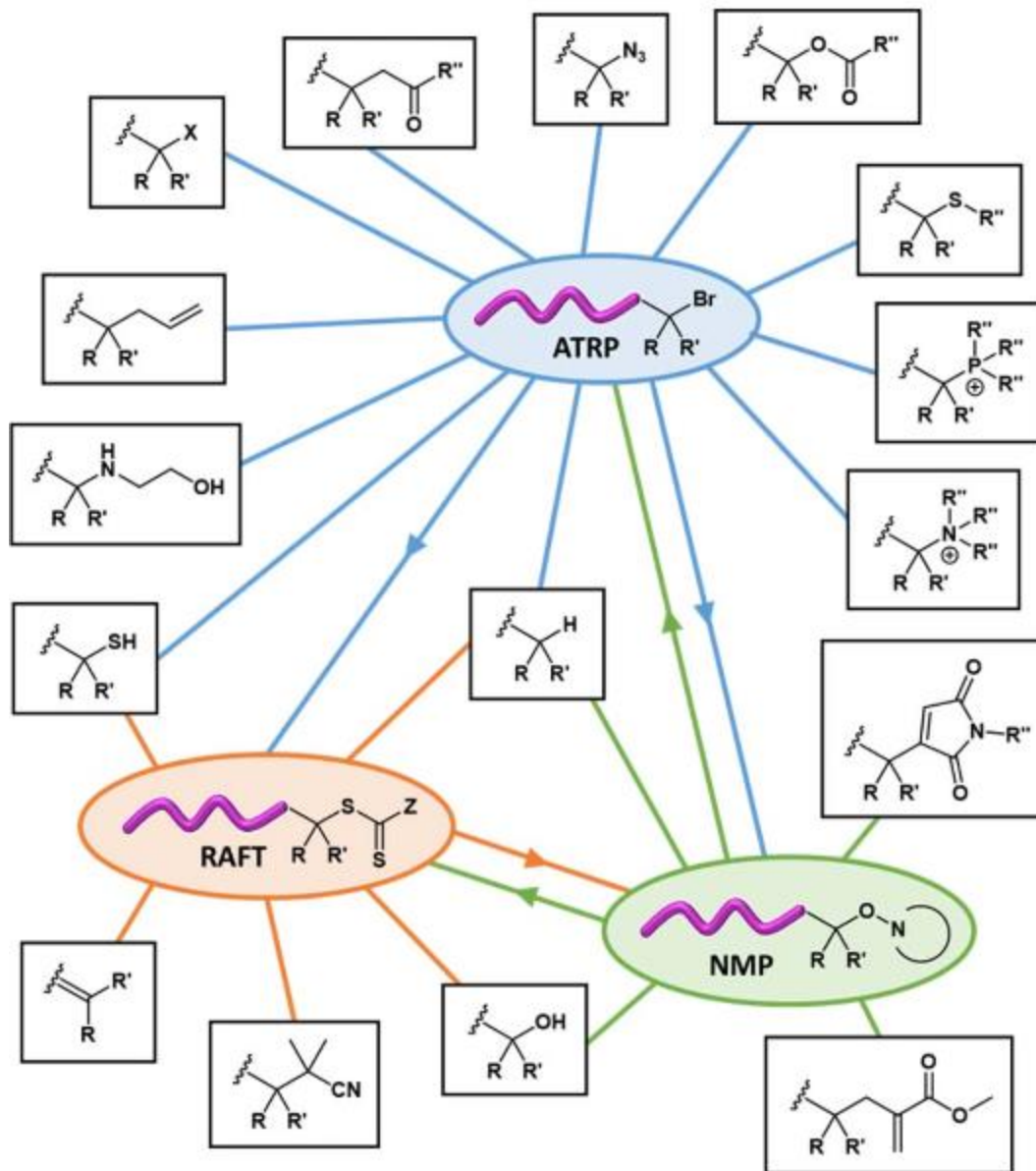


Figure 1.9 Overview of some possible chain-end functional groups for the three main controlled radical polymerizations. Most research has focused on the introduction of ω -chain ends, yet functionalization of the α -end group is also possible through the use of appropriate initiators. Figure reprinted with permission from *J. Polym. Sci., Part A Polym. Chem*, **2019**, 57, 716–725 (Reference #30) © 2019 John Wiley & Sons, Inc. CCC License Number 4695020653131.

These controlled radical polymerization and polymer chain-end modification strategies have allowed for significant advancements toward the functionalization of poly(acrylic acid) for targeted applications. For instance, in 2010, Fellows and coworkers revealed that by simply modifying the initiator for the ATRP of *tert*-butyl acrylate to a variety of long and short chain alkyl groups followed by hydrolysis of the resulting polymer (see **Figure 1.5, Protected Polymerization**), they could access a number of α chain-end modified PAA structures with narrow polydispersities.³⁶ This library of polymers revealed that PAAs possessing long chain alkyl groups could provide preferential formation of calcium oxalate crystals and thus proved more useful in industrial water system applications over their short-chain PAA counterparts. Similarly, RAFT polymerization techniques have provided access to various chain-transfer agents resulting in PAA libraries with diverse ω -chain end modifications.³² These strategies have effectively resulted in PAAs with various long and short chain alkyl and hydroxyl groups. However, in order to achieve a more complete understanding of how various end groups will affect the properties of PAA, a wider breadth of chain-end chemistries would need to be accessed. **Chapter 4** will introduce a novel pathway to obtain tailored and well-defined PAA chain-ends with more versatile functional groups *via* a universal and scalable synthetic method. This synthesis provides a more user-friendly method to produce PAA derivatives with a wide variety of chain ends so that a more complete catalog of potential PAA additives can be screened for any given application. Also, by expanding the range of PAA chain-ends and simplifying the synthetic process to produce these polymers, the overall structure-property relationship between PAA chain-end chemistry and macroscale polymer behaviour can be further understood.

1.4 References

- 1 American Chemical Society, Materials Science, <https://www.acs.org/content/acs/en/careers/college-to-career/chemistry-careers/materials-science.html>, (accessed August 10, 2019).
- 2 K. L. Bicker, S. L. Wiskur and J. J. Lavigne, in *Chemosensors: Principles, Strategies, and Applications, First Edition*, eds. B. Wang and E. V. Anslyn, John Wiley & Sons, Inc., 1st edn., 2011, pp. 275–295.
- 3 K. C.-F. Leung, C.-P. Chak, C.-M. Lo, W.-Y. Wong, S. Xuan and C. H. K. Cheng, *Chem. Asian J.*, 2009, **4**, 364–381.
- 4 E. Kaiser, R. L. Colescott, C. D. Bossinger and P. I. Cook, *Anal. Biochem.*, 1970, **34**, 595–598.
- 5 L. A. Cole, *Clin. Chem. Lab. Med.*, 2011, **50**, 617–630.
- 6 F. Gaggini, A. Porcheddu, G. Reginato, M. Rodriguez and M. Taddei, *J. Comb. Chem.*, 2004, **6**, 805–810.
- 7 T. Fan, W. Xu, J. Yao, Z. Jiao, Y. Fu, D. Zhu, Q. He, H. Cao and J. Cheng, *ACS Sens.*, 2016, **1**, 312–317.
- 8 K. E. Secor and T. E. Glass, *Org. Lett.*, 2004, **6**, 3727–3730.
- 9 H. Li, Q. Chen, J. Zhao and Q. Ouyang, *Anal. Methods*, 2014, **6**, 6271–6277.
- 10 U. Khulal, J. Zhao, W. Hu and Q. Chen, *RSC Adv.*, 2016, **6**, 4663–4672.
- 11 B. Kuswandi, Jayus, A. Restyana, A. Abdullah, L. Y. Heng and M. Ahmad, *Food*

- Control*, 2012, **25**, 184–189.
- 12 Y. Hu, X. Ma, Y. Zhang, Y. Che and J. Zhao, *ACS Sens.*, 2016, **1**, 22–25.
- 13 A. Pacquit, K. T. Lau, H. McLaughlin, J. Frisby, B. Quilty and D. Diamond, *Talanta*, 2006, **69**, 515–520.
- 14 T. Lin, Y. Wu, Z. Li, Z. Song, L. Guo and F. Fu, *Anal. Chem.*, 2016, **88**, 11022–11027.
- 15 X. Sun, Y. Wang and Y. Lei, *Chem. Soc. Rev.*, 2015, **44**, 8019–8061.
- 16 L. Feng, C. J. Musto, J. W. Kemling, S. H. Lim and K. S. Suslick, *Chem. Commun.*, 2010, **46**, 2037–2039.
- 17 S. F. Liu, A. R. Petty, G. T. Sazama and T. M. Swager, *Angew. Chem. Int. Ed.*, 2015, **54**, 6554–6557.
- 18 G. A. Sotzing, J. N. Phend, R. H. Grubbs and N. S. Lewis, *Chem. Mater*, 2000, **12**, 593–595.
- 19 E. Mertz and S. C. Zimmerman, *J. Am. Chem. Soc.*, 2003, **125**, 3424–3425.
- 20 A. T. Hoang, Y. B. Cho, J.-S. Park, Y. Yang and Y. S. Kim, *Sens. Actuators, B*, 2016, **230**, 250–259.
- 21 N. A. Rakow, A. Sen, M. C. Janzen, J. B. Ponder and K. S. Suslick, *Angew. Chem. Int. Ed.*, 2005, **44**, 4528–4532.
- 22 S. Helmy, F. A. Leibfarth, S. Oh, J. E. Poelma, C. J. Hawker and J. Read de Alaniz, *J. Am. Chem. Soc.*, 2014, **136**, 8169–8172.

- 23 S. Helmy, S. Oh, F. A. Leibfarth, C. J. Hawker and J. Read De Alaniz, *J. Org. Chem.*, 2014, **79**, 11316–11329.
- 24 M. M. Lerch, W. Szymański and B. L. Feringa, *Chem. Soc. Rev.*, 2018, **47**, 1910–1937.
- 25 T. Spychaj, *Prog. Org. Coat.*, 1989, **17**, 71–88.
- 26 S. Liufu, H. Xiao and Y. Li, *J. Colloid Interface Sci.*, 2005, **281**, 155–163.
- 27 Y. Qi, Z. Ye, A. Fok, B. N. Holmes, M. Espanol, M.-P. Ginebra and C. Aparicio, *ACS Biomater. Sci. Eng.*, 2018, **4**, 2758–2766.
- 28 A. Akar and N. Öz, *Macromol. Mater. Eng.*, 1999, **273**, 12–14.
- 29 K. Kabiri, H. Omidian, M. J. Zohuriaan-Mehr and S. Doroudiani, *Polym. Compos.*, 2011, **32**, 277–289.
- 30 D. J. Lunn, S. Seo, S. Lee, R. Bou Zerdan, K. M. Mattson, N. J. Treat, A. J. McGrath, W. R. Gutekunst, J. Lawrence, A. Abdilla, A. Anastasaki, A. S. Knight, B. V. K. J. Schmidt, M. W. Bates, P. G. Clark, J. P. Derocher, A. K. Van Dyk and C. J. Hawker, *J. Polym. Sci., Part A Polym. Chem.*, 2019, **57**, 716–725.
- 31 A. Foissy, A. El Attar and J. M. Lamarche, *J. Colloid Interface Sci.*, 1983, **96**, 275–287.
- 32 W. O. S. Doherty, C. M. Fellows, S. Gorjian, E. Senogles and W. H. Cheung, *J. Appl. Polym. Sci.*, 2004, **91**, 2035–2041.
- 33 A. D. Wallace, A. Al-Hamzah, C. P. East, W. O. S. Doherty and C. M. Fellows, *J. Appl. Polym. Sci.*, 2010, **116**, 1165–1171.

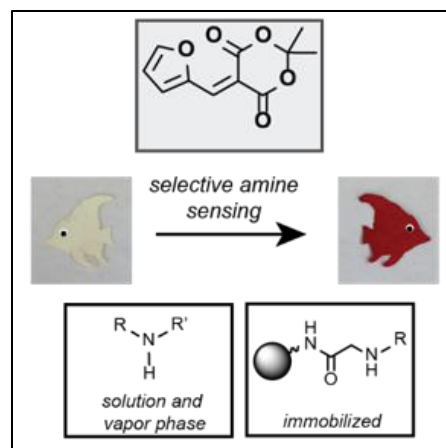
- 34 A. A. Al-Hamzah, C. P. East, W. O. S. Doherty and C. M. Fellows, *Desalination*, 2014, **338**, 93–105.
- 35 D. J. Lunn, E. H. Discekici, J. Read de Alaniz, W. R. Gutekunst and C. J. Hawker, *J. Polym. Sci., Part A Polym. Chem*, 2017, **55**, 2903–2914.
- 36 C. P. East, A. D. Wallace, A. Al-Hamzah, W. O. S. Doherty and C. M. Fellows, *J. Appl. Polym. Sci.*, 2010, **115**, 2127–2135.

CHAPTER 2

A VERSATILE AND HIGHLY SELECTIVE COLORIMETRIC SENSOR FOR DETECTION OF AMINES[‡]

2.1 Abstract

The utility of Meldrum's activated furan (MAF) for the colorimetric detection of sub parts per million (ppm) levels of amines in solution, on solid supports, and as vapors is presented. MAF is synthesized in one step from inexpensive and commercially available starting materials and exhibits high selectivity for primary and secondary amines in the presence of competing nucleophiles. The reaction between activated furans and amines results in a distinct color change, discernable by the naked eye. Ultraviolet-visible (UV-vis) absorption spectroscopy was utilized to monitor reactions in



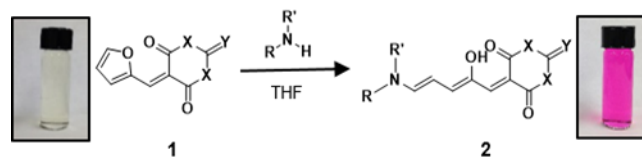
[‡] Reproduced with permission: Y. J. Diaz, Z. A. Page, A. S. Knight, N. J. Treat, J. R. Hemmer, C. J. Hawker and J. Read de Alaniz, *Chem. Eur. J.*, **2017**, *23*, 3562–3566. © John Wiley & Sons, Inc. CCC License Number 4695030584584.

solution and determine detection limits. Additionally, solutions of MAF were useful as stains for thin layer chromatography and for monitoring solid phase synthesis of peptides and peptidomimetics. Finally, MAF was used to detect volatile amines released from fish samples, demonstrating potential for food spoilage applications.

2.2 Introduction

The ability to selectively sense amine-containing molecules is pertinent to a variety of research and commercial applications, including chemical synthesis,¹ drug detection,^{3,23} and environmental monitoring.^{5-12,24} Emerging methods that track changes in resistivity^{13,13,14} and luminescence^{7,15-17,23} have allowed increased sensitivity and selectivity with chemiresistors^{13,14,18} and fluorescence-sensors^{7,15,19-22} providing sub-ppm limits of detection. However these systems often require complex synthetic methods and the use of secondary equipment for amine identification. Additionally, the majority of these sensors are limited to detection of volatile and primary amines.

In addressing the challenges with these techniques, colorimetric sensors are attractive alternatives due to their simple and rapid detection of amines in solution, as vapors, and on solid supports.²⁵ Recent improvements have also provided competitive sensitivities (<1 ppm).^{11,26,27} For example, polyacrylonitrile nanofibers have been used for the visible detection of ammonia vapors of < 1 ppm.^{11,26} Suslick and coworkers have achieved < 1 ppm sensitivities by utilizing a combination of metalloporphyrins and pH acid/base indicators in colorimetric arrays with the additional benefit of merging modern digital imaging and pattern recognition techniques.²⁷ Although advances to colorimetric sensors have allowed for the



Scheme 2.1 General reaction for activated furan-based amine sensor. Activated furan (**1**) reacts with ammonia, or a primary or secondary amine to form a colored DASA (**2**). Inset: Photographs of Meldrum's activated furan in tetrahydrofuran (THF) (20 mM, left) and 5 min after the addition of diethylamine (200 ppm, right).

identification and quantification of specific analytes, these methods often involve the use of specialized equipment and are restricted to the detection of volatile amines, limiting their use as a general amine colorimetric sensor. Recent investigation into new negative photoswitches, termed donor acceptor Stenhouse adducts (DASA)s, revealed an avenue to increasing the versatility and selectivity of colorimetric detection of amines.^{28,29} The ring opening of activated furans with secondary amines is a rapid and efficient reaction that produces DASAs, which possess high molar absorptivity values ($\epsilon_{\lambda_{max}} \approx 10^5 \text{ M}^{-1}\text{cm}^{-1}$).³⁰⁻³² The facile synthesis of activated furans from commercially available and inexpensive starting materials coupled with the high ϵ of the DASA product indicated the potential of activated furans as colorimetric sensors.³¹

This chapter presents a simple methodology to monitor the presence of amines in solution, on solid supports, and as vapors that is available to non-experts (**Scheme 2.1**). These activated furan-based sensors combine the sensitivity of state-of-the-art detectors with the ability to distinguish various amines by the naked eye. In illustrating the utility of this novel system across different fields, applications including thin layer chromatography (TLC) staining, solid phase peptide/peptoid synthesis, and food spoilage detection were demonstrated.

2.3 Colorimetric Detection in Solution

Activated furan-carbon acids (**1**) are rapidly synthesized by reacting furfural ($\approx \$2/\text{kg}$), a derivative of non-edible biomass, with cyclic 1,3-dicarbonyl compounds on water.^{30,31} Conveniently, both Meldrum's acid activated furan (MAF, compound **3**) and 1,3-dimethyl barbituric acid activated furan (BAF, compound **5**) (**Figure 2.1**) precipitate out of the reaction mixture and can be isolated in near quantitative yields by filtration.³¹ Additionally, MAF and BAF have excellent stability under ambient conditions as well as when dissolved in non-nucleophilic organic solvents (e.g., tetrahydrofuran and dichloromethane), as evidenced by monitoring the solution over time using nuclear magnetic resonance (NMR) spectroscopy

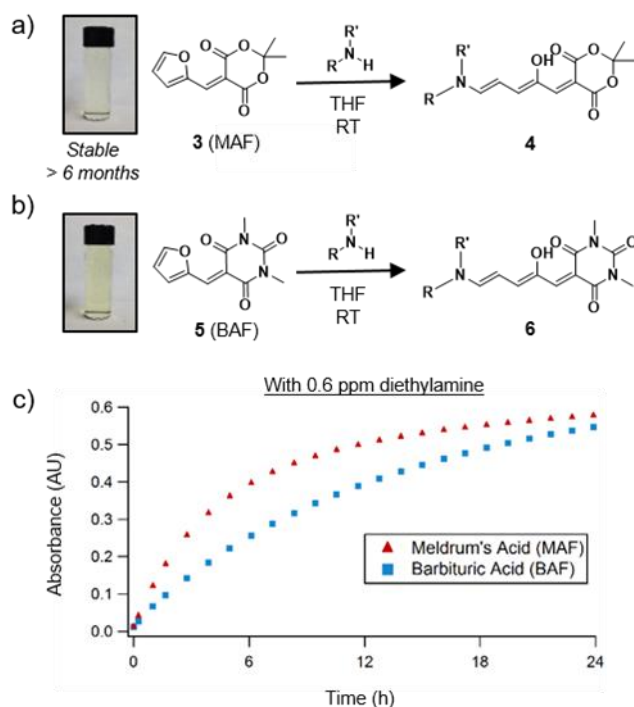


Figure 2.1 General reaction with amines for **a)** MAF, **3**, and **b)** BAF, **4** (photographs represent respective 20 mM solutions of MAF and BAF in THF). **c)** Reaction of MAF (red triangles) and BAF (blue squares) with DEA (0.6 ppm).

(**Figure S2.1**). These activated furans then react rapidly with amines to produce highly colored and thermodynamically stable triene forms of DASAs (**2**).^{30–32} Although DASAs are light-responsive dyes, basic “donors”, such as aliphatic amines, require a highly nonpolar matrix (e.g., toluene, hexanes) for photoswitching (color bleaching) to be observed, making them excellent candidates for amine sensing (**Figure S2.2**).^{32–34}

UV-Vis absorption spectroscopy was utilized to compare the optical properties and amine reactivities of MAF and BAF. For equimolar solutions (10 μM in THF) of the two activated furans, MAF solution was found to be colorless to the naked eye, while BAF solution was slightly yellow (**Figure 2.1a, 2.1b**). The near colorless initial MAF solutions are favorable for sensing applications, given the more distinguishable “turn-ON” of color that occurs upon amine exposure (**Figure S2.3-S2.5**). Introducing 0.6 ppm diethylamine (DEA) to MAF and BAF solutions (20 mM in THF), and monitoring the reactions *in situ*, revealed that MAF reacts ~ 2 times faster (**Figure 2.1c**). Given the beneficial optical properties and faster response time of MAF based sensor, it was selected for in-depth investigation. Initially, the limit of detection by eye for DEA in a 20 mM solution of MAF (in THF) was found to be ~ 0.4 ppm after 1 h of exposure (**Figure S2.6**). Significantly, other secondary amines, primary amines, and ammonia were all found to form the characteristic pink color ($\lambda_{\text{max}} \approx 532$ nm), however, with varying reaction rates (**Figure S2.7**). After 5 min, the absorbance of **4** using DEA is 11-fold higher than the reaction with butylamine (1° amine), and 33-fold higher than the reaction with

ammonia (**Figure 2.2**). The same trend was observed for other 2° and 1° amines; 10 ppm of dimethylamine and piperidine (2° amines) resulted in pink color after 5 min, while 100 ppm of cadaverine (a common biogenic 1° amine³⁵) was required to turn the solution pink within 5 min (**Figure S2.7**). This difference in reaction rates and absorbance provides a pathway to distinguish between primary and secondary amines in solution. To establish selectivity for amines, the MAF solution was reacted with other nucleophiles, such as water, alcohols, thiols,

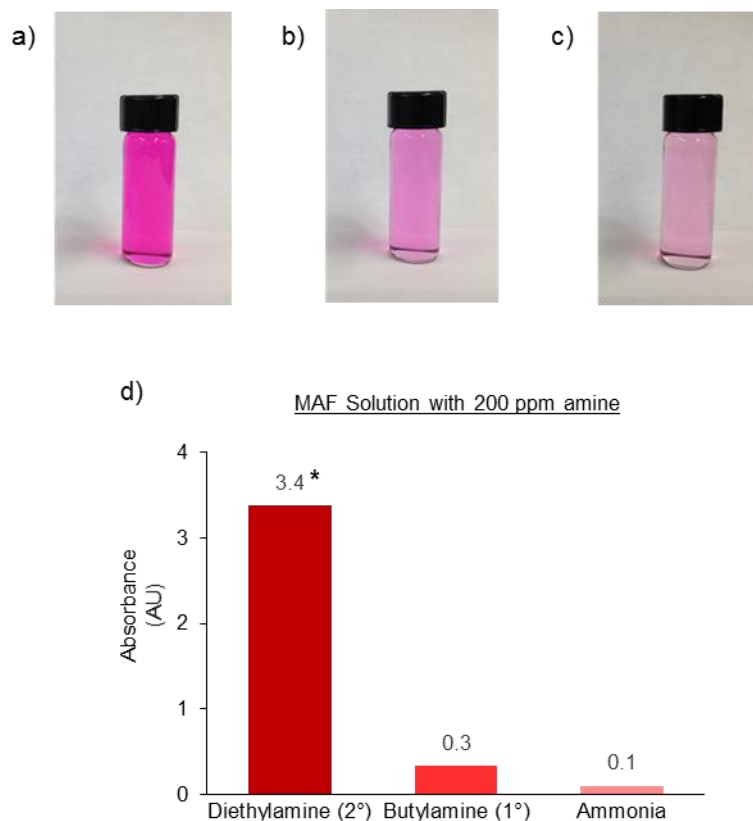


Figure 2.2 Images of MAF solution (20 mM in THF) after reacting for 5 min with **a**) DEA (2° amine) **b**) butylamine (1° amine), and **c**) ammonia and **d**) absorption of MAF solutions at 532 nm (λ_{maxDASA}) after reacting for 5 min with 200 ppm DEA (2° amine), butylamine (1° amine), and ammonia. *For DEA the absorption was measured by diluting the parent solution four fold given the high DASA molar absorptivity and high concentration that cannot accurately be measured with UV-Vis absorption.

and organophosphorus compounds (**Figure 2.3**). As expected only amines were found to be reactive with the MAF solution, highlighting the amine-selectivity.

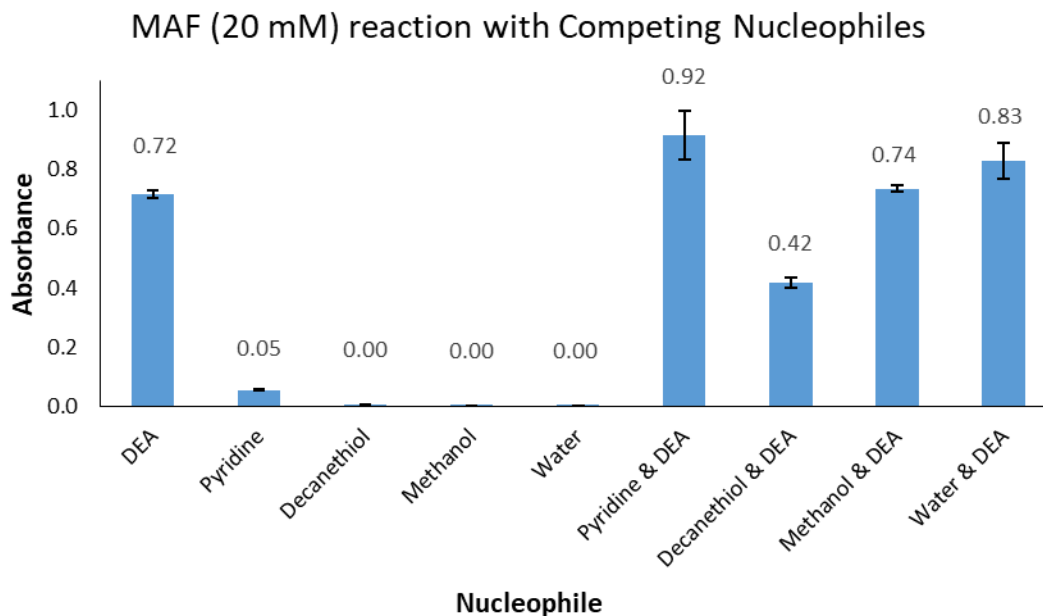


Figure 2.3 Reaction of 20 mM Meldrum's activated furan solution with 20 ppm of diethylamine, pyridine, decanethiol, methanol, and water. Selective detection of diethylamine (DEA) in the presence of representative 3° amine (pyridine), thiol (decanethiol), alcohol (methanol), and water.

2.4 Colorimetric Detection on Solid Supports

To showcase MAF as an amine-selective stain on solid supports, in particular for thin layer chromatography, a tryptamine-based synthetic sequence was monitored (**Figure 2.4**). TLC staining is one of the most common methods to track the progress of a chemical reaction and determine chromatographic purification conditions. Although the ability to rapidly distinguish different amine moieties by eye is beneficial for synthetic chemists, traditional stains, such as ninhydrin,³⁶ often do not provide this distinction.

Tryptamine derivatives are prevalent in the pharmaceutical industry and natural product synthesis, making them exemplary candidates for TLC staining with MAF. Four derivatives, possessing various aliphatic and/or conjugated amines, were synthesized from tryptamine (**Figure S2.8**), spotted onto silica TLC plates, and stained with MAF (20 mM in THF). After staining for < 1 min at room temperature, a wide range of vibrant colors became apparent, making it possible to clearly distinguish the different reaction stages by eye (**Figure 2.4** and **Figure S2.9**). By comparison, the traditional and commercially available Ninhydrin stain could not provide this same level of detection (**Figure 2.5** and **Figure S2.10**). To quantify the color difference between stained tryptamine derivatives, ΔE^* values were determined following International Commission on Illumination (CIE) guidelines (See **Section 2.7.4**).^{37–39} All pairs had ΔE^* values > 5, which is generally considered to be

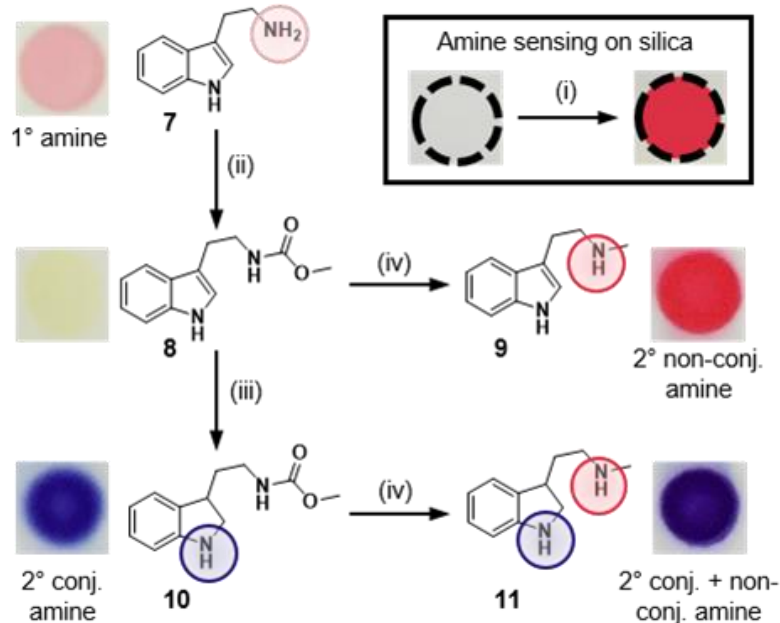


Figure 2.4 Tryptamine-based synthesis and TLC staining with MAF (20 mM in THF). Reagents and conditions: **i**) secondary amine. **ii**) methyl chloroformate, NaOH(aq):DCM (1:1), rt, > 95%. **iii**) Et₃SiH, CF₃COOH, 60 °C, 48%. **iv**) LAH, THF, 60 °C, > 95%.

distinguishable by eye (**Figure S2.11**).^{39–41} This supported that MAF stains are an effective method to distinguish between amine-containing compounds with subtle chemical differences.

MAF solutions were further used to stain amine-functional resins found in solid phase synthesis of peptides and peptidomimetics. For modular solid phase synthesis, the quantitative conversion at each synthetic step is critical for obtaining the desired product.⁴² As such, stains have been developed to identify the presence of 1° and 2° amines.^{43–47} However, commonly used stains such as ninhydrin⁴³ (a.k.a., Kaiser test) and chloranil,⁴⁴ used for detection of 1° and 2° amines respectively, are unstable and require the use of toxic reagents such as acetaldehyde and potassium cyanide. To highlight the ease of reaction monitoring with MAF, peptide and peptoid-functionalized resins were tested. A stable stock solution of MAF in THF (200 mM) was prepared and diluted tenfold into methanol prior to adding 2–3 drops to functionalized

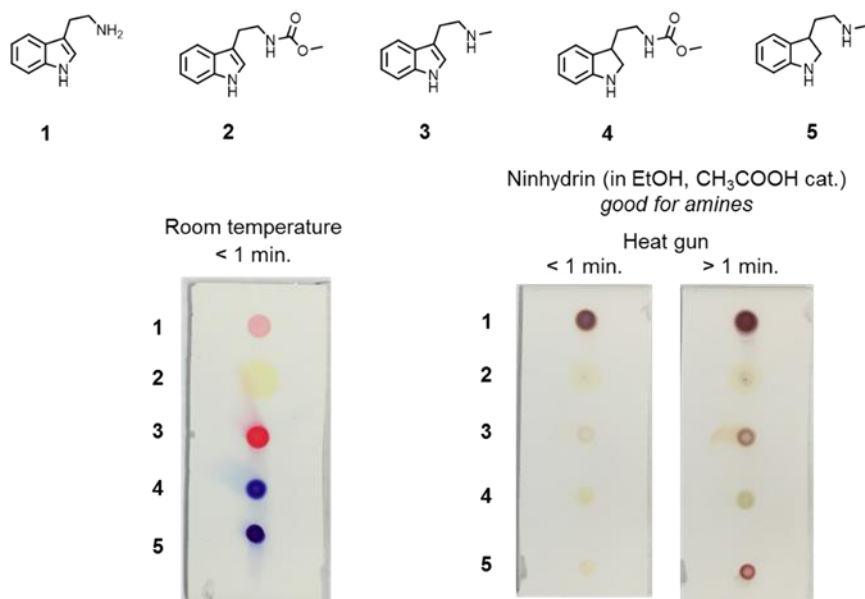


Figure 2.5 Comparison of Meldrum's activated furan (20 mM THF) TLC stain to traditional Ninhydrin TLC stain

resins. For peptides (1° amines), exposure to MAF resulted in beads with a light pink color in 5 min with heat (**Figure 2.6a**). For this, a test tube containing beads was dipped into a bath of boiling water, similar to the procedure used for the Kaiser test.⁴³ However, unlike the Kaiser test, the MAF solution is capable of sensing 1° and 2° amines, allowing for the detection of all amino acids and many peptidomimetics (**Figure S2.12**). The addition of 2-3 drops of MAF solution to resin-bound peptoids, immediately turned the beads bright pink under ambient conditions (**Figure 2.6b**). These results confirmed that MAF stains are a simple and effective alternative to classic methods used to determine reaction completion in solid phase peptide and peptoid synthesis.

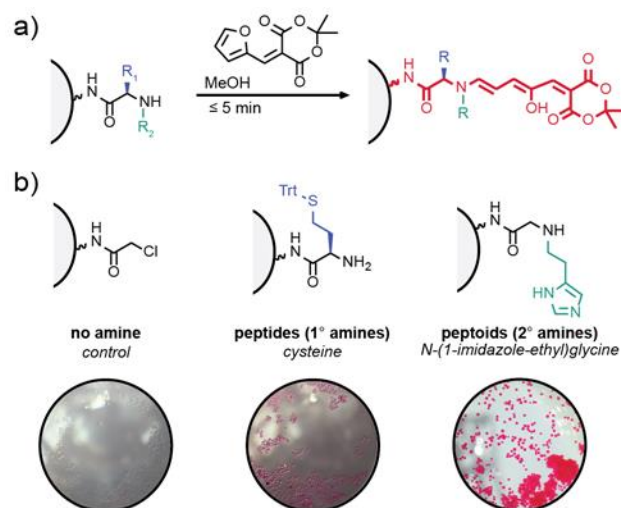


Figure 2.6 a) General reaction between MAF and resin bound peptides/peptoids. **b)** Images of resin beads 5 min after adding 2-3 drops of a MAF solution (20 mM methanol) where 1° amine containing beads (peptides) turn pale pink after heating and 2° amine containing beads (peptoids) turn bright pink under ambient conditions. Control image represents resin beads (no amine) after heating for 5 min.

2.5 Colorimetric Detection in Vapor Phase

Given the facile detection of amines in solution and on solid supports with MAF, we chose to investigate its utility to sense amine vapors. Detection of amine vapors is important for various applications, including food spoilage,^{4-7,18,48,49} where volatile amines such as dimethylamine (DMA) and ammonia are released from aging meat.³⁵ To evaluate the sensitivity of this sensor toward volatile amines, MAF was exposed to known concentrations of amine vapors. First, nylon filter membranes were dipped into a 450 mM solution of MAF in THF, dried, and sealed in septa-capped scintillation vials. The MAF coated filters were then exposed to vapors of DMA and ammonia. After 5 min, the filters were removed from the vials and a digital image of the filter membrane was captured. Calculating ΔE^* for each image revealed that filter membrane exposed to 0.5 ppm of DMA and ammonia vapors is distinguishable ($\Delta E^* > 5$)³⁹⁻⁴¹ from the MAF coated reference (no amine exposure) (**Figure 2.7**). Although MAF has a similar limit of detection for both vapors, the relative change in color for the 2° amine provides ΔE^* values of 68 at 2 ppm DMA, as compared to 31 at 50 ppm ammonia. The more pronounced color change for the secondary amine is consistent with prior observations made for amines in solution and on solid supports. This demonstrated the ability to use MAF coated nylon filters for quick and sensitive detection of volatile amines.

To expand the utility of this sensor to applications in food spoilage, the release of volatile amines from two commercially important fish samples, cod and tilapia, was studied. Freshly thawed fish samples (~15 g) were sealed into separate glass jars containing five nylon filter membranes coated with MAF solutions in THF at concentrations ranging from 56 to

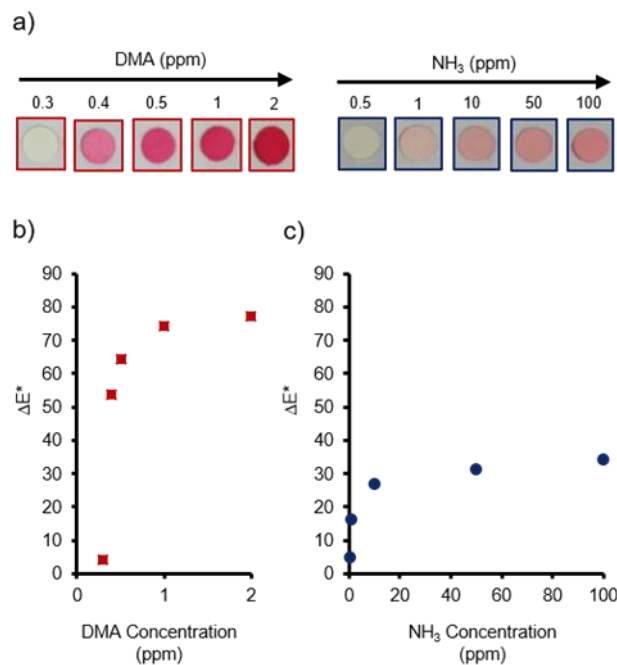


Figure 2.7 a) Images of nylon filters that correspond to data points from graphs b and c. Visual responses of MAF coated nylon filters after 5 min amine exposures to b) 0.3, 0.4, 0.5, 1, and 2 ppm DMA (red squares, detection limit of ~ 0.4 ppm) and c) 0.5, 1, 10, 50, and 100 ppm ammonia (blue circles, detection limit of ~ 0.5 ppm).

450 mM (see **Figure S2.13** for experimental setup). As a control, an analogous setup was constructed with no added fish samples.

The sensors were monitored over the course of 48 h with time lapse imaging (**Figure 2.8**). Interestingly, the cod sample resulted in a noticeable change in color after ~ 8 h, while the tilapia had a significantly delayed response, changing color after ~ 24 h (**Figure 2.8**). Ultimately, ΔE^* values of 60 and 38 were obtained for the cod and tilapia samples (respectively) after 48 h relative to the control sample, highlighting the very distinct color change for MAF samples upon exposure to volatile amines. These results show the potential applicability for this type of sensor in real-time monitoring of food spoilage.

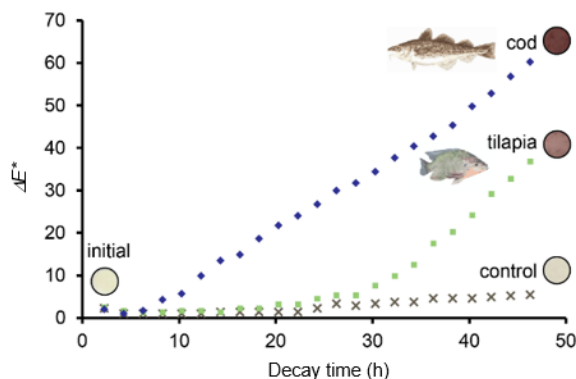


Figure 2.8 Change in color of MAF coated nylon filters over time in the presence of cod (blue diamonds), tilapia (green squares) and air only (black x's, control) at room temperature.

2.6 Conclusion

Meldrum's activated furan has been identified as a versatile and simple to use sensor for the selective detection of amines in solution, on solid supports, and in the vapor phase. With an amine detection limit < 1 ppm MAFs are among the most sensitive, all organic, colorimetric tests for amines, highlighting the capacity of activated furans to be used as simpler alternatives to state-of-the-art sensors. Further utility of activated furans for sensing in organic synthesis, drug detection, and food spoilage applications are currently under investigation.

2.7 Experimental

2.7.1 Materials and equipment

All commercially obtained reagents were used without purification. Ammonia solution (0.5 M in THF) and Nylon-based filter paper (MAGNA) were purchased from Fisher-Scientific. All other reagents and solvents were purchased from Sigma-Aldrich. Fish samples were purchased from Whole Foods Market and stored at -22 °C. Fish samples were then

allowed to thaw to room temperature before use. Broad spectrum handheld light was purchased from The Home Depot and used as is.

UV-Vis spectroscopy was performed on a Shimadzu UV3600 UV-NIR Spectrometer. Analytical TLC was performed using commercial Whatman flexible TLC plates. ¹H NMR spectra were recorded on a Varian 400 MHz spectrometer, using solvent signal for calibration. Time-lapse imaging was performed using a smartphone and the free application Lapse It.

2.7.2 Activated furan synthesis

Meldrum's activated furan and barbituric acid activated furan were synthesized according to literature procedures.^{31,32}

2.7.3 Amine sensing in solution

All sensing reactions were completed using a 20 mM solution of Meldrum's acid activated furan in THF unless stated otherwise. Additionally, the following method was used to conduct detection of amines in solution:

A 20 mM stock solution of Meldrum's acid furan adduct in THF (**A**) was prepared through serial dilutions. This solution was left to equilibrate overnight. In addition, a 1 μL/1 mL stock solution of amine in THF (**B**) was prepared (higher accuracy of this solution can be achieved by preparing a solution with higher volume, i.e 15 μL/15 mL). For highly volatile amines such as dimethylamine and ammonia, dilutions were prepared from a commercially obtained solution of amine in THF. Dimethylamine dilutions were prepared from a 2.0 M solution in THF and ammonia dilutions were prepared from a 0.5 M solution in THF.

Various amounts of **(B)** were added to a 2 mL solution of **(A)** in order to achieve each concentration of amine. For example, diethylamine has a molecular weight of 73.14 g/mol and density of 0.707 g/mL. To achieve 2 mL of a 10 ppm diethylamine solution, 25 μL of **(B)** containing diethylamine was added to 1975 μL of **(A)** to create a 122 μM solution of diethylamine. Using molecular weight and density, this is found to be 10^{-5} g amine/g THF or 10 ppm diethylamine. To reach even lower ppm values, serial dilutions of **(B)** were conducted. After 5 min, solutions were analyzed using a UV-Vis Spectrometer and an image of the reaction vial was obtained with a smartphone.

2.7.4 Quantifying Color: International Commission on Illumination (CIE)

Guidelines

For this protocol, the software Adobe Photoshop was used to quantify colors in images using CIE guidelines with chromatic values $L^*a^*b^*$ representing lightness (L^*) and color opponent red/green (a^*) and yellow/blue (b^*) dimensions (**Figure 2.9**). The distance between

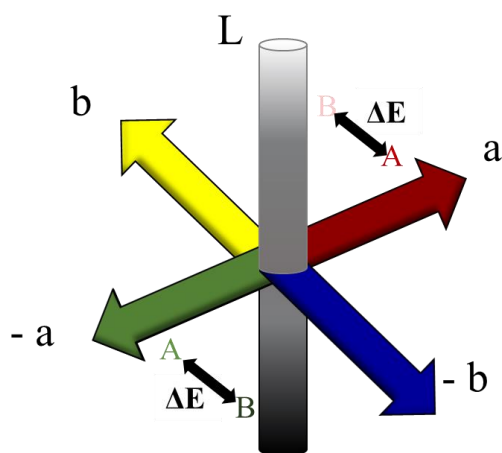


Figure 2.9 Visual representation of the color space utilized by CIE guidelines.⁵¹ The distance between two colors in this space is defined as Delta E (ΔE^*).

two chromatic values in color space, defined as Delta E (ΔE^*), is a metric often used to differentiate two colors.³⁷⁻³⁹ A ΔE^* value > 5 is considered to be distinguishable by eye.³⁹⁻⁴¹

2.8 Supplemental Results

2.8.1 Stability of sensor solution

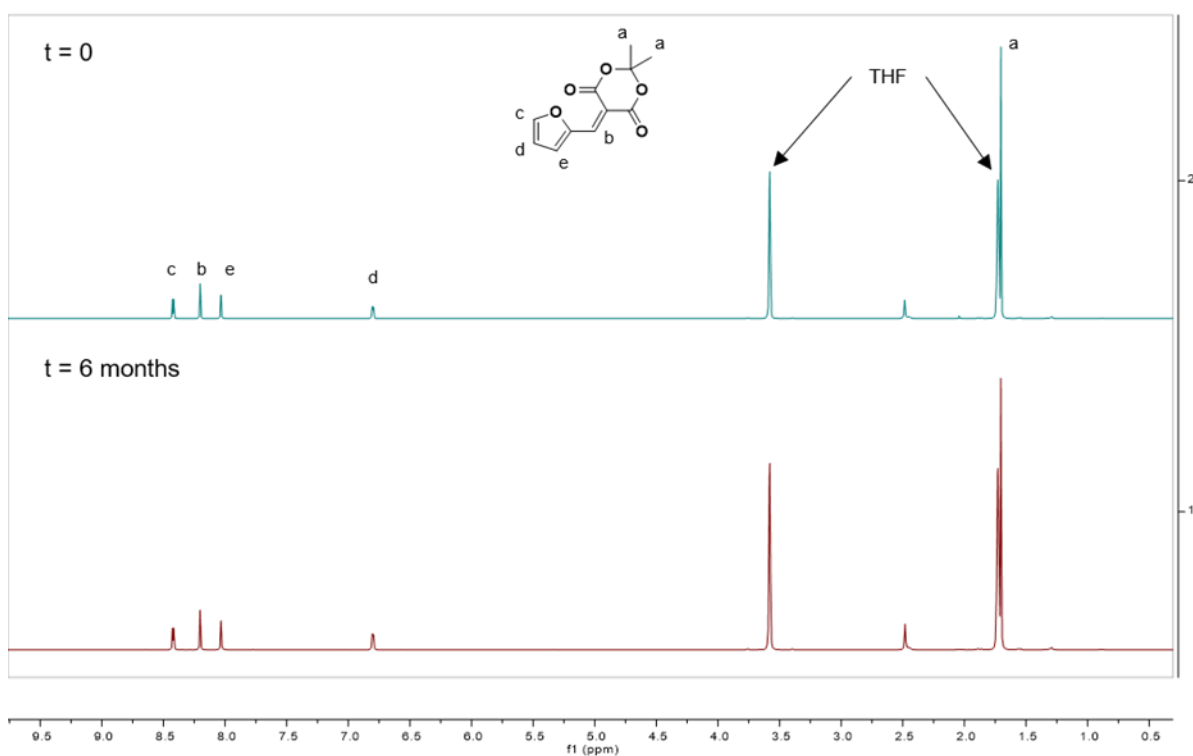


Figure S2.1 ¹H NMR spectra showing the stability of MAF solution over time: 20 mM Meldrum's activated furan in deuterated THF-d₈ at time = 0 (top blue spectrum) and time = 6 months (bottom, red spectrum). ¹H NMR (400 MHz, THF-d₈) δ 8.42 (d, $J = 3.8$ Hz, 1H), 8.20 (s, 1H), 8.03 (d, $J = 1.4$ Hz, 1H), 6.83 – 6.77 (m, 1H), 1.70 (s, 6H).

2.8.2 Optical properties and reactivity of activated furan solution

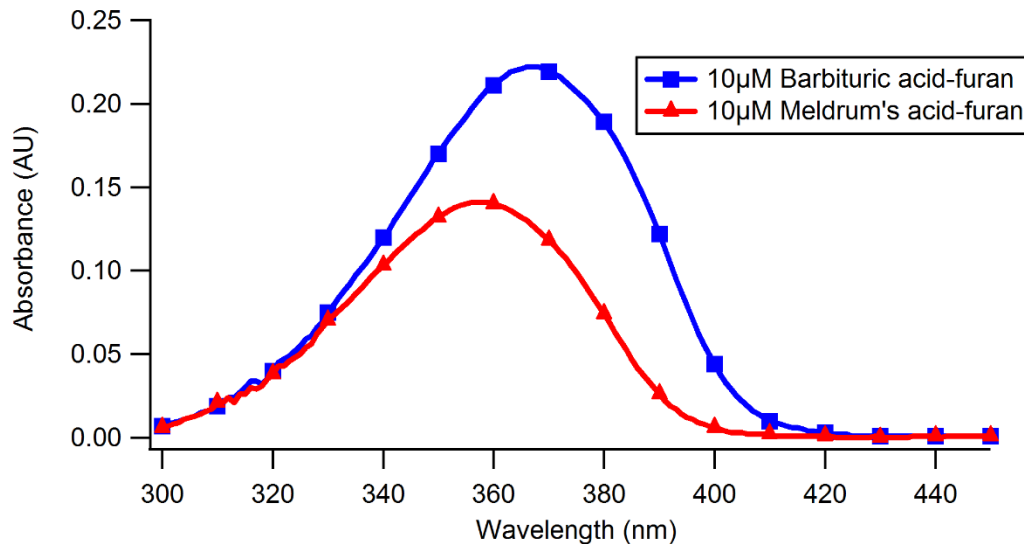


Figure S2.2 UV-Vis analysis of photostability of DASA product. Absorption of DASA product formed after reaction of 20 mM Meldrum's activated furan solution with 20 ppm diethylamine and 24 h in dark, exposed to light from a broad spectrum handheld light, and under ambient conditions.

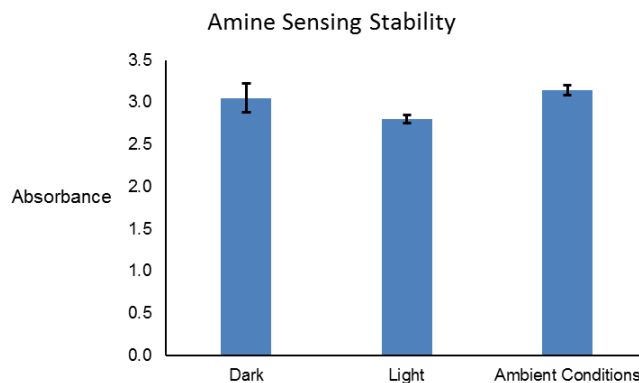


Figure S2.3 Comparison of 10 μM solutions in THF of Meldrum's acid activated furan (red triangle) and barbituric acid activated furan (blue squares).

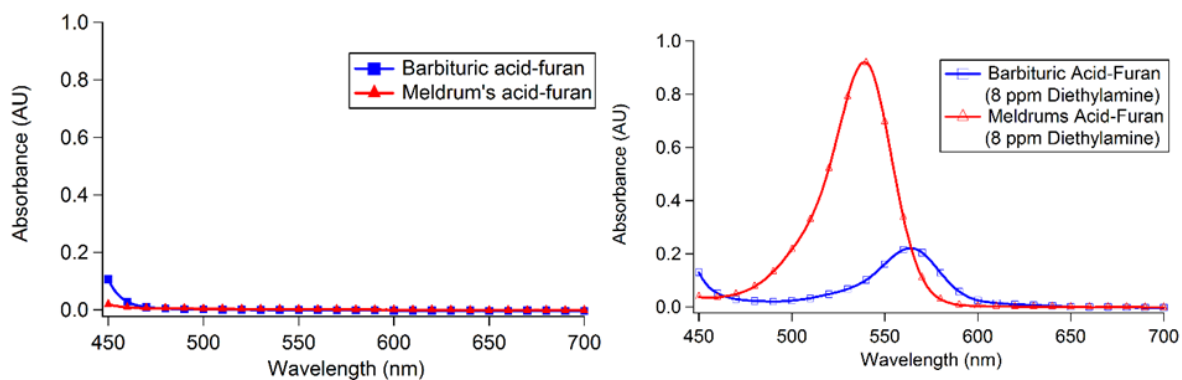


Figure S2.4 UV/Vis absorption of 20 mM solutions in THF of activated furans **a)** before addition of amine and **b)** 5 min after addition of ~10 ppm diethylamine.

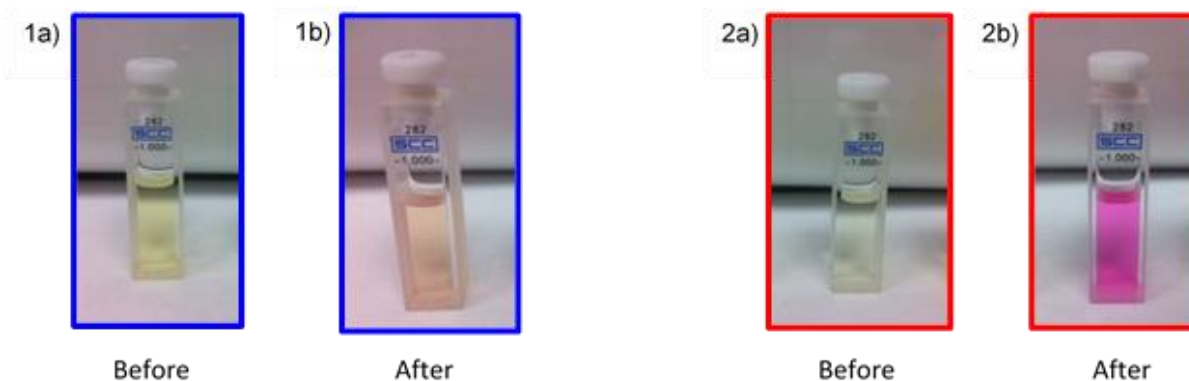


Figure S2.5 Pictorial representation of 20 mM solutions in THF of **1)** barbituric acid activated furan and **2)** Meldrum's acid activated furan **a)** before and **b)** after reaction with ~10 ppm diethylamine for 5 min.

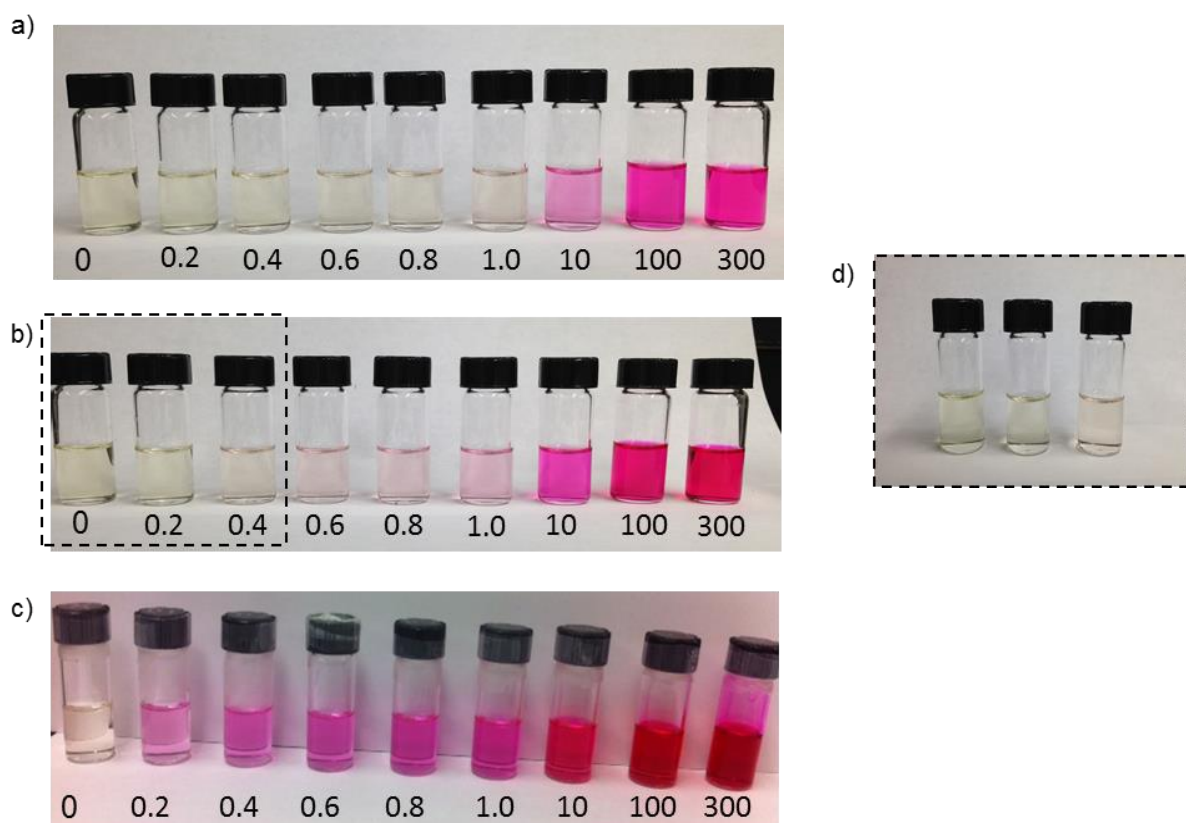


Figure S2.6 Images from reaction with MAF (20 mM THF) and diethylamine after addition of amine at **a)** 5 min **b)** 1 h **c)** 24 h and **d)** expanded image of 0, 0.2, and 0.4 ppm at 1 h after addition of amine. Limit of detection by eye for diethylamine (2° amine) within 1 h is ~0.4 ppm.

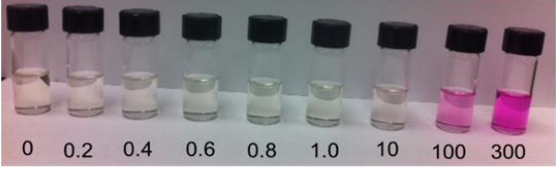
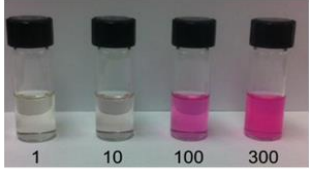
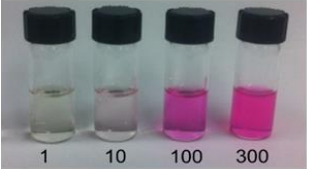
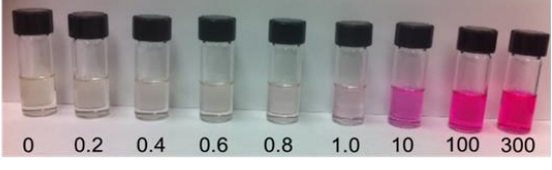
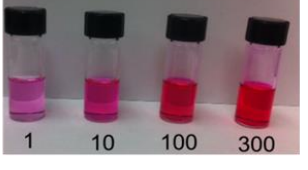
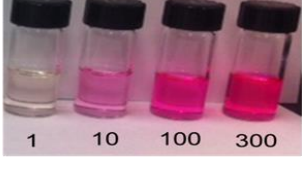
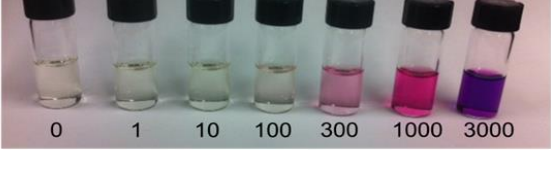
<chem>CCCCN</chem> (1°) Butylamine ppm:	
<chem>CCCCCCN</chem> (1°) Cadaverine ppm:	
<chem>CCCCNC(CCCN)CC</chem> (1° / 2°) Spermidine ppm:	
<chem>CCNCC</chem> (2°) Diethylamine ppm:	
<chem>C1CCNCC1</chem> (2°) Piperidine ppm:	
<chem>CN(C)C</chem> (2°) Dimethylamine ppm:	
<chem>N</chem> Ammonia ppm:	

Figure S2.7a Sensitivity measurements of amines 5 min after reaction with amine

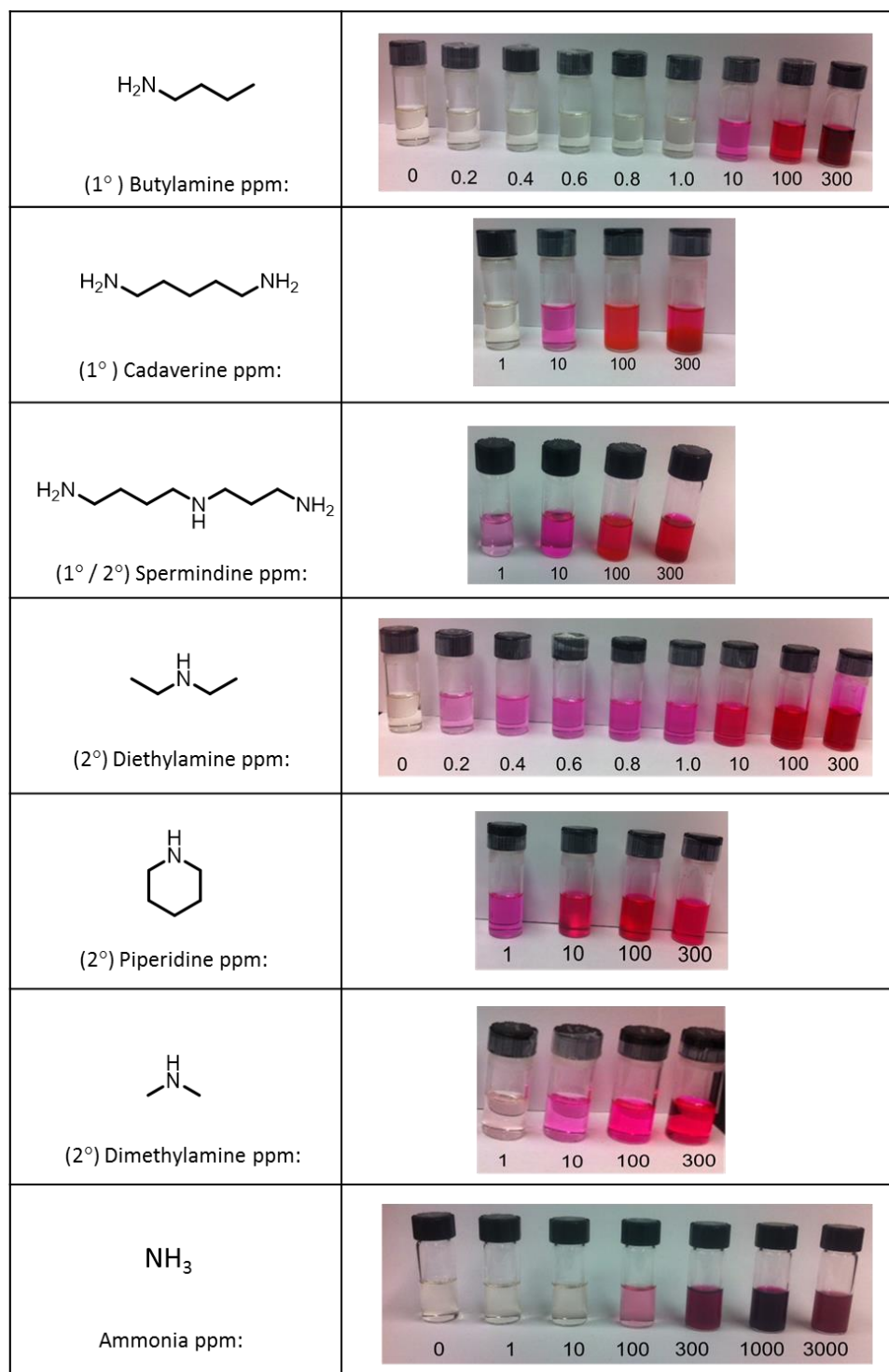


Figure S2.7b Sensitivity measurements of amines 24 h after reaction with amine

2.8.3 Amine sensing on solid supports

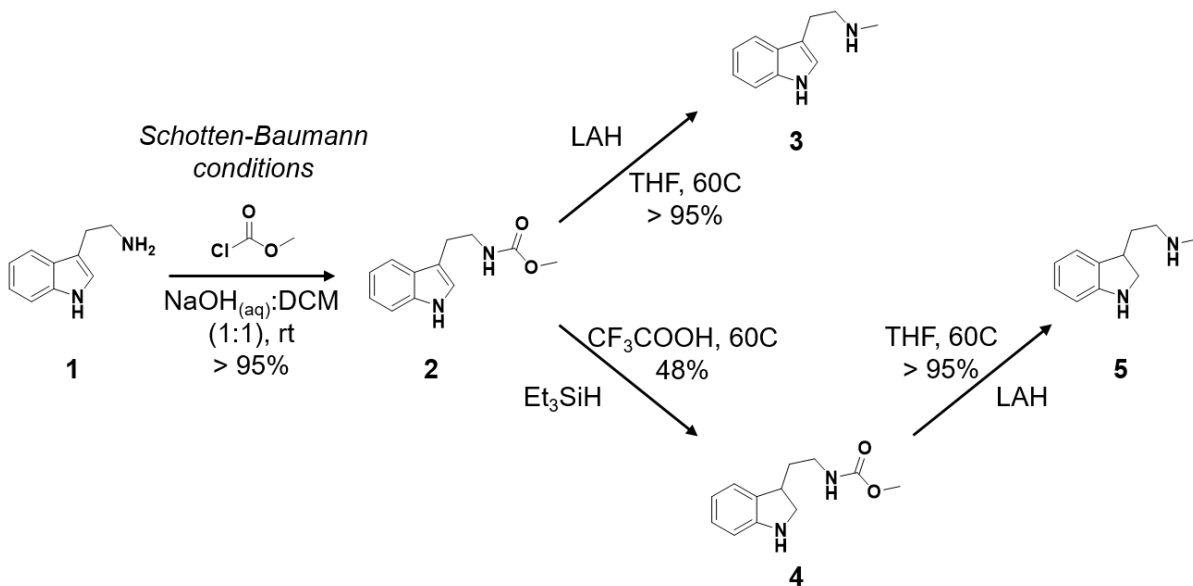


Figure S2.8 Synthetic scheme for tryptamine derivatives to be detected with MAF stain.⁵⁰

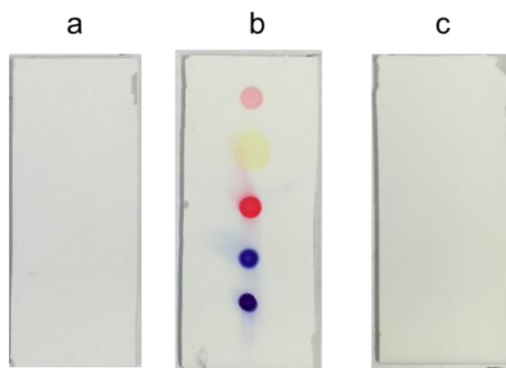


Figure S2.9 Comparison of TLC plates **a)** Spotted with tryptamine derivatives and no MAF stain **b)** Spotted with tryptamine derivatives and coated with MAF stain, < 1 min, room temp **c)** coated with MAF stain, no spots of tryptamine derivatives

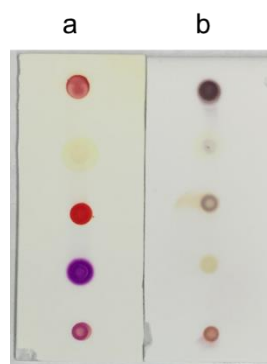
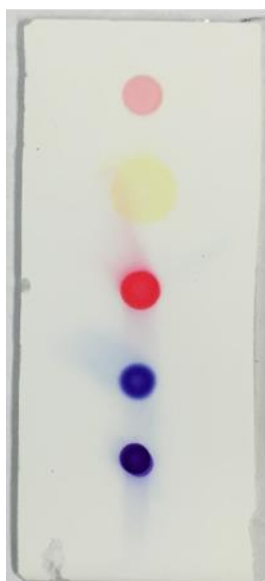


Figure S2.10 Images of stains upon standing for 10 min **a)** Meldrum's activated furan, no heating
b) Ninhydrin, heat







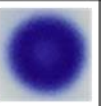
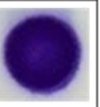




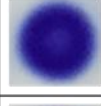
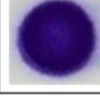
ΔE^*						
		23	22	87	101	98
			34	66	88	85
				84	114	112
					105	104
						8
						

Figure S2.11 ΔE^* values for each TLC spot relative to each other

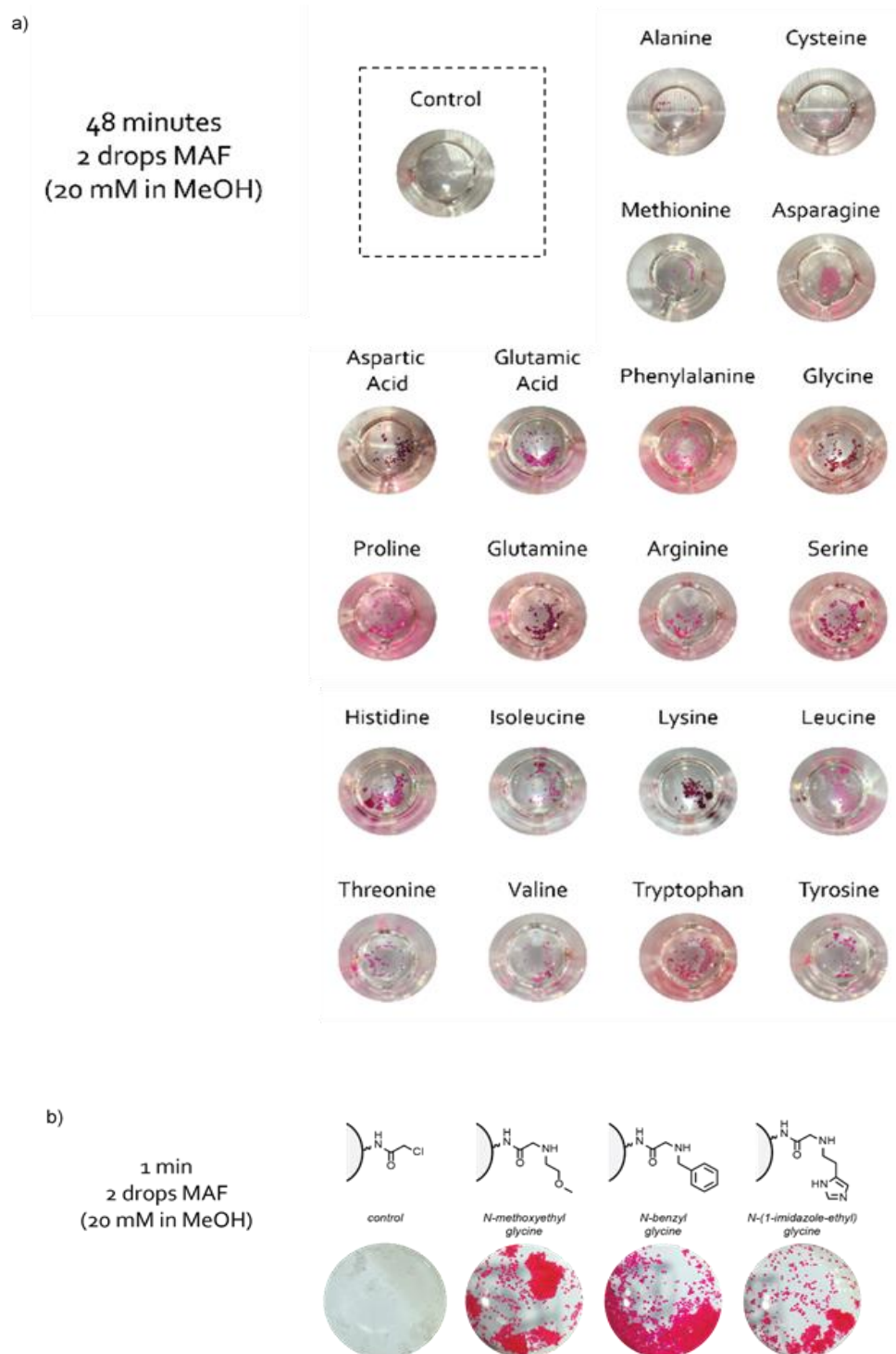


Figure S2.12 Images of **a)** commercial peptide functionalized resins and **b)** N-substituted glycine monomers after reaction with MAF (20 mM methanol).

2.8.4 Set up for food spoilage detection monitoring

Prior to use, the frozen cod and tilapia samples were allowed to thaw at room temperature for 2-3 h. Filter paper substrates for sensing were prepared as stated above with MAF solutions at concentrations of 100 mg/mL (450 μ M), 50 mg/mL (225 μ M), 25 mg/mL (112 μ M), and 12.5 mg/mL (56 μ M). The substrates were attached to a glass jar as seen in **Figure S2.13** and sealed in the presence of the cod and tilapia samples. A third jar, containing no fish, was used as a control. The substrates were monitored over the course of 48 h with time lapse imaging (**Figure S2.13**). Adobe Photoshop was then used to quantify the color of these sensors.

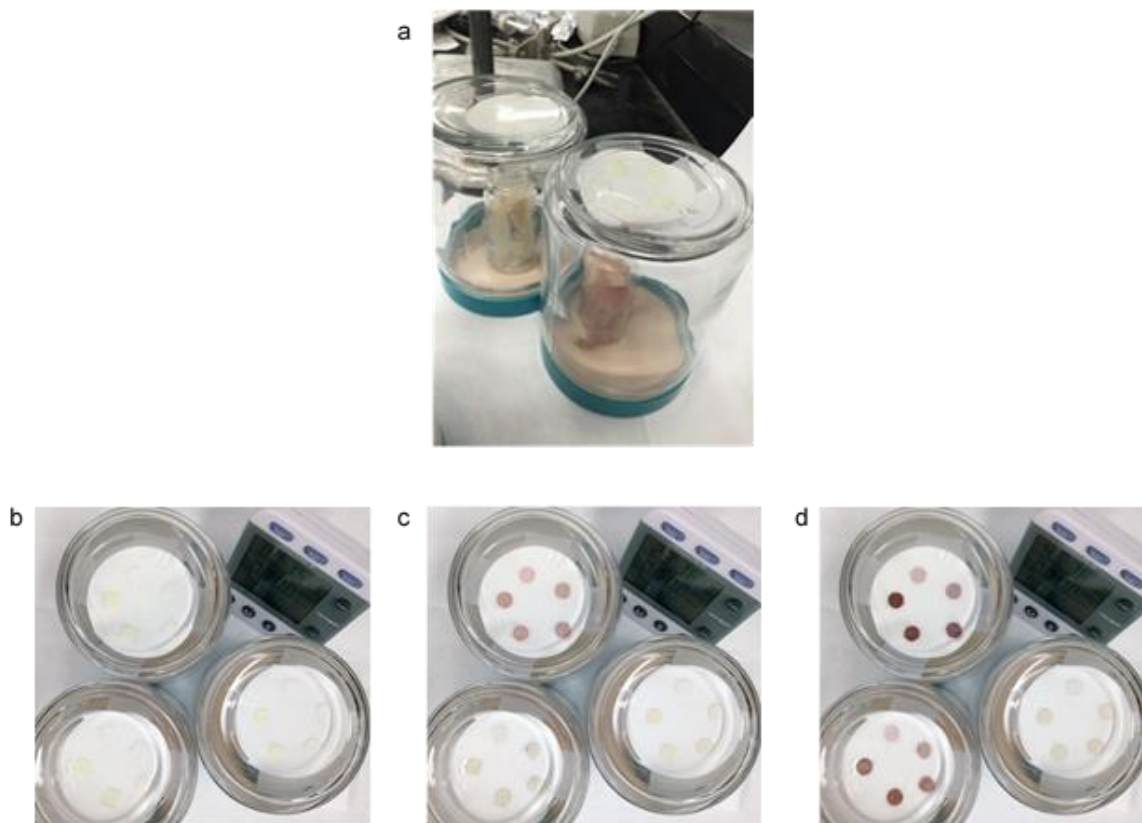


Figure S2.13 a) Experimental set up for food spoilage detection and images of sensors after addition of fish samples at a) $t = 16$ seconds b) $t = 23$ h and c) $t = 46$ h

2.9 References

- 1 F. Gaggini, A. Porcheddu, G. Reginato, M. Rodriguez and M. Taddei, *J. Comb. Chem.*, 2004, **6**, 805–810.
- 2 T. Fan, W. Xu, J. Yao, Z. Jiao, Y. Fu, D. Zhu, Q. He, H. Cao and J. Cheng, *ACS Sens.*, 2016, **1**, 312–317.
- 3 K. E. Secor and T. E. Glass, *Org. Lett.*, 2004, **6**, 3727–3730.
- 4 H. Li, Q. Chen, J. Zhao and Q. Ouyang, *Anal. Methods*, 2014, **6**, 6271–6277.
- 5 U. Khulal, J. Zhao, W. Hu and Q. Chen, *RSC Adv.*, 2016, **6**, 4663–4672.
- 6 B. Kuswandi, Jayus, A. Restyana, A. Abdullah, L. Heng and M. Ahmad, *Food Control*, 2012, **25**, 184–189.
- 7 Y. Hu, X. Ma, Y. Zhang, Y. Che and J. Zhao, *ACS Sens.*, 2016, **1**, 22–25.
- 8 A. Pacquit, K. Lau, H. McLaughlin, J. Frisby, B. Quilty and D. Diamond, *Talanta*, 2006, **69**, 515–520.
- 9 T. Lin, Y. Wu, Z. Li, Z. Song, L. Guo and F. Fu, *Anal. Chem.*, 2016, **88**, 11022–11027.
- 10 X. Sun, Y. Wang and Y. Lei, *Chem. Soc. Rev.*, 2015, **44**, 8019–8061.
- 11 Z. Li and K. S. Suslick, *ACS Sens.*, 2016, **1**, 1330–1335.
- 12 L. Feng, C. J. Musto, J. W. Kemling, S. H. Lim and K. S. Suslick, *Chem. Commun.*, 2010, **46**, 2037–2039.
- 13 S. F. Liu, A. R. Petty, G. T. Sazama and T. M. Swager, *Angew. Chem. Int. Ed.*, 2015, **54**, 6554–6557.

- 14 G. A. Sotzing, J. N. Phend, R. H. Grubbs and N. S. Lewis, *Chem. Mater.*, 2000, **12**, 593–595.
- 15 M. Gao, S. Li, Y. Lin, Y. Geng, X. Ling, L. Wang, A. Qin and B. Z. Tang, *ACS Sens.*, 2015, **1**, 179–184.
- 16 J. Kumpf and U. H. F. Bunz, *Chem. Eur. J.*, 2012, **18**, 8921–8924.
- 17 S. Rochat and T. M. Swager, *Angew. Chem. Int. Ed.*, 2014, **53**, 9792–9796.
- 18 S. Bhadra, C. Narvaez, D. J. Thomson and G. E. Bridges, *Talanta*, 2015, **134**, 718–723.
- 19 P. A. Peixoto, A. Boulangé, M. Ball, B. Naudin, T. Alle, P. Cosette, P. Karuso and X. Franck, *J. Am. Chem. Soc.*, 2014, **136**, 15248–15256.
- 20 G. J. Mohr, C. Demuth and U. E. Spichiger-Keller, *Anal. Chem.*, 1998, **70**, 3868–3873.
- 21 E. Mertz and S. C. Zimmerman, *J. Am. Chem. Soc.*, 2003, **125**, 3424–3425.
- 22 A. R. Longstreet, M. Jo, R. R. Chandler, K. Hanson, N. Zhan, J. J. Hrudka, H. Mattoussi, M. Shatruk and D. T. McQuade, *J. Am. Chem. Soc.*, 2014, **136**, 15493–15496.
- 23 T. Fan, W. Xu, J. Yao, Z. Jiao, Y. Fu, D. Zhu, Q. He, H. Cao and J. Cheng, *ACS Sens.*, 2016, **1**, 312–317.
- 24 H. Li, Q. Chen, J. Zhao and Q. Ouyang, *Anal. Methods*, 2014, **6**, 6271–6277.
- 25 K. L. Bicker, S. L. Wiskur and J. J. Lavigne, in *Chemosensors: Principles, Strategies, and Applications, First Edition*, eds. B. Wang and E. V. Anslyn, John Wiley & Sons, Inc., 1st edn., 2011, pp. 275–295.
- 26 A. T. Hoang, Y. B. Cho, J.-S. Park, Y. Yang and Y. S. Kim, *Sens. Actuators, B*, 2016,

- 230**, 250–259.
- 27 N. A. Rakow, A. Sen, M. C. Janzen, J. B. Ponder and K. S. Suslick, *Angew. Chem. Int. Ed.*, 2005, **44**, 4528–4532.
- 28 A. Rico-Yuste, V. González-Vallejo, E. Benito-Peña, T. De Las Casas Engel, G. Orellana and M. Cruz Moreno-Bondi, *Anal. Chem.*, 2016, **88**, 3959–3966.
- 29 R. Blue, D. G. Uttamchandani and O. Farish, *IEEE Trans. Instrum. Meas.*, 1998, **47**, 964–966.
- 30 S. Helmy, F. A. Leibfarth, S. Oh, J. E. Poelma, C. J. Hawker and J. Read de Alaniz, *J. Am. Chem. Soc.*, 2014, **136**, 8169–8172.
- 31 S. Helmy, S. Oh, F. A. Leibfarth, C. J. Hawker and J. Read De Alaniz, *J. Org. Chem.*, 2014, **79**, 11316–11329.
- 32 J. R. Hemmer, S. O. Poelma, N. Treat, Z. A. Page, N. D. Dolinski, Y. J. Diaz, W. Tomlinson, K. D. Clark, J. P. Hooper, C. Hawker and J. Read De Alaniz, *J. Am. Chem. Soc.*, 2016, **138**, 13960–13966.
- 33 S. Singh, K. Friedel, M. Himmerlich, Y. Lei, G. Schlingloff and A. Schober, *ACS Macro Lett.*, 2015, **4**, 1273–1277.
- 34 A. Balamurugan and H.-I. Lee, *Macromolecules*, 2016, **49**, 2568–2574.
- 35 X. Nicolay and K. Kristbergsson, *Odors in the food industry*, 2006.
- 36 S. Ruhemann, *Trans. Chem. Soc.*, 1910, **97**, 2025–2031.
- 37 F. Pedreschi, J. León, D. Mery and P. Moyano, *Food Res. Int.*, 2006, **39**, 1092–1098.

- 38 K. L. Yam and S. E. Papadakis, *J. Food. Eng.*, 2004, **61**, 137–142.
- 39 R. W. G. Hunt and M. R. Pointer, *Measuring Colour: Fourth Edition*, 2011.
- 40 G. Sharma, W. Wu and E. N. Dalal, *Color. Res. App*, 2005, **30**, 21–30.
- 41 A. R. Robertson, *Color. Res. App*, 1977, **2**, 7–11.
- 42 M. Amblard, J.-A. Fehrentz, J. Martinez and G. Subra, *Mol. Biotechnol.*, 2006, **33**, 239–254.
- 43 E. Kaiser, R. L. Colescott, C. D. Bossinger and P. I. Cook, *Anal. Biochem.*, 1970, **34**, 595–598.
- 44 T. Christensen, *Acta Chem. Scand.*, 1979, **B33**, 763–766.
- 45 S. Claerhout, D. S. Ermolat’ev and E. V. Van Der Eycken, *J. Comb. Chem*, 2008, **10**, 580–585.
- 46 C. Blackburn, *Tetrahedron Lett.*, 2005, **46**, 1405–1409.
- 47 S. J. Yang, X. Z. Tian and I. Shin, *Org. Lett.*, 2009, **11**, 3438–3441.
- 48 A. Pacquit, J. Frisby, D. Diamond, K. T. Lau, A. Farrell, B. Quilty and D. Diamond, *Food Chem.*, 2007, **102**, 466–470.
- 49 M. K. Morsy, K. Zór, N. Kostesha, T. S. Alstrøm, A. Heiskanen, H. El-Tanahi, A. Sharoba, D. Papkovsky, J. Larsen, H. Khalaf, M. H. Jakobsen and J. Emnéus, *Food Control*, 2016, **60**, 346–352.
- 50 M. Righi, F. Topi, S. Bartolucci, A. Bedini, G. Piersanti and G. Spadoni, *J. Org. Chem.*, 2012, **77**, 6351–6357.

51 S. Sands, Delta E: A Key to Understanding Lightfastness Readings,

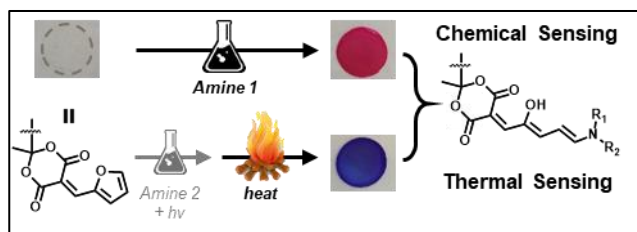
<https://www.justpaint.org/delta-e/>.

CHAPTER 3

STABLE ACTIVATED FURAN AND DASA POLYMER CONJUGATES AS CHEMICAL AND THERMAL SENSORS[‡]

3.1 Abstract

The development and application of novel activated furan copolymers is reported. This platform provides a colorimetric method for sensing amines in



aqueous media through the generation of a highly colored donor-acceptor Stenhouse adduct (DASA). The resulting DASA-polymer conjugates, which are obtained after amine sensing, are characterized to determine fundamental structure-property relationships for this emerging class of negative photochromic species.

[‡] Reproduced with permission from Q. Chen*, Y. J. Diaz*, M. C. Hawker, M. R. Martinez, Z. A. Page, S. X. Zhang, C. J. Hawker and J. Read de Alaniz, *Macromolecules*, **2019**, 52, 4370–4375.
© 2019 American Chemical Society

*These authors contributed equally.

3.2 Introduction

Colorimetric sensors are coveted for their ability to quickly and efficiently respond to different stimuli such as pH, heat, or light with a change in color that is visible to the naked eye.¹⁻⁵ To improve the stability and prevent leaching of such molecular sensors, a number of elegant strategies have been developed, including direct attachment to polymeric backbones.^{1-3,6,7} This strategy of covalent attachment to a polymer support has proven useful in a wide span of applications including the detection of explosives,^{8,9} nerve agents,^{10,11} and heavy metals.^{1,6,12-14} In particular, there has been a growing interest in the chemistry of DASAs due to their ease of preparation, high molar absorptivity, and tailored response to heat or chemical stimuli.^{12,15-17} DASA-based sensors leverage highly colored and thermodynamically stable triene-enol architectures based on amine “donor” and carbon acid “acceptor” end groups (**Figure 3.1**). Due to its chemical and physical properties, various derivatives of DASA have been utilized as photoswitches and colorimetric sensors.¹⁸ This chapter is intended to focus on the new and emerging uses of DASA for colorimetric sensing and the readers are referred to recent publications for a thorough review on its application for photoswitches.¹⁸⁻⁴⁶

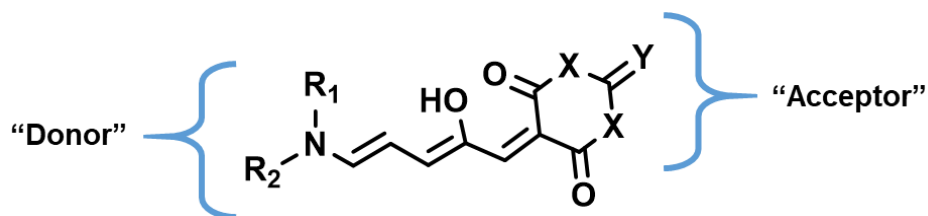


Figure 3.1 General structure for donor-acceptor Stenhouse adduct (DASA)

Prior to the work presented in this chapter, three approaches were developed that take advantage of the highly colored form of DASA as a sensing platform (**Figure 3.2**). The Read de Alaniz group reported a thermally activated “turn-ON” sensor, where a hydroxyl-terminated polybutadiene (HTPB) matrix stabilizes the meta-stable and colorless cyclic derivative until friction from an impact facilitates a thermal transition to the open, colored triene structure (**Figure 3.2a**).¹⁶ Although this approach has been powerful for visualizing high strain-rate events without specialized equipment, it has been limited to HTPB based polymers, which are hydrophobic and rubbery. Such hydrophobic matrix facilitates the reversion from a colorless to colored form for the embedded DASA derivative in the solid state. Additionally, Lee and Wang independently developed a “turn-OFF” (colored to colorless) DASA-based polymer

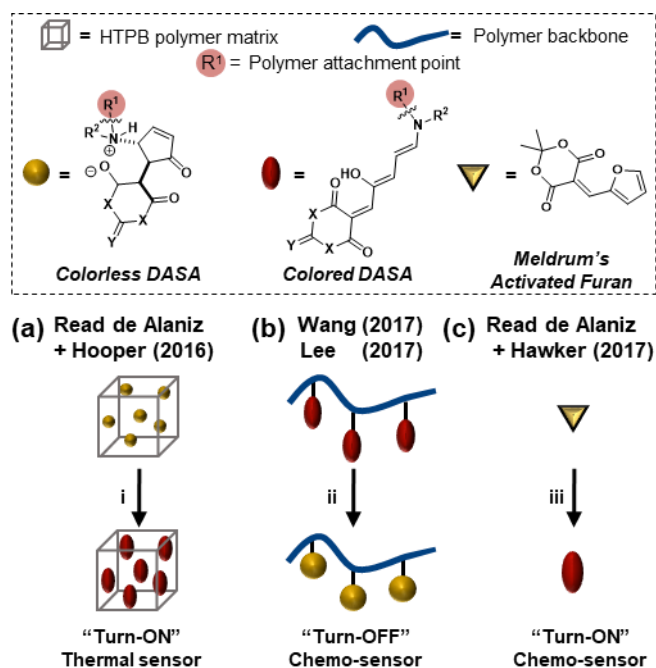


Figure 3.2 a) DASA based thermal sensing examined by our group, b) DASA based “Turn-OFF” chemo-sensors developed by Wang and Lee groups; polymers attached *via* DASA donor and c) “Turn-ON” chemo-sensor, investigated by our group. Reagents and conditions: i) heat *via* high impact event, ii) nerve agent mimics (Lee) and metal ions (Wang), iii) amine.

chemical sensor for nerve agents¹² and metal ions¹⁷ (**Figure 3.2b**). However, a “turn-OFF” color detection limits the sensitivity of these systems, and its non-reversible nature only allows for a single-use. In 2017, the Read de Alaniz and Hawker groups reported an alternative DASA-based sensing platform that allowed for “turn-ON” detection and enabled the sensing of amines (**Figure 3.2c** and **Chapter 2**).¹⁵ In this study, the colorimetric detection of sub-ppm levels of amines could be achieved when the activated furan is physically adsorbed onto a solid support. However, low surface robustness resulted in leaching of DASA molecules into solution and reduced the utility of this approach as an all-purpose sensor.

This chapter describes the development of a versatile and scalable platform for controlling the reactivity and stability of activated furans and DASA groups in aqueous media and their subsequent performance as amine sensors. Key to these advances is the development of an easily tunable polymer matrix that provides efficient access to covalently bound conjugates for fundamental structure-property studies. Significantly, by modulating the polymer glass transition temperature (T_g) reversible switching of DASA isomers can be tuned over a broad range of temperatures, providing access to novel colorimetric thermal sensors using the same platform (**Figure 3.3**).

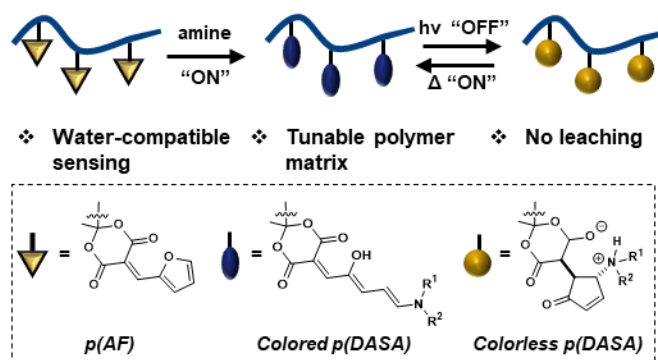
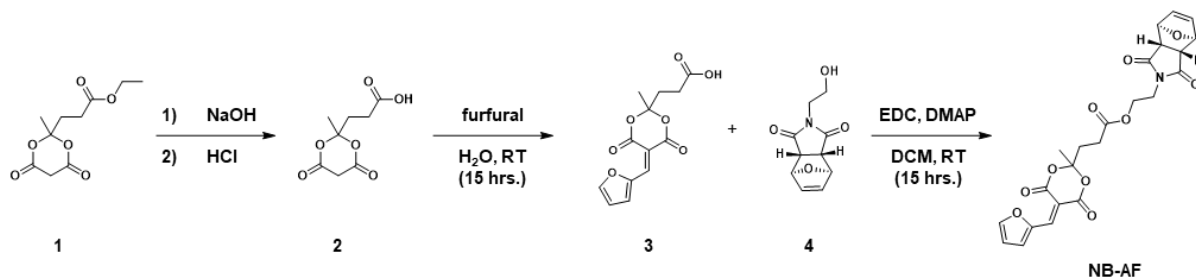


Figure 3.3 A “Turn-ON” chemo and thermal sensor based on activated furan [p(AF)] and DASA [p(DASA)] polymer conjugates.

3.3 Synthesis of Functional Meldrum's Acid Activated Furan



Scheme 3.1 Synthetic scheme for oxa-norbornene Meldrum's acid activated furan monomer (NB-AF)

Initial investigations focused on the synthesis and ring-opening metathesis polymerization (ROMP) of an activated furan monomer (**NB-AF**) that would allow for the facile incorporation of DASA acceptor units along the polymer backbone (**Scheme 3.1**). In examining common acceptors used in the synthesis of DASA adducts, our attention was drawn to activated furans derived from Meldrum's acid (MAF). Although MAF systems were previously found to possess favorable optical properties and response times when used as a sensor (see **Chapter 2**),¹⁵ the lack of functional handle for covalent attachment to a monomer or polymer backbone restricted the utility of these building blocks. To address this limitation, a new carboxylic acid functionalized activated furan, **3**, based on Meldrum's acid was prepared. Synthesis of **1** on a 80+ gram scale employed malonic acid and ethyl levulinate as inexpensive starting materials.^{47,48} Treatment of **1** with sodium hydroxide followed by an acidic workup furnished **2** and finally Knoevenagel condensation with furfural led to the desired activated furan **3** in 85% yield over two steps. Steglich esterification of oxa-norbornene derivative **4** with the activated furan **3** then produced a Meldrum's acid activated furan monomer (**NB-AF**). Importantly, carboxylic acid **3** and **NB-AF** were stable and could be stored at room

temperature under ambient conditions with no observable degradation or instability over extended periods (> 1 year) (**Figure S3.14 and S3.15**).

3.4 Early Studies – Activated Furan Polymerization Compatibility

Two methods of covalent attachment were considered for the incorporation of **NB-AF** to a polymer backbone: a) direct polymerization, which provides a more straightforward synthetic route to functional polymers with control over molecular weight, composition, and architecture⁴⁹ and b) post-polymerization functionalization, which is an attractive alternative for functional groups that are incompatible with polymerization techniques (**Figure 3.4**).^{50,51} For instance, early studies by Dr. Zachariah A. Page and Mr. Michael R. Martinez from the Hawker group revealed that a DASA monomer was incompatible with free radical

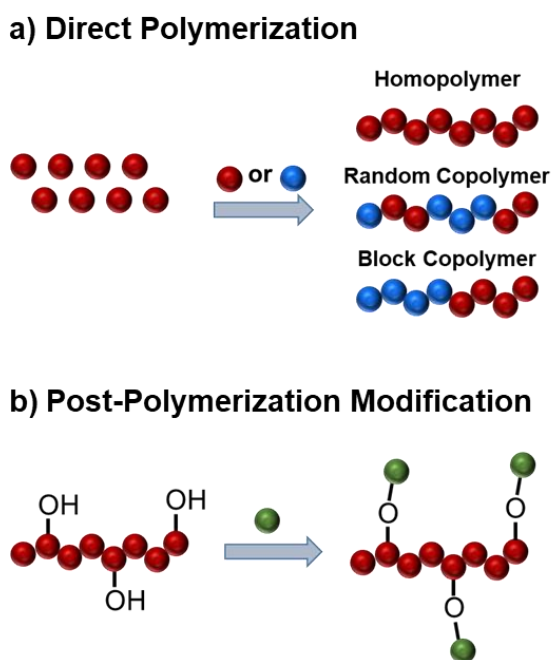


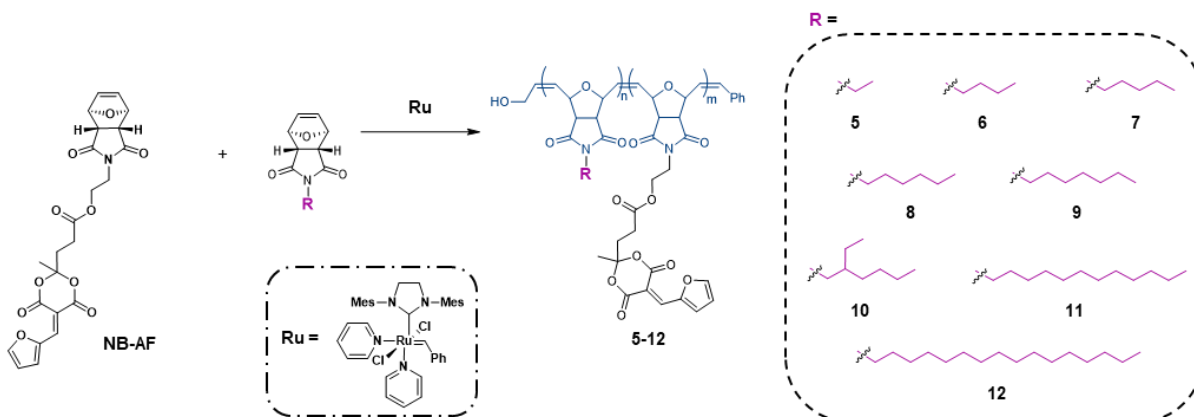
Figure 3.4 Schematic representation of methods for polymer functionalization. **a)** Direct polymerization of functional groups giving good control over polymer architecture, molecular weight, and dispersity and **b)** modification of an existing pendant group, here showing one example of hydroxyl pendent transformation to alternative functional group.

polymerization conditions, where the triene backbone of DASA quickly decomposed in the presence of free radicals. Similar assessments to the compatibility of the activated furan to free radical conditions also resulted in decomposition. However, with the oxa-norbornene **NB-AF** in hand, subsequent attempts at direct polymerization revealed that ROMP could be utilized to produce well-controlled activated furan polymers.

3.5 Creating a Highly Tunable Sensor *via* Ring Opening Metathesis

Polymerization

The ROMP utilizing bispyridine ruthenium (Grubbs) initiator⁵² with oxa-norbornene monomers of various alkyl chain lengths was investigated (**Scheme 3.2**). The simplicity of this process coupled with the availability of **NB-AF** allows for a range of activated furan-based polymers to be prepared on gram scale. All polymers (**5-12**) were prepared based on an activated furan monomer incorporation of ~ 30 mol%. Significantly, ¹H NMR spectroscopy revealed a product ratio of 7:3, in agreement with the feed ratio. Additionally, size exclusion chromatography (SEC) in chloroform revealed polystyrene equivalent molecular weights of ~28 kg mol⁻¹ with narrow distributions ($\mathcal{D} = 1.10$). Differential scanning calorimetry (DSC) of the various compositions further reveals a systematic decrease in T_g , with increased length of the side chain. For example, copolymers prepared with butyl (**6**), hexyl (**8**), and octyl (**10**) oxa-norbornene comonomers possessed decreasing T_g s of 104 °C, 83 °C, and 72 °C, respectively (See **Section 3.12.4**). The well-defined and tunable nature of the copolymers prepared, illustrate the controlled nature of the polymerization and the compatibility of the DASA-based acceptor **NB-AF** for ROMP procedures.



Scheme 3.2 Ring-opening metathesis copolymerization of NB-AF with oxa-norbornene derivatives of different chain lengths to produce polymeric activated furans (5-12). Ru = bispyridine ruthenium (Grubbs) initiator⁵².

3.6 Facilitating Use of DASA Dyes for Sensors in Aqueous Media

The detection of amine-containing compounds is attractive for various industrial and research applications including chemical synthesis⁵³ and environmental monitoring.^{8,54–62} In particular, applications such as food spoilage and on-site water contamination benefit from the use of water as a “green” solvent for sensing.^{63–69} To date, the degradation and spontaneous cyclization of the colored, triene form of DASA adducts in water has limited their utility as aqueous sensors, while the inability to covalently attach the activated furan to solid supports has led to unacceptable levels of leaching.¹⁸ To demonstrate the utility of these activated furan polymers as a broad platform for sensing, a spin coated film of **12** was prepared on a pre-cleaned cover glass slip to produce a transparent film (~1 μm). Note that alternative polymers **5-11** produced similar films (**Section 3.12.1**). The thin film was then dipped into a solution of diethylamine (300 ppm in water) and a vibrant pink color, characteristic of the triene-enol form of DASA was observed (3 min at 75 °C, **Figure 3.5a**). It should be noted that at temperatures

lower than 75 °C, detection still proceeded albeit at a slower rate. Of particular note, the highly colored form of DASA did not show signs of discoloration or leaching into the aqueous solution, in stark contrast to non-covalently attached analogs (**Figure 3.5b**).¹⁸ The stability of this open form of DASA in water clearly demonstrates the importance of covalently attaching the activated furan moiety to the polymer backbone.

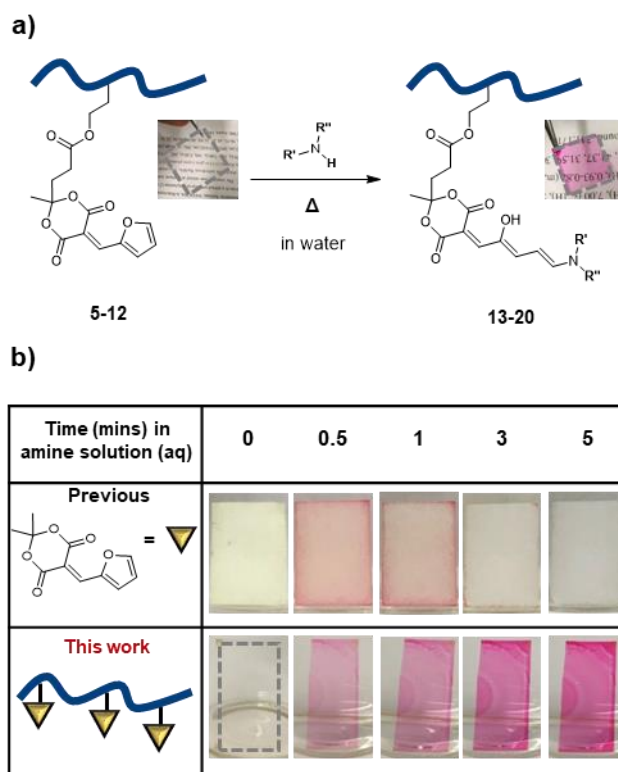


Figure 3.5 a) General reaction for polymeric activated furan detection of amines. Poly (oxa-norbornene activated furan) (**5-12**) reacts with amine to form the colored polymeric DASA (**13-20**). Inset: Photograph of thin films of the polymeric activated furan **12** (left) and 3 min after exposure to diethylamine in water (300 ppm, 75 °C, right). **b)** Representative stability of amine sensor films over time after exposure to diethylamine in water (300 ppm). The polymeric activated furan presented in this dissertation provides improved stability over their non-covalently bound counterparts.

3.7 Sensitivity of Polymeric Activated Furan for Amine Detection

To evaluate the sensitivity of our sensor toward aqueous amine solutions, films of activated furan polymer **11** were exposed to known concentrations of four representative amine solutions: a secondary alkyl amine (diethylamine), primary alkyl amine (*n*-butylamine), secondary aryl amine (indoline), and primary aryl amine (*p*-methoxyaniline). Polymer films were first dipped into aqueous solutions of each amine (10 – 300 ppm) at 75 °C. After 3 min,

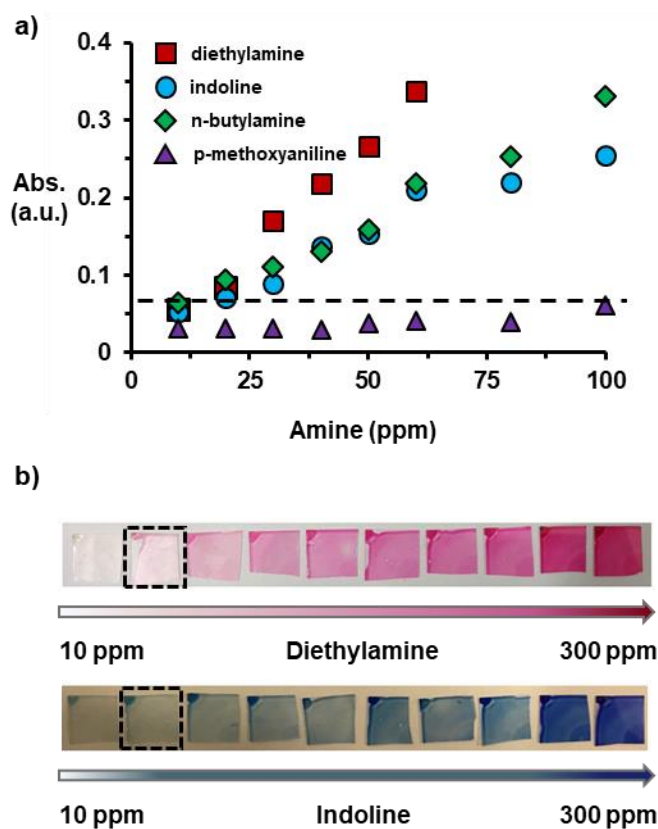


Figure 3.6 a) Expanded view of UV-vis absorption response for polymer film **11** to aqueous amine solutions (10 – 100 ppm, 75 °C for 3 min) where dotted line outlines limit of detection (LOD) and **b)** images of corresponding thin films after exposure to aqueous solutions of diethylamine and indoline between 10 – 300 ppm (75 °C for 3 min) where dotted boxes display LOD. See Section 3.12.6 for images of thin films for alternative amines and for full absorbance spectra. LOD for diethylamine, indoline, *n*-butylamine, and *p*-methoxyaniline were found to be 20 ppm, 10 ppm, 20 ppm, and 100 ppm respectively.

the films were removed from the solution and the absorbance of each film was measured *via* UV-vis spectroscopy (**Figure 3.6**). The limit of detection for aqueous solutions of diethylamine, *n*-butylamine, indoline, and *p*-methoxyaniline were found to be 20 ppm, 10 ppm, 20 ppm, and 100 ppm respectively. For images of films exposed to a range of primary and secondary alkyl and aryl amines see **Figure S3.7- S3.12**. This facile introduction of DASA-based acceptor units to solid supports/polymer films not only enables the “turn-ON” detection of amines in water, but also creates a nanoenvironment that allows for the intriguing possibility of using DASA photoswitches in water.

3.8 Influence of Glass Transition Temperature (T_g)

To evaluate the effect of the polymer T_g on the response time and sensitivity of this system, UV-vis absorption spectroscopy was used to monitor the color change of thin films upon exposure to aqueous solutions containing ppm levels of diethylamine. Individual spin cast films of activated furan polymers **6-12** were therefore prepared (see **Section 3.12.1**) and exposed to solutions of diethylamine in water (50 ppm at 50 °C) with the absorbance of each film ($\lambda_{\text{max}} = 540$ nm) being determined after 30 min. A direct correlation between the T_g of the polymer and the response/sensitivity of the film was observed (**Figure 3.7a**). This trend may be due to the increasing flexibility of the polymer matrix that allows for the conversion of the activated furan into the highly colored DASA form (**13-20**). To support this observation, the change in sensitivity of the thin films to diethylamine was probed at temperatures above and below the T_g of the polymer matrix. Films of polymer **12** ($T_g = 72$ °C) were first dipped into aqueous solutions of diethylamine (50 ppm) at temperatures between 0 °C and 90 °C. After 3

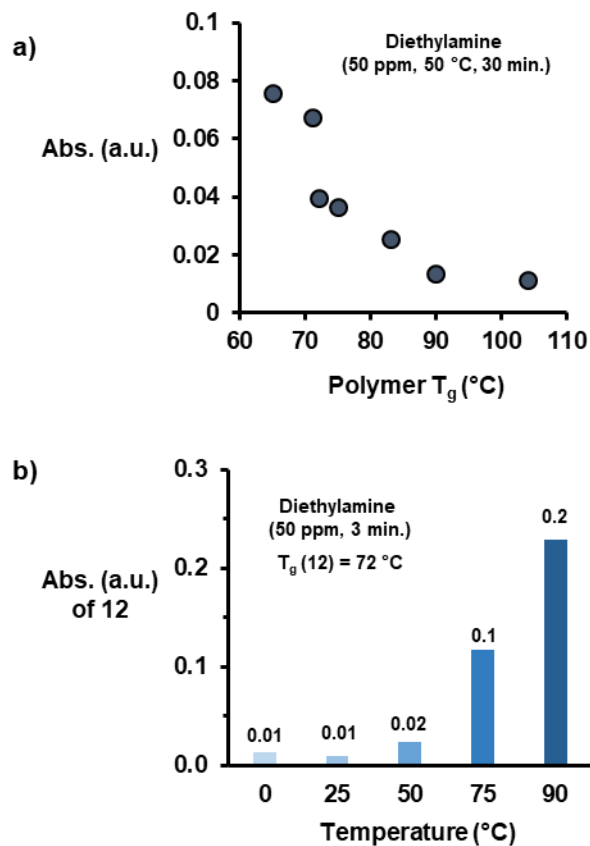


Figure 3.7 a) Reaction of polymer films (6-12) with aqueous diethylamine solution (50 ppm, 50 °C, 30 min) compared to the corresponding T_g of the polymer matrix and **b)** reaction of polymeric activated furan film 12 with aqueous solution of diethylamine (50 ppm, 3 min) at varying temperatures. An absorbance value ≥ 0.1 a.u. can be visible by the naked eye.

min, the absorbance of the films ($\lambda_{\max} = 540$ nm) were determined by UV-vis spectroscopy (**Figure 3.7b**). At temperatures below the T_g , the change in absorbance with 3 min of amine exposure is negligible. However, at temperatures above the polymer's T_g , a rapid increase in absorbance was observed on exposure to aqueous solutions containing 50 ppm of diethylamine. These studies highlight the sensitivity and versatility of this polymeric platform coupled with the ability to tune the properties of activated furan-based polymers to enable detection over defined temperature ranges.

3.9 Polymeric Activated Furan as a Thermal Sensor

The ability to efficiently tune the response as a function of T_g encouraged us to evaluate this platform as a thermal sensor. Temperature sensing is pertinent to a multitude of applications spanning body temperature regulators to explosive testing.⁶ Previous work published from the Read de Alaniz group demonstrated that 2nd generation DASA adducts can reversibly switch in a polymer matrix. In this example, light was used to convert the highly colored DASA form into the colorless, compact form, followed by heating to recover the highly colored form. Notably, glass transition temperature played an important role in the conversion rates, especially for the thermal recovery.³⁶ Exploration into the photoswitching capabilities of a DASA compound covalently bounded to a poly(oxa-norbornene) backbone revealed similar results (**Figure 3.8**).

Encouraged by these observations, we envisioned that the ability to tune the T_g of these ROMP-based activated furan polymers could be leveraged for thermal sensing applications. To investigate the utility of these materials as DASA based thermal sensors, polymer films **7**, **8**, **9**, and **11** were first exposed to indoline to obtain a range of 2nd generation, highly colored triene adducts (denoted **15**, **16**, **17**, and **19** respectively). Specifically, reaction with this secondary aryl amine resulted in thin films with the characteristic blue color of 2nd generation systems (see **Section 3.12.5**). Upon irradiation, a near colorless film is obtained indicating the transformation of the DASA triene to the colorless cyclopentenone form (**Figure 3.9b**, labeled “initial”). Importantly, these colorless films were stable at lower temperatures (0 °C) for one month, in contrast to previously reported DASA-polymer conjugates.^{12,17,31,32,36} To test these ROMP-based DASA polymers as thermal sensors, each film was slowly heated from 50 to

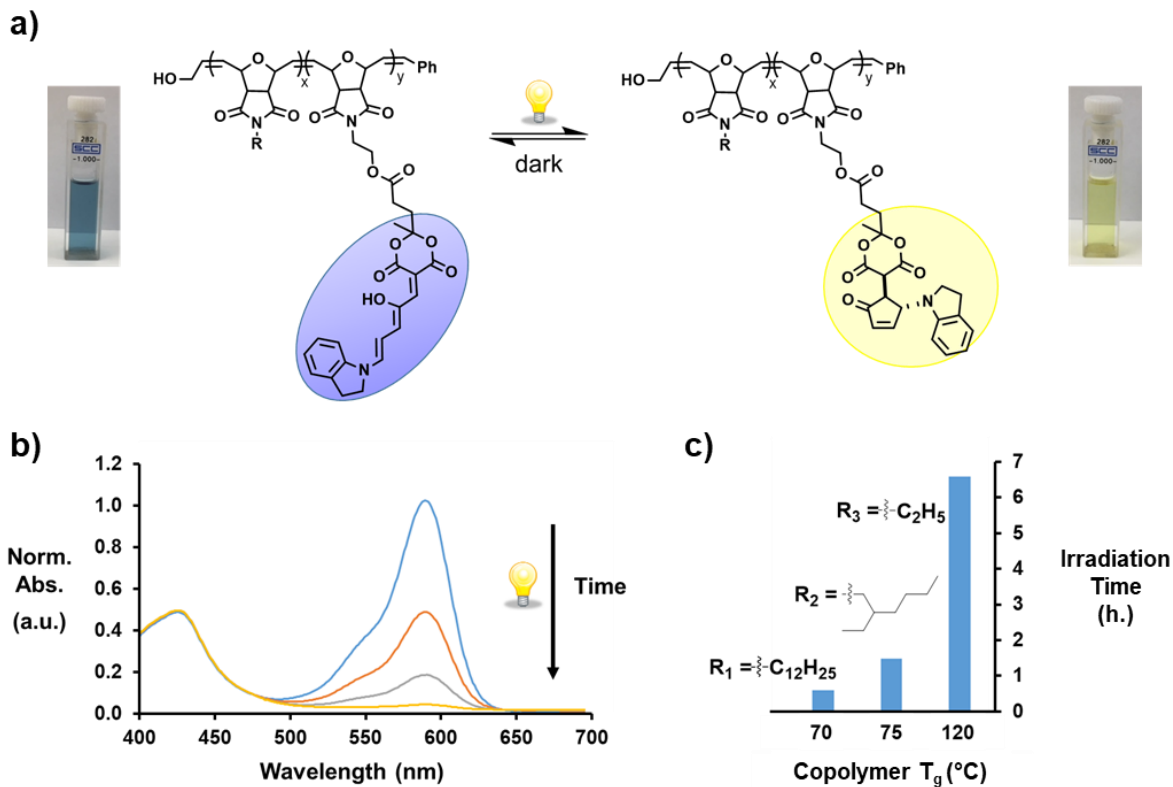


Figure 3.8 a) Reaction scheme for photoswitching of a poly(oxa-norbornene) with pendant DASA compounds. When irradiated with light the polymer solution turns from blue to yellow. This is reversible upon introduction of heat to the solution. **b)** UV-vis spectra denoting the change in λ_{max} for the polymer solution over time upon irradiation with light. **c)** As the polymer T_g increases, a longer period of irradiation is required for complete photoswitching.

100 °C (5 °C increments with holds for 3 min) followed by image analysis. To quantify the color difference between each film at various temperatures, ΔE^* values were determined following International Commission on Illumination guidelines as previously described (**Figure 3.9a**).¹⁵ Significantly, polymers with lower T_g s underwent isomerization from the colorless cyclopentenone to the colored triene at lower temperatures than their higher T_g counterparts, where a ΔE^* value = 20 was used as a benchmark value that indicates visual detection by eye is possible. For example, DASA films based on polymers **15**, **16**, **17**, and **19**

(possessing decreasing T_g values of 90, 83, 75, and 65 °C respectively) required corresponding temperatures of 85, 80, 75, and 70 °C to reach ΔE^* values = 20 (**Figure 3.9**, highlighted in blue). These results confirm the potential of the DASA films for use as stable and convenient thermal sensors with small differences (≥ 5 °C) in temperature exposure being detectable by the naked eye.

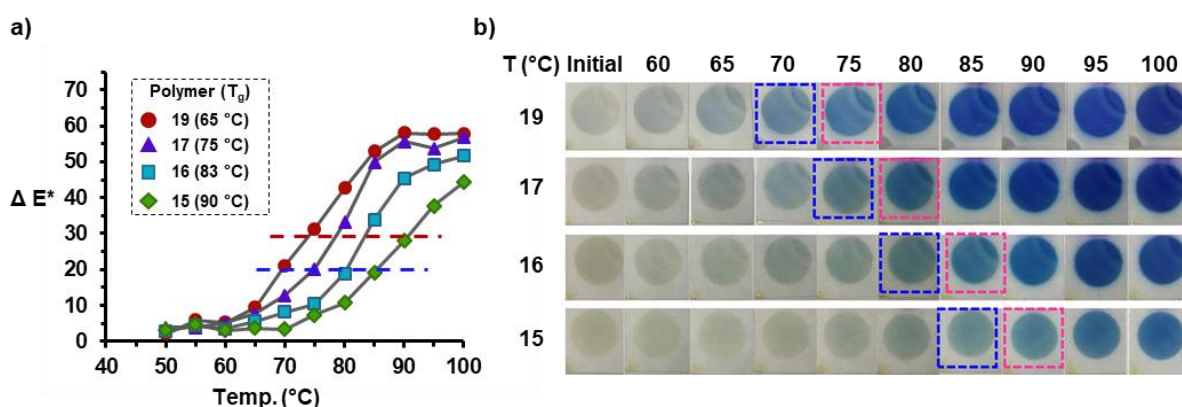


Figure 3.9 a) Visual responses of bleached polymeric DASA films **15**, **16**, **17**, and **19** to slow increase in temperatures (1.5 °C per min) and b) Images for corresponding films after exposure to different temperatures. Blue (bottom and left) and red (top and right) dotted lines indicate polymer films at ΔE^* values = 20 and 30 respectively.

3.10 Conclusion

Activated furan based poly(oxa-norbornene)s were prepared by ROMP copolymerization and found to have significant utility as amine and thermal sensors through facile formation of donor-acceptor Stenhouse adducts. In addition, the covalent bonding to poly(oxa-norbornene) backbones permits the first example of water-compatible sensing with DASA dyes. By tailoring the comonomer, the photo/thermal reversibility of the DASA isomers

could be tuned and maintained in the polymer matrix, which was exploited for use in thermal sensing. Future mechanistic studies into the relationship between amine structure, polymer T_g , and sensor reactivity will provide an expanded insight into the structure/property link in activated furan and DASA polymeric systems. Additionally further development of this platform as a general use sensor and as a polymeric photoswitch is currently being investigated.

3.11 Experimental

3.11.1 Materials and equipment

All commercial chemicals were obtained from *Sigma Aldrich*, *TCI Europe* or *Fisher Scientific* and, unless otherwise noted, all reagents were used as received without further purification. All polymers solutions were filtered through a 0.45 μm TEFLON SYR FILTER before spin coating.

^1H NMR and ^{13}C NMR spectra were recorded on Varian spectrometers (600 MHz) and Varian spectrometers (150 MHz), respectively and were reported in ppm and determined with residual signals of the deuterated solvents (TMS, 0.00; CDCl_3 , 7.26; $\text{DMSO-}d_6$, 2.50 for ^1H NMR and CDCl_3 , 77.0; $\text{DMSO-}d_6$, 39.5 for ^{13}C NMR). Differential scanning calorimetry measurements were carried out using Q2000 DSC V24.11 instrument from 30 $^\circ\text{C}$ to 150 $^\circ\text{C}$ at a heating rate of 20 $^\circ\text{C}/\text{min}$ and a cooling rate of 20 $^\circ\text{C}/\text{min}$ under an N_2 flow of 50 mL/min. The GC-HRMS and ESI-HRMS analysis were performed on a Waters GCT Premier high resolution time-of-flight mass spectrometer. The UV-vis absorption spectra of solution and transparent polymer films were measured on an Agilent Technologies G1103A UV-vis spectrophotometer. Size exclusion chromatography was performed at ambient temperature

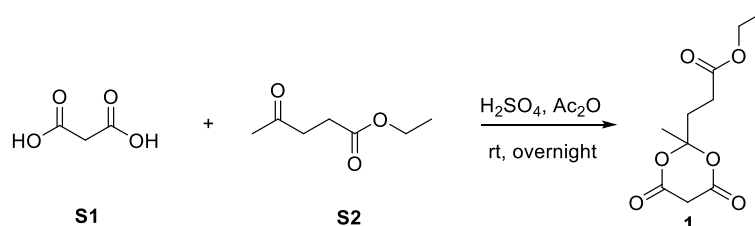
using chloroform with 0.25% triethylamine as the mobile phase in a Waters 2695 separation module with a Waters 2414 refractive index detector. The hydroxy grown on cover glass used for spin-coating was grown by PSDP-UVT Pro Novascan Ozone Cleanser. Polymer film was prepared by spin-coating on a WS-400-6NPP-LITE Spin Processor. The film thickness of polymer film was measured by a Bruker DektakXT Stylus Profilometer.

3.11.2 Quantification of color from images

Description of protocol for quantification of color from images can be found in Section 2.7.4.

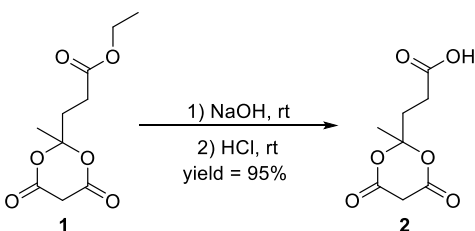
3.11.3 Synthesis and characterization of monomers and polymers

Synthesis of oxa-norbornene activated furan monomer (NB-AF)



Ethyl 3-(2-methyl-4,6-dioxo-1,3-dioxan-2-yl)propanoate (1):^{47,48} Concentrated sulfuric acid (1ml) was added dropwise to a stirring mixture of malonic acid **S1** (18.7 g, 180 mmol) and acetic anhydride (25.6 g, 24.15 ml, 251 mmol) in a 250 mL Erlenmeyer flask. To this, ethyl levulinate **S2** (28.9 g, 28.44 ml, 200 mmol) was added dropwise at room temperature. This was then stirred at room temperature ~ 15 h. To this, a 10% brine: ethyl acetate mixture (100 ml) was added. The organic layer was then separated, washed (2 × 50 ml) with brine, and dried over magnesium sulfate. The combined organic layers were then concentrated *via* rotary

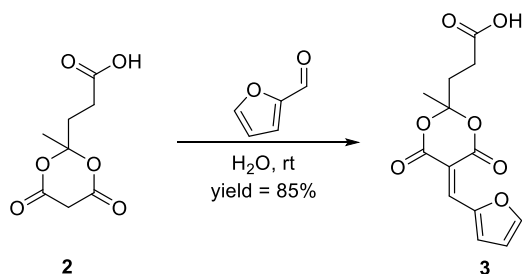
evaporation until a thick yellow/orange product is observed. The resulting oil can then be crystallized from a 1:3 mixture of ethanol and water to give the desired ester functionalized Meldrum's acid **1** as a light yellow solid (32 - 40% yield). ^1H NMR (600 MHz, CDCl_3) δ 4.15 (q, $J = 7.1$ Hz, 2 H), 3.75 (d, $J = 20.6$ Hz, 1H), 3.61 (d, $J = 20.6$ Hz, 1H), 2.52 (t, $J = 7.3$ Hz, 2 H), 2.34 (t, $J = 7.3$ Hz, 2 H) 1.75 (s, 3H), 1.26 (t, $J = 7.1$ Hz, 3 H)) ppm; ^{13}C NMR (150 MHz, CDCl_3) δ 172.0, 162.5, 106.8, 61.1, 36.4, 35.0, 28.1, 25.9, 14.1 ppm; HRMS (ES+) Exact mass cald. for $\text{C}_{10}\text{H}_{14}\text{O}_6$ $[\text{M}-\text{H}]^-$: 229.0713, found: 229.0718.



3-(2-methyl-4,6-dioxo-1,3-dioxan-2-yl)propanoic acid (2): 1 M NaOH (aq, 25 mL) was added to **1** (18.1 g, 78.6 mmol) in an Erlenmeyer flask. The pH of the solution was found to be ~ 6 with pH paper. To this suspension liquid, 18.5 mL of 6 M NaOH (aq) was added dropwise. As the solid begins to dissolve, pH is increased to 12 \sim 14. Additional 6 M NaOH was stirred into the mixture until all solid was dissolved and solution maintained a pH of 12-14. This was then stirred for ~ 30 min assuring that pH was maintained at $\sim 12-14$. Then 3 M HCl (aq) was added slowly to achieve a pH $\sim 2-3$ during which time product was precipitated as a white solid. Crude product was collected *via* vacuum filtration and rinsed with 1 M HCl (aq) x 3, followed by a single rinse with DI water. The product was collected as a white solid with a little viscosity (15.0 g, 95%). ^1H NMR (600 MHz, DMSO) δ 12.28 (s, 1 H), 4.20 (d, $J = 20.5$ Hz, 1 H), 3.82 (d, $J = 20.5$ Hz, 1 H), 2.38 (t, $J = 7.7$ Hz, 2 H), 2.20 (t, $J = 7.7$ Hz, 2 H), 1.70 (s, 3 H) ppm; ^{13}C

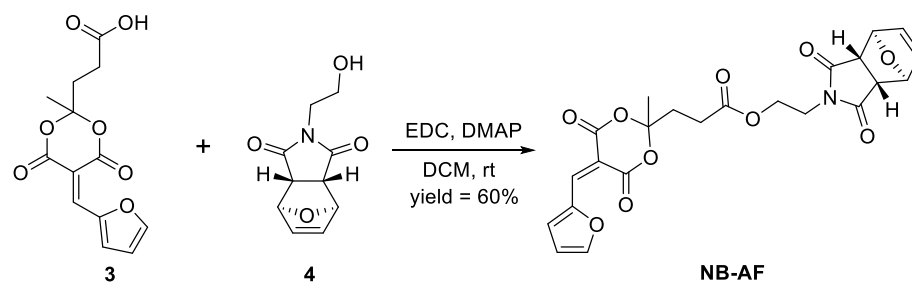
NMR (150 MHz, DMSO) δ 173.8, 164.3, 106.9, 37.2, 35.0, 28.2, 25.6 ppm; HRMS (ES+)

Exact mass calcd. for $C_8H_{10}O_6$ [M-H]⁻: 201.0405, found: 201.0410.



3-(5-(furan-2-ylmethylene)-2-methyl-4,6-dioxo-1,3-dioxan-2-yl)propanoic acid (3):

Meldrum's carboxylic acid **2** (10 g, 42 mmol) was suspended in water (900 mL). To this, distilled furfural (5.3 g, 47 mmol) was added dropwise. Mixture turned yellow instantly. This was then left to stir ~15 h and then monitored by TLC (dichloromethane: methanol = 9:1). Once the starting material was consumed, the reaction was filtered to yield a yellow solid. Crude product was washed with water to afford product as a yellow solid. (80 - 90% yield). ¹H NMR (600 MHz, DMSO) δ 12.29 (s, 1 H), 8.32 (s, 1 H), 8.27 (d, *J* = 3.8 Hz, 1 H), 8.12 (s, 1 H), 6.95 (m, 1 H), 2.42 (t, *J* = 7.2 Hz, 2 H), 2.22 (t, *J* = 7.2 Hz, 2 H), 1.69 (s, 3 H) ppm; ¹³C NMR (150 MHz, DMSO) δ 173.2, 162.3, 159.4, 151.9, 149.3, 139.4, 127.6, 115.5, 107.8, 105.2, 34.5, 27.9, 25.2 ppm; HRMS (ES+) Exact mass calcd. for $C_{13}H_{12}O_7$ [M-H]⁻: 232.0510, found: 279.0495.



2-(1,3-dioxo-1,3,3a,4,7,7a-hexahydro-2H-4,7-epoxyisoindol-2-yl)ethyl 3-(5-(furan-2-ylmethylene)-2-methyl-4,6-dioxo-1,3-dioxan-2-yl)propanoate (NB-AF): **3** (1.79 g, 6.39 mmol) and **4**⁶ (2.0 g, 9.56 mmol) were suspended in dry DCM (70 mL). Then 4-dimethylaminopyridine (DMAP) (47 mg, 0.32 mmol) in DCM (3 mL) was added to the solution which was then cooled to 0 °C. After, a suspension of 1-ethyl-3-(3-dimethylaminopropyl)carbodiimide (EDC) (1.48 g, 9.56 mmol) in dry DCM (20 mL) was added dropwise to the reaction mixture. This solution was brought to room temperature and left to stir ~ 15 h until **3** was consumed and solution slightly brown. This organic solution was then extracted several times with water to remove starting material **4**. Organic layer was then dried over magnesium sulfate and solvent was removed under reduced pressure to obtain a yellow solid. The product was further purified by column chromatography utilizing a mobile phase of ethyl acetate: hexanes (3:1) to yield a solid yellow product (60% yield). ¹H NMR (600 MHz, CDCl₃) δ 8.45 (d, *J* = 3.8 Hz, 1 H), 7.85 (s, 1 H), 6.75 (d, *J* = 3.8 Hz, 1 H), 6.50 (s, 2 H), 5.25 (s, 2 H), 4.24 (t, *J* = 5.2 Hz, 2 H), 3.75 (t, *J* = 5.2 Hz, 2 H), 2.87 (s, 1 H), 2.53 (t, *J* = 8.0 Hz, 2 H), 2.30 (t, *J* = 8.0 Hz, 2 H) ppm; ¹³C NMR (150 MHz, CDCl₃) δ 176.0, 150.5, 150.2, 141.4, 136.5, 136.5, 128.2, 115.3, 105.0, 80.9, 61.0, 47.5, 37.7, 34.9, 28.0, 26.0 ppm; HRMS (ES⁺) Exact mass calcd. for C₂₃H₂₂NO₁₀ [M+Na]⁺: 494.1058, found: 494.1073.

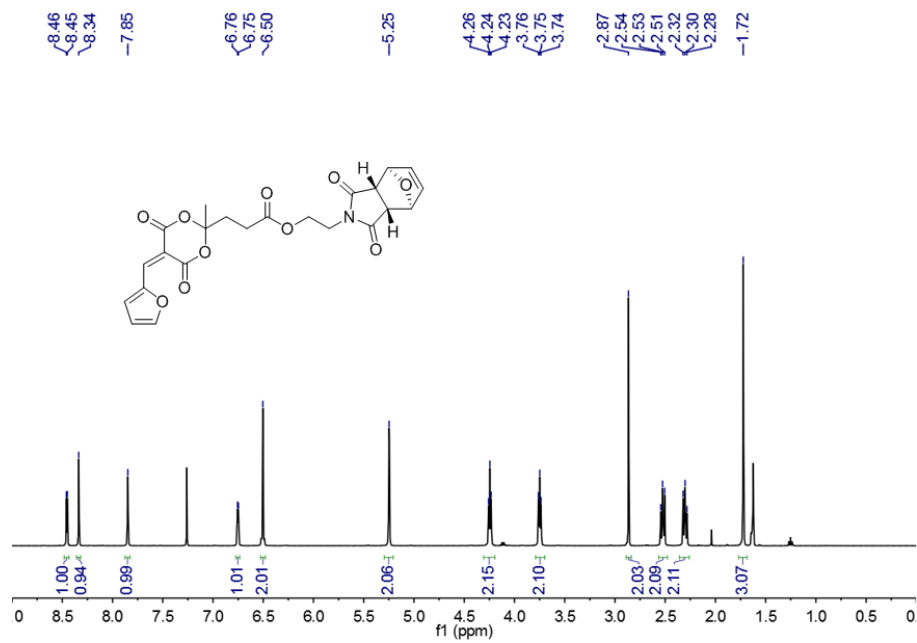


Figure 3.10 ^1H NMR spectra of NB-AF.

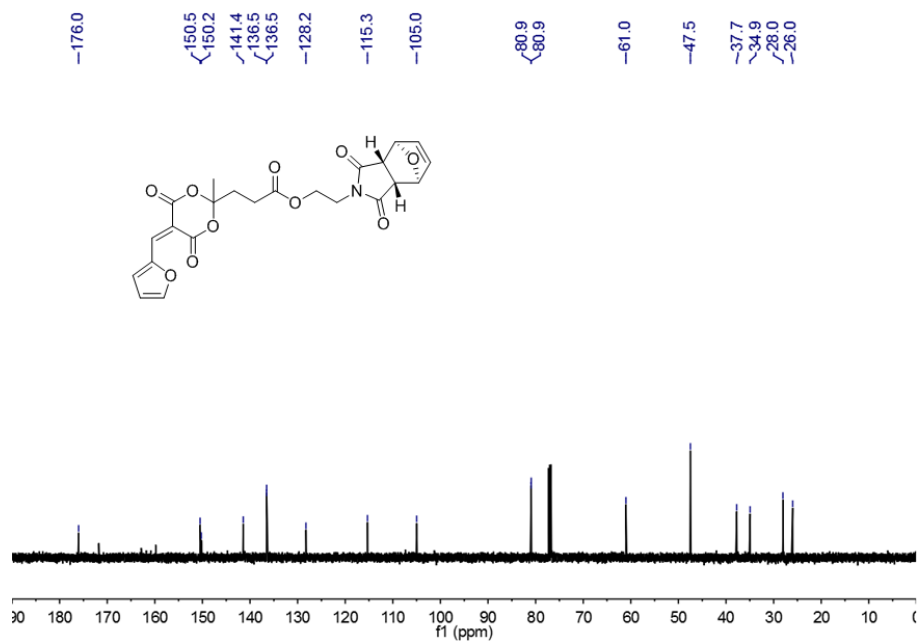
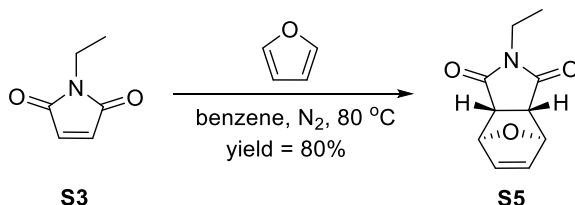


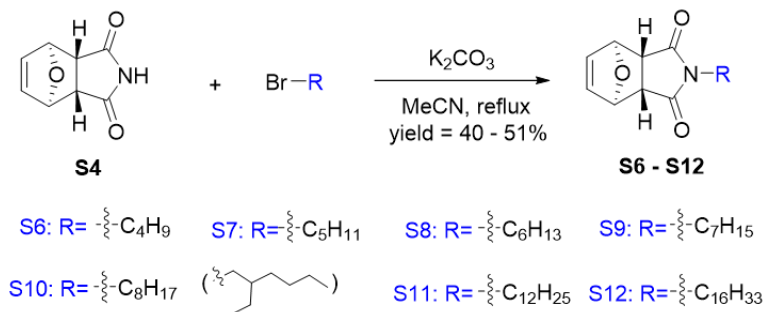
Figure 3.11 ^{13}C NMR spectra of NB-AF.

Synthesis of monomers S5- S12



(3aR,4S,7R,7aS)-2-ethyl-3a,4,7,7a-tetrahydro-1H-4,7-epoxyisoindole-1,3(2H)-dione

(S5)⁷⁰: 1-ethyl-1H-pyrrole-2,5-dione **S3** (2 g, 16 mmol) and furan (10.88 g, 160 mmol) were added to a flame dried 250 mL reaction flask with condenser and stir bar under a N₂ blanket. Toluene (110 mL) was then added to this and the solution was heated to 90 °C in an oil bath. This solution was mixed for ~ 15 h at which point no starting material was observed by ¹H NMR spectroscopy. Solution was then cooled to room temperature and concentrated *via* rotary evaporation to obtain a white solid. Re-crystallization in diethyl ether (100 mL) at -20 °C, followed by vacuum filtration yields the product as a light yellow solid (2.47 g, 80%). ¹H NMR (400 MHz, CDCl₃) δ 6.51 (s, 2 H), 5.27 (s, 2 H), 3.53 (q, *J* = 7.2 Hz, 3 H), 2.83 (s, 2 H), 1.16 (t, *J* = 7.2 Hz, 2 H) ppm; ¹³C NMR (100 MHz, CDCl₃) δ 176.0, 136.5, 80.9, 47.4, 33.9, 12.9 ppm; HRMS (EI+) Exact mass calcd. for C₁₀H₁₁NO₃ [M-C₄H₄O]⁺: 125.0477, found: 125.0480.



General method to synthesize S6-S12:⁷¹ Norbornene imide **S4**⁷² (1g, 1 eq) was dissolved in acetonitrile (MeCN) (45 mL) in a 50 mL round bottom flask. To this solution, K₂CO₃ (1.675 g, 2 eq) and 1-bromo-2-ethylhexane (1.29 mL, 1.2 eq) were added dropwise under N₂. The solution was refluxed for 12 h. This was cooled to room temperature and then filtered under vacuum. MeCN was removed under rotary evaporation to obtain a liquid (**S8 and S10**) or solid (**S6, S7, S9, S11 and S12**) mixed crude product. Diethyl ether was used to dissolve the crude product and this was washed with brine (1:1) four times. The organic layer was then dried with anhydrous sodium sulfate then filtered. The organic solvent was removed by rotary evaporation. Then column chromatography with a mobile phase of EtOAc: hexane = 1:1 was used to obtain the corresponding product. Yield = 40 ~ 51%.

(3aR,4S,7R,7aS)-2-butyl-3a,4,7,7a-tetrahydro-1H-4,7-epoxyisoindole-1,3(2H)-dione

(S6): ¹H NMR (600 MHz, CDCl₃) δ 6.48 (s, 2 H), 5.24 (t, *J* = 7.2 Hz, 2 H), 3.45 (t, *J* = 7.4 Hz, 2 H), 2.80 (s, 2 H), 1.51 (m, 2 H), 1.27 (m, 2 H), 0.89 (t, *J* = 7.4 Hz, 2 H) ppm; ¹³C NMR (150 MHz, CDCl₃) δ 176.3, 136.5, 80.9, 47.4, 38.8, 29.6, 19.9, 13.6 ppm; HRMS (EI+) Exact mass calcd. for C₁₂H₁₅NO₃ [M-C₄H₄O]⁺: 153.0788, found: 153.0790.

(3aR,4S,7R,7aS)-2-pentyl-3a,4,7,7a-tetrahydro-1H-4,7-epoxyisoindole-1,3(2H)-dione

(S7): ^1H NMR (600 MHz, CDCl_3) δ 6.49 (t, $J = 0.9$ Hz, 2 H), 5.24 (t, $J = 0.9$ Hz, 2 H), 3.63-3.32 (m, 2H), 2.80 (s, 2 H), 1.53 (m, 2 H), 1.30 (m, 2 H), 1.24 (m, 2H), 0.85 (t, $J = 7.2$ Hz, 2 H) ppm; ^{13}C NMR (150 MHz, CDCl_3) δ 176.3, 136.5, 80.9, 47.4, 39.0, 31.3, 27.5, 26.3, 22.4, 13.9 ppm; HRMS (EI+) Exact mass calcd. for $\text{C}_{13}\text{H}_{17}\text{NO}_3$ [$\text{M}-\text{C}_4\text{H}_4\text{O}$] $^+$: 167.0946, found: 167.0947.

(3aR,4S,7R,7aS)-2-hexyl-3a,4,7,7a-tetrahydro-1H-4,7-epoxyisoindole-1,3(2H)-dione

(S8): ^1H NMR (600 MHz, CDCl_3) δ 6.49 (t, $J = 0.9$ Hz, 2 H), 5.24 (t, $J = 0.9$ Hz, 2 H), 3.47-3.42 (m, 2H), 2.81 (s, 2 H), 1.54-1.52 (m, 2 H), 1.27-1.24 (m, 6 H), 0.86-0.84 (m, 3 H) ppm; ^{13}C NMR (150 MHz, CDCl_3) δ 176.3, 136.5, 80.9, 47.4, 39.0, 28.8, 27.3, 22.2, 13.9 ppm; HRMS (EI+) Exact mass calcd. for $\text{C}_{14}\text{H}_{19}\text{NO}_3$ [$\text{M}-\text{C}_4\text{H}_4\text{O}$] $^+$: 181.1103, found: 181.1101.

(3aR,4S,7R,7aS)-2-heptyl-3a,4,7,7a-tetrahydro-1H-4,7-epoxyisoindole-1,3(2H)-dione

(S9): ^1H NMR (600 MHz, CDCl_3) δ 6.49 (s, 2 H), 5.24 (s, 2 H), 3.45-3.43 (m, 2H), 2.80 (s, 2 H), 1.54-1.51 (m, 2 H), 1.26-1.21 (m, 9 H), 0.85 (t, $J = 6.9$ Hz, 3 H) ppm; ^{13}C NMR (150 MHz, CDCl_3) δ 176.3, 136.5, 80.9, 47.4, 39.0, 31.3, 27.5, 26.3, 22.4, 13.9 ppm; HRMS (EI+) Exact mass calcd. for $\text{C}_{15}\text{H}_{21}\text{NO}_3$ [$\text{M}-\text{C}_4\text{H}_4\text{O}$] $^+$: 195.1259, found: 195.1265.

(3aR,4S,7R,7aS)-2-(2-ethylhexyl)-3a,4,7,7a-tetrahydro-1H-4,7-epoxyisoindole-1,3(2H)-dione (S10):

^1H NMR (600 MHz, CDCl_3) δ 6.51 (s, 2 H), 5.26 (s, 2 H), 3.37 (d, $J = 7.6$ Hz, 2 H), 2.82 (s, 2 H), 1.74 (m, 1H), 1.28-1.20 (m, 9H), 0.88-0.85 (m, 6H) ppm; ^{13}C NMR (150 MHz, CDCl_3) δ 176.5, 136.5, 80.9, 47.3, 42.8, 37.3, 30.1, 28.3, 23.5, 22.9, 14.0, 10.3 ppm; HRMS (EI+) Exact mass calcd. for $\text{C}_{16}\text{H}_{23}\text{NO}_3$ [$\text{M}-\text{C}_4\text{H}_4\text{O}$] $^+$ 209.1416, found: 209.1419.

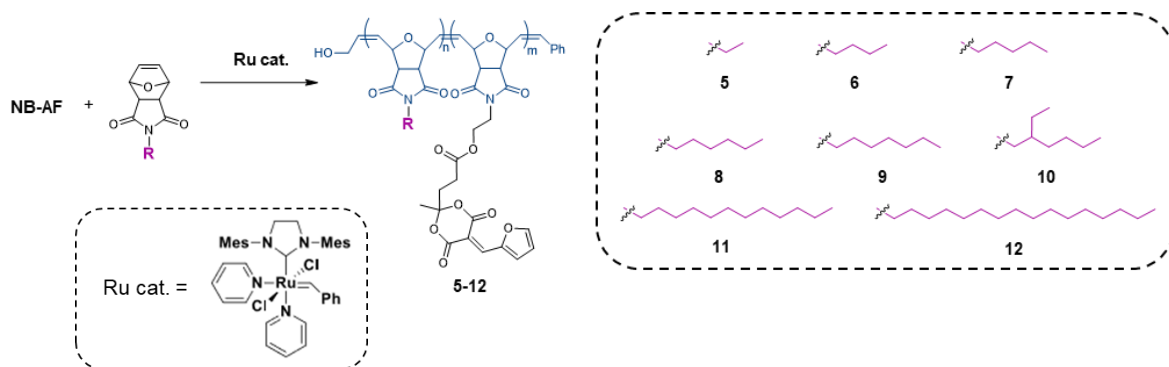
(3aR,4S,7R,7aS)-2-dodecyl-3a,4,7,7a-tetrahydro-1H-4,7-epoxyisoindole-1,3(2H)-dione

(S11): ^1H NMR (600 MHz, CDCl_3) δ 6.51 (s, 2 H), 5.26 (s, 2 H), 3.47-3.44 (m, 2H), 2.82 (s, 2 H), 1.30-1.24 (m, 20 H), 0.88 (t, $J = 7.0$ Hz, 3 H) ppm; ^{13}C NMR (150 MHz, CDCl_3) δ 176.3, 136.5, 80.9, 47.4, 39.0, 31.9, 29.6, 29.5, 29.5, 29.3, 29.1, 27.6, 26.7, 22.7 ppm; HRMS (EI+) Exact mass calcd. for $\text{C}_{20}\text{H}_{31}\text{NO}_3$ [M-C $_4\text{H}_4\text{O}$]: 265.2042, found: 265.2042.

(3aR,4S,7R,7aS)-2-hexadecyl-3a,4,7,7a-tetrahydro-1H-4,7-epoxyisoindole-1,3(2H)-dione (S12):

^1H NMR (600 MHz, CDCl_3) δ 6.51 (s, 2 H), 5.26 (s, 2 H), 3.46 (m, 2H), 2.82 (s, 2 H), 1.31-1.24 (m, 28 H), 0.88 (t, $J = 7.0$ Hz, 3 H) ppm; ^{13}C NMR (150 MHz, CDCl_3) δ 176.2, 136.5, 80.9, 47.4, 39.0, 31.9, 29.7, 29.7, 29.6, 29.6, 29.6, 29.5, 29.5, 29.3, 29.1, 27.6, 26.7, 22.7, 14.1 ppm; HRMS (EI+) Exact mass calcd. for $\text{C}_{20}\text{H}_{31}\text{NO}_3$ [M-C $_4\text{H}_4\text{O}$]: 321.2668, found: 321.2677.

Synthesis of co-polymers 5-12



General method to synthesize 5-12: Within a N_2 atmosphere glove box, **NB-AF** (225 mg) and each of **S5-S12** (500 mg) were dissolved in dry DCM (2.5 mL) in a 1 dram vial. Meanwhile, a concentrated solution of bispyridine ruthenium catalyst⁵² (22 mg/ mL) in dry

DCM was also prepared in the glove box. Then 0.54 mL of DCM solution of ruthenium catalyst solution (11.9 mg) was rapidly added into the quickly stirring **NB-AF** solution. This solution was then stirred for an additional 30 min. Reaction was then removed from the glovebox and quenched with two drops of butenediol. This was then stirred for an additional 20 min. Reaction mixture was then added dropwise to quickly stirring, cold methanol and a light yellow solid was precipitated. Product was then collected *via* vacuum filtration. (Yield \approx 89%). $\bar{M}_n = 1.02 \sim 1.06$. $M_w = 41k \sim 78k$. **NB-AF** wt% = 29 ~ 31% by ^1H NMR spectroscopy.

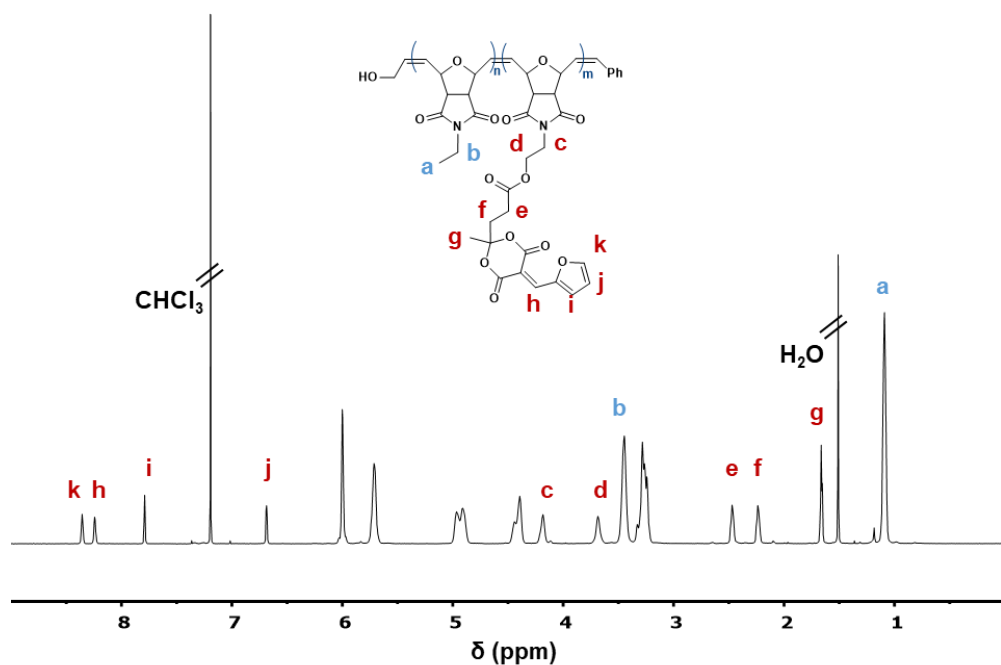


Figure 3.12 Representative example of ^1H NMR spectra for activated furan polymer conjugates. NMR shown illustrates polymer 5.

3.12 Supplemental Results

3.12.1 Polymer thin film preparation

The polymers were first dissolved in dioxane (100 mg/mL), then filtered through a 0.45 μm syringe filter. Meanwhile each glass substrate was precleaned *via* sonication in dilute cuvette cleaning solution (Hellmanex III purchased from Sigma-Aldrich), followed by deionized water, acetone, and finally isopropanol for 15 min each. Substrates were then dried under N_2 and ozone treated (~ 10 min) (**Figure S3.1a**). Each solution was then spin coated onto a precleaned glass substrate ($\sim 22 \times 22 \text{ mm}^2$) at 600 rpm to prepare films of **5-12** (**Figure S3.1b**). Film thickness was determined to be approximately 1050 \sim 1300 nm using profilometry (**Figure S3.2**). These films could then be exposed to aqueous solutions of amine to produce thin films of the open isomer of DASA **13-20** (specific derivative varies depending on amine utilized) (**Figure S3.1c**)

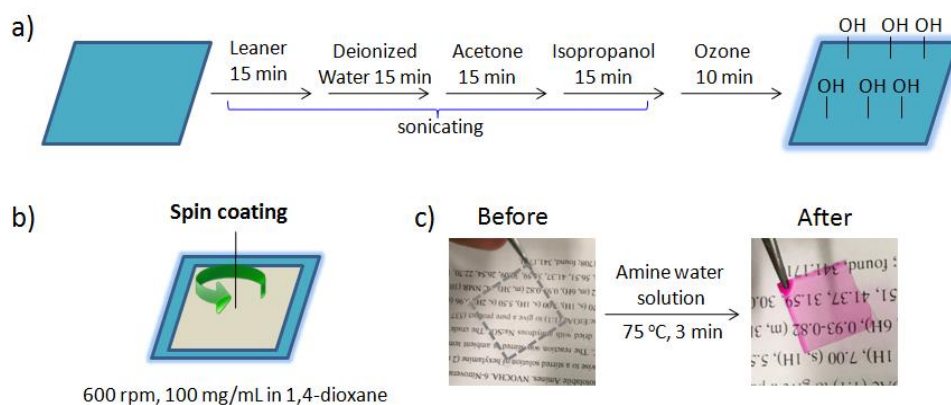


Figure S3.1 a) Schematic diagram of precleaning cover glasses and growing hydroxy films. b) Conditions for spin coating of polymer **5-12**. c) Polymer films prepared by spin coating before and after detect amine in water.

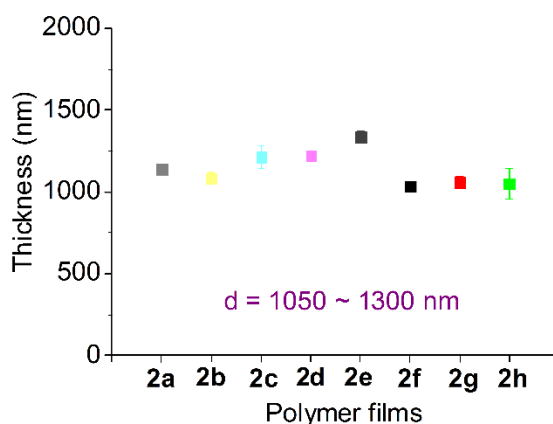


Figure S3.2 Thickness of polymer films 5-12.

3.12.2 Stability of small molecule activated furan and DASA in aqueous environment

Small molecule activated furan and a small molecule donor acceptor Stenhouse adduct were dissolved in dioxane (23 mg / mL). Each small molecule was then drop cast onto a filter paper and dried under ambient conditions. The AF filter paper was then placed into a diethylamine aqueous solution (300 ppm) at 75 °C (**Figure S3.3a**). The DASA filter paper was put in aqueous solution at 75 °C (**Figure S3.3b**).

It was observed that the AF filter paper initially developed a pink color indicating the formation of DASA on the filter paper as expected. However, after 1 min the film began exhibit discoloration. As previously shown, the pink color gradually disappears indicating the instability of the small molecule DASA compound in water. Similarly, when a small molecule DASA was introduced to an aqueous environment, it also instantly began to show the same discoloration and leaching as has been observed in the literature.¹⁸

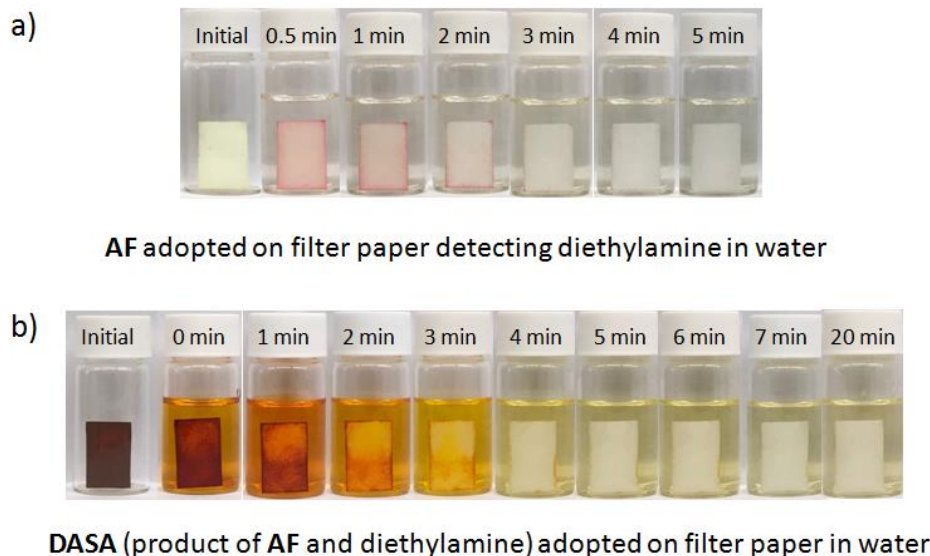


Figure S3.3 a) Photos of AF on filter paper detecting diethylamine in water (300 ppm) at 75 °C with time. b) Photos of DASA on filter paper put in water at 75 °C with time.

3.12.3 Leaching studies for small molecule DASA and AF versus polymeric activated furan

In order to further verify the leaching of DASA into its aqueous environment, remaining aqueous solutions from **Figure S3.3** were analyzed by ^1H NMR and mass spectroscopy (**Figure S3.4b and c**). This was then compared to a coated filter paper with polymer **12** that was also introduced to an aqueous solution of diethylamine (300 ppm, 75 °C) (**Figure S3.4a**). The residual aqueous solution from the coated film **12** after reaction with diethylamine did not show signs of leaching from the polymer film. In contrast, the residual aqueous solution from the AF coated filter paper demonstrated leaching and decomposition of the resulting DASA (**Figure S3.4b**). ^1H NMR and mass spectroscopy revealed three compounds remaining in solution: 1) diethylamine 2) a Meldrum's acid derivative formed from

decomposition of the activated furan with $[M-H^-] = 392.1$, and 3) and unidentified side product with $[M-H^-] = 436.1$. Additionally, the residual aqueous solution from the DASA coated revealed, as well-known in the literature, that a small molecule DASA will indeed leach into a water solution. Interestingly 1H NMR and mass spectroscopy of the residual aqueous solution determined that DASA will leach into the aqueous environment without apparent decomposition. However, as previously stated, the small molecule DASA will instantly begin to close irreversibly in water (**Figure S3.4c**). This indicated that polymer **12** film is more stable and applicable than a small molecule activated furan or DASA physically adopted on filter paper.

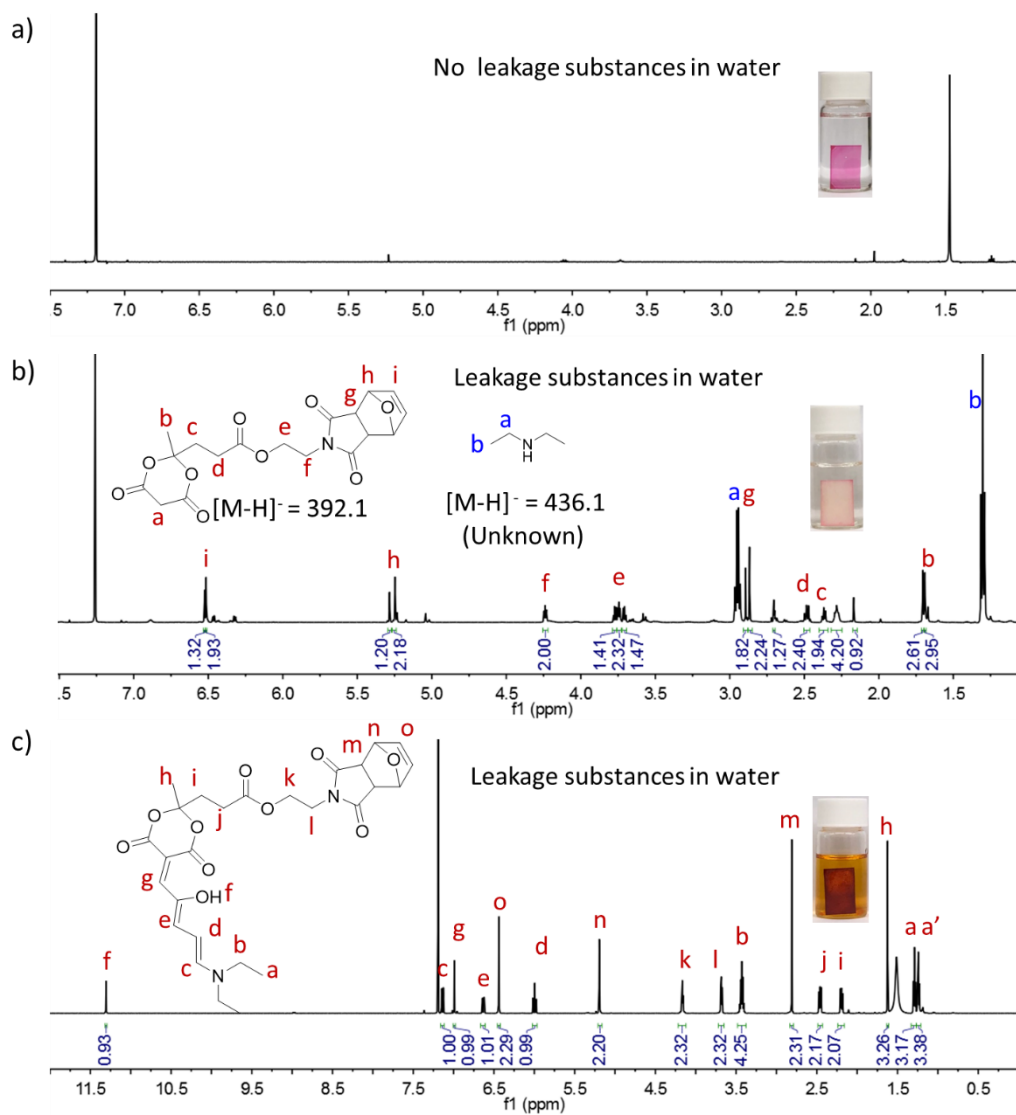


Figure S3.4 Leakage test in aqueous solution of amine sensors. ^1H NMR of the residual substances in water of **a)** polymer **11** film and **b)** AF filter paper after detecting diethylamine in water (300 ppm), and **c)** DASA filter paper put in water at 75 °C for 20 min.

3.12.4 Glass transition temperatures for co-polymers 6-12

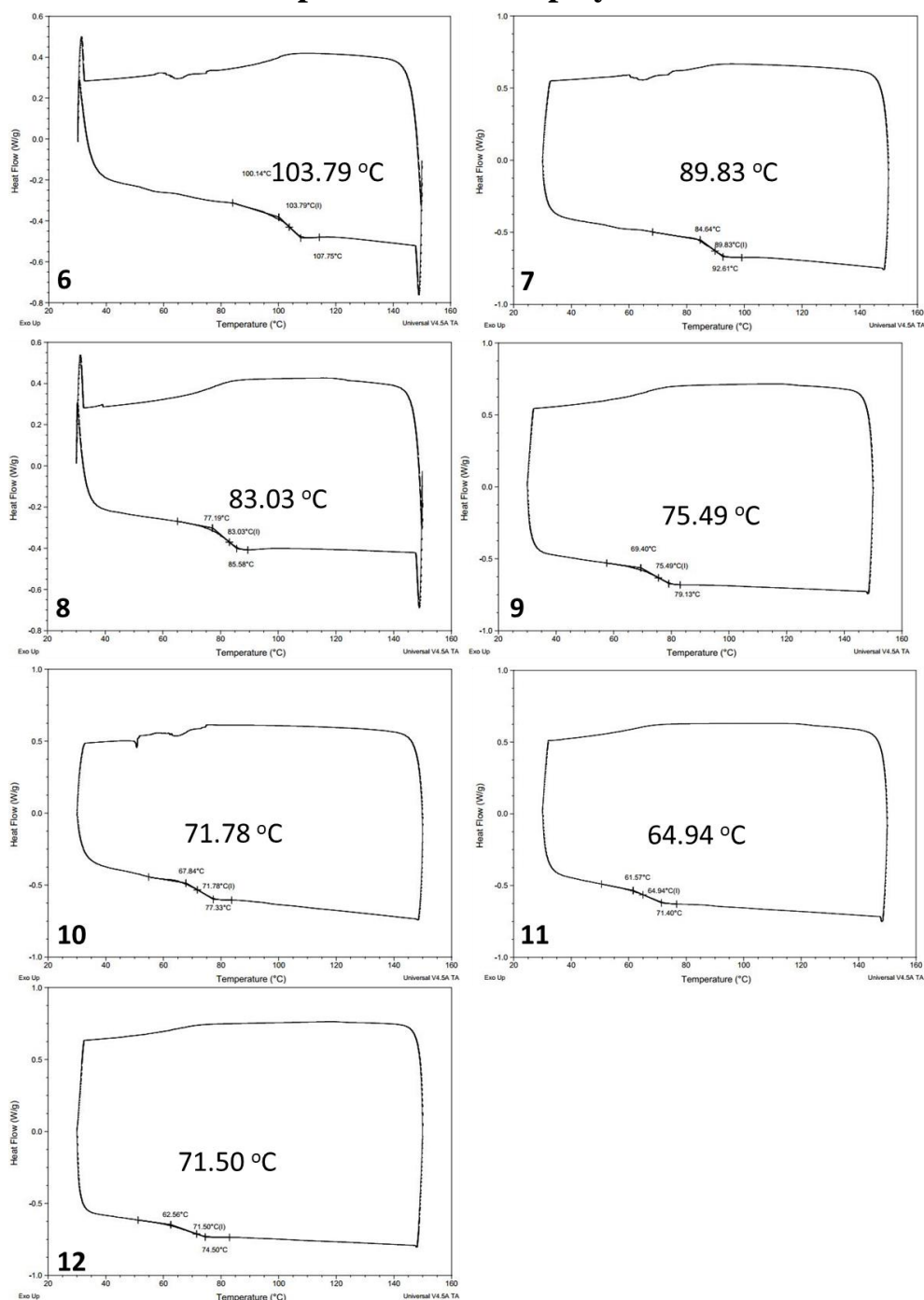


Figure S3.5 Representative DSC traces of **6-12** with heat/cool cycle run from 30 °C to 150 °C. T_g s were determined from the 2nd heat cycle onset point.

3.12.5 Temperature effect on amine detection

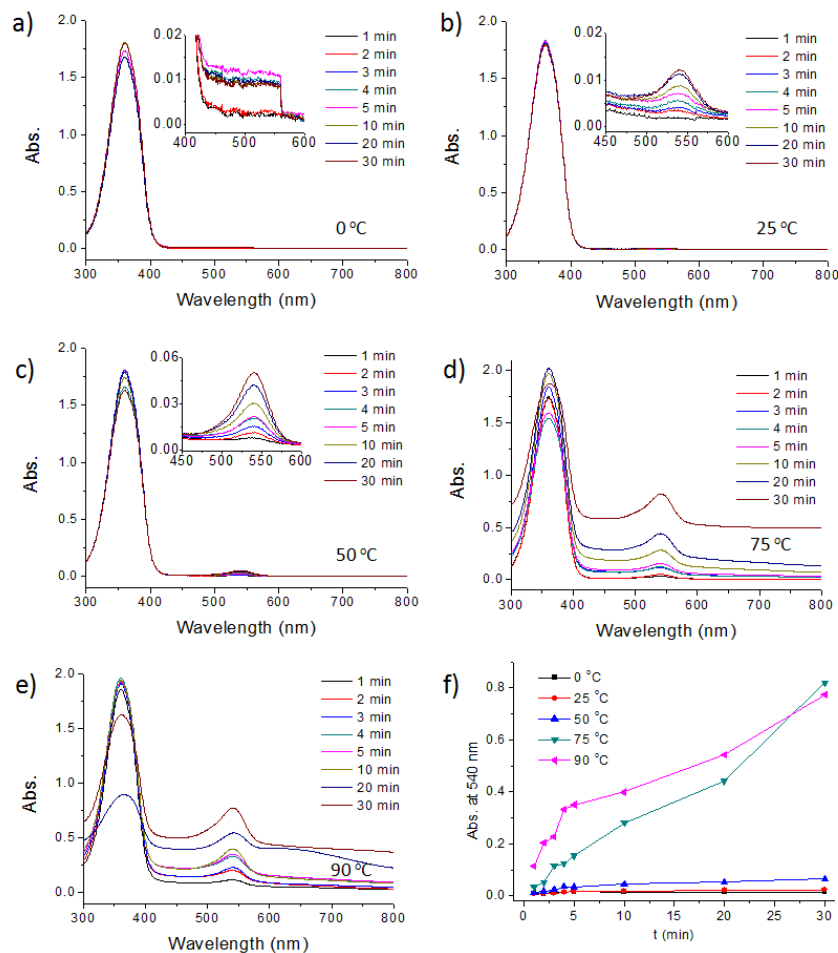


Figure S3.6 UV-vis spectra of polymer **12** detecting diethylamine (50 ppm) in water over time at **a)** 0 °C, **b)** 25 °C, **c)** 50 °C, **d)** 75 °C, **e)** 90 °C, respectively. **f)** Plot of absorption at $\lambda = 540$ nm of film **12** detecting diethylamine over time.

Amine detection sensitivity increases with **12** as the temperature increases (**Figure S3.6**). This is most noticeable at temperatures above the T_g of polymer **12** (72 °C). We believe that at temperatures above the T_g the increased flexibility of the polymer matrix allows for easier/faster conversion of the activated furan to the open DASA form. It is worth noting that at high temperatures (> 90 °C) or at long reaction times at moderate temperatures (> 75 °C),

de-adhesion of the polymer from the film makes analysis by UV-vis challenging. Therefore 5 min and 75 °C seems to be a suitable amine detecting condition for polymer **11** film.

3.12.6 Amine detection scope of polymeric activated furan

As expected, activated furan polymer film **11** (used as a representative example) was able to detect for various primary, secondary alkyl, and secondary aryl amines (**Figure S3.7 and S3.8**). This included 1: methylamine, 2: 1-propylamine, 3: 1-butylamine, 4: 2-(4,5-dihydrooxazol-2-yl)ethan-1-amine, 5: dimethylamine, 6: diethylamine, 7: dipropylamine, 8: dibutylamine, 9: pyrrolidine, 10: N-methylbutan-1-amine, 11: dibenzylamine, 12: indoline, 13: 2-methylindoline, 14: 4-methoxy-N-methylaniline, 15: 1,2,3,4-tetrahydroquinoline, 16: 4-methoxyaniline. For amines 1-12 an amine concentration of 50 ppm was used for detection and for 13-15 a slightly higher concentration (150 ppm) was required to achieve similar UV-vis response.

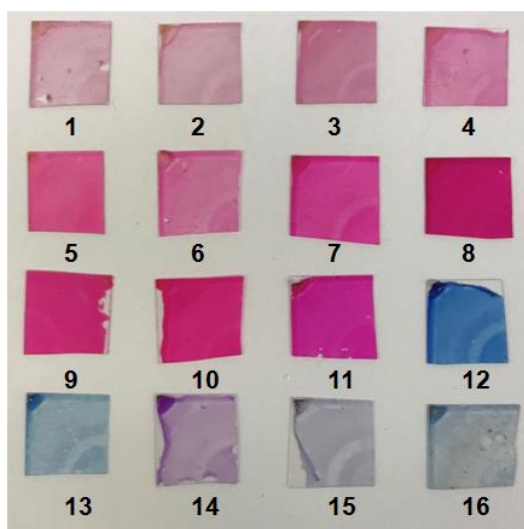


Figure S3.7 Photos of spin casted polymer film **11** after detecting different amines (see text above for full list of amines).

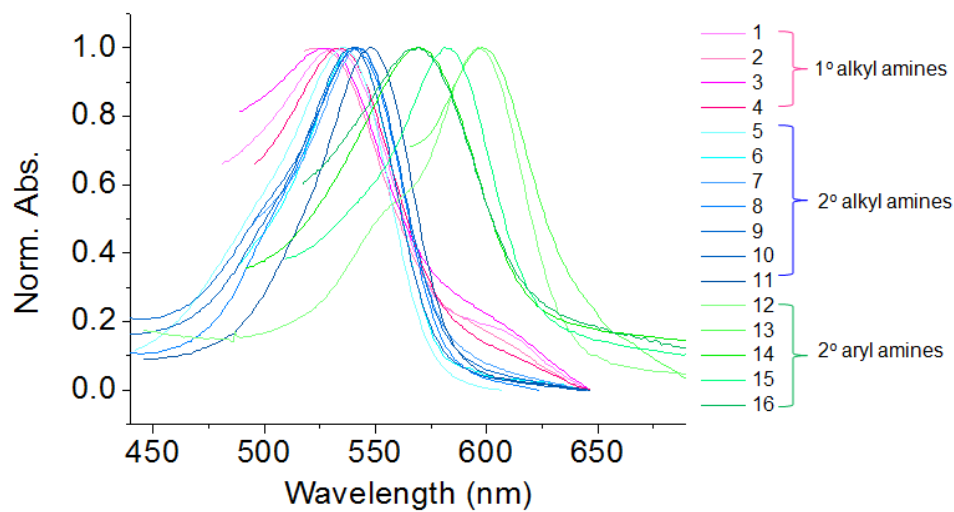


Figure S3.8 Normalized absorption spectra of **11** film (spin-coating) after detecting various amines (see text of **section 3.12.6** for full list) in aqueous solution at 75 °C for 3 min. Absorption spectra for amines 1-16 correspond to pictures for 1-16 in **Figure S3.7**.

3.12.7 Limit of detection for various amines with activated furan polymer film

Four representative amines were chosen to determine the amine limit of detection of polymer **11** film, including secondary alkyl amine (diethylamine), primary alkyl amine (*n*-butylamine), secondary aryl amine (indoline), and primary aryl amine (*p*-methoxyaniline). Each amine was measured three times. The limits of detection of activated furan polymer **11** film for diethylamine, *n*-butylamine, indoline, and *p*-methoxyaniline are approximately 10 ppm, 10 ppm, 10 ppm and 100 ppm, respectively (all $\lambda_{\max} \geq 0.05$ a.u.).

Limit of detection for diethylamine

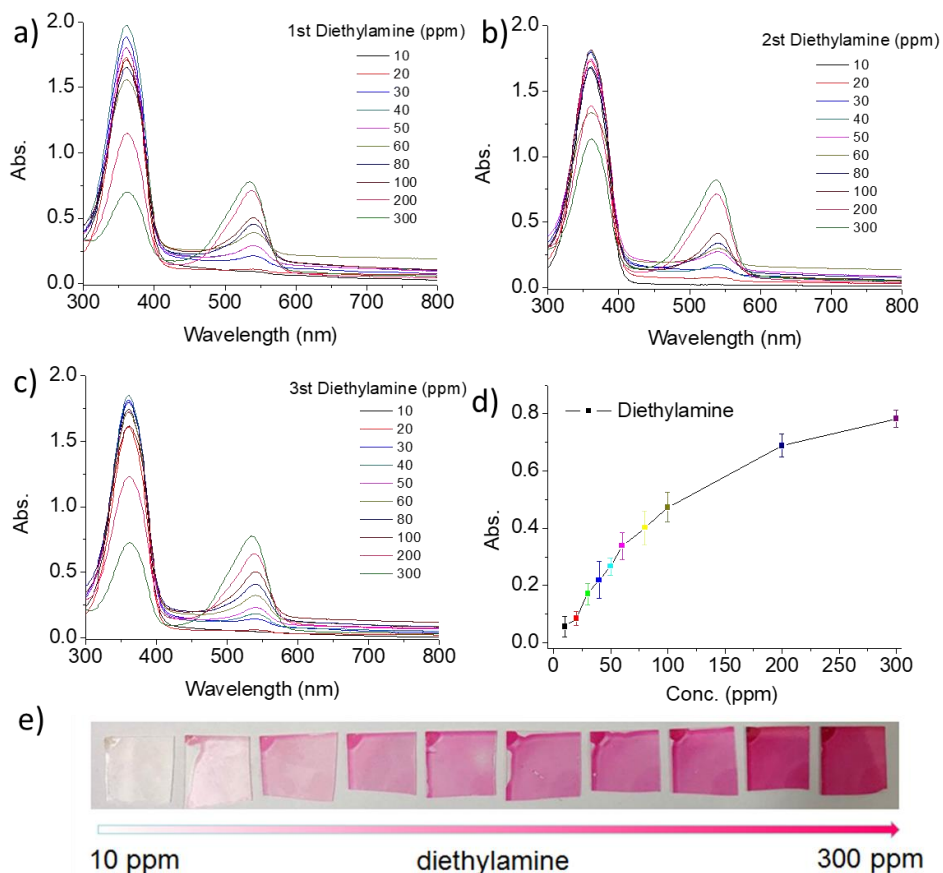


Figure S3.9 UV-vis spectrum of polymer **11** film in different concentrations of diethylamine aqueous solution at 75 °C for 3 min. This test was repeated three times as (a), (b) and (c). (d) Plot of absorption of **11** vs. concentration of diethylamine (e) Photos of **11** detecting diethylamine of different concentration. The limit of detection for diethylamine in water of polymer **11** film is 20 ppm ($\lambda_{\max} \geq 0.06$ a.u.).

Limit of detection of polymer film 11 for n-butylamine

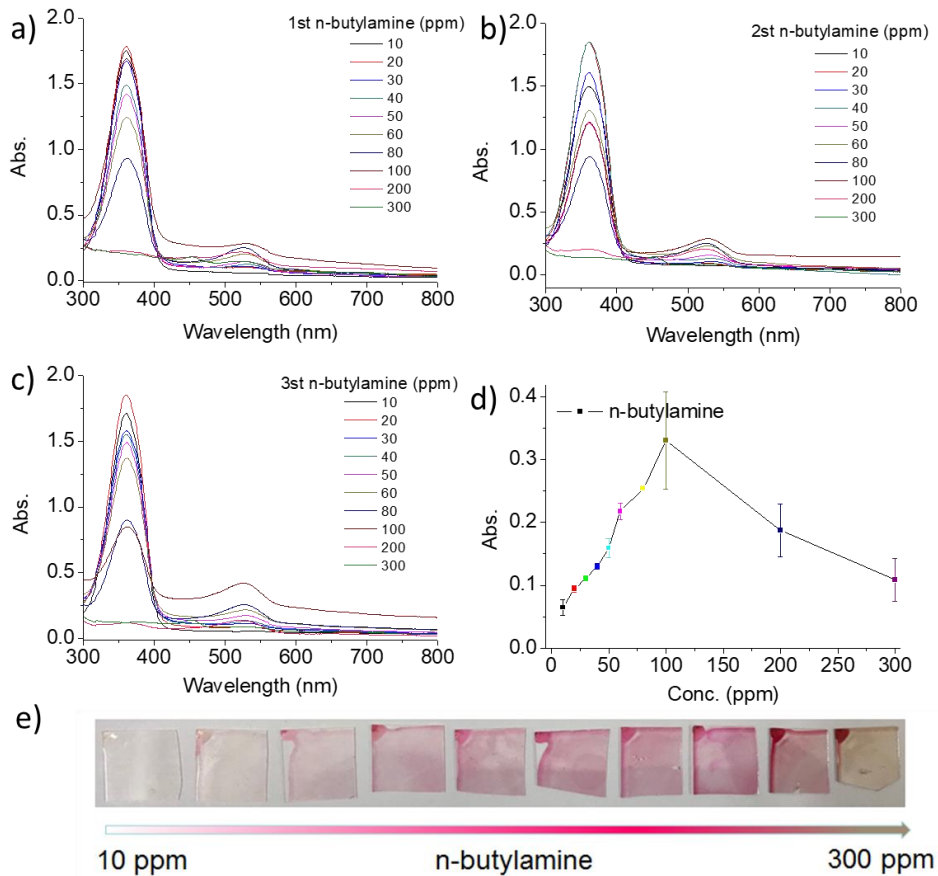


Figure S3.10 UV-vis spectrum of polymer **11** film in different concentrations of n-butylamine aqueous solution at 75 °C for 3 min. This test was repeated three times as (a), (b) and (c). (d) Plot of absorption of **11** vs. concentration of n-butylamine. (e) Photos of **11** detecting n-butylamine of different concentrations. The limit of detection for n-butylamine in water of polymer **11** film is 10 ppm ($\lambda_{\text{max}} \geq 0.06$ a.u.).

Limit of detection of polymer film 11 for indoline

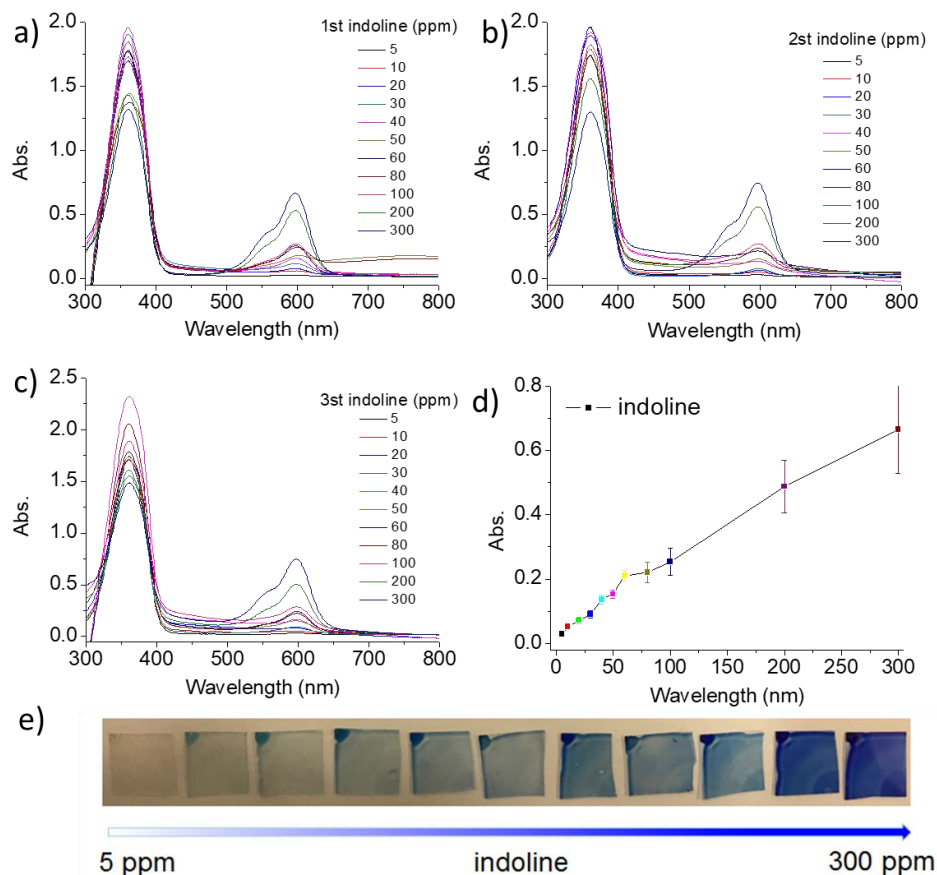


Figure S3.11 UV-Vis spectrum of polymer **11** film in different concentrations of indoline aqueous solution at 75 °C for 3 min. This test was measured three times as (a), (b) and (c). (d) Plot of absorption of **11** with concentration of indoline with error bar. (e) Photos of **11** detecting indoline of different concentration. The limit of detection for indoline in water of polymer **11** film is 20 ppm ($\lambda_{\text{max}} \geq 0.06$ a.u.).

Limit of detection of polymer film 11 for p-methoxyaniline

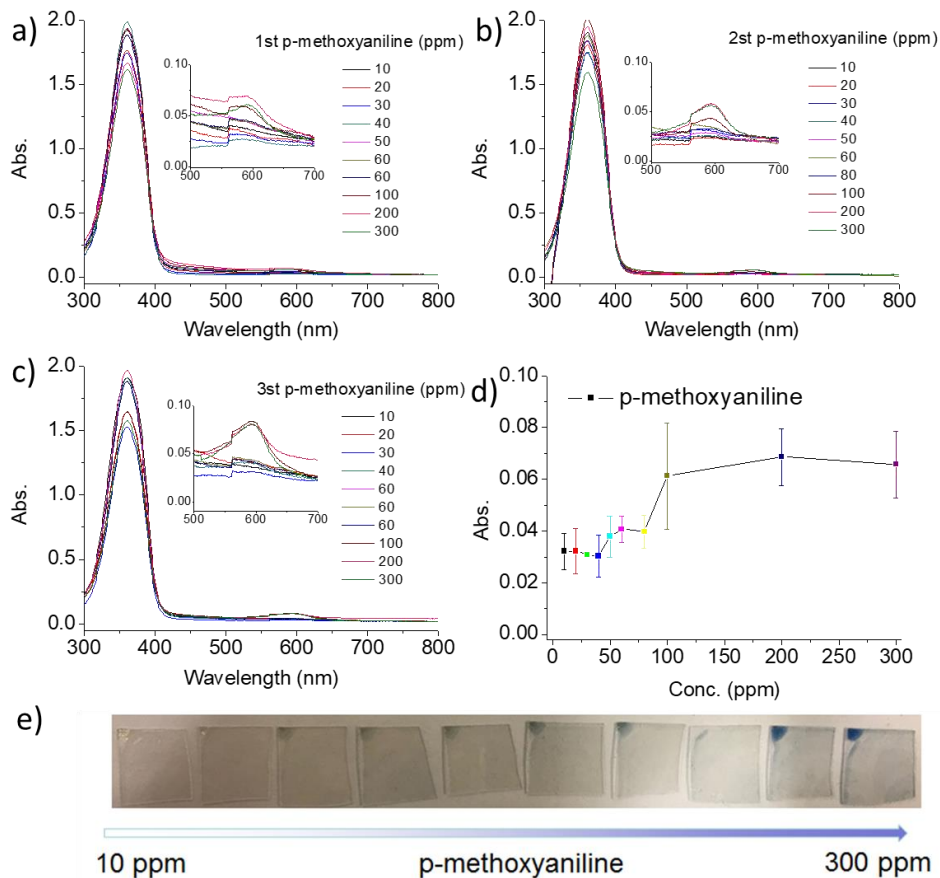


Figure S3.12 UV-vis spectrum of polymer **11** film in different concentration of p-methoxyaniline aqueous solution at 75 °C for 3 min. This test was measured three times as (a), (b) and (c). (d) Plot of absorption of **11** with concentration of p-methoxyaniline. (e) Photos of **11** detecting p-methoxyaniline of different concentration. The limit of detection for p-methoxyaniline in water of polymer **11** film is 100 ppm ($\lambda_{\max} \geq 0.06$ a.u.).

3.12.8 Stability of thermal sensor

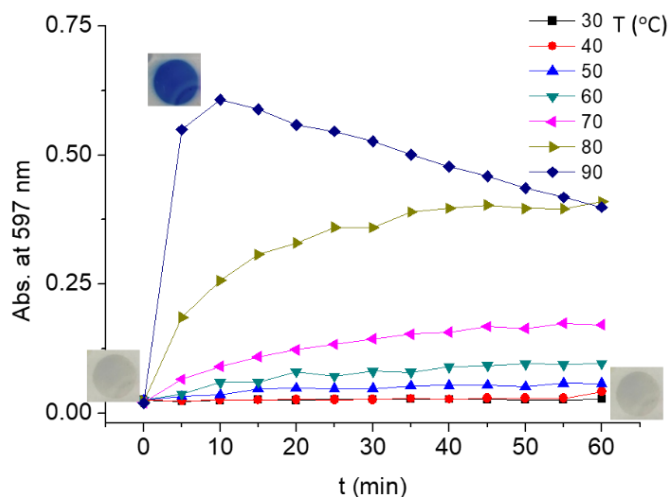


Figure S3.13 Plot of absorption at 597 nm of polymer **18** film (after reaction with 1500 ppm indoline) in response to different temperatures over time. Inset: Photographs of irradiated indoline derivative of polymer **18** initially (left), at 90 °C after 10 min (middle), and at 30 °C after 60 min (right).

In order to determine the ideal storage temperature for activated furan polymeric films, polymer **18** was coated onto a glass slide. This was then exposed to 1500 ppm indoline to form a blue colored open DASA derivative. The colorless, closed isomer of DASA could then be obtained with irradiation. This film was then exposed to various temperatures (30 °C – 90 °C) and monitored over 60 min. Every 5 min, the absorbance of the polymer film was collected (**Figure S3.13**).

At temperatures > 50 °C, the irradiated polymer film will gradually develop the blue color characteristic of the open DASA form over time. When maintained at room temperature (25 °C) to 40 °C, the colorless films were found to be stable up to 12 h. Finally, when the polymer films were stored within the freezer (approximately -20 °C) they were found to be stable for more than one month.

3.12.9 Stability of carboxylic acid activated furan **3** over time

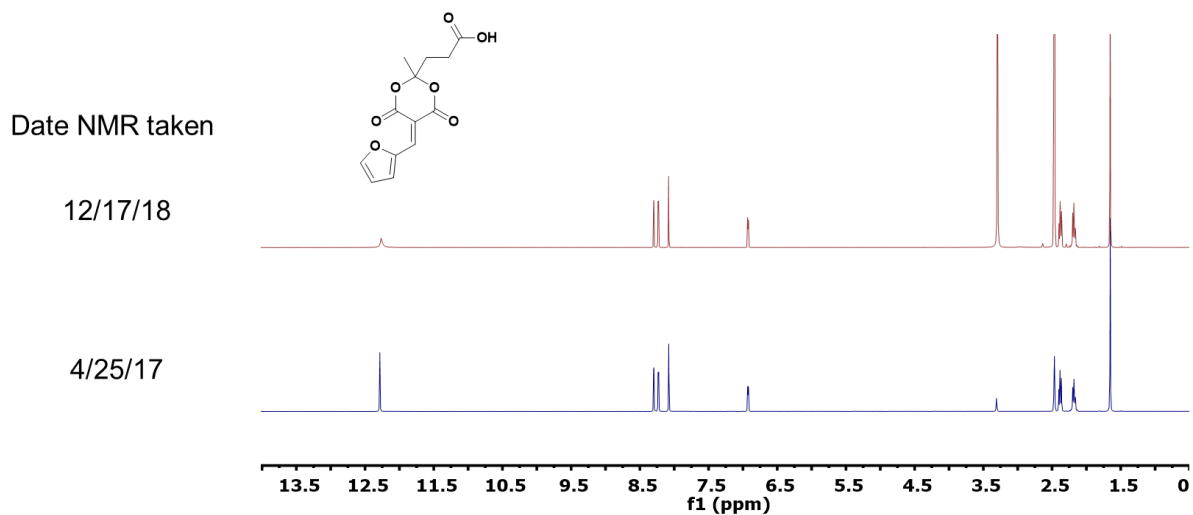


Figure S3.14 ^1H NMR spectroscopy comparison of **3** immediately after preparation (4/25/17) and after 20 months under ambient conditions at room temperature (12/17/18). Compound shows no observable degradation after > 1.5yrs.

3.12.10 Stability of oxa-norbornene Meldrum's activated furan (NF-AF) over time

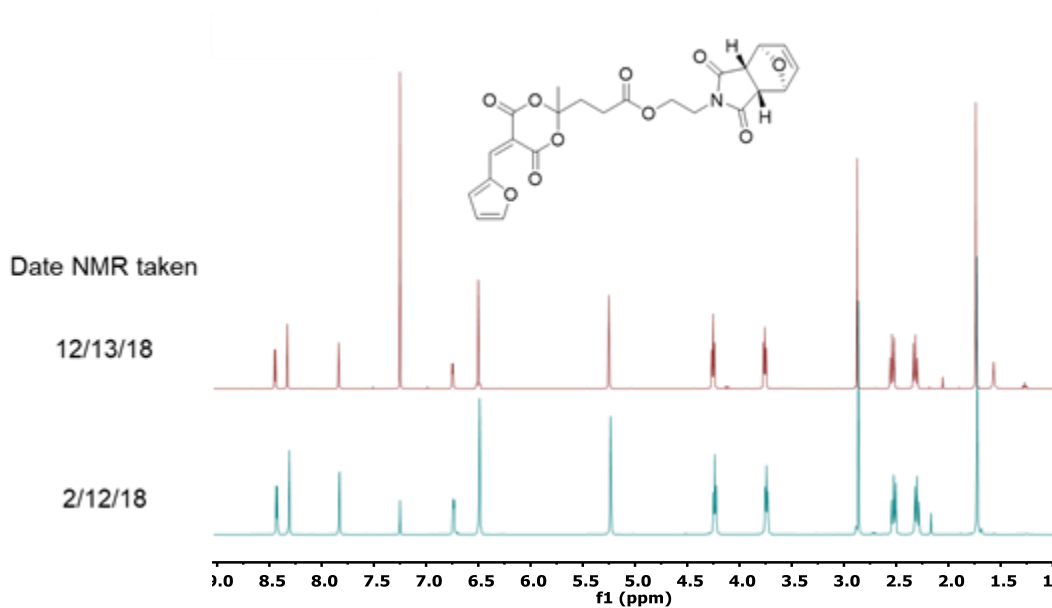


Figure S3.15 ¹H NMR spectroscopy comparison of **NB-AF** immediately after preparation (2/12/18) and after 10 months under ambient conditions at room temperature (12/13/18). Compound shows no observable degradation after 10 months.

3.13 References

- 1 K. L. Bicker, S. L. Wiskur and J. J. Lavigne, in *Chemosensors: Principles, Strategies, and Applications, First Edition*, eds. B. Wang and E. V. Anslyn, John Wiley & Sons, Inc., 1st edn., 2011, pp. 275–295.
- 2 H. N. Kim, Z. Guo, W. Zhu, J. Yoon and H. Tian, *Chem. Soc. Rev.*, 2011, **40**, 79–93.
- 3 S. W. Thomas 3rd, G. D. Joly and T. M. Swager, *Chem. Soc. Rev.*, 2007, **107**, 1339–1386.
- 4 Y. Shen, M. Kuang, Z. Shen, J. Nieberle, H. Duan and H. Frey, *Angew. Chem. Int. Ed.*, 2008, **47**, 2227–2230.
- 5 X. Wang, T.-W. Chang, G. Lin, M. R. Gartia and G. L. Liu, *Anal. Chem.*, 2017, **89**, 611–615.
- 6 W. S. P. Carvalho, M. Wei, N. Ikpo, Y. Gao and M. J. Serpe, *Anal. Chem.*, 2018, **90**, 459–479.
- 7 X. Feng, L. Liu, S. Wang and D. Zhu, *Chem. Soc. Rev.*, 2010, **39**, 2411–2419.
- 8 X. Sun, Y. Wang and Y. Lei, *Chem. Soc. Rev.*, 2015, **44**, 8019–8061.
- 9 J. Jaworski, K. Yokoyama, C. Zueger, W.-J. Chung, S.-W. Lee and A. Majumdar, *Langmuir*, 2011, **27**, 3180–3187.
- 10 H. N. Kim, W. X. Ren, J. S. Kim and J. Yoon, *Chem. Soc. Rev.*, 2012, **41**, 3210–3244.
- 11 E. Coronado, J. R. Galan-Mascaros, C. Martí-Gastaldo, E. Palomares, J. R. Durrant, R.

- Vilar, M. Gratzel and M. K. Nazeeruddin, *J. Am. Chem. Soc.*, 2005, **127**, 12351–12356.
- 12 A. Balamurugan and H. Lee, *Macromolecules*, 2016, **49**, 2568–2574.
- 13 J.-M. Kim, Y. B. Lee, D. H. Yang, J.-S. Lee, G. S. Lee and D. J. Ahn, *J. Am. Chem. Soc.*, 2005, **127**, 17580–17581.
- 14 C. Belger, J. G. Weis, E. Egap and T. M. Swager, *Macromolecules*, 2015, **48**, 7990–7994.
- 15 Y. J. Diaz, Z. A. Page, A. S. Knight, N. J. Treat, J. R. Hemmer, C. J. Hawker and J. Read de Alaniz, *Chem. Eur. J.*, 2017, **23**, 3562–3566.
- 16 B. P. Mason, M. Whittaker, J. Hemmer, S. Arora, A. Harper, S. Alnemrat, A. McEachen, S. Helmy, J. Read De Alaniz and J. P. Hooper, *Appl. Phys. Lett.*, 2016, **108**, 041906.
- 17 D. Zhong, Z. Cao, B. Wu, Q. Zhang and G. Wang, *Sens. Actuators B.*, 2018, **254**, 385–392.
- 18 M. M. Lerch, W. Szymański and B. L. Feringa, *Chem. Soc. Rev.*, 2018, **47**, 1910–1937.
- 19 J. Ahrens, T. Bian, T. Vexler and R. Klajn, *ChemPhotoChem*, 2017, **1**, 230–236.
- 20 S. Helmy, F. A. Leibfarth, S. Oh, J. E. Poelma, C. J. Hawker and J. Read de Alaniz, *J. Am. Chem. Soc.*, 2014, **136**, 8169–8172.

- 21 J. R. Hemmer, Z. A. Page, K. D. Clark, F. Stricker, N. D. Dolinski, C. J. Hawker and J. Read De Alaniz, *J. Am. Chem. Soc.*, 2018, **140**, 10425–10429.
- 22 S. Jia, J. D. Du, A. Hawley, W.-K. Fong, B. Graham and B. J. Boyd, *Langmuir*, 2017, **33**, 2215–2221.
- 23 M. M. Lerch, M. J. Hansen, W. A. Velema, W. Szymanski and B. L. Feringa, *Nat. Commun.*, 2016, **7**, 1–10.
- 24 M. M. Lerch, M. Di Donato, A. D. Laurent, M. Medved', A. Iagatti, L. Bussotti, A. Lapini, W. J. Buma, P. Foggi, W. Szymański and B. L. Feringa, *Angew. Chem. Int. Ed.*, 2018, **57**, 8063–8068.
- 25 A. D. Laurent, M. Medved' and D. Jacquemin, *ChemPhysChem*, 2016, **17**, 1846–1851.
- 26 M. M. Lerch, S. J. Wezenberg, W. Szymanski and B. L. Feringa, *J. Am. Chem. Soc.*, 2016, **138**, 6344–6347.
- 27 M. M. Lerch, M. Medved, A. Lapini, A. D. Laurent, A. Iagatti, L. Bussotti, W. Szymański, W. J. Buma, P. Foggi, M. Di Donato and B. L. Feringa, *J. Phys. Chem. A.*, 2018, **122**, 955–964.
- 28 N. Mallo, P. T. Brown, H. Iranmanesh, T. S. C. MacDonald, M. J. Teusner, J. B. Harper, G. E. Ball and J. E. Beves, *Chem. Commun.*, 2016, **52**, 13576–13579.
- 29 S. O. Poelma, S. S. Oh, S. Helmy, A. S. Knight, G. L. Burnett, H. T. Soh, C. J. Hawker and J. Read De Alaniz, *Chem. Commun.*, 2016, **52**, 10525–10528.
- 30 A. Belhboub, F. Boucher and D. Jacquemin, *J. Mater. Chem. C.*, 2017, **5**, 1624–1631.

- 31 O. Rifaie-Graham, S. Ulrich, N. F. B. Galensowske, S. Balog, M. Chami, D. Rentsch, J. R. Hemmer, J. Read De Alaniz, L. F. Boesel and N. Bruns, *J. Am. Chem. Soc.*, 2018, **140**, 8027–8036.
- 32 G. Sinawang, B. Wu, J. Wang, S. Li and Y. He, *Macromol. Chem. Phys.*, 2016, **217**, 2409–2414.
- 33 S. Singh, K. Friedel, M. Himmerlich, Y. Lei, G. Schlingloff and A. Schober, *ACS Macro Lett.*, 2015, **4**, 1273–1277.
- 34 C. Tonnelé, B. Champagne, L. Muccioli and F. Castet, *Phys. Chem. Chem. Phys.*, 2018, **20**, 27658–27667.
- 35 F.-Y. Tang, J.-N. Hou, K.-X. Liang, Y. Liu, L. Deng and Y.-N. Liu, *New J. Chem.*, 2017, **41**, 6071–6075.
- 36 S. Ulrich, J. R. Hemmer, Z. A. Page, N. D. Dolinski, O. Rifaie-Graham, N. Bruns, C. J. Hawker, L. F. Boesel and J. Read De Alaniz, *ACS Macro Lett.*, 2017, **6**, 738–742.
- 37 B. Wu, T. Xue, W. Wang, S. Li, J. Shen and Y. He, *J. Mater. Chem. C.*, 2018, **6**, 8538–8545.
- 38 B. K. Wright, University of Victoria, 2014.
- 39 S. Yang, J. Liu, Z. Cao, M. Li, Q. Luo and D. Qu, *Dye. Pigm.*, 2018, **148**, 341–347.
- 40 J. N. Bull, E. Carrascosa, N. Mallo, M. S. Scholz, G. da Silva, J. E. Beves and E. J. Bieske, *J. Phys. Chem. Lett.*, 2018, **9**, 665–671.

- 41 Y. Chen, Z. Li, H. Wang, Y. Pei, Y. Shi and J. Wang, *Langmuir*, 2018, **34**, 2784–2790.
- 42 M. Di Donato, M. M. Lerch, A. Lapini, A. D. Laurent, A. Iagatti, L. Bussotti, S. P. Ihrig, M. Medved, D. Jacquemin, W. Szymański, W. Jan Buma, P. Foggi and B. L. Feringa, *J. Am. Chem. Soc.*, 2017, **139**, 15596–15599.
- 43 N. D. Dolinski, Z. A. Page, F. Eisenreich, J. Niu, S. Hecht, J. Read de Alaniz and C. J. Hawker, *ChemPhotoChem*, 2017, **1**, 125–131.
- 44 C. García-Iriepe and M. Marazzi, *Materials (Basel)*, 2017, **10**, 1025.
- 45 S. Helmy, S. Oh, F. A. Leibfarth, C. J. Hawker and J. Read De Alaniz, *J. Org. Chem.*, 2014, **79**, 11316–11329.
- 46 J. R. Hemmer, S. O. Poelma, N. Treat, Z. A. Page, N. D. Dolinski, Y. J. Diaz, W. Tomlinson, K. D. Clark, J. P. Hooper, C. Hawker and J. Read De Alaniz, *J. Am. Chem. Soc.*, 2016, **138**, 13960–13966.
- 47 PTC Int., WO2006019146A1, 2006.
- 48 US7442809B, 2004.
- 49 G. Odian, *Principles of Polymerization*, John Wiley & Sons, Inc., 4th edn., 2004.
- 50 M. A. Gauthier, M. I. Gibson and H.-A. Klok, *Angew. Chem. Int. Ed.*, 2008, **48**, 48–58.
- 51 A. S. Goldmann, M. Glassner, A. J. Inglis and C. Barner-Kowollik, *Macromol. Rapid.*

- Commun.*, 2013, **34**, 810–849.
- 52 C. M. Bates, A. B. Chang, N. Momčilović, S. C. Jones and R. H. Grubbs, *Macromolecules*, 2015, **48**, 4967–4973.
- 53 F. Gaggini, A. Porcheddu, G. Reginato, M. Rodriguez and M. Taddei, *J. Comb. Chem.*, 2004, **6**, 805–810.
- 54 C. Han, L. Zeng, H. Li and G. Xie, *Sens. Actuators B.*, 2009, **137**, 704–709.
- 55 H. Li, Q. Chen, J. Zhao and Q. Ouyang, *Anal. Methods*, 2014, **6**, 6271–6277.
- 56 U. Khulal, J. Zhao, W. Hu and Q. Chen, *RSC Adv.*, 2016, **6**, 4663–4672.
- 57 B. Kuswandi, Jayus, A. Restyana, A. Abdullah, L. Heng and M. Ahmad, *Food Control*, 2012, **25**, 184–189.
- 58 Y. Hu, X. Ma, Y. Zhang, Y. Che and J. Zhao, *ACS Sens.*, 2016, **1**, 22–25.
- 59 A. Pacquit, K. Lau, H. McLaughlin, J. Frisby, B. Quilty and D. Diamond, *Talanta*, 2006, **69**, 515–520.
- 60 T. Lin, Y. Wu, Z. Li, Z. Song, L. Guo and F. Fu, *Anal. Chem.*, 2016, **88**, 11022–11027.
- 61 Z. Li and K. S. Suslick, *ACS Sens.*, 2016, **1**, 1330–1335.
- 62 L. Feng, C. J. Musto, J. W. Kemling, S. H. Lim and K. S. Suslick, *Chem. Commun.*, 2010, **46**, 2037–2039.
- 63 J. Kumpf and U. H. F. Bunz, *Chem. Eur. J.*, 2012, **18**, 8921–8924.

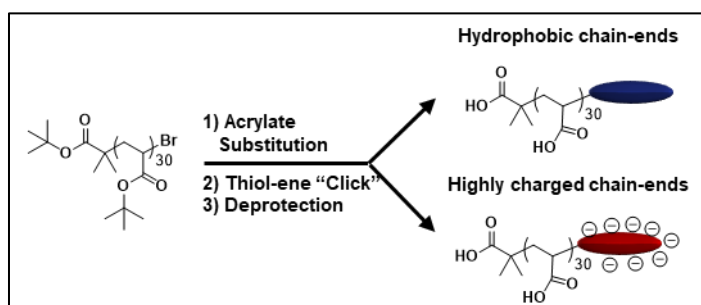
- 64 J. Freudenberg, J. Kumpf, V. Schäfer, E. Sauter, S. J. Wörner, K. Brödner, A. Dreuw and U. H. F. Bunz, *J. Org. Chem.*, 2013, **78**, 4949–4959.
- 65 M. Comes, M. D. Marcos, R. Martínez-Mañez, F. Sancenón, L. A. Villaescusa, A. Graefe and G. J. Mohr, *J. Mater. Chem.*, 2008, **18**, 5815–5823.
- 66 C. Ren, J. S. Lee and T. E. Glass, *Supramol. Chem.*, 2014, **26**, 607–611.
- 67 P. Montes-Navajas, L. A. Baumes, A. Corma and H. Garcia, *Tetrahedron Lett.*, 2009, **50**, 2301–2304.
- 68 L. Cai, Y. Zhao, S. Gong, L. Dong and C. Wu, *Chromatographia*, 2003, **58**, 615–621.
- 69 Y. Sun, L. Liang, X. Zhao, L. Yu, J. Zhang, G. Shi and T. Zhou, *Water Res.*, 2009, **43**, 41–46.
- 70 M. V. Gil, V. Luque-Agudo, E. Román and J. A. Serrano, *Synlett*, 2014, **25**, 2179–2183.
- 71 J.-Y. Wu, C.-D. Kuo, C.-Y. Chu, M.-S. Chen, J.-H. Lin, Y.-J. Chen and H.-F. Liao, *Molecules*, 2014, **19**, 6911–6928.
- 72 E. H. Discekici, A. H. St. Amant, S. N. Nguyen, I. H. Lee, C. J. Hawker and J. Read De Alaniz, *J. Am. Chem. Soc.*, 2018, **140**, 5009–5013.

CHAPTER 4

A UNIVERSAL AND SCALABLE SYNTHESIS OF WELL-DEFINED POLY(ACRYLIC ACID)S WITH TAILORED CHAIN END CHEMISTRIES

4.1 Abstract

The synthesis of a low dispersity acrylate-terminated poly(*tert*-butyl acrylate) enables facile access to well-defined



poly(acrylic acid)s (PAA) with tailorable chain end chemistries. This synthesis allows for the incorporation of both hydrophobic and highly charged ω -chain ends through a universal procedure while also allowing for the simple modification of the α -end group. A number of examples including a dodecyl and sulfonate-terminated poly(acrylic acid), each with low dispersity, were synthesized to demonstrate the tunability for this technique. A combination of

size exclusion chromatography (SEC), nuclear magnetic resonance (NMR), and matrix-assisted laser desorption ionization time of flight mass (MALDI-ToF-MS) spectrometry were used to confirm full conversion of the end group along with the retention of a narrow molecular weight distribution. This tailorable and accessible procedure simplifies the synthetic process to produce well-defined PAAs with a wide variety of chain ends and will facilitate further studies into the structure-property relationship between PAA chain end chemistry and macroscale polymer behavior toward targeted applications.

4.2 Introduction

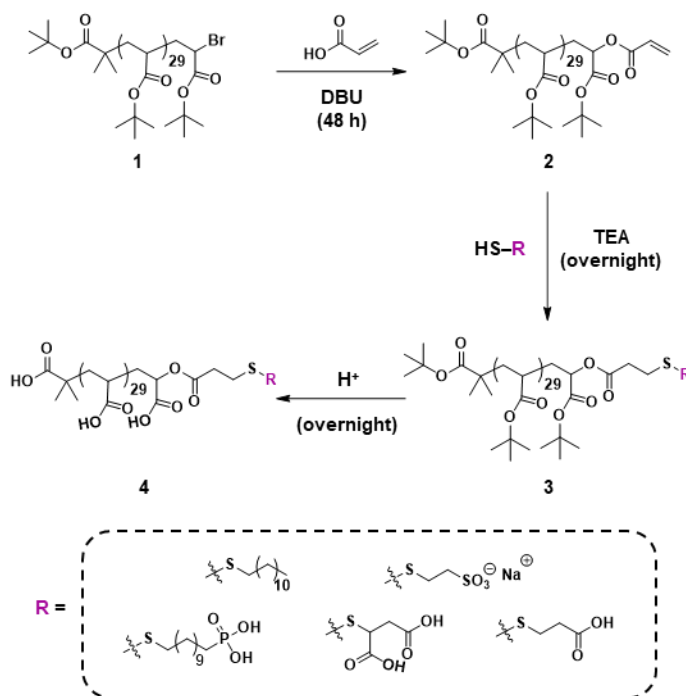
Poly (acrylic acid)s have found use in a wide variety of industrially relevant applications such as dispersants¹, coatings,² scale inhibition,³⁻⁵ and mineralization control.^{6,7} Their versatility has led to the investigation of the critical relationship between PAA architecture, dispersity, and performance.⁸⁻¹¹ In particular, it was discovered that for low molecular weight PAAs, the end-group functionalization had a direct influence on the utility of these polymers. For example, Cheung and Fellows separately revealed that by simply modifying the length and hydrophobicity of the PAA chain end, they could significantly vary the crystallization and scale inhibition of calcium oxalate for applications in industrial water systems.^{12,13} In addition, it was found that a precise control over the dispersity of these polymers was critical in controlling characteristics such as viscosity and dispersion capability.^{14,15} Although a systematic analysis of the relationship between chain end composition and polymer properties would be beneficial for further analyzing the utility of PAAs for these applications, the ability to simply and affordably tailor end group functionalization of narrowly dispersed PAAs remains a fundamental challenge.

The field of controlled living radical polymerizations has contributed many advancements toward the modification of polymer chain ends.¹⁶ For example, Fellows and coworkers modified the initiator for the atom transfer radical polymerization (ATRP) of *tert*-butyl acrylate followed by hydrolysis to access a number of α chain end modified PAA derivatives with narrow dispersities.¹⁷ Alternatively ω -end-group modifications of PAAs have been realized through the use of various chain-transfer agents throughout reversible-addition fragmentation chain-transfer (RAFT) polymerization.¹³ These strategies have been effective in providing chain end modified PAAs that include long or short alkyl chains and hydroxyl groups. However, in order to provide a more in-depth analysis of the effect of chain ends on the unique properties of PAA, a wider breath of specialized end groups needs to be accessed such as highly charged species.

Herein, we introduce a universal method to access a library of PAA derivatives with more versatile chain end chemistries that allows for the easy combination of both α and ω -chain end modification while maintaining low dispersity. Through the facile and scalable synthesis of an acrylate-terminated poly(*tert*-butyl acrylate) we provide a synthetic framework that allows for the incorporation of a wide range of alkyl or highly charged end groups to the poly(acrylic acid) backbone *via* thiol-Michael addition (thiol-ene “click”) (**Scheme 4.1**). Due to the nature of this transformation, a strict control over the molecular weight and dispersity of these compounds is also maintained. Hydrolysis with trifluoroacetic acid then produces the targeted PAAs without influence or cleavage of the modified chain end. These chain end modifications were all performed under ambient conditions without the necessity of inert gas or deoxygenation procedures. Furthermore, the high efficiency of the “click” reaction, allowed

for the use of minimal thiol equivalence (equiv.), thus increasing the overall affordability of this method and expanding its potential for industrial use.

4.3 Synthesis of Bromine-Terminated PtBA



Scheme 4.1 Schematic representation for the synthesis of ω chain end modified poly(acrylic acid)s from an acrylate-terminated poly(tert-butyl acrylate).

The synthesis of bromine-terminated poly(*tert*-butyl acrylate) (PtBA) (**1**) was accomplished utilizing a slightly modified literature procedure¹⁸ for UV-light mediated ATRP to achieve high chain end fidelity. A *tert*-butyl α -bromoisobutyrate (*t*B-BiB) initiator was chosen to provide opportunity for further modification of the α -terminus since the hydrophobic *tert*-butyl moiety of both the initiation site and backbone are removed to give the acid form upon deprotection. However, alternative initiators can be used in order to provide additional

tunability to the α -end group.¹² A combination of ¹H NMR and MALDI-ToF-MS were used to ensure quantitative functionalization with a single bromine ω -chain end (**Figure S4.1-S4.4**).

4.4 Synthesis of Acrylate-Terminated PtBA

Although bromine chain ends have previously been used to successfully introduce a wide variety of functional groups to poly(acrylate)s by S_N2 substitution, an excess of the substituting reagent is often required to achieve full chain end conversion and is not ideal for various industrial applications.¹⁸ To address this, an acrylate-terminated PtBA (**2**) was prepared using commodity materials. This end group would more readily react with low equivalents of thiols through the highly efficient thiol-Michael addition (thiol-ene “click”) and subsequent hydrolysis could produce the targeted poly(acrylic acid) (**4**) with the desired chain end (**Scheme 4.1**). Displacement of the bromine chain end was facilitated by non-nucleophilic base, 1, 8- diazobicyclo [5.4.0]undec-7-ene (DBU), and this transformation can be accomplished over the course of 48 h in a common screw cap vial without the need for deoxygenation. Furthermore, this procedure would allow for the introduction of not only large hydrophobic chain ends to the PAA backbone, but also charged and hydrophilic species.

Initial synthetic attempts for the acrylate-terminated PtBA were performed with a 1:1 ratio of the DBU to acrylic acid according to literature procedures for PtBA macromonomers.⁸ ¹H NMR showed complete disappearance of the proton next to the bromine end group (~4.12 ppm) which indicated complete substitution of the bromine with acrylic acid. However, further analysis of this modified structure by SEC and MALDI-ToF-MS revealed bimodal molecular weight distributions (**Figure S4.42**). Although the lower molar mass distribution aligned well with the expected size of the acrylate-terminated PtBA, the second distribution

possessed twice the molecular weight of the predicted structure, suggesting an unexpected chain-chain coupling. Ultimately, control over the ratio of DBU: acrylic acid was essential in preventing coupling reactions. In fact, a modified ratio of DBU: acrylic acid (5:10) was found to produce the acrylate-terminated *Pt*BA (**2**) on 12+ gram scales with average yield recoveries of 70%. Higher reaction scales are possible, but would likely require further optimization in processing. ¹H NMR comparison of bromine-terminated *Pt*BA (**1**) to the acrylate modified product (**2**) demonstrated high conversion based on the shift of methine proton from 4.1 ppm (adjacent to bromine) to 4.6 ppm (**Figure 4.1b**, top, red and middle, green respectively). This is accompanied by the addition of three new proton peaks in the 5.5 – 6.5 ppm region, which are characteristic of the vinyl peaks for the acrylate chain end. More interestingly, under these conditions, SEC analysis reveals that low dispersity ($M_{n,SEC} = 3800$, $D = 1.1$) is maintained after the transformation from the bromine-terminated *Pt*BA to the acrylate derivative (**Figure 4.2a** and **4.2b** respectively). MALDI-ToF-MS confirms the primary molar distribution to be the addition of one *t*BA repeat unit (128 Da) per peak (**Figure 4.3**). Additionally, there is quantitative agreement between the observed and expected mass of the sodium adduct confirming the presence of a *tert*-butyl α -chain end and an acrylate ω -end group. A minor, secondary mass distribution was also observed and attributed to the cleavage of the *tert*-butyl group, which is typically detected during the ionization process of *p*(*t*BA) derivatives.¹⁸ This synthesis method provides a common route to *Pt*BA with a variety of different chain ends (**Scheme 4.1**).

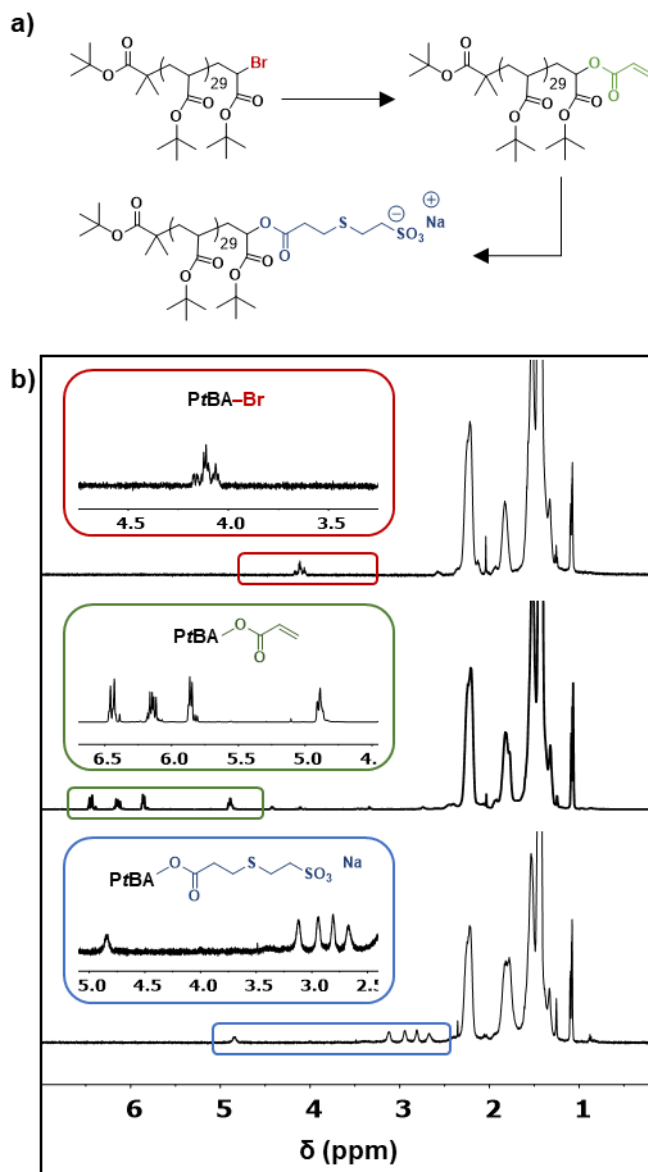


Figure 4.1 a) Synthetic scheme for the transformation of bromine-terminated PtBA to a sulfonate-terminated PtBA and b) Comparison of the ^1H NMR spectra for sulfonate-terminated PtBA and its bromine-terminated (top, red) and acrylate-terminated (middle, green) analogues. Similar spectra are obtained for each chain end of interest.

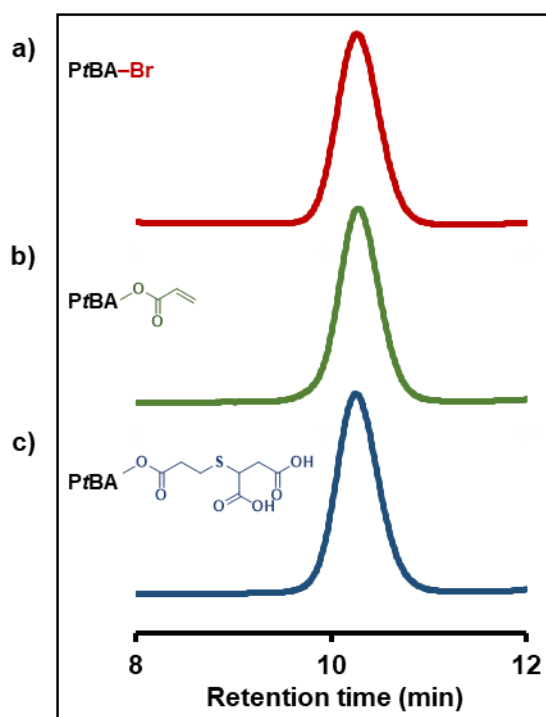


Figure 4.2 SEC comparison of an **a)** acrylate-terminated and **b)** bromine-terminated PtBA in comparison to the **c)** di-carboxylic acid analogue shows that a low molecular weight dispersity is maintained throughout all transformations. Similar comparisons are obtained for all chain end modified polymers.

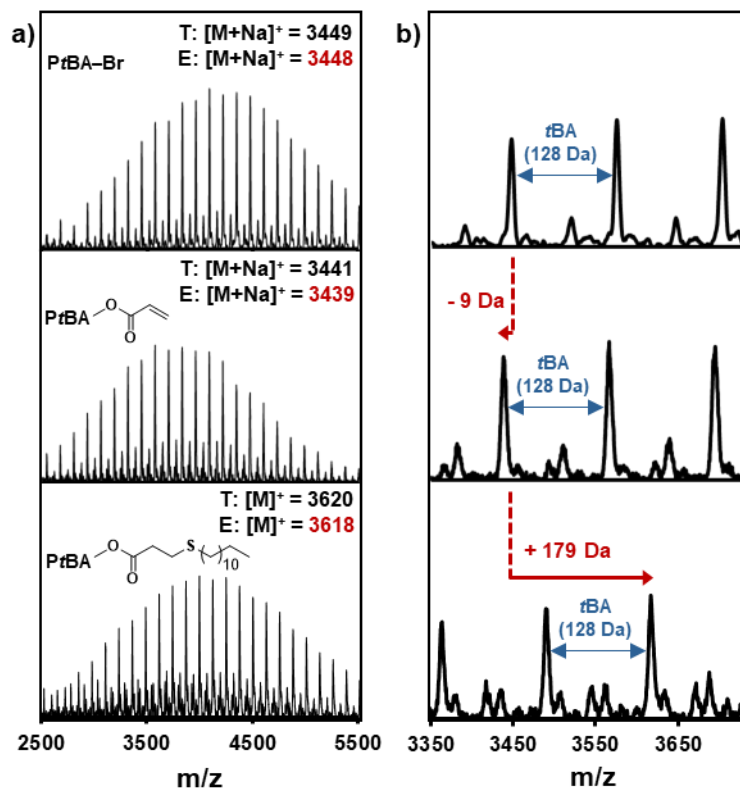


Figure 4.3 a) MALDI-ToF-MS spectrum of PtBA initiated by tB-BiB and terminated with either bromine (top), acrylate (middle), or dodecyl (bottom). **b)** The expanded view of each spectrum highlights the mass loss (9 Da) observed from the transformation of the bromine PtBA (top) to the acrylate PtBA (middle) and finally a large increase of mass (179 Da) that corresponds to the successful addition of a dodecyl chain end (bottom). Similar spectra are obtained for all unique chain ends.

4.5 Synthesis of Charged Chain End Modified PtBAs

To demonstrate the efficiency of this method in providing hydrophilic and charged end group modified PtBAs, sodium 2-mercaptoethanesulfonate, 11-mercaptoundecylphosphonic acid, 3-mercaptopropionic acid and mercaptosuccinic acid were utilized for the Michael addition with acrylate-terminated PtBA. For these transformations, two equivalents of thiol were used to “click” a sulfonate, phosphonic acid, carboxylic acid, or di-carboxylic acid group respectively to the ω -chain end of the PtBA (**Scheme 4.1**). In the presence of triethylamine, the chain end modified PtBA can be obtained with up to 80% mass recovery with high chain end fidelity as determined by ^1H NMR and MALDI-ToF-MS spectroscopy. From ^1H NMR, a slight upfield shift of the methine peak from the acrylate chain end is observed (see **Section 4.10** for full characterization). Additionally, the characteristic vinyl peaks of the acrylate chain end are replaced by several new peaks that correspond to the transformed functional group. An example of this conversion is illustrated for the sulfonate derivative where the small upfield shift from 4.90 to 4.84 ppm is observed for the methine signal (**Figure 4.1**). New proton peaks for the sulfonate end also appear from 3.19 - 2.58 ppm in lieu of the previous vinyl signals. Furthermore, SEC analysis was utilized to confirm that a low dispersion is maintained throughout all chain end modifications (**Figure 4.2**). A representative example of this characterization is demonstrated for the dicarboxylic acid derivative, showing that a monomodal peak is retained from the bromine-terminated PtBA (**Figure 4.2a**) throughout all modifications (**Figure 4.2b and 4.2c**). In order to confirm the purity for this series of chain end transformations, the Ellman’s test, which is sensitive to thiols, was conducted.¹⁹ No color change was observed when several drops of the Ellman’s test reagent

was added to a DMF solution of each polymer, demonstrating the absence of free thiol groups. Finally, MALDI-ToF-MS was used to confirm a high agreement between the expected mass for a *Pt*BA initiated by *t*B-BiB and terminated with each charged species individually. Careful analysis of the isotropic pattern for each chain end modified polymer identified a full transformation from the acrylate-terminated *Pt*BA to each of the sulfonate, phosphonic acid, carboxylic acid, or dicarboxylic acid ω -terminated *Pt*BA derivatives respectively (See **Section 4.10** for full characterization).

4.6 Synthesis of Dodecyl-Terminated *Pt*BA

The ability to introduce a hydrophobic chain end to a comparatively hydrophilic polymer, such as poly(acrylic acid), is desirable for a number of applications such as scale inhibition, dispersants, and surfactants.² Direct S_N2 reaction of thiols with bromine-terminated poly(acrylates)¹⁸ or the use of initiators with long alkyl chains for ATRP,¹² either fail to incorporate highly charged species or require the use of increased amount of thiol.

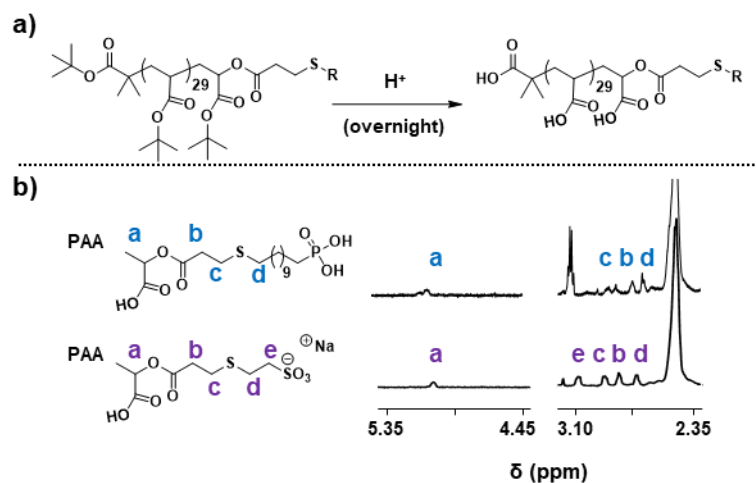
To demonstrate the efficiency of this new method, we chose to compare the synthesis of a dodecyl-terminated *Pt*BA via S_N2 transformation to our thiol-ene “click” procedure. While the S_N2 transformation of bromine-terminated *Pt*BA to dodecyl-terminated *Pt*BA required ~10 equivalents of both thiol and base, the thiol-ene “click” reaction from our procedure utilized only 2 equivalents of dodecanethiol and catalytic amounts of triethylamine (TEA) to produce *Pt*BA with hydrophobic chain end (**Figure S4.6-S4.10**). ¹H NMR comparison reveals the high chain end fidelity for each reaction where a shift of the methine proton near the bromine or acrylate end group respectively was observed (**Figure S4.11** and **S4.43**). In the case of the thiol-ene “click” reaction, the vinyl peaks which are characteristic of the acrylate chain end

disappear with a corresponding appearance of new proton peaks for the dodecyl end-group (**Figure S4.11**). Furthermore, SEC characterization showed that polymers prepared *via* both methods possessed a narrow molar mass distribution (**Figure S4.12** and **S4.44**). MALDI-ToF-MS spectroscopy was further used to confirm the initial mass loss (9 Da) that is expected for the transformation of the bromine-terminated *PtBA* to the acrylate-terminated *PtBA* along with the large mass increase (179 Da) that is observed with the final incorporation of the dodecyl ω -chain end (**Figure 4.3**). This analysis served to confirm the near quantitative agreement of the expected and observed mass for a *tB*-BiB initiated and dodecyl-terminated *PtBA*.

4.7 Synthesis of Chain End Modified PAA: From Hydrophobic to Charged Species

With an efficient method for synthesis of the *PtBA* derivatives on hand, a simple deprotection of the *t*-butyl groups with trifluoroacetic acid (TFA) will produce the targeted PAA derivatives in > 95% yield (**Figure 4.4a**). This can be accomplished in a screw cap vial after an overnight reaction and the pure deprotected polymer can then be recovered from precipitation into hexanes. Full deprotection of the backbone and initiator can be confirmed by ^1H NMR in deuterated methanol where the methyl peak corresponding to the *t*-butyl groups disappears and the protons of the *PtBA* backbone shift (see **Section 4.10** for full characterization). Furthermore, if deuterated TFA is added to the NMR sample, the residual water peak (~ 4.9 ppm) can be shifted downfield to reveal chain end peaks which are much more defined, confirming high chain end fidelity (**Figure S4.40**). Comparison of three representative PAA derivatives highlights this retention of end groups (**Figure 4.4**, see

Section 4.10 for full spectra). It is important to note that the unique chain end signals for each of these derivatives can still be identified after full deprotection, demonstrating that all chain ends remain intact.



4.8 Conclusion

A general method for the preparation of poly(acrylic acid)s with uniquely modified ω -chain ends was introduced. This synthetic framework utilizes an acrylate-terminated poly(*tert*-butyl acrylate) polymer to selectively “click” a variety of chain end species (from hydrophobic to hydrophilic and charged groups) to a narrowly disperse P*t*BA. A simple deprotection of the *t*-butyl groups on the backbone then produces a well-defined poly(acrylic acid) with distinctive chain end chemistries. The structural fidelity of these materials was verified through ^1H NMR spectroscopy, SEC, and MALDI-ToF-MS. This transformation can be accomplished under ambient conditions and with limited thiol equivalence in multi-gram scales, thus expanding the

utility of this process for industrial applications. Moreover, this method provides the tools necessary to access a greater range of modified poly(acrylic acid)s so that a more complete catalog of potential PAA derivatives can be screened for any given application.

4.9 Experimental

4.9.1 Materials and equipment

All chemicals were used as received without further purification unless otherwise noted. Copper (II) bromide, trifluoroacetic acid (TFA), *tert*-butyl α -bromoisobutyrate, 1,8-Diazabicyclo[5.4.0]undec-7-ene (DBU), triethylamine (TEA), sodium 2-mercaptoethanesulfonate, and 11-mercaptopundecylphosphonic acid were obtained from *Sigma Aldrich*. Tris[2-(dimethylamino)ethyl]amine (Me₆-Tren), 1-dodecanethiol, acrylic acid, 3-mercaptopropionic acid, and mercaptosuccinic acid were obtained from *Fisher Scientific*. *Tert*-butyl acrylate (TBA) monomer was also received from *Sigma Aldrich* and passed through a column of basic alumina (~150 mesh, Brockmann I grade) prior to use in order to remove the inhibitor.

Nuclear magnetic resonance spectra were recorded on a Varian spectrometer (600 MHz) and were reported in δ units, parts per million (ppm) and determined with residual signals of the deuterated solvents (CDCl₃, 7.26 ppm or MeOD, 3.31 ppm). Size exclusion chromatography (SEC) for molecular weight analysis, relative to linear polystyrene standards, was performed on a Waters e2695 separation module equipped with a Waters 2414 refractive index and 2996 photodiode array detector using THF as eluent at a flow rate of 0.3 mL/min. Fourier Transform Infrared (FT-IR) spectroscopy was measured on a Nicolet iS10 FT-IR

spectrometer equipped with a Smart Diamond ATR accessory in transmission mode for 64 scans. Matrix-assisted laser desorption ionization time of flight mass spectrometry was conducted using a Bruker Microflex LRF MALDI-ToF-MS, equipped with a 60 Hz nitrogen laser at 337 nm. Solutions in DCM/ chloroform of dithranol were used as a matrix and 0.7 μ L sample (10 μ g/ mL) was applied to the target plate. Spectra were recorded in linear mode.

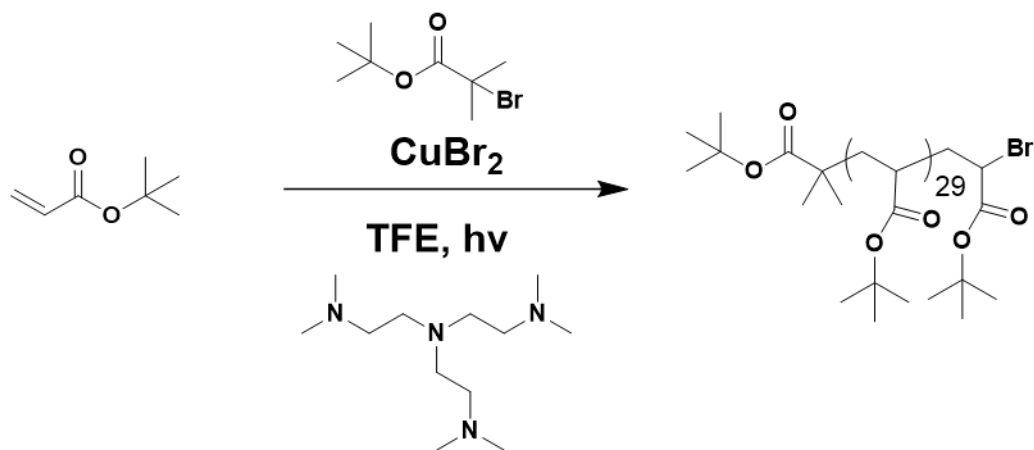
4.10 Supplemental Results

4.10.1 Bromine-terminated PtBA: synthesis and characterization

General conditions for the polymerization of tert-butyl acrylate (tBA) utilizing photo induced ATRP

Bromine-terminated PtBA was synthesized following a slightly modified literature protocol.¹⁸ Copper (II) bromide (CuBr_2) (9.3 mg, 0.04 mmol, 0.02 equiv.) was suspended in 2,2,2-trifluoroethanol (TFE) (10.0 mL) in a scintillation vial equipped with magnetic stir bar. Tris[2-(dimethylamino)ethyl]amine ($\text{Me}_6\text{-Tren}$) (58.0 mg, 67 μ L, 0.25 mmol, 0.12 equiv.) was then added to this heterogeneous mixture and sonicated until all copper was dissolved. Then filtered (passed through a short column of basic alumina) tBA (10.0 g, 11.4 mL, 78.0 mmol, 37.5 equiv.) followed by tB-BiB (0.46 g, 0.39 mL, 2.08 mmol, 1.0 equiv.) were added to the vial before sealing the vial with a septum and purging with nitrogen for 15 min. Polymerization commenced upon exposure of the degassed reaction mixture to UV light. Samples were taken periodically and conversions were measured using ^1H NMR spectroscopy. A degree of polymerization (DP) = 30 (~80% conversion) was obtained within 4 hr and the copper residue was removed *via* precipitation into cold, stirring methanol/ water (1:1). The product was then dried in a vacuum oven (final yield: 85%).

^1H NMR (600 MHz, CDCl_3 , δ): 4.20 – 4.02 (m, CH_2CHBr at terminal repeat unit), 2.38 – 2.09 (m, CH_2CH of backbone), 1.95 – 1.49 (m,m, aliphatic protons of backbone), 1.49 -1.27 (*tert*-butyl protons of backbone and initiator), 1.11 – 1.05 (2 x CH_3 of initiator). SEC (THF, RI, PS standard): $M_n = 3800 \text{ g mol}^{-1}$, $\text{Đ} = 1.11$. MALDI-ToF-MS: calc'd for $\text{C}_{183}\text{H}_{315}\text{BrNaO}_{52}$, $[\text{M}+\text{Na}]^+ = 3449.3$; observed = 3447.8.



Scheme S4.1 Synthetic scheme for photo-initiated ATRP to make bromine-terminated PtBA starting material.

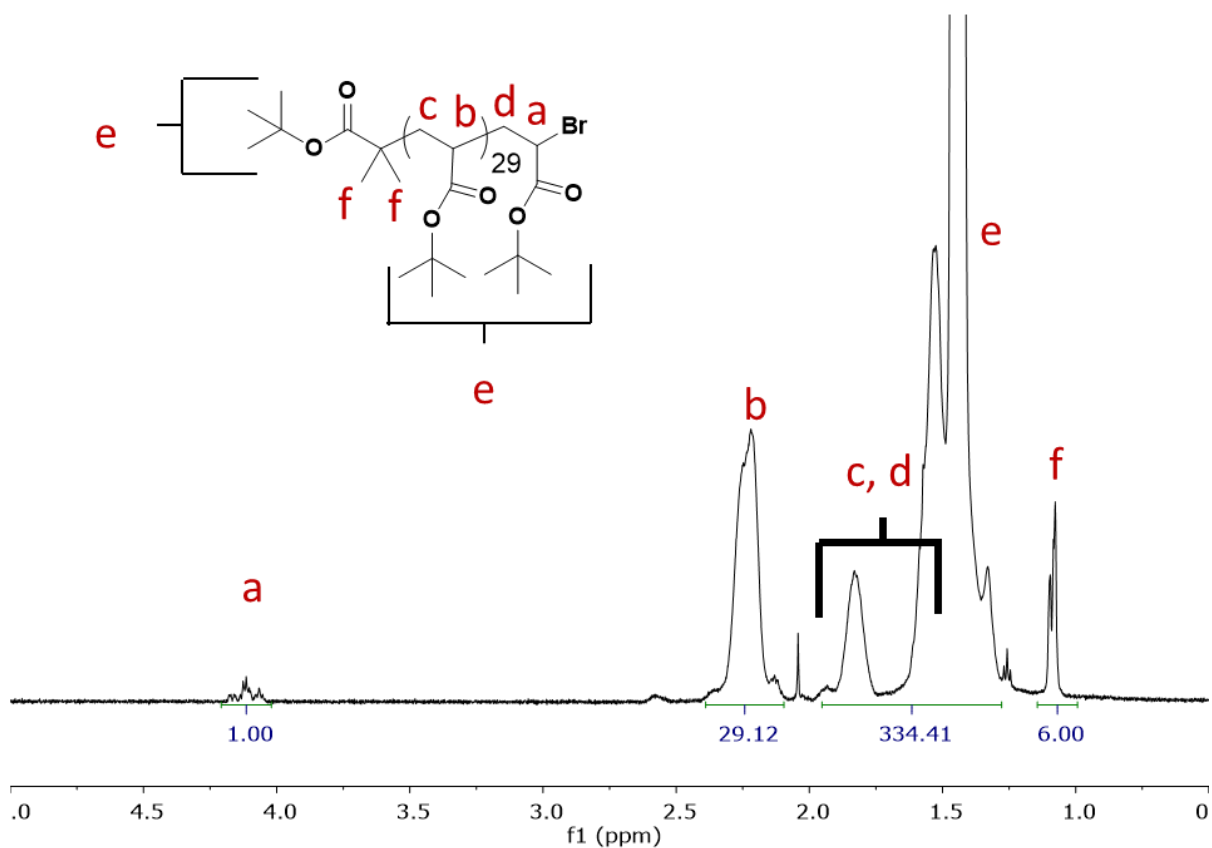


Figure S4.1 ¹H NMR of bromine-terminated PtBA (DP = 30) obtained via UV-mediated ATRP. Quantitative comparison of the methine proton *a* and the methyl hydrogens *f* indicate high chain end fidelity is achieved (*f* ~100%).

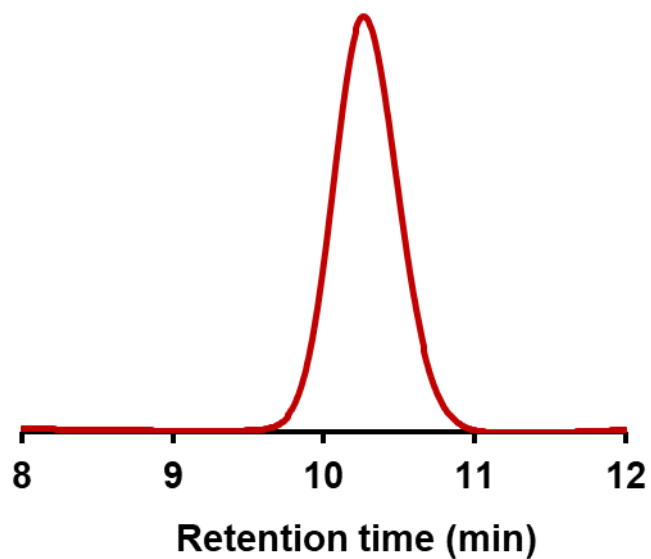


Figure S4.2 SEC trace of bromine-terminated PtBA ($DP = 30$, $M_n = 3800 \text{ g mol}^{-1}$, $\mathcal{D} = 1.11$).

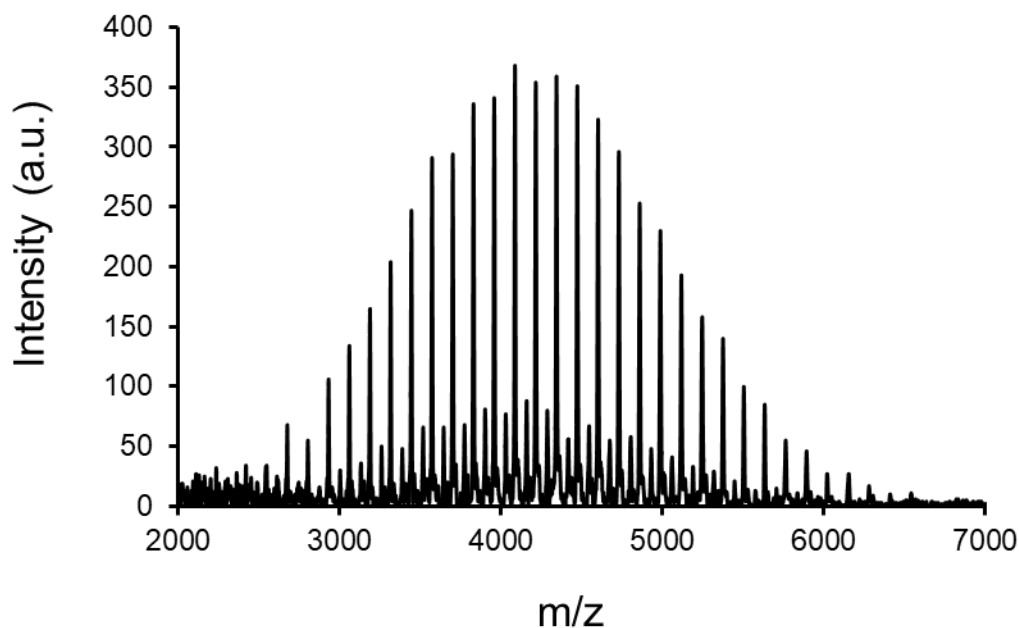


Figure S4.3 MALDI-ToF-MS distribution of bromine-terminated PtBA

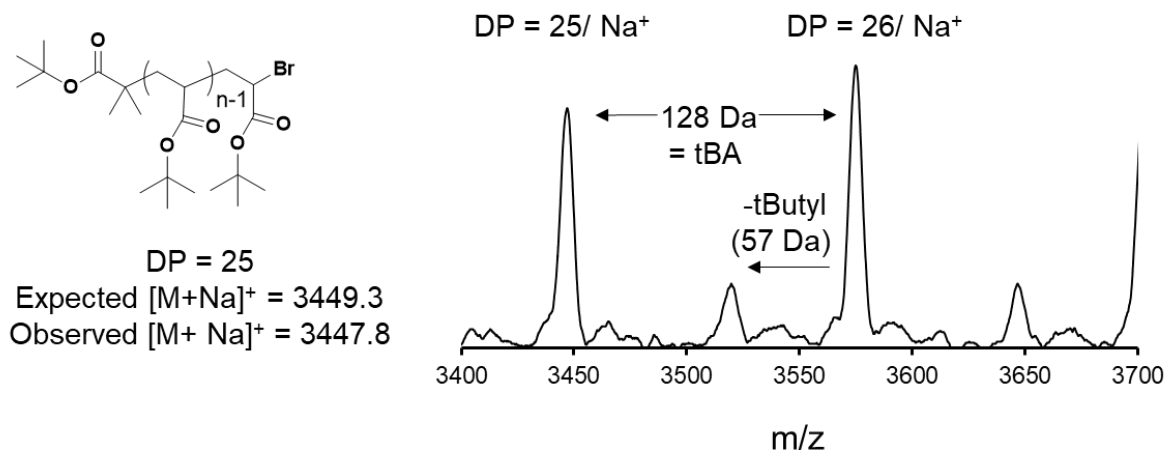


Figure S4.4 An expanded view of the MALDI-ToF-MS spectrum shows an even spacing between peaks corresponding to one *t*BA repeat unit. Agreement between the expected and observed mass of the sodium adduct indicates an accurate assignment of the expected structure and chain ends. Note an additional set of polydisperse peaks is observed corresponding to loss of a *t*BA group during ionization.

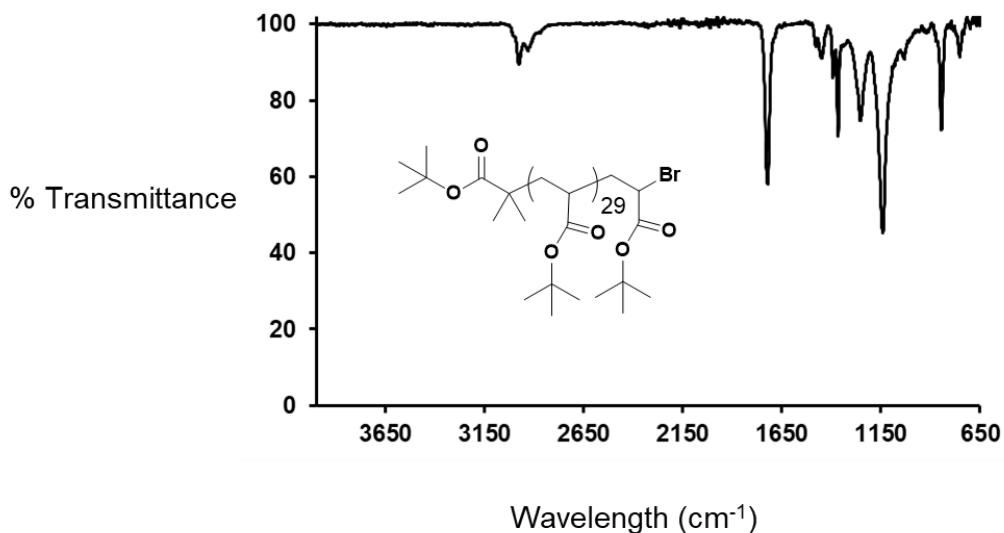
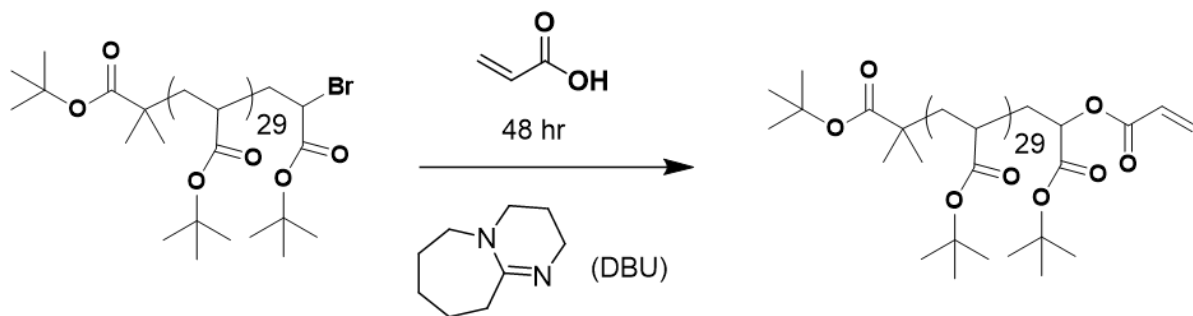


Figure S4.5 FT-IR analysis for bromine-terminated *Pt*BA derivative showing a sharp signal corresponding to *t*BA groups.

4.10.2 Acrylate-terminated PtBA: synthesis and characterization

Acrylate-terminated PtBA was synthesized following a modified literature procedure.⁸ Bromine-terminated PtBA (6.0 g, 1.5 mmol, 1.0 equiv.) was dissolved in dimethylformamide (DMF) (12.0 mL) in a scintillation vial equipped with magnetic stir bar. To this, DBU (1.1 g, 1.1 mL, 7.5 mmol, 5.0 equiv.) was added followed immediately by the slow and dropwise addition of acrylic acid while stirring (1.1 g, 1.0 mL, 15 mmol, 10.0 equiv.). This vial was sealed and the reaction was left to proceed for 48 h. The acrylic acid was then quenched by adding the entire reaction solution dropwise to 160.0 mL saturated sodium bicarbonate (aqueous) solution. To this, 160.0 mL ethyl acetate was added to dissolve the polymer. The two layers are allowed to separate. The organic layer is then extracted three more times. The first with 160.0 mL sodium bicarbonate solution, the second with 160.0 mL brine, and finally with 160.0 mL deionized water. Any emulsions are separated by adding brine to the mixture (final yield: 70%).

¹H NMR (600 MHz, CDCl₃, δ): 6.50 – 5.80 (3 x vinyl proton at chain end), 4.95 – 4.83 (CH₂CH of terminal repeat unit), 2.43 – 2.00 (m, CH₂CH of backbone), 2.00 – 1.49 (m, aliphatic protons of backbone), 1.49 – 1.29 (*tert*-butyl protons of backbone and initiator), 1.11 – 1.05 (2 x CH₃ of initiator). SEC(THF, RI, PS standard): M_n = 3800 g mol⁻¹, Đ = 1.11. MALDI-ToF-MS: calc'd for C₁₈₆H₃₁₈NaO₅₄, [M+Na]⁺ = 3441.4; observed = 3438.8.



Scheme S4.2 Reaction scheme for synthesis of acrylate-terminated PtBA. Precise control over acrylic acid: DBU ratio (10:5) is essential to prevent unwanted side reactions.

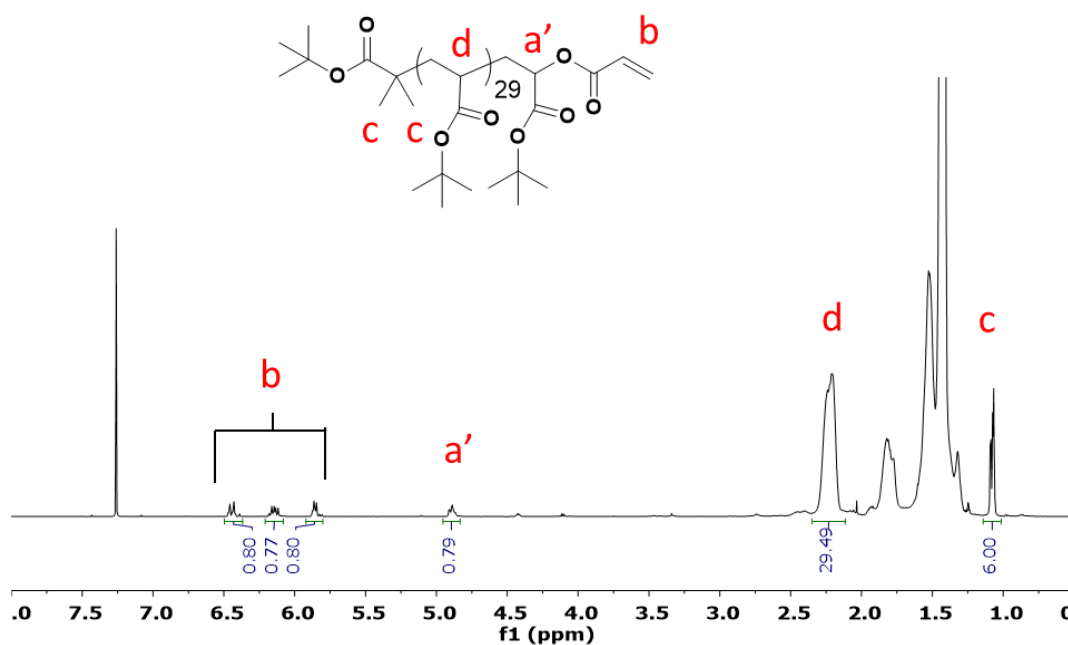


Figure S4.6 ^1H NMR spectroscopy for the newly prepared acrylate-terminated PtBA demonstrates the formation of highly characteristic vinyl peaks from $\delta = 5.5 - 6.5$ ppm along with a high chain end fidelity.

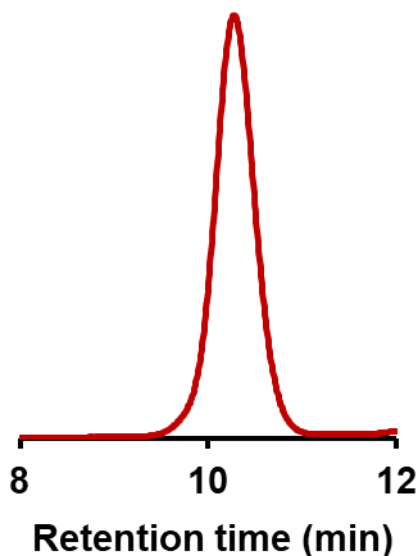


Figure S4.7 Size exclusion chromatography (THF) of acrylate-terminated *Pt*BA displaying the retention of low dispersity material after transformation from the bromine-terminated starting material ($DP = 30$, $M_n = 3800 \text{ g mol}^{-1}$, $D = 1.11$).

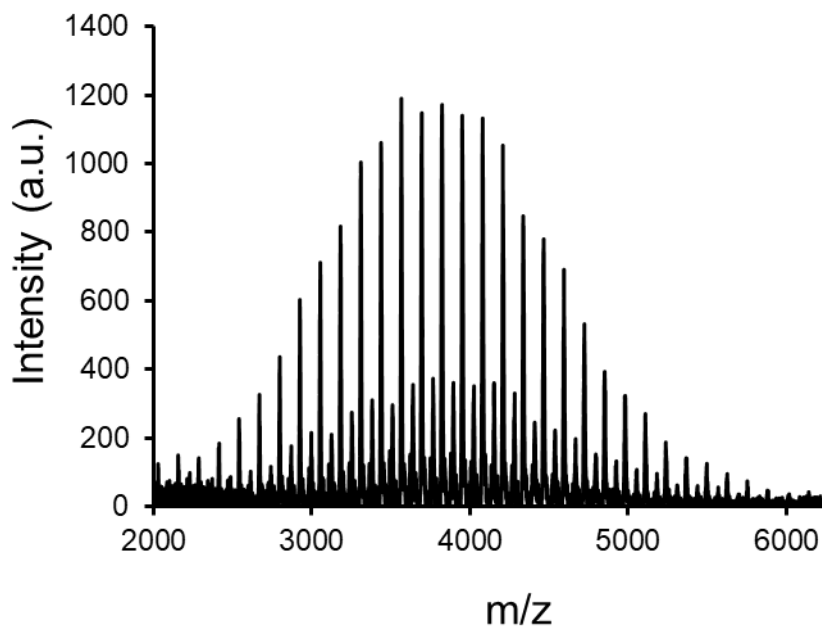


Figure S4.8 MALDI-ToF-MS spectrum of *Pt*BA initiated by *t*B-BiB and possessing an acrylate chain end.

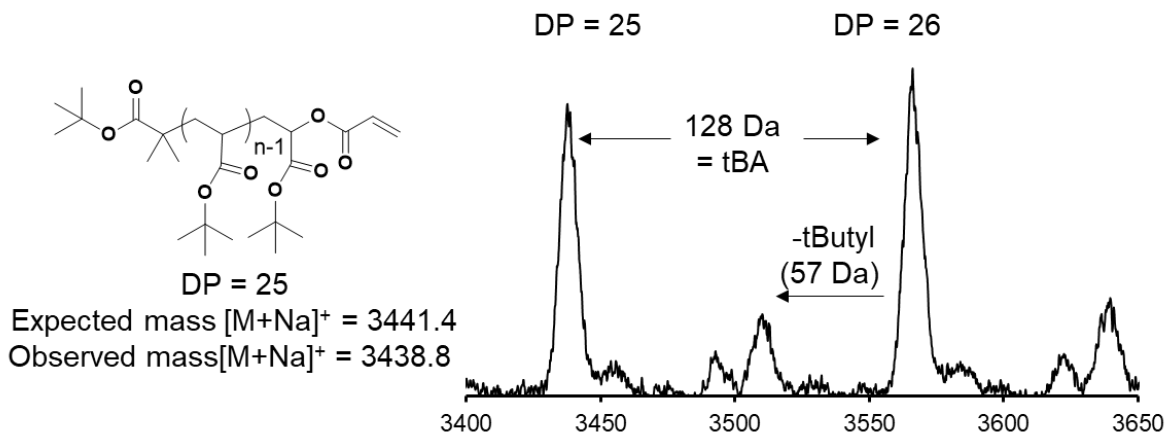


Figure S4.9 Expanded view of the *PtBA* showing a major set of polydisperse peaks corresponding to acrylate chain end and one minor distribution corresponding to loss of a *tert*-butyl group. Close agreement between the expected and observed mass of the sodium adduct indicates an accurate assignment of the expected structure and chain ends.

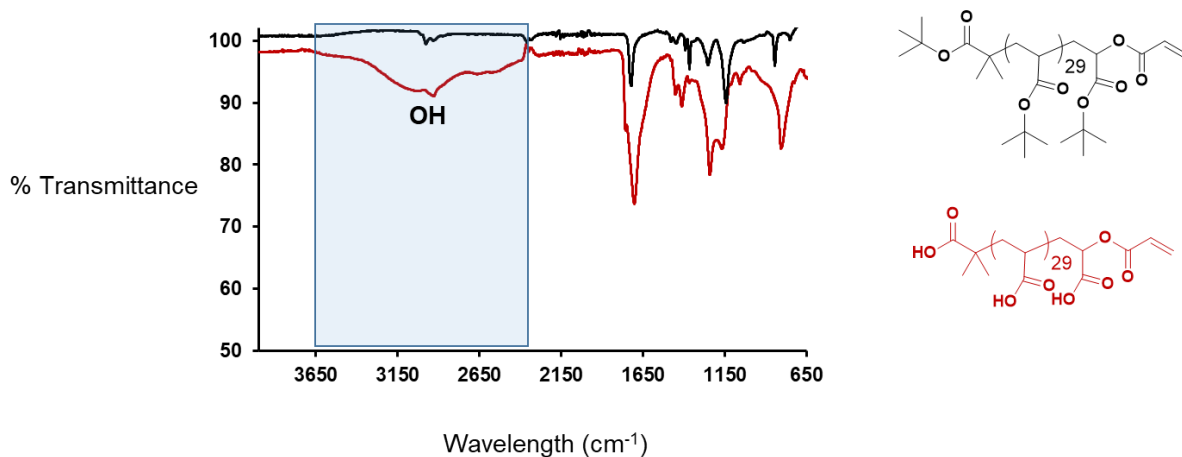


Figure S4.10 Comparison of acrylate-terminated *PtBA* (black) and acrylate-terminated PAA (red) by FT-IR shows the appearance of a broad OH peak signaling the deprotection of the *tBA* groups.

4.10.3 Dodecyl-terminated PAA: synthesis and characterization

Acrylate-terminated PtBA (3.0 g, 0.75 mmol, 1.0 equiv.) was dissolved in dimethylformamide (DMF) (6.0 mL) in a scintillation vial equipped with magnetic stir bar. To this 1-dodecanethiol (304 mg, 0.36 mL, 1.5 mmol, 2.0 equiv.) and triethylamine (15.0 mg, 21 μ L, 0.15 mmol, 0.2 equiv.) were added. The vial was then sealed with a cap and the reaction was left to proceed overnight for approximately 15 h. The DMF and TEA were removed *via* rotary evaporation of a toluene: DMF (3:1) azeotrope. This crude product was then dissolved in TFA (3.0 mL) in a scintillation vial equipped with magnetic stir bar and sealed with a screw cap then allowed to react overnight, under a N₂ purge, for approximately 15 h. The TFA was then evaporated *via* rotary evaporation and the crude product was dissolved in minimal THF before precipitating into cold, stirring hexanes. The product was then rinsed with cold hexanes and dried *in vacuo* (final yield: 82%).

PtBA intermediate: ¹H NMR (600, CDCl₃, δ): 4.91 – 4.60 (CH₂CH of terminal repeat unit), 2.83 – 2.70 (bt, COOCH₂CH₂ at chain end), 2.70 – 2.55 (bt, COOCH₂CH₂ at chain end), 2.55 – 2.45 (bt, SCH₂(CH₂)₁₀CH₃ at chain end), 2.43 – 2.00 (m, CH₂CH of backbone), 2.00 – 1.49 (m, aliphatic protons of backbone), 1.49 – 1.29 (*tert*-butyl protons of backbone and initiator), 1.29 – 1.19 (SCH₂(CH₂)₁₀CH₃ at chain end), 1.11 – 1.05 (2 x CH₃ of initiator), 0.90 – 0.85 (bt CH₃ of chain end). SEC (THF, RI, PS standard): M_n = 4200 g mol⁻¹, Đ = 1.10. MALDI-ToF-MS: calc'd for C₁₉₈H₃₄₄O₅₄S, [M]⁺ = 3620.5; observed = 3617.6.

PAA product: ^1H NMR (600 MHz, MeOD + TFA-d, δ): 5.10 – 4.98 (CH_2CH of terminal repeat unit), 2.80 – 2.55 (m,m,m, $\text{COOCH}_2\text{CH}_2\text{SCH}_2$ at chain end), 2.55 – 2.30 (m, CH_2CH of backbone), 2.10 – 1.32 (m, aliphatic protons of backbone), 1.32 – 1.20 (10 x CH_2 of chain end), 1.19 – 1.10 (2 x CH_3 of initiator), 0.86 – 0.82 (m, CH_3 of chain end).

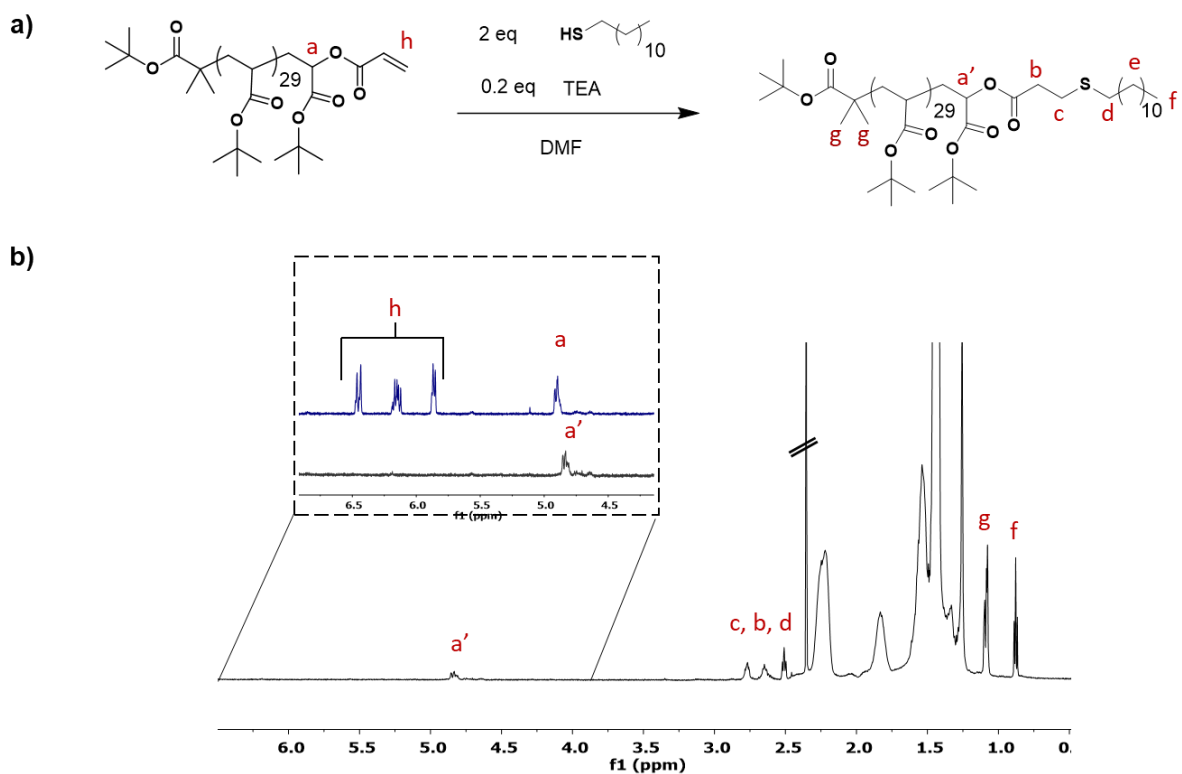


Figure S4.11 a) Reaction scheme for transformation of acrylate-terminated PtBA to a hydrophobic, dodecyl-terminated PtBA. b) ^1H NMR spectroscopy for dodecyl-terminated PtBA showing < 5% acrylate-terminated starting material remaining (inset denoted *a* and *h*).

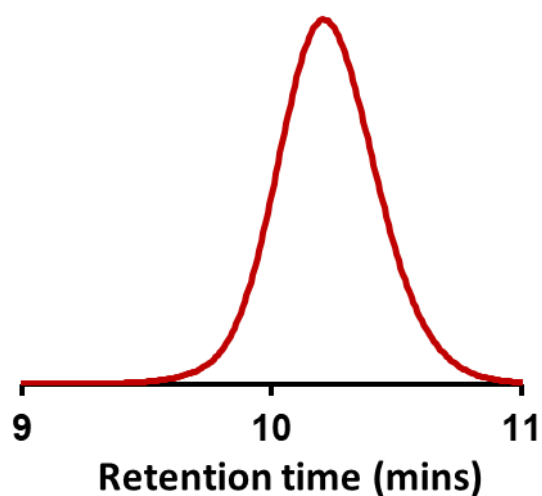


Figure S4.12 SEC (THF) trace after the transformation of the acrylate-terminated *Pt*BA to the dodecyl-terminated derivative. A low dispersity is maintained ($DP = 30$, $M_n = 4200 \text{ g mol}^{-1}$, $\mathcal{D} = 1.10$).

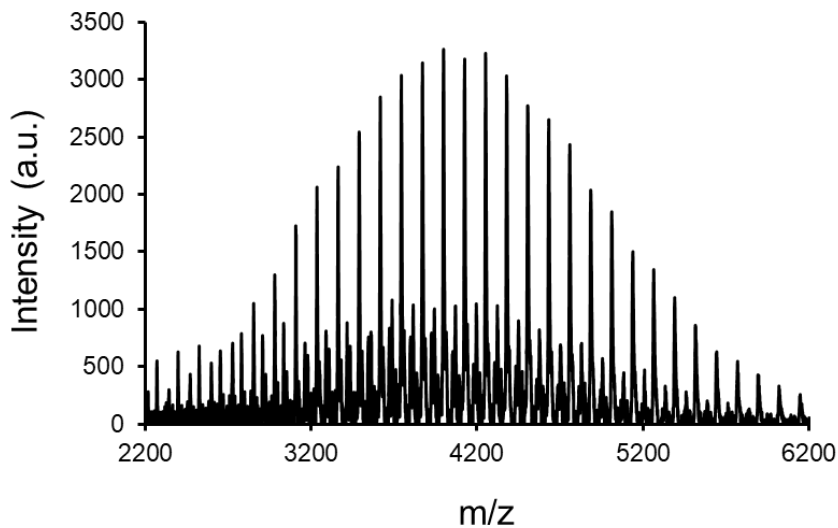
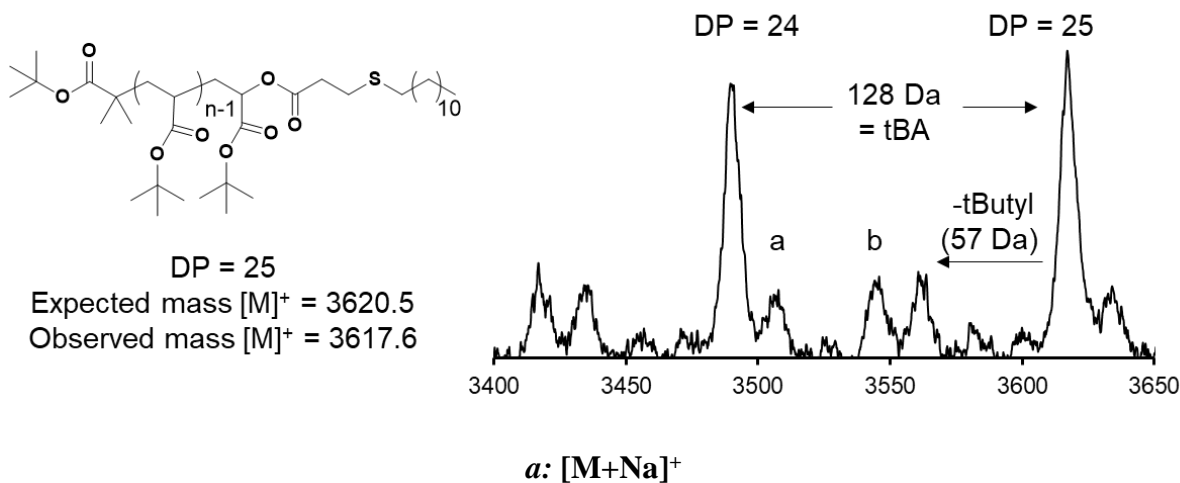
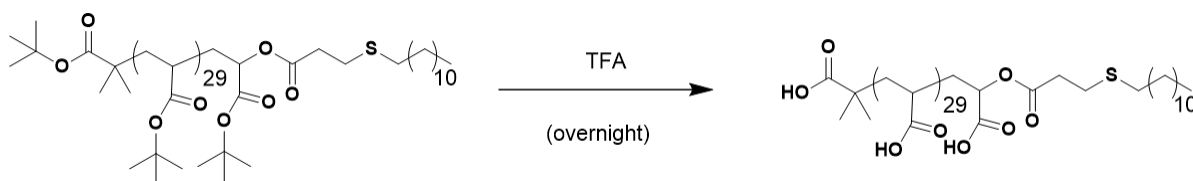


Figure S4.13 MALDI-ToF-MS spectrum of *Pt*BA initiated by *t*B-BiB and possessing a dodecyl chain end.



b: acrylate-terminated PtBA (< 5% by 1H NMR)

Figure S4.14 Expanded view of the PtBA derivative showing a major set of polydisperse peaks corresponding to dodecyl chain end and three minor distributions corresponding to either loss of *tert*-butyl group, PtBA with sodium adduct (labeled *a*), or the acrylate-terminated starting material (labeled *b*). NMR spectroscopy shows the remaining acrylate-terminated PtBA content to be < 5%. Agreement between the expected and observed mass of the sodium adduct indicates an accurate assignment of the expected structure and chain ends.



Scheme S4.3 Reaction scheme for deprotection of PtBA terminated with hydrophobic dodecyl group with TFA to produce the targeted dodecyl-terminated PAA.

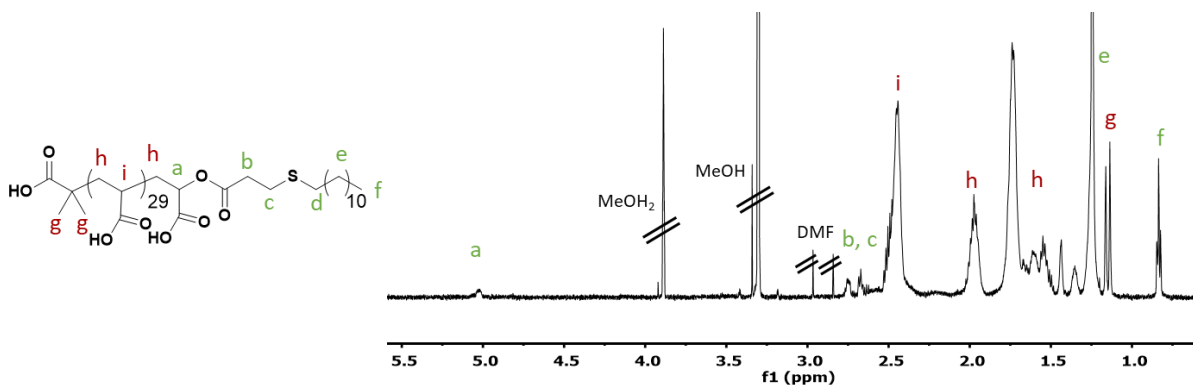


Figure S4.15 ^1H NMR spectroscopy for dodecyl-terminated PAA in deuterated methanol with added d-TFA. Addition of acid allows for full identification of chain ends.

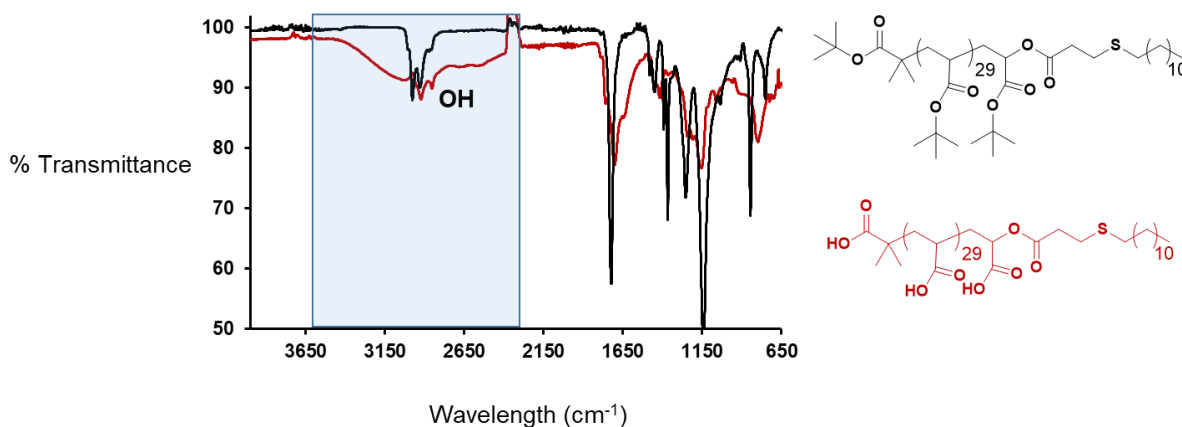


Figure S4.16 Comparison of dodecyl-terminated PtBA (black) and dodecyl-terminated PAA (red) by FT-IR shows the appearance of a broad OH peak and the disappearance of the sharp tBA peaks.

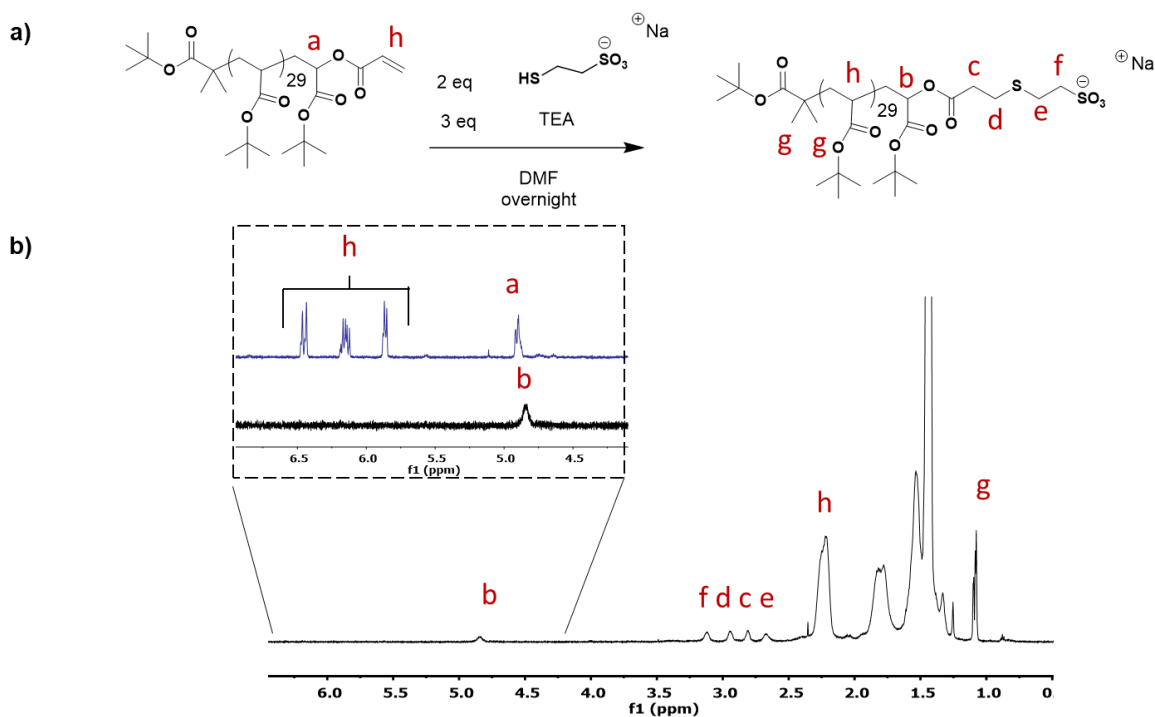
4.10.4 Sulfonate-terminated PAA: synthesis and characterization

Acrylate-terminated PtBA (3.5 g, 0.88 mmol, 1.0 equiv.) was dissolved in dimethylformamide (DMF) (7.0 mL) in a scintillation vial equipped with magnetic stir bar. To this, sodium 2-mercaptoethanesulfonate (290 mg, 1.76 mmol, 2.0 equiv.) and triethylamine (267 mg, 368 μL , 2.64 mmol, 3.0 equiv.) were added. The vial was then sealed with a screw

cap and the reaction was left to proceed overnight for approximately 15 h. The DMF and TEA were removed *via* rotary evaporation of a toluene: DMF (3:1) azeotrope. This crude product was then dissolved in minimal THF and then precipitated into stirring MeOH: H₂O (1:1) to remove residual thiol. The resulting *Pt*BA intermediate was then dissolved in TFA, (3.0 mL) in a scintillation vial equipped with magnetic stir bar and sealed with a screw cap then allowed to react overnight, under a N₂ purge, for approximately 15 h. Finally, TFA was removed *via* rotary evaporation (final yield: 80%).

*Pt*BA intermediate: ¹H NMR (600, CDCl₃, δ): 4.91 – 4.74 (CH₂CH of terminal repeat unit), 3.19 – 3.03 (m, SCH₂CH₂SO₃ at chain end) 3.03 – 2.88 (m, COOCH₂CH₂ at chain end), 2.88 – 2.75 (m, SCH₂CH₂SO₃ at chain end), 2.75 – 2.58 (m, SCH₂CH₂SO₃ at chain end), 2.43 – 2.00 (m, CH₂CH of backbone), 2.00 – 1.49 (m, aliphatic protons of backbone), 1.49 – 1.29 (*tert*-butyl protons of backbone and initiator), 1.11 – 1.05 (2 x CH₃ of initiator). Note that SEC characterization was not completed due to incompatibility of charged chain end with SEC column. MALDI-ToF-MS: calc'd for C₁₈₃H₃₁₁NaO₅₇S₂, [M+Na]⁺ – *t*-butyl = 3676.5; observed = 3674.7.

PAA product: ¹H NMR (600 MHz, MeOD + TFA-d, δ): 5.10 – 4.98 (CH₂CH of terminal repeat unit), 3.15 – 3.03 (m, CH₂SO₃ at chain end), 2.98 – 2.88 (m, COCH₂CH₂S at chain end), 2.88 – 2.76 (COCH₂CH₂S at chain end), 2.76 – 2.67 (SCH₂CH₂SO₃ at chain end), 2.66 – 2.30 (m, CH₂CH of backbone), 2.10 – 1.32 (m, aliphatic protons of backbone), 1.19 – 1.10 (2 x CH₃ of initiator).



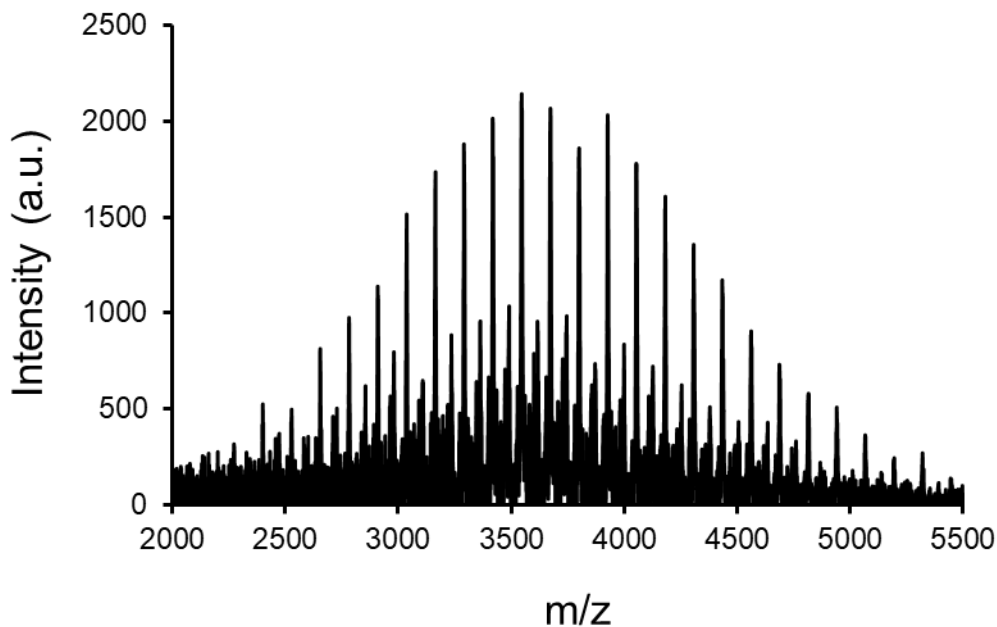


Figure S4.18 MALDI-ToF-MS spectrum shows sulfonate-terminated and *t*B-BiB initiated *Pt*BA.

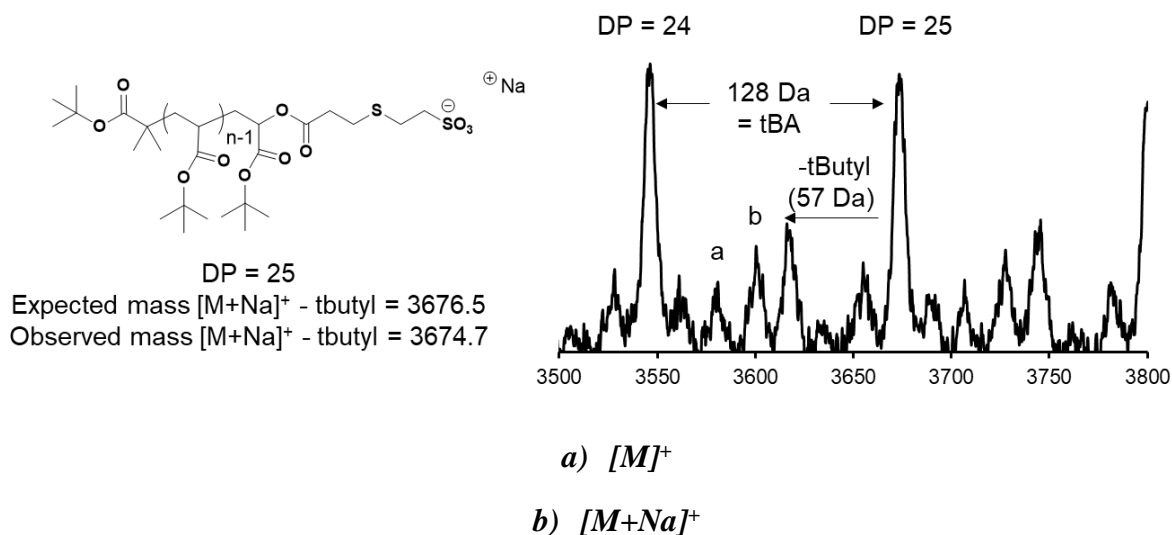
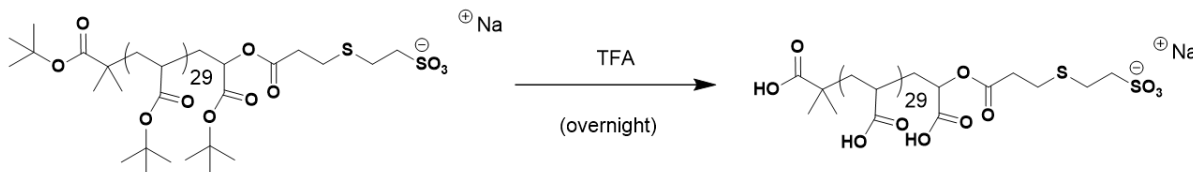


Figure S4.19 Expanded view of the sulfonate-terminated *Pt*BA shows an even spacing (128 Da) between peaks corresponding to addition of one *t*BA repeat unit per peak. Near quantitative agreement between the expected and observed mass of the sodium adduct with the loss of *tert*-butyl group indicates an accurate assignment of the expected structure and chain ends. Alternative distributions include loss of *t*-Butyl group during ionization, the sulfonate-terminated product sans sodium ion (**a**), and the sodium adduct of the sulfonate-terminated *Pt*BA (**b**).



Scheme S4.4 Reaction scheme for formation of sulfonate-terminated PAA via deprotection of PABA derivative with TFA.

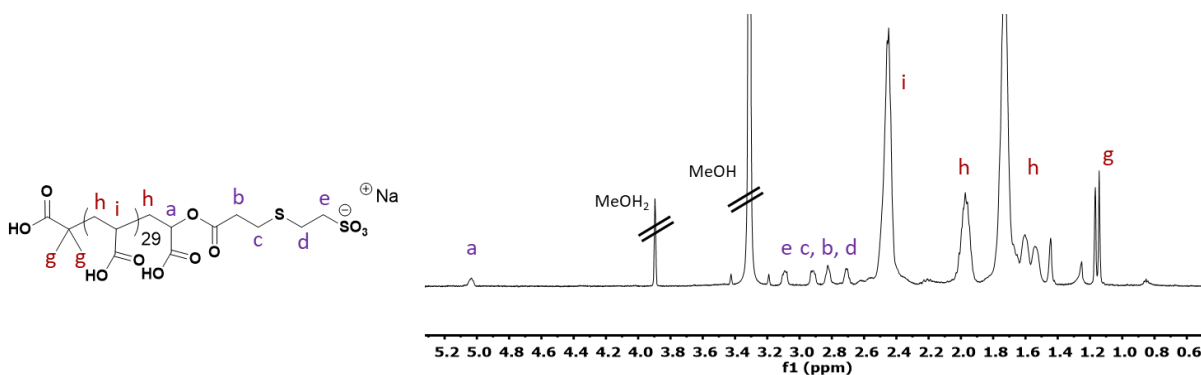


Figure S4.20 ^1H NMR spectroscopy of sulfonate PAA derivative showing clearly defined chain end peaks. This confirms that chain end fidelity is maintained throughout deprotection of PABA.

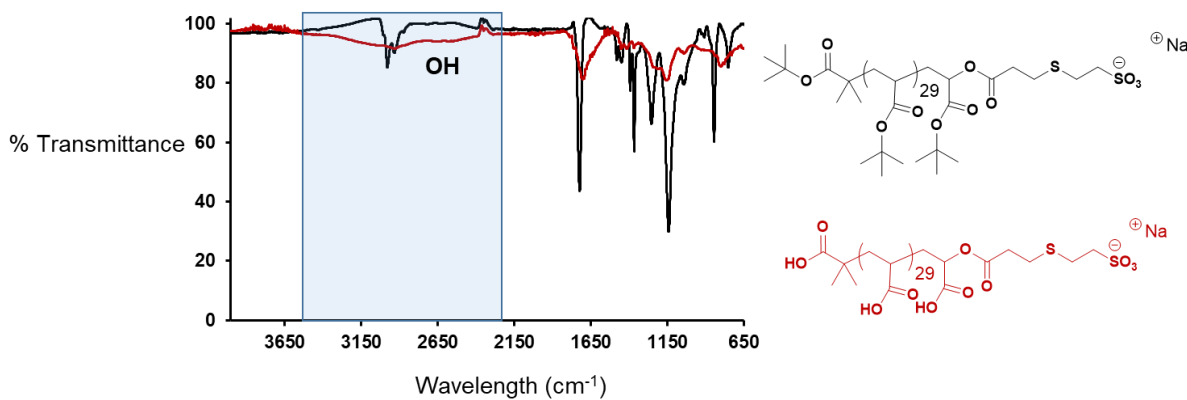


Figure S4.21 FR-IR comparison of the sulfonate-terminated PABA (black) with its deprotected PAA counterpart (red) reveals the appearance of a broad OH peak to signify deprotection of *t*BA groups.

4.10.5 Phosphonic acid-terminated PAA: synthesis and characterization

The synthesis and work up for this compound was identical to that of the dodecyl-terminated PAA except that the substitution occurred with 2.0 equiv. of 11-mercaptoundecylphosphonic acid and 3.0 equiv. of triethylamine rather than 2.0 equiv. of 1-dodecanethiol and 0.2 equiv. of triethylamine (final yield: 75%).

PtBA intermediate: ^1H NMR (600, CDCl_3 , δ): 4.91 – 4.74 (CH_2CH of terminal repeat unit), 2.83 – 2.43 (m, m, m, $\text{COOCH}_2\text{CH}_2\text{SCH}_2$ at chain end), 2.43 – 2.00 (m, CH_2CH of backbone), 2.00 – 1.49 (m, aliphatic protons of backbone and 6H at chain end), 1.49 – 1.29 (*tert*-butyl protons of backbone and initiator), 1.29 – 1.19 (14H at chain end), 1.11 – 1.05 (2 x CH_3 of initiator). Note that SEC characterization was not completed due to incompatibility of chain end with SEC column. MALDI-ToF-MS: calc'd for $\text{C}_{197}\text{H}_{342}\text{Na}_2\text{O}_{57}\text{PS}$, $[\text{M}+2\text{Na}-\text{H}]^+$ – *t*-butyl = 3673.5; observed = 3674.5.

PAA product: ^1H NMR (600 MHz, MeOD + TFA-*d*, δ): 5.12 – 5.00 (CH_2CH at terminal repeat unit), 2.94 – 2.60 (m, m, m, $\text{COOCH}_2\text{CH}_2\text{SCH}_2$ at chain end), 2.60 – 2.30 (m, CH_2CH of backbone), 2.10 – 1.30 (m, aliphatic protons of backbone and 6H at chain end), 1.30 – 1.20 (14H at chain end), 1.20 – 1.08 (2 x CH_3 of initiator). ^{31}P (600, MeOD, δ) 30.44 – 26.18 (bs).

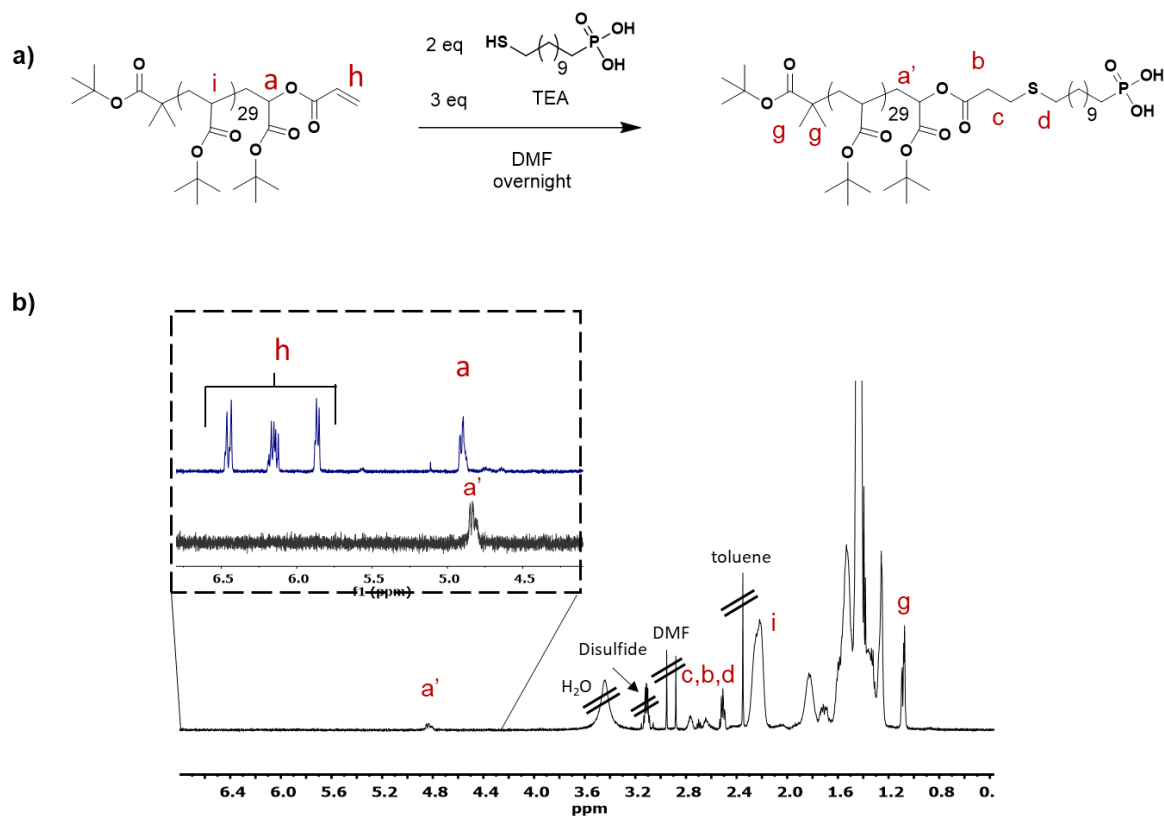


Figure S4.22 a) Synthesis of the phosphonic-terminated PtBA and b) ^1H NMR spectrum showing loss of vinyl peaks for acrylate-terminated starting material (inset: upper blue trace) and providing evidence of phosphonic acid chain end creation (labeled a' and $b-d$).

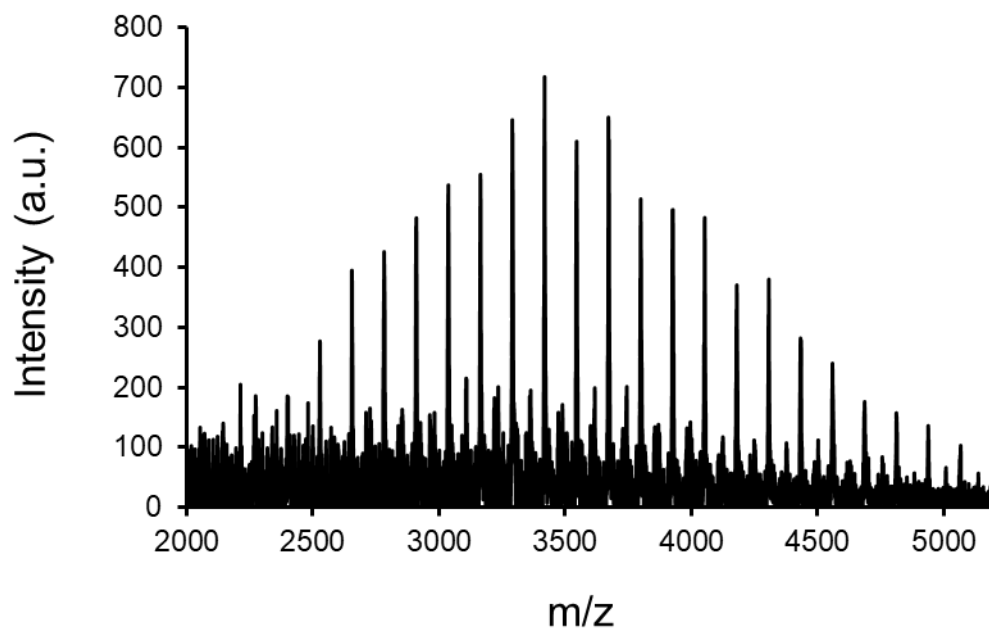
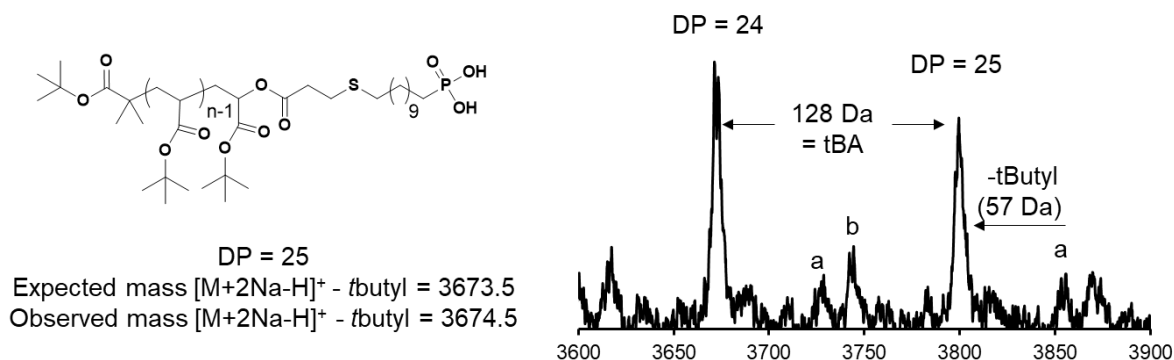
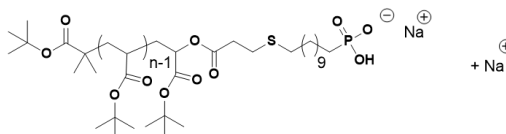


Figure S4.23 MALDI-ToF-MS spectrum of *Pt*BA terminated with phosphonic acid and initiated with *t*B-BiB.



a) $[M+ 2Na -H]^+$: See below for di-sodium adduct observed



b) $[M+ 3Na - 2H]^+$: See below for tri-sodium adduct observed

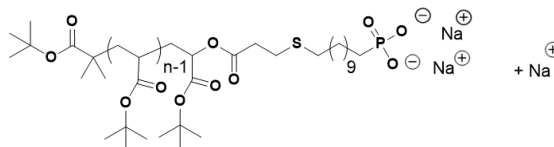
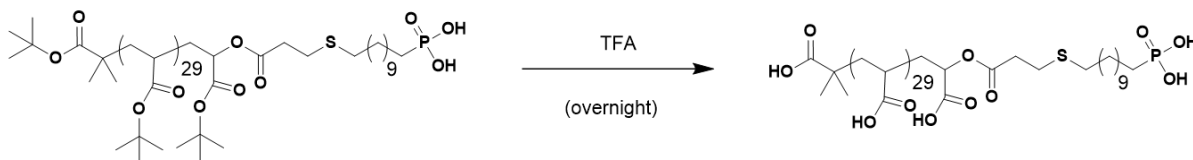


Figure S4.24 Expanded view of MALDI-ToF-MS spectrum for the phosphonic acid-terminated PtBA. Near quantitative agreement between the expected and observed mass of the di-sodium adduct minus *tert*-butyl group indicates an accurate assignment of the expected structure and chain ends. Additional distributions include the di-sodium adduct (**a**) as well as a tri-sodium adduct (**b**).



Scheme S4.5 Reaction scheme for formation of phosphonic acid-terminated PAA via deprotection of PtBA derivative with TFA.

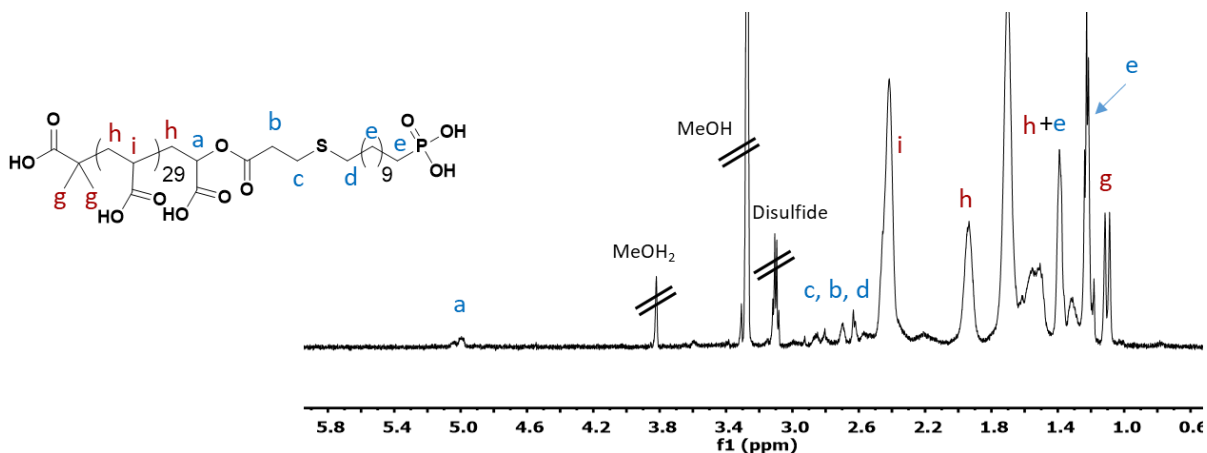
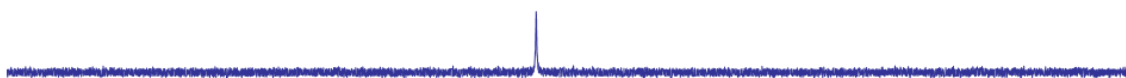
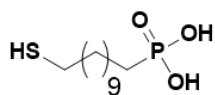


Figure S4.25 Purified ^1H NMR spectroscopy for the full transformation of acrylate-terminated PzBA to phosphonic acid-terminated PAA. NMR is run in a mixture of deuterated methanol and deuterated TFA (d-TFA) for added clarity of chain ends.

a)



b)

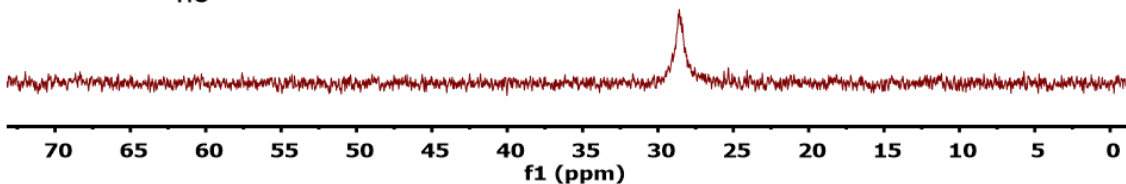
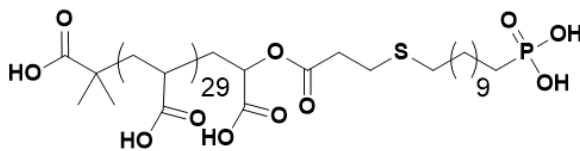


Figure S4.26 Analysis of ^{31}P NMR spectrum shows a shift in phosphine signal and slight broadening from a) small molecule 11, mercaptoundecylphosphonic acid to b) phosphonic acid-terminated PAA as expected with covalent bonding of phosphine group to polymer chain end.

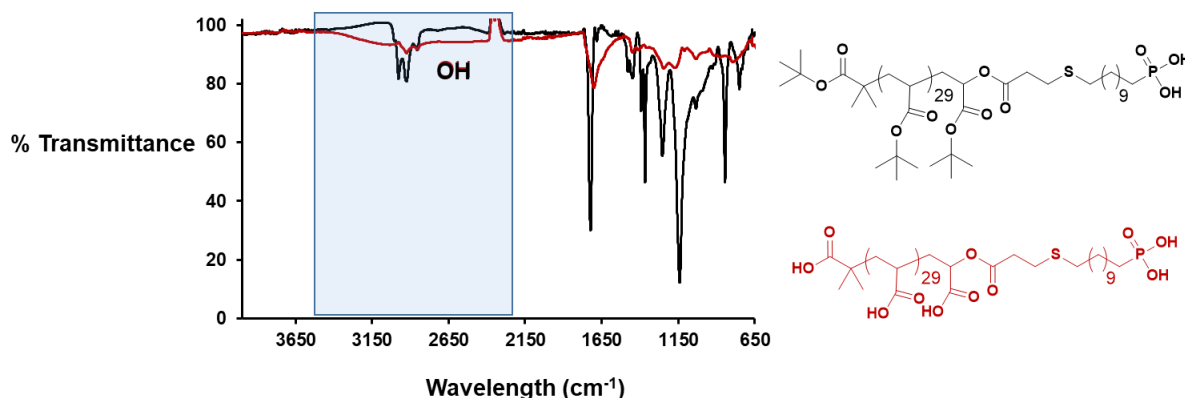


Figure S4.27: Highly charged species such as the phosphonic acid-terminated PtBA (black) and PAA (red) demonstrate a clear difference between the sharp *t*BA peaks and broad OH peaks respectively.

4.10.6 Carboxylic acid-terminated PAA: synthesis and characterization

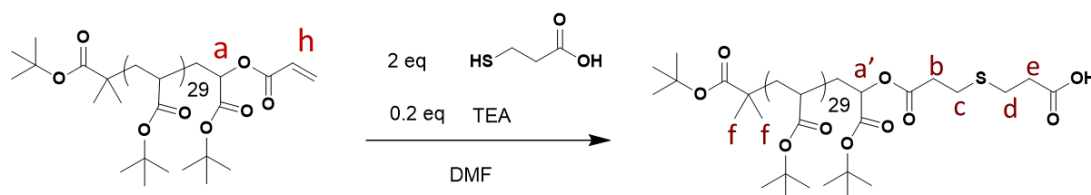
The synthesis for the carboxylic acid-terminated PtBA intermediate for this compound was identical to that of the dodecyl-terminated PtBA intermediate (see synthesis of dodecyl-terminated PAA) except that the transformation occurred with 3-mercaptopropionic acid rather than 1-dodecanethiol. The synthesis for the carboxylic acid-terminated PAA differed as follows. After an overnight reaction, the DMF and TEA were removed *via* rotary evaporation of a toluene: DMF (3:1) azeotrope. This crude product was then dissolved in a minimal amount of THF and precipitated into a cold, stirring 1:1 mixture of MeOH: H₂O (4xs) to remove remaining thiol. The PtBA intermediate was then dissolved in TFA (3.0 mL) in a scintillation vial equipped with magnetic stir bar and sealed with a screw cap then allowed to react overnight, under a N₂ purge, for approximately 15 h. The TFA was then evaporated *via* rotary evaporation (final yield: 55%).

PtBA intermediate: ¹H NMR (600, CDCl₃, δ): 4.91 – 4.79 (CH₂CH of terminal repeat unit), 3.00 – 2.52 (4 x CH₂ peaks of the chain end), 2.43 – 2.00 (m, CH₂CH of backbone), 2.00

– 1.49 (m, aliphatic protons of backbone), 1.49 – 1.29 (*tert*-butyl protons of backbone and initiator), 1.11 – 1.05 (2 x CH_3 of initiator). SEC (THF, RI, PS standard): $M_n = 3900 \text{ g mol}^{-1}$, $D = 1.11$. MALDI-ToF-MS: calc'd for $C_{189}H_{324}NaO_{56}S$, $[M+Na]^+ = 3547.6$; observed = 3546.5.

PAA product: 1H NMR (600 MHz, MeOD + TFA-d, δ): 5.10 – 4.98 (CH_2CH of terminal repeat unit), 2.84 – 2.57 (4 x CH_2 peaks of the chain end), 2.55 – 2.15 (m, CH_2CH of backbone), 2.10 – 1.48 (m, aliphatic protons of backbone), 1.19 – 1.13 (2 x CH_3 of initiator).

a)



b)

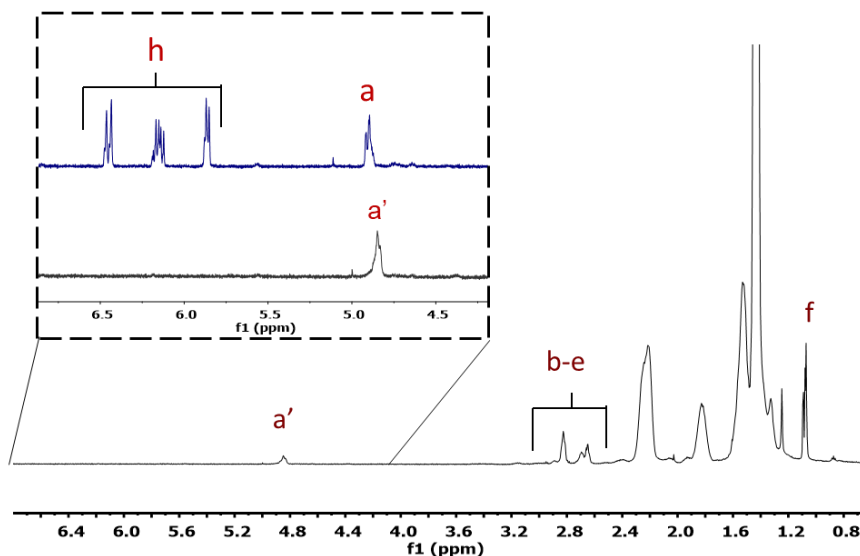


Figure S4.28 a) Transformation of acrylate-terminated PtBA to carboxylic acid-terminated product and b) 1H NMR displaying full loss of vinyl signals from acrylate starting material. The emergence of peaks corresponding to the new carboxylic acid end-group (a' and $b - e$) is also observed.

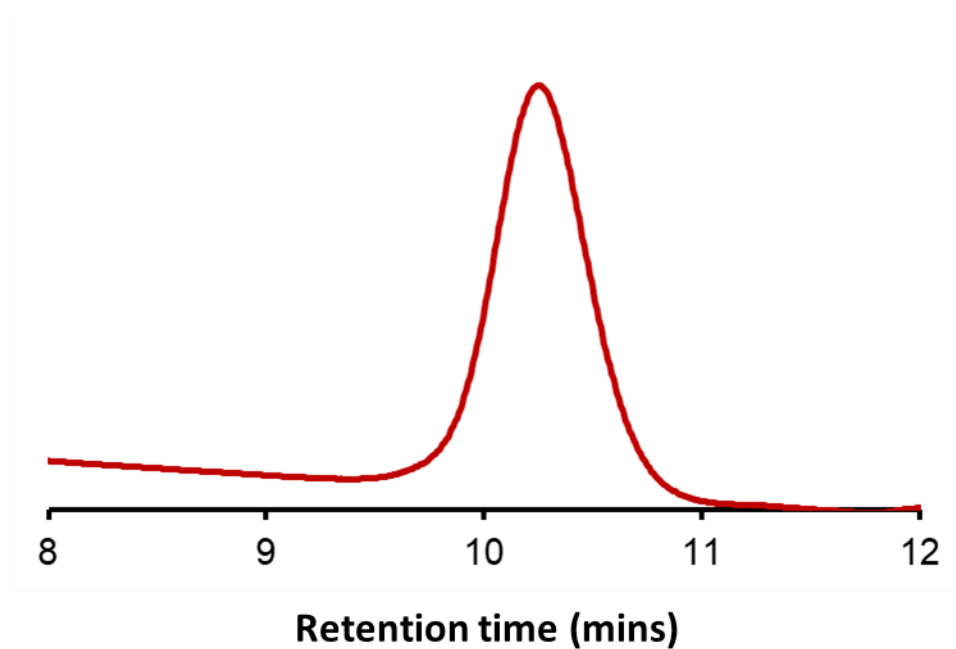


Figure S4.29 Size exclusion chromatography for carboxylic acid-terminated *Pt*BA demonstrates retention of low dispersity throughout transformation ($DP = 30$, $M_n = 3900 \text{ g mol}^{-1}$, $D = 1.11$).

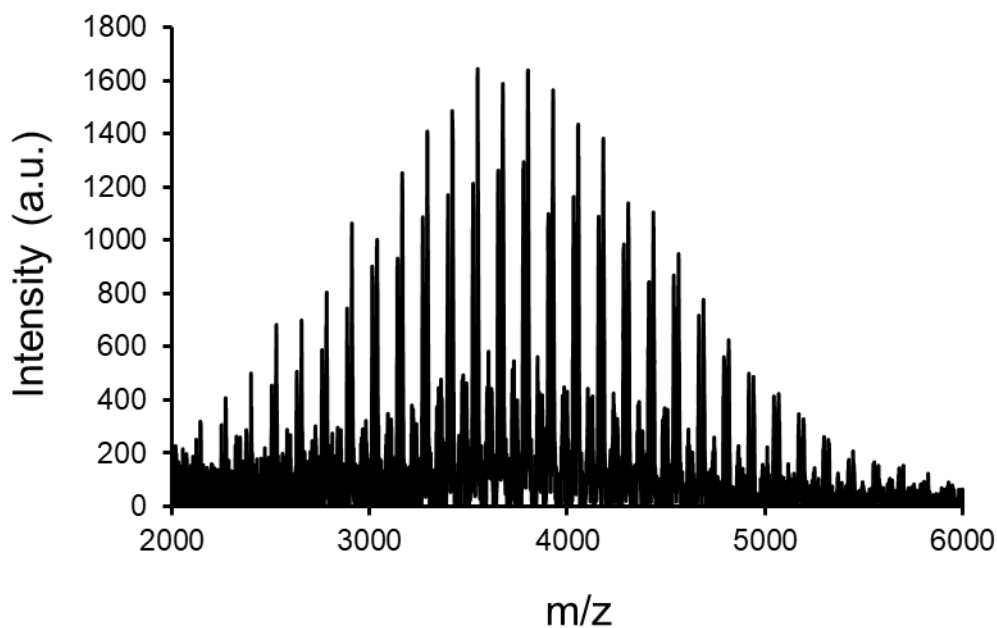


Figure S4.30 MALDI-ToF-MS spectrum of *Pt*BA initiated by *t*B-BiB and possessing a carboxylic acid chain end.

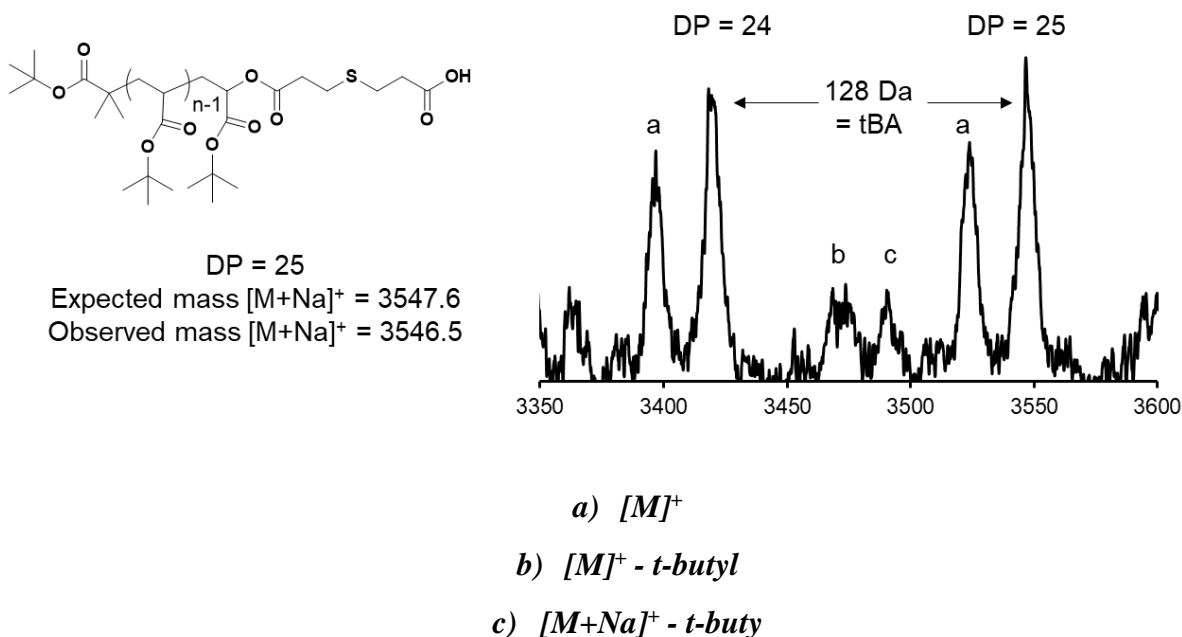
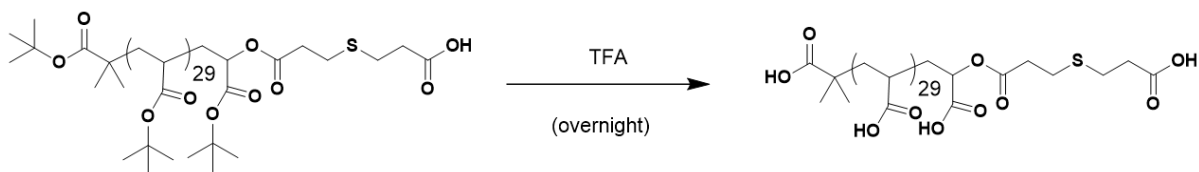


Figure S4.31 Expanded view of the PtBA showing two major sets of polydisperse peaks corresponding to the PtBA with carboxylic acid end group and *t*B-BiB initiator with and without a sodium ion (**a**). Two minor peaks correlate to each adduct respectively with the loss of a *tert*-butyl group (denoted **c** and **b** respectively). Quantitative agreement between the expected and observed mass of the sodium adduct indicates an accurate assignment of the expected structure and chain ends.



Scheme S4.6 Scheme for the acid deprotection of carboxylic acid-terminated PtBA to form the targeted PAA product.

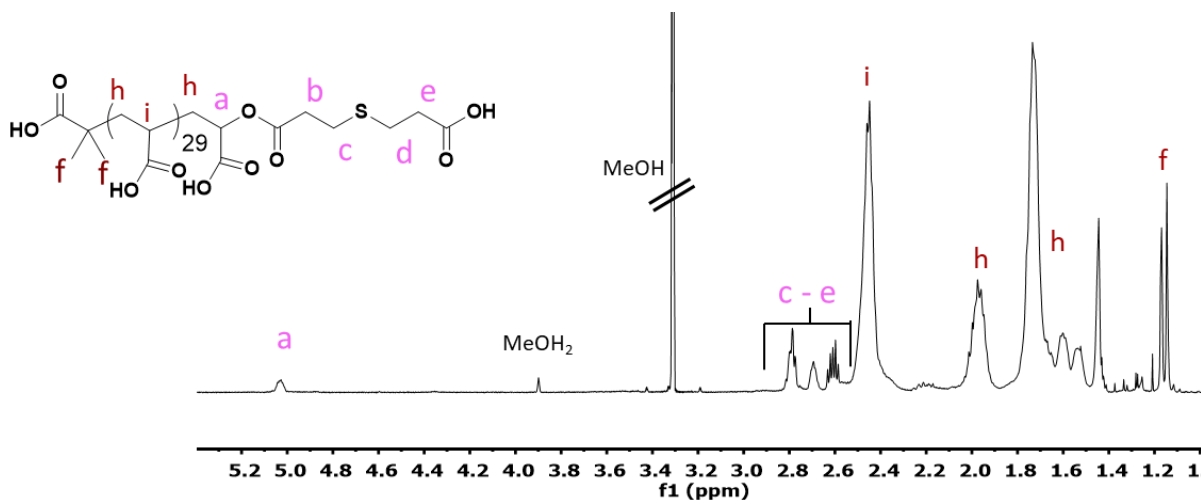


Figure S4.32 ^1H NMR spectrum for the fully deprotected carboxylic acid-terminated PtBA (or the PAA). Unique peaks from chain end (*a* and *c-e*) remain fully visible.

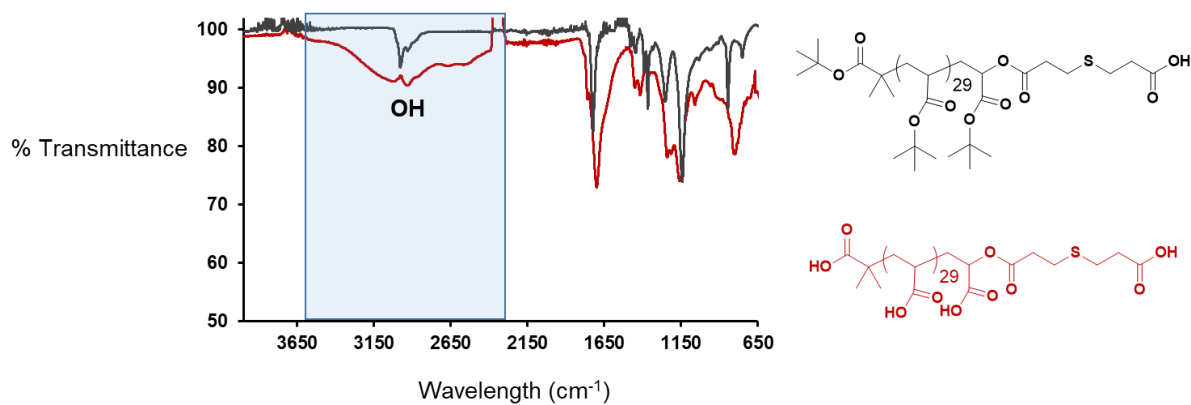


Figure S4.33 Comparison of carboxylic acid-terminated PtBA (black) and carboxylic acid-terminated PAA (red) by FT-IR shows the appearance of a broad OH peak and the disappearance of the sharp *t*BA peaks.

4.10.7 Dicarboxylic acid-terminated PAA: synthesis and characterization

The synthesis for the dicarboxylic acid-terminated *Pt*BA intermediate for this compound was identical to that of the dodecyl-terminated *Pt*BA intermediate (see synthesis of dodecyl-terminated PAA except that the transformation occurred with mercaptosuccinic acid rather than 1-dodecanethiol. The synthesis for the PAA product differs as follows. After an overnight reaction, the DMF and TEA were removed *via* rotary evaporation of a toluene: DMF (3:1) azeotrope. This crude product was then dissolved in 80.0 mL ethyl acetate and extracted with brine 4xs. If further purification was required, then the product was re-dissolved in minimal THF and precipitated into 1:1 MeOH: H₂O (2xs). This *Pt*BA intermediate was then dissolved in TFA (3.0 mL) in a scintillation vial equipped with magnetic stir bar and sealed with a screw cap then allowed to react overnight, under a N₂ purge, for approximately 15 h. Finally, TFA was removed *via* rotary evaporation (final yield: 65%).

*Pt*BA intermediate: ¹H NMR (600, CDCl₃, δ): 4.91 – 4.74 (CH₂CH of terminal repeat unit), 3.85 – 3.63 (SCHCH₂ of chain end), 3.13 – 2.63 (3 x CH₂ peaks of the chain end), 2.53 – 2.00 (m, CH₂CH of backbone), 2.00 – 1.49 (m, aliphatic protons of backbone), 1.49 – 1.29 (*tert*-butyl protons of backbone and initiator), 1.11 – 1.05 (2 x CH₃ of initiator). SEC (THF, RI, PS standard): M_n = 3800 g mol⁻¹, Đ = 1.12. MALDI-ToF-MS: calc'd for C₁₈₅H₃₁₂O₅₈S, [M]⁺ – *t*-butyl = 3417.9; observed = 3423.2.

PAA product: ¹H NMR (600 MHz, MeOD + TFA-d, δ): 5.09 – 4.97 (CH₂CH of terminal repeat unit), 3.72 – 3.62 (CH₂CH of chain end), 3.06 – 2.62 (3 x CH₂ peaks of the chain end), 2.62 – 2.12 (m, CH₂CH of backbone), 2.10 – 1.48 (m, aliphatic protons of backbone), 1.19 – 1.13 (2 x CH₃ of initiator).

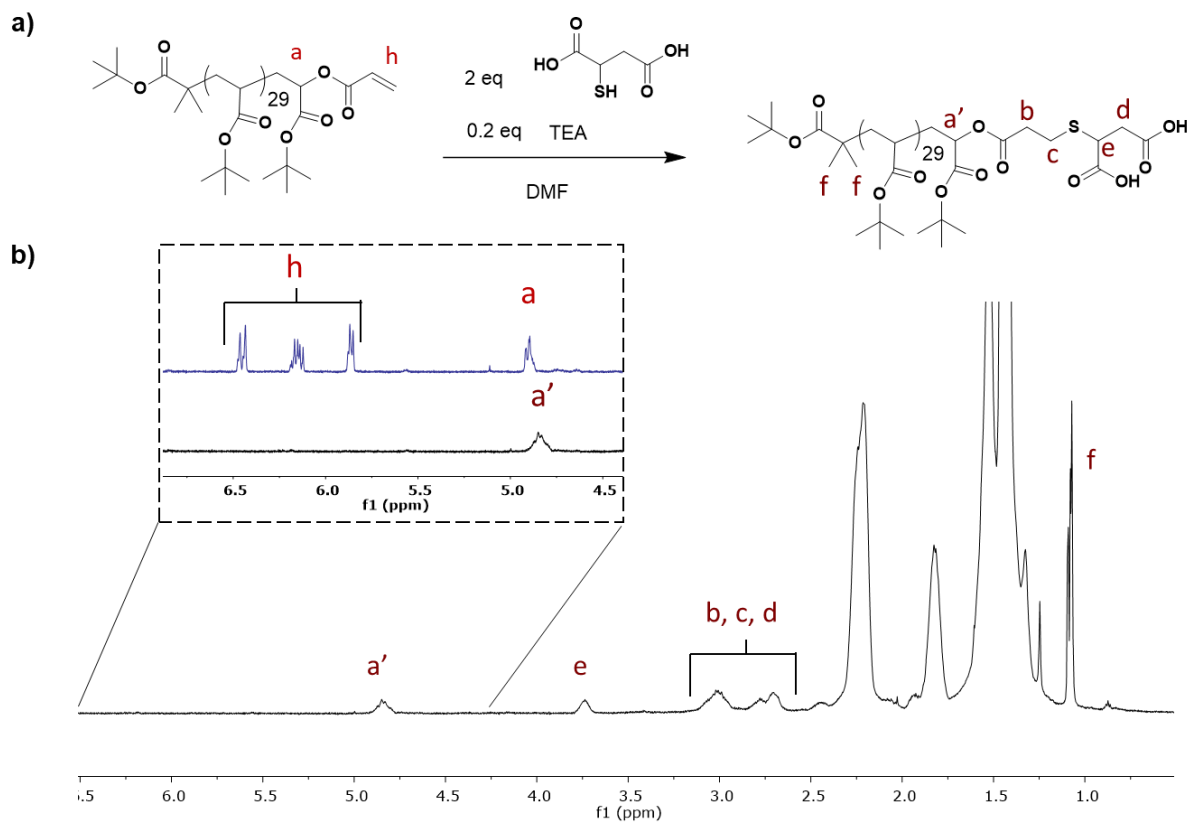


Figure S4.34 a) Reaction scheme for formation of a dicarboxylic acid-terminated PtBA and b) ¹H NMR spectrum for product displaying full conversion from acrylate-terminated starting material (inset upper, blue trace).

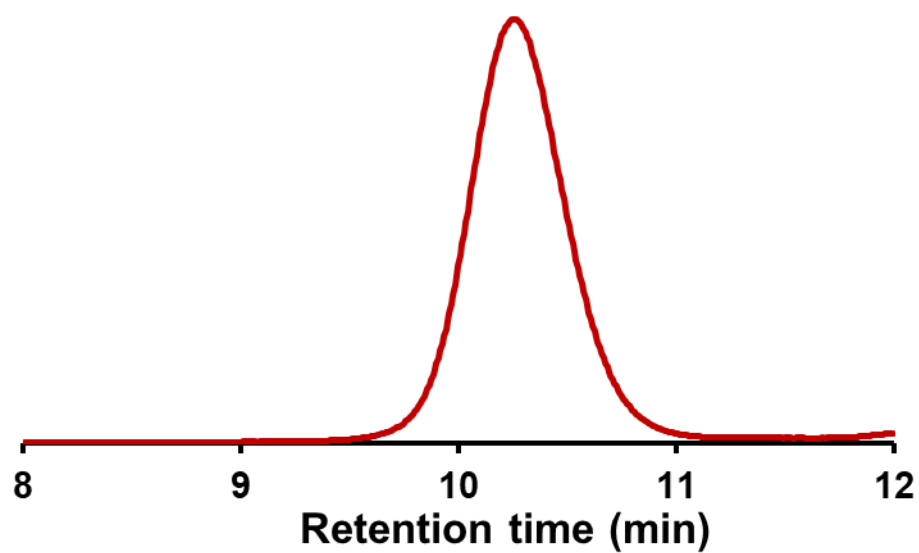


Figure S4.35 SEC trace of dicarboxylic acid-terminated *PtBA* ($DP = 30$, $M_n = 2800 \text{ g mol}^{-1}$, $D = 1.12$).

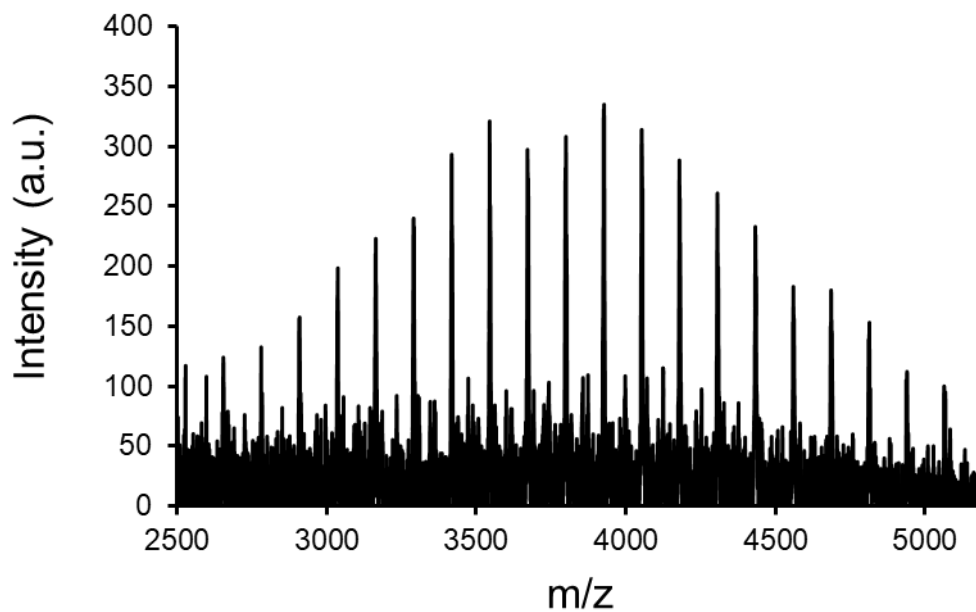


Figure S4.36 MALDI-ToF-MS distribution of dicarboxylic acid-terminated *PtBA*.

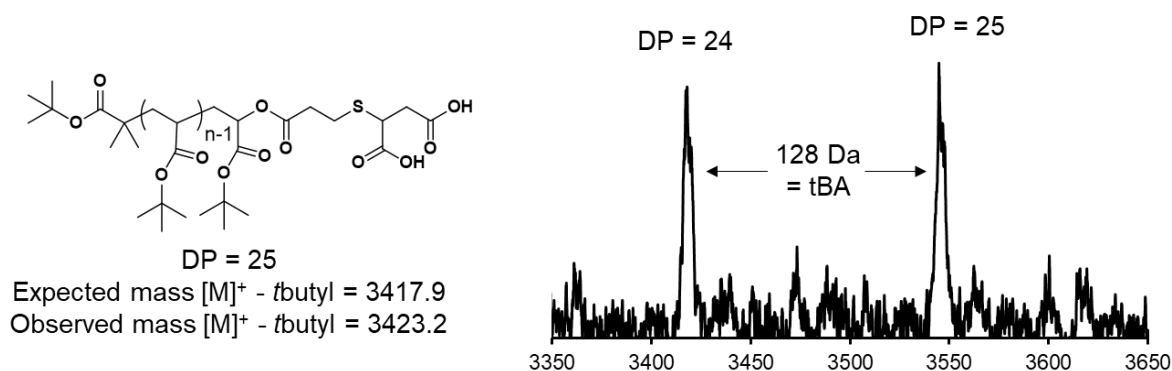
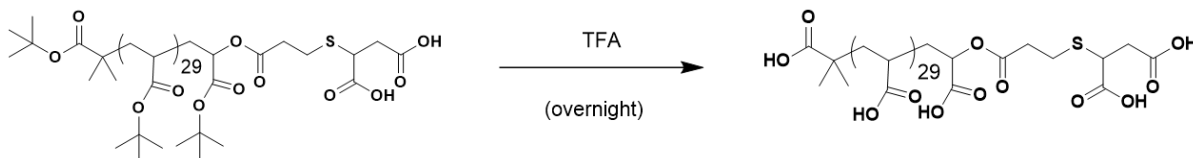


Figure S4.37 Expanded view of the dicarboxylic acid-terminated PtBA shows an even spacing between peaks corresponding to one tBA repeat unit. The main distribution observed corresponds to the dicarboxylic acid product with the loss of tert-butyl group during ionization.



Scheme S4.7 Reaction scheme for the formation of dicarboxylic acid-terminated PAA via deprotection of tert-butyl groups with TFA.

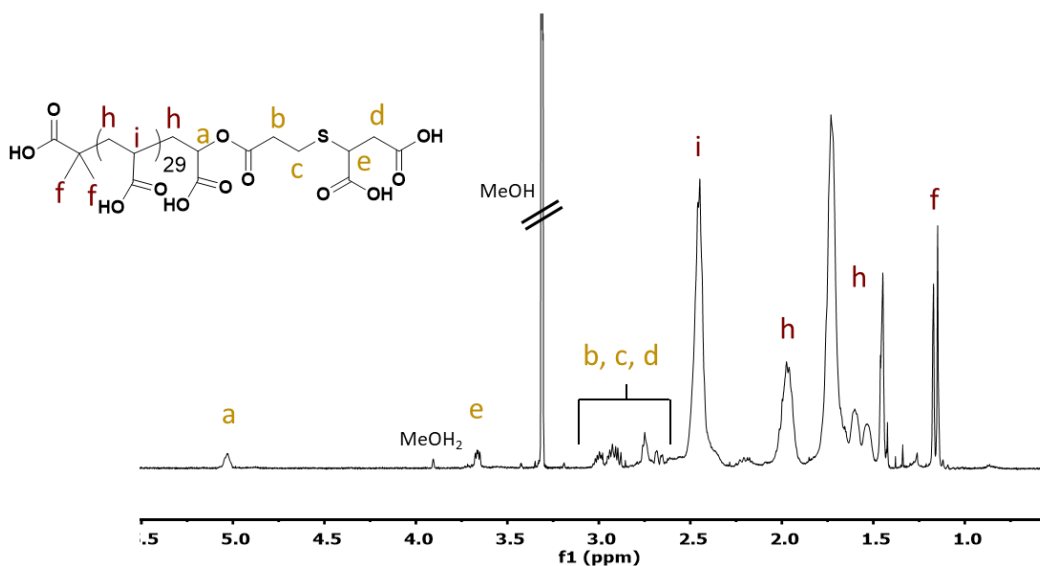


Figure S4.38 Full deprotection of the dicarboxylic acid PtBA along with complete retention of newly formed chain end is demonstrated by ¹H NMR spectroscopy.

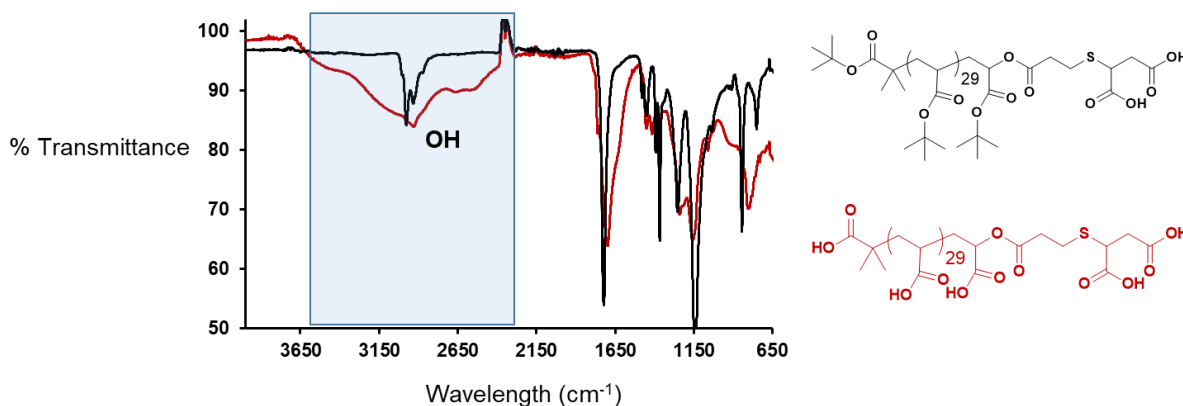


Figure S4.39 FR-IR comparison of the dicarboxylic acid-terminated PtBA (black) with its deprotected PAA counterpart (red) reveals the appearance of a broad OH peak to signify deprotection of *t*BA groups.

4.10.8 Comparison of ¹H NMR analysis with and without d-TFA treatment

NMR analysis of PAA derivatives were originally performed in deuterated methanol. This allowed for only partial identification of chain ends post PtBA deprotection due to the overlap of the proton chain end signals with the H₂O signal (**Figure 40a**). Addition of deuterated TFA (d-TFA) to the NMR sample sufficiently shifted the residual H₂O peak downfield such that a proper analysis of all chain end peaks was possible (**Figure 40b**). The appearance of an additional peak at $\delta=3.86$ ppm is identified as the formation of protonated methanol (see section 9). Furthermore, this treatment leaves the polymer unaffected as demonstrated by the quantitative agreement in polymer peak integration before and after acid treatment.

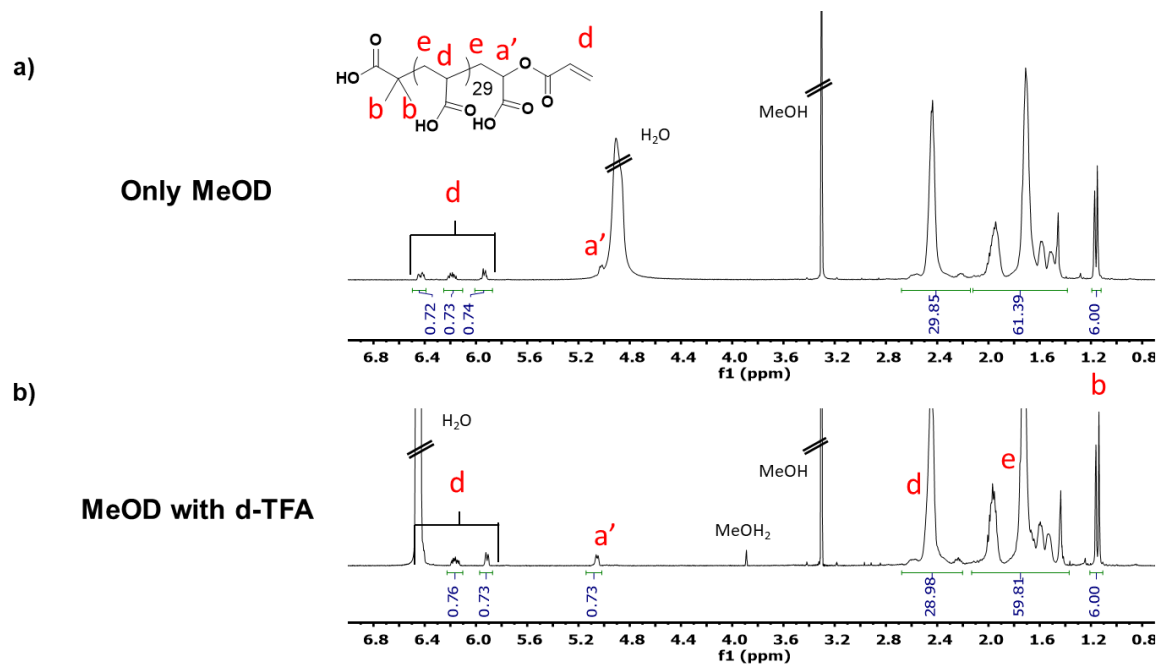


Figure S4.40 a) ^1H NMR comparison for an acrylate-terminated PAA in only d-MeOH and b) after treatment with d-TFA. Acid treatment allows for full characterization of polymer end groups and leaves polymer unaffected.

4.10.9 Control NMR of d-MeOH with d-TFA

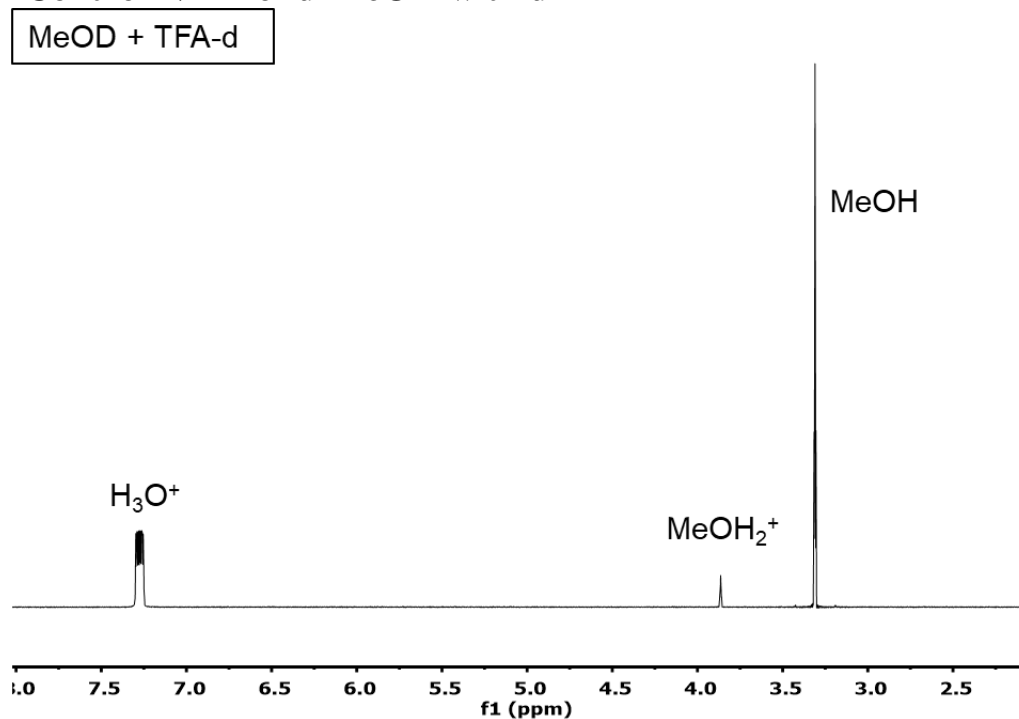


Figure S4.41 A downfield shift for the aqueous peak in the ¹H NMR for d-MeOH is observed with the addition of d-TFA. An additional peak corresponding to protonated methanol can also be observed at $\delta=3.86$ ppm.

4.10.10 Comparing synthesis of acrylate-terminated PtBA product under acidic and basic conditions.

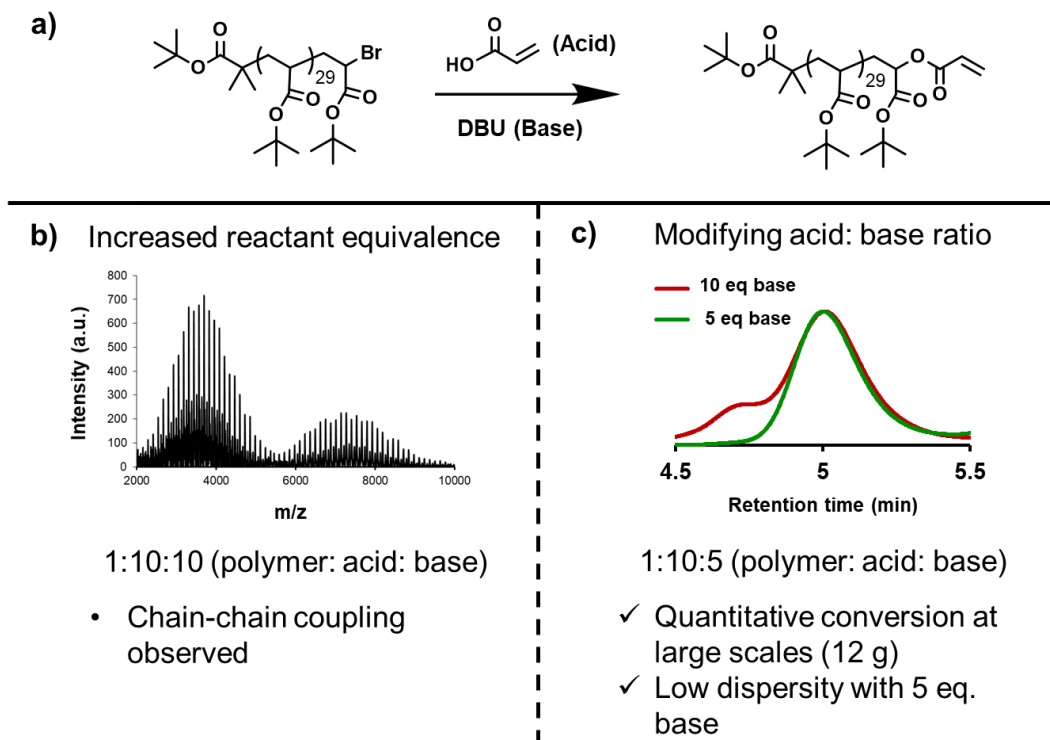


Figure S4.42 **a)** Reaction scheme for synthesis of acrylate-terminated PtBA, **b)** Matrix-assisted laser desorption ionization time of flight mass spectrometry of acrylate-terminated PtBA product showing a high molecular weight shoulder when 10 equivalents of base was utilized, and **c)** Size exclusion chromatography comparison of product when utilizing 10 equiv. of base (red trace) versus using only 5 equiv. of base (green trace). SEC analysis also shows a high molecular weight shoulder appearing when a higher base equiv. is used.

4.10.11 Characterization for synthesis of dodecyl-terminated PtBA via S_N2 substitution

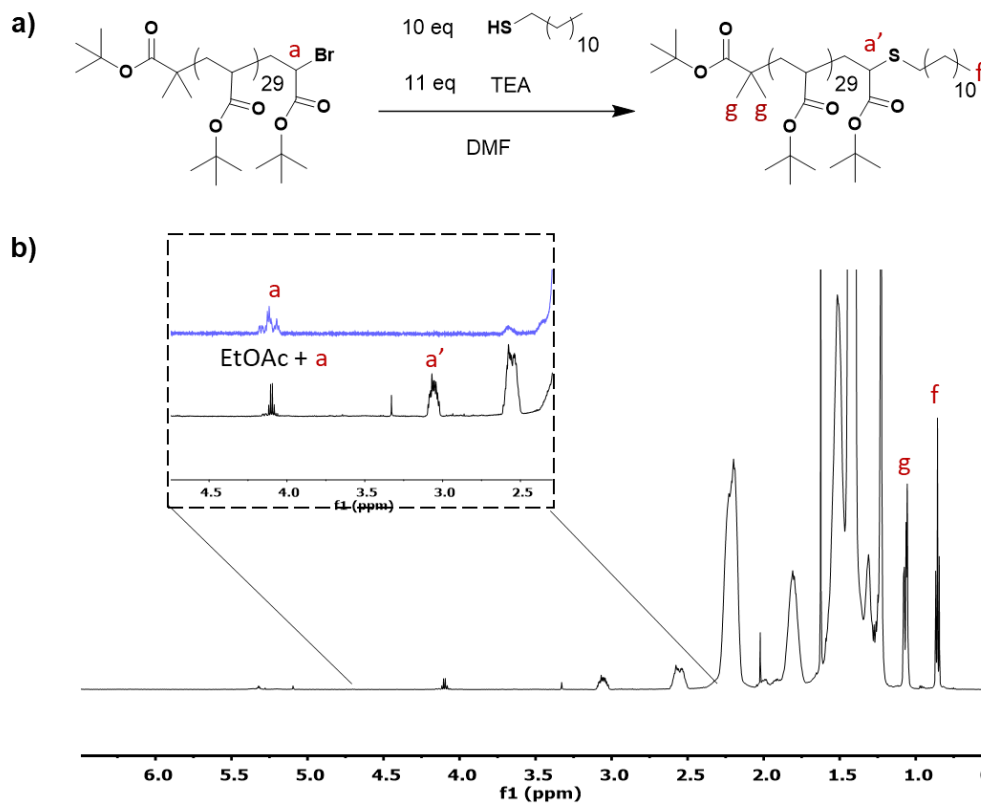


Figure S4.43 a) Reaction scheme for synthesis of dodecyl-terminated PtBA via S_N2 substitution of thiol to bromine-terminated PtBA and b) ¹H NMR of dodecyl-terminated product showing a shift of methine peak from the bromine-terminated starting material (inset: blue, top spectra labeled **a**) to the shifted peak adjacent to the sulfur (labeled **a'**).

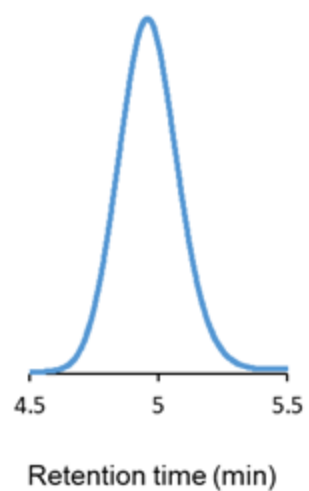


Figure S4.44 SEC trace after the transformation of the bromine-terminated PBA to the dodecyl-terminated derivative

4.11 References

- 1 S. Liufu, H. Xiao and Y. Li, *J. Colloid Interface Sci.*, 2005, **281**, 155–163.
- 2 T. Spychaj, *Prog. Org. Coat.*, 1989, **17**, 71–88.
- 3 J. E. Loy, J. Guo and S. J. Severtson, *Ing. Eng. Chem. Res.*, 2004, **43**, 1882–1887.
- 4 A. D. Wallace, A. Al-Hamzah, C. P. East, W. O. S. Doherty and C. M. Fellows, *J. Appl. Polym. Sci.*, 2010, **116**, 1165–1171.
- 5 W. O. S. Doherty, *Ing. Eng. Chem. Res.*, 2006, **45**, 642–647.
- 6 Y. Qi, Z. Ye, A. Fok, B. N. Holmes, M. Espanol, M.-P. Ginebra and C. Aparicio, *ACS Biomater. Sci. Eng.*, 2018, **4**, 2758–2766.
- 7 A. Akar and N. Öz, *Macromol. Mater. Eng.*, 1999, **273**, 12–14.
- 8 D. J. Lunn, S. Seo, S. Lee, R. Bou Zerdan, K. M. Mattson, N. J. Treat, A. J. McGrath, W. R. Gutekunst, J. Lawrence, A. Abdilla, A. Anastasaki, A. S. Knight, B. V. K. J. Schmidt, M. W. Bates, P. G. Clark, J. P. Derocher, A. K. Van Dyk and C. J. Hawker, *J. Polym. Sci., Part A Polym. Chem.*, 2019, **57**, 716–725.
- 9 A. Alhamzah and C. M. Fellows, *Desalination*, 2014, **332**, 33–43.
- 10 D. N. Misra, *Langmuir*, 1991, **7**, 2422–2424.
- 11 L. Shallcross, K. Roche, C. J. Wilcock, K. T. Stanton, T. Swift, S. Rimmer, P. V. Hatton and S. G. Spain, *J. Mater. Chem. B.*, 2017, **5**, 6027–6033.

- 12 A. A. Al-Hamzah, C. P. East, W. O. S. Doherty and C. M. Fellows, *Desalination*, 2014, **338**, 93–105.
- 13 W. O. S. Doherty, C. M. Fellows, S. Gorjian, E. Senogles and W. H. Cheung, *J. Appl. Polm. Sci.*, 2004, **91**, 2035–2041.
- 14 J. Loiseau, N. Döerr, J. M. Suau, J. B. Egraz, M. F. Llauro, C. Ladaviere and J. Claverie, *Macromolecules*, 2003, **36**, 3066–3077.
- 15 C. Ladaviere, N. Dörr and J. P. Claverie, *Macromolecules*, 2001, **34**, 5370–5372.
- 16 D. J. Lunn, E. H. Discekici, J. Read de Alaniz, W. R. Gutekunst and C. J. Hawker, *J. Polym. Sci., Part A Polym. Chem*, 2017, **55**, 2903–2914.
- 17 C. P. East, A. D. Wallace, A. Al-Hamzah, W. O. S. Doherty and C. M. Fellows, *J. Appl. Polm. Sci.*, 2010, **115**, 2127–2135.
- 18 A. Anastasaki, J. Willenbacher, C. Fleischmann, W. R. Gutekunst and C. J. Hawker, *Polym. Chem.*, 2017, **8**, 689–697.
- 19 G. L. Ellman, *Arch. Biochem. Biophys.*, 1959, **82**, 70–77.

APPENDIX A

INVESTIGATING THE INFLUENCE OF CHAIN END ON DISPERSANT AND BIO-MINERALIZATION CONTROL

A1 Introduction

In **Chapter 4**, the utility of poly(acrylic acid)s (PAA) for an expansive range of industrially relevant applications including dispersants, scale inhibition, and mineralization control was introduced. In addition, it was discussed that small changes in the polymer's architecture or dispersity were found to significantly influence their macromolecular properties and effectiveness toward these applications. **Chapter 4** also described a synthetic method that facilitated the synthesis of tailored PAA derivatives with unique chain end chemistries. **Appendix A** describes initial studies on the utility of this new synthetic method to target high performance dispersants and bio-mineral crystallization control.

A2 The Influence of PAA Chain End on Dispersant Performance

In paint and coating formulations, titanium dioxide (TiO_2) is widely used due to its favorable physicochemical properties as a white pigment.¹ For these applications, control over TiO_2 aggregation is critical in producing suitable end-use properties including stability, opacity, and gloss. To obtain proper dispersion of these inorganic pigments, water soluble polymers, such as PAA, have been used.¹⁻³

Preliminary structure-property studies have revealed that microstructure changes to the PAA can directly influence the polymer's effectiveness as a dispersant.⁴⁻⁶ An on-going collaboration between our group and Dow Chemical seeks to expand the current understanding on how control over polymer design can unlock coveted properties. Specifically, this collaboration aims to uncover how the chain end chemistry of PAA can influence the polymer's utility as a dispersant for improved paint formulations.

At UCSB, several PAA derivatives possessing a variety of chain end chemistries were synthesized *via* the facile universal synthesis presented in **Chapter 4**. Furthermore, several grams of each chain end modified PAA derivative were transferred to Dow Chemical and various field experiments are underway to discover how these polymers' interactions with different metal surfaces differ from that of commercial formulations. This knowledge on the structure-performance relationship will then be applied to create more targeted PAA derivatives that will produce enhanced paint coating formulations.

A3 The Effect of PAA Chain End on the Morphology and Size of Hydroxyapatite Crystals

While a study on the influence of the chain end on dispersant performance is being conducted at Dow, our group has concurrently performed similar assessments into the influence of the chain end on bio-mineral crystal formation.

Hydroxyapatite (HA) nanocrystals are prevalent in a range of biological systems including human bones and teeth. It has been shown that the structure of these systems depends on the interaction of biological apatites with organic polymers such as collagen type I or amelogenin.⁷⁻¹⁰ Studies to replicate such systems have included the use of poly(acrylic acid) to produce HA crystals that more closely mimic the size and morphology of those observed in nature.¹¹⁻¹⁴ These investigations have revealed that crystal structure control relies on the architecture¹² and molecular weight^{11,13} of the PAA. In order to provide a more thorough understanding into the formation mechanism of HA crystals and the structure-property relationship of the PAA, we chose to specifically investigate the influence of PAA chain end on this bio-mineral crystallization.

Several PAA derivatives with unique chain end chemistries were first prepared *via* the new synthetic method described in **Chapter 4**. HA crystals were then synthesized according to literature procedures^{12,14} in the presence of these PAA derivatives. Thermogravimetric analysis was used to demonstrate incorporation of polymer into each composite (**Figure A.1**). For a control sample with no polymer additive, a gradual mass loss of < 4% was observed up to 800 °C. In contrast, composite materials that included PAA resulted in more mass loss below 400 °C with an overall loss of < 6% up to 800 °C.

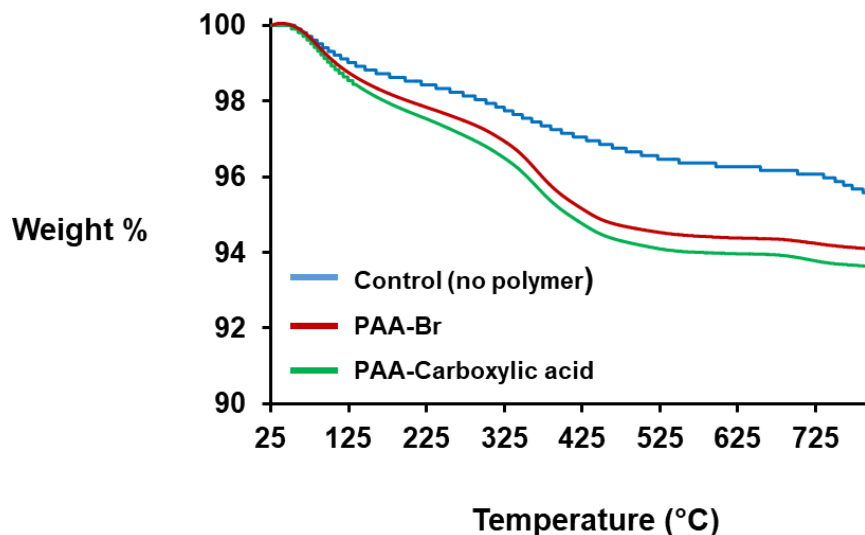


Figure A.1 Thermogravimetric analysis of HA crystals prepared **a**) in the absence of PAA (blue, top trace), **b**) with bromine-terminated PAA (red, middle trace), and **c**) with carboxylic acid-terminated PAA (green, bottom trace).

Furthermore, crystal size and morphology for each composite were analyzed *via* transmission electron microscopy. For example, crystals prepared in the presence of a phosphonic acid-terminated PAA produced more plate-like crystallites while sharper, more needle-like structures were observed in those crystals prepared with sulfonate-terminated PAA (**Figure A.2**). Detailed characterization studies are underway to investigate if different structures can be produced by simply tuning the chain end of the PAA.

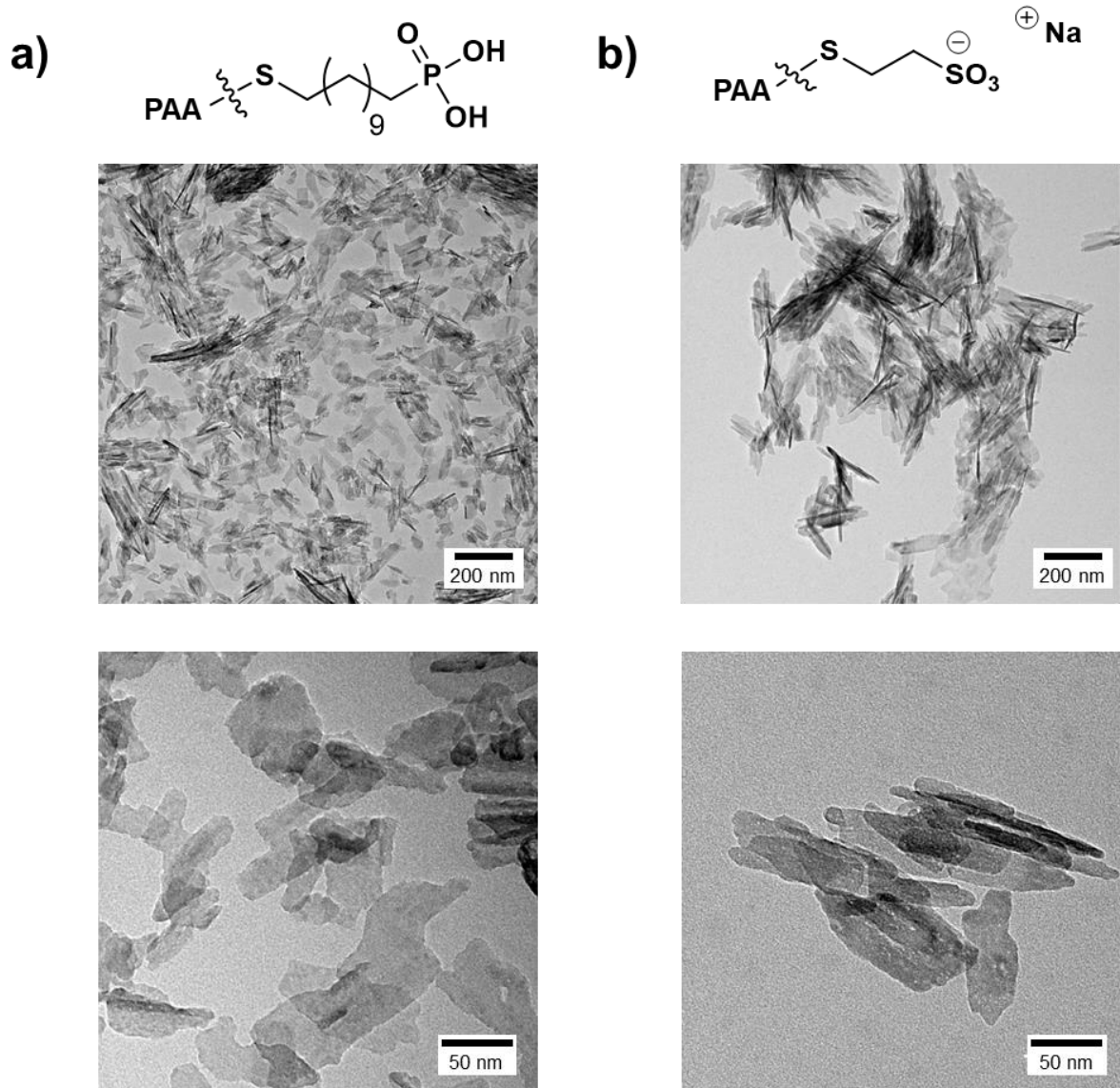


Figure A.2 Transmission electron microscopy comparison of HA crystals prepared with **a)** phosphonic acid-terminated PAA, that produces plate-like crystals and **b)** sulfonate-terminated PAA that produces more needle-like structures.

A4 References

- 1 S. Farrokhpay, *Adv. Colloid Interface Sci.*, 2009, **151**, 24–32.
- 2 S. Liufu, H. Xiao and Y. Li, *J. Colloid Interface Sci.*, 2005, **281**, 155–163.
- 3 K. Esumi, H. Toyoda, T. Suhara and H. Fukui, *Colloids Surf., A*, 1998, **145**, 145–151.
- 4 D. J. Lunn, S. Seo, S. Lee, R. Bou Zerdan, K. M. Mattson, N. J. Treat, A. J. McGrath, W. R. Gutekunst, J. Lawrence, A. Abdilla, A. Anastasaki, A. S. Knight, B. V. K. J. Schmidt, M. W. Bates, P. G. Clark, J. P. Derocher, A. K. Van Dyk and C. J. Hawker, *J. Polym. Sci., Part A Polym. Chem.*, 2019, **57**, 716–725.
- 5 S. Farrokhpay, G. E. Morris, D. Fornasiero and P. Self, *Colloids Surf., A*, 2005, **253**, 183–191.
- 6 S. Farrokhpay, G. E. Morris, D. Fornasiero and P. Self, *J. Colloid Interface Sci.*, 2004, **274**, 33–40.
- 7 A. G. Fincham, J. Moradian-Oldak and J. P. Simmer, *J. Struct. Biol.*, 1999, **126**, 270–299.
- 8 M. J. Olszta, X. Cheng, S. S. Jee, R. Kumar, Y.-Y. Kim, M. J. Kaufman, E. P. Douglas and L. B. Gower, *Mater. Sci. Eng., R*, 2007, **28**, 77–116.
- 9 X. Yang, L. Wang, Y. Qin, Z. Sun, Z. J. Henneman, J. Moradian-Oldak and G. H. Nancollas, *J. Phys. Chem. B*, 2010, **114**, 2293–2300.
- 10 X. Y. Liu and S. W. Lim, *J. Am. Chem. Soc.*, 2003, **125**, 888–895.
- 11 Y. Qi, Z. Ye, A. Fok, B. N. Holmes, M. Espanol, M.-P. Ginebra and C. Aparicio, *ACS Biomater. Sci. Eng.*, 2018, **4**, 2758–2766.
- 12 L. Shallcross, K. Roche, C. J. Wilcock, K. T. Stanton, T. Swift, S. Rimmer, P. V Hatton and S. G. Spain, *J. Mater. Chem. B.*, 2017, **5**, 6027–6033.
- 13 D. N. Misra, *Langmuir*, 1991, **7**, 2422–2424.
- 14 K. J. Roche and K. T. Stanton, *J. Cryst. Growth*, 2015, **409**, 80–88.

APPENDIX B

TUNABLE VISIBLE AND NEAR
INFRARED PHOTOSWITCHES[‡]

[‡] Reprinted with permission from J. R. Hemmer, S. O. Poelma, N. Treat, Z. A. Page, N. D. Dolinski, Y. J. Diaz, W. Tomlinson, K. D. Clark, J. P. Hooper, C. Hawker and J. Read De Alaniz, *J. Am. Chem. Soc.*, **2016**, *138*, 13960–13966.

Tunable Visible and Near Infrared Photoswitches

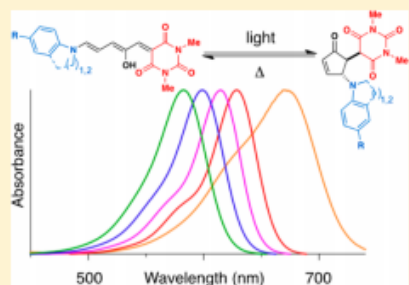
James R. Hemmer,[†] Saemi O. Poelma,[†] Nicolas Treat,[‡] Zachariah A. Page,[‡] Neil D. Dolinski,[‡] Yvonne J. Diaz,[†] Warren Tomlinson,[§] Kyle D. Clark,[†] Joseph P. Hooper,[§] Craig Hawker,^{‡,†} and Javier Read de Alaniz^{*,†}

[†]Department of Chemistry and Biochemistry and [‡]Materials Department, Materials Research Laboratory, University of California, Santa Barbara, California 93106, United States

[§]Department of Physics, Naval Postgraduate School, 1 University Circle, Monterey, California 93943, United States

Supporting Information

ABSTRACT: A class of tunable visible and near-infrared donor–acceptor Stenhouse adduct (DASA) photoswitches were efficiently synthesized in two to four steps from commercially available starting materials with minimal purification. Using either Meldrum's or barbituric acid "acceptors" in combination with aniline-based "donors", an absorption range spanning from 450 to 750 nm is obtained. Additionally, photoisomerization results in complete decoloration for all adducts, yielding fully transparent, colorless solutions and films. Detailed investigations using density functional theory, nuclear magnetic resonance, and visible absorption spectroscopies provide valuable insight into the unique structure–property relationships for this novel class of photoswitches. As a final demonstration, selective photochromism is accomplished in a variety of solvents and polymer matrices, a significant advantage for applications of this new generation of DASAs.



INTRODUCTION

Photoswitches have long held the interest of the scientific community for their ability to alter molecular structure, and thus properties, using light as a stimulus.^{1–3} Upon photoexcitation, the photoswitch transforms from a thermodynamically stable state to a metastable photostationary state. In the photostationary state, molecules will return to equilibrium by thermal relaxation or upon photoirradiation with a different wavelength. The resulting change in structure can modify absorption, polarity, and/or free volume. Not surprisingly, numerous applications have taken advantage of these property changes including switching of surface polarity,⁴ membrane permeability,⁵ nanoparticle clustering,^{6,7} as well as controlling the properties of biologically active molecules.^{8–12} Additionally, photoswitches have been used to create mechanical actuators¹³ and mechanical sensors¹⁴ (mechanophores).

Although photoswitches have been extensively studied for over a century, the most widely used classes, including azobenzene,¹⁵ diarylethene,¹⁶ dihydroazulene,¹⁷ and spiroopyran,¹⁸ often reside in a colorless thermodynamically stable state that requires high-energy ultraviolet (UV) light for activation. The use of UV light comes with inherent limitations for a range of applications that arise from irreversible chemical damage and limited penetration depth in many materials. Alternatively, low-energy visible light-activated photoswitches, described as negative photochromes owing to their colored thermodynamically stable state, have the potential to overcome such limitations yet are far less common.^{19–23}

In the past decade, advances with azobenzene-based photoswitches demonstrated by Aprahamian,^{24,25} Hecht,²⁶ Herges,²⁷ and Woolley⁸ have allowed for visible light isomerization across a broad range of wavelengths. However, in these photochromic systems, switching occurs between two colored states. This feature limits their use in applications such as sensing that benefit from a more notable color change.²⁸ Although conversion from colorless-to-colored is routine for spiroopyran derivatives, they have been shown to fatigue quickly upon repeated cycling experiments. Exposure to high-energy UV light and the presence of singlet and triplet oxygen have been identified as key factors leading to degradation.^{29,30} To address these challenges, we sought to design a robust and highly tunable photoswitch platform using inexpensive reagents and simple syntheses to provide a colored-to-colorless transformation using visible light.

Donor–acceptor Stenhouse adducts (DASAs) are a new class of negative photoswitches that can be synthesized easily in two steps from commercially available starting materials.³¹ The colored DASA becomes colorless upon irradiation with visible light. This process initiates with a light-controlled alkene isomerization followed by a thermal 4π electrocyclozation to the colorless state. In initial work, we described DASAs containing alkyl-based amine "donors" (electron-rich) and Meldrum's or barbituric acid "acceptors" (electron-deficient) that display

Received: July 19, 2016
Published: October 4, 2016

visible light absorption, high fatigue resistance, and a significant polarity and color change upon switching.³² However, with these first-generation DASAs, wavelength tunability was limited to 545 and 570 nm for the Meldrum's and barbituric acid derivatives, respectively.³¹ Additionally, reversible photoswitching was only possible in nonpolar solvents such as toluene, and reversible switching could not be observed in solid-supported matrices.^{33,34} To improve the performance of DASA-based photoswitches, we have designed a new system that overcomes these limitations while retaining the facile two-step synthetic approach from commercially available materials. Specifically, we report a study using secondary aniline-derivatives as donors to provide wavelength tunable DASA photochromes (Figure 1)

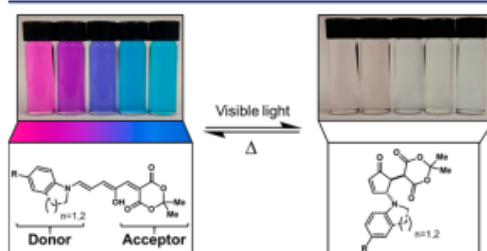


Figure 1. General structure for second generation donor–acceptor Stenhouse adducts containing aniline-based donors and a Meldrum's acid acceptor. The thermodynamically stable colored “open” isomer (left) can be converted into the photostationary colorless “closed” isomer (right) with visible light irradiation.

that absorb visible and near-IR light (ranging from 450 to 750 nm) in solvents of varying polarity as well as in polymer matrices. Detailed characterization to elucidate structure–property relationships for these second generation aniline-based donors is also provided. We show that wavelength tunability can be exploited in systems where two different DASAs can be independently switched in both solution and polymer films.

RESULTS AND DISCUSSION

Synthesis. We have developed a two-step procedure from commercially available starting materials for the synthesis of aniline-based DASAs (Figure 2a). First, an activated furan-carbon acid is generated by condensing furfural, an inexpensive (~\$2/kg) byproduct from nonedible biomass, with either Meldrum's or barbituric acid. The synthesis is performed in water at either room temperature (barbituric acid) or 70 °C (Meldrum's acid), where the pure product precipitates out of solution as a yellow solid in near quantitative yield.³¹ Isolation and purification are accomplished by filtration and subsequent washing with water. Second, the activated furan adduct is mixed with a secondary aniline derivative either neat using 3–5 equiv of the amine or in solution using 1 equiv. Less nucleophilic aniline derivatives, such as *N*-methylaniline, require neat conditions for optimal yields, whereas more electron-rich/nucleophilic anilines, such as indoline or 5-methoxyindole, can be run in tetrahydrofuran (THF) or dichloromethane (DCM). Purification is accomplished by trituration with hexanes, diethyl ether, or THF, yielding the desired DASA products as dark lustrous solids.

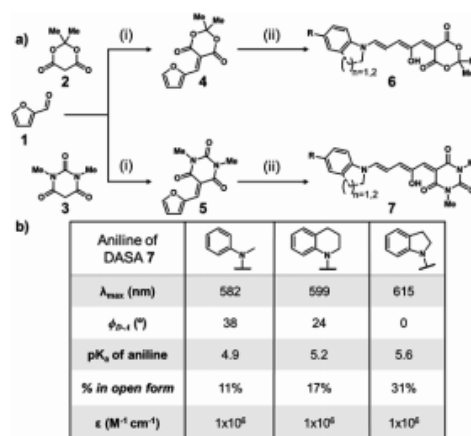


Figure 2. Synthesis and characterization of aniline-based donor–acceptor Stenhouse adducts. (a) top: Meldrum's acid acceptor; bottom: Barbituric acid acceptor. Reagents and conditions: (i) H₂O and (ii) aniline-derivative, neat, DCM, MeOH or THF. (b) Select properties of three representative secondary aniline-based DASAs highlighting stark differences for subtle changes in chemical structure; *N*-methylaniline, tetrahydroquinoline, and indoline from left to right.

With efficient access to a range of aniline-based DASAs, it was evident immediately that subtle differences in the aniline donor results in dramatic changes in color and the ability to switch reversibly in a number of solvents. Probing aniline-based DASAs bearing *N*-methylaniline, tetrahydroquinoline, and indoline donors in detail revealed a number of property trends that could be correlated back to the structure, including peak absorption (λ_{max}), calculated dihedral angle between the donor and acceptor (Φ_{D-A}), negative log of the acid dissociation constant (p*K*_a) of the donor amine, open/close equilibrium percentage, and molar absorptivity (ϵ), (Figure 2b; characterization data for all DASAs is provided in Table S1).

Property Studies. The bathochromic shift in absorption of the aniline-based DASAs relative to the alkyl-based DASAs was the first property we sought to evaluate. Meldrum's acid and barbituric acid acceptors were both synthesized and characterized with representative absorption spectra given for the barbituric acid derivatives in Figure 3 (the full barbituric acid and Meldrum's acid derivatives are described in Figures S1 and S2). The same absorption trends are observed for both barbituric and Meldrum's acid-based DASAs, but all wavelengths are bathochromically shifted by approximately 25 nm for the barbituric structures. The peak absorptions for *N*-methylaniline (8), tetrahydroquinoline (9), and indoline (10) are 582, 599, and 615 nm, respectively (Figures 2b and 3). The wavelength could be extended further by incorporating electron donating groups at the para position of the cyclic anilines, such as methoxy (11) and *N,N*-dialkyl (12), which led to red-shifts in absorption (λ_{max} = 629 and 669 nm, respectively) compared to that of native indoline (λ_{max} = 615 nm). The most notable structural difference between these derivatives and the alkyl-based DASAs is the presence of an aromatic ring, where homoconjugation may result in a bathochromic absorption shift due to enhanced hybridization of molecular orbitals between the electron-rich donors and acceptor groups, an effect

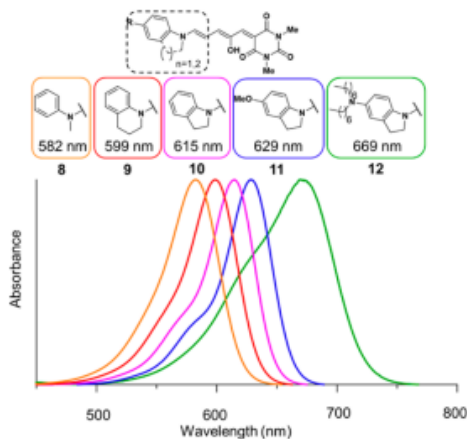


Figure 3. Representative absorption spectra for aniline-based DASAs highlighting the wavelength tunability with barbituric acid derivatives. Measured as 10 μM solutions in DCM.

commonly observed with “push-pull” systems in organic semiconductors.^{35,36} Using readily available aniline-based donors, the absorbance maxima of barbituric-based DASAs were tuned from 582 to 669 nm.

In contrast to the cyclic indoline derivatives, acyclic derivatives such as *p*-methoxy-*N*-methylaniline do not lead to a significant change in λ_{max} compared to unsubstituted *N*-methylaniline (Figure 4 and Figure S3). For the difference

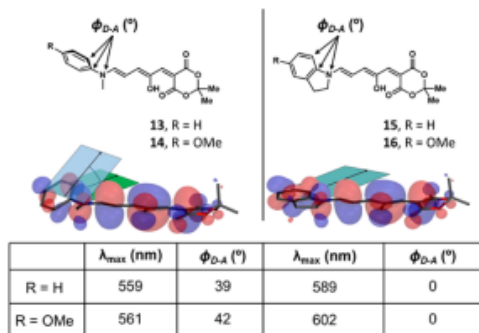


Figure 4. Computational density functional theory modeling of representative aniline DASAs, determining HOMO orbital overlap, energy gap (represented by λ_{max}), and dihedral angle between donor and acceptor ($\Phi_{\text{D,A}}$).

between acyclic- and cyclic-substituted *N*-methylaniline derivatives to be addressed, density functional theory (DFT) calculations at the B3LYP/6-31G(d) level were performed to identify the dihedral angle between the donor and acceptor groups ($\Phi_{\text{D,A}}$), and the character of the highest occupied molecular orbitals (HOMOs) overlap (Figures 2b and 4 and Figures S4 and S5). *N*-Methylaniline (8 and 15) derivatives were found to have a substantial out-of-plane twist ($\Phi_{\text{D,A}} \approx 40^\circ$), whereas indoline (10 and 16) derivatives were planar

($\Phi_{\text{D,A}} \approx 0^\circ$). As a consequence, indoline derivatives have more HOMO overlap/conjugation, resulting in a narrowing of the energy gap (E_g)/bathochromic shift of ~ 30 nm relative to the corresponding *N*-methylaniline derivatives. Even more striking than the difference between the acyclic and cyclic anilines is the effect of a donating group para to the aniline nitrogen. Because the *N*-methylaniline is out of plane, a donating group, such as *p*-methoxy, has little impact on the wavelength and only results in a 2 nm bathochromic shift compared to its unsubstituted counterpart. However, in the indoline case, the addition of a *p*-methoxy group causes a 13 nm redshift. Planarity of the aryl ring in the aniline donor is therefore critical for increasing conjugation and extending the absorption maxima wavelength. Of note, these trends can be predicted using DFT calculations (Figure S6).

The molar absorptivities (ϵ) for *N*-methylaniline (8), tetrahydroquinoline (9) and indoline (10) barbituric acid derivatives were determined through a combination of NMR and absorption spectroscopies at equilibrium (Figure S7). The ϵ values for these derivatives are uniformly high at $\sim 10^6 \text{ M}^{-1} \text{ cm}^{-1}$. The strong dye character for DASAs highlights their potential for colorimetric sensing applications because the naked eye can identify even minute amounts ($<1 \text{ mg/mL}$).

During the molar absorptivity investigations, it was observed that an equimolar solution of *p*-methoxy-*N*-methylaniline derivative (14) in dichloromethane (DCM) appeared darker and required more time to switch with visible light than that of the corresponding *N*-methylaniline derivative (13). Because the intensity of color and rate of switching is a critical property for numerous applications of negative photochromes, we sought to better understand this observation. All aniline-based DASAs are isolated in a nearly all open triene (colored) form via precipitation, as seen with ^1H NMR spectroscopy (see Supporting Information (SI)); however, given time to thermally equilibrate in solution, the aniline derivatives partially cyclize to the closed cyclopentenone (transparent) form. This process could be monitored by ^1H NMR, and it was determined that the equilibrium position could be approximately correlated to the $\text{p}K_a$ of the aniline derivatives (Figures S9–S13). For example, the percent of open colored form in CD_2Cl_2 goes from 2 to 12 to 41% for the *p*-chloro-*N*-methylaniline (S1), *N*-methylaniline (13), and *p*-methoxy-*N*-methylaniline (14) derivatives, respectively (determined by ^1H NMR). As expected, substitution of aniline derivatives will affect basicity,³⁷ and the $\text{p}K_a$ of the conjugate acid of *p*-chloro-*N*-methylaniline, *N*-methylaniline, and *p*-methoxy-*N*-methylaniline increases from 4.0 to 4.9 to 5.9. This relationship between $\text{p}K_a$ and percent of open form in DCM also exists for the cyclic aniline derivatives. The respective conjugate acid $\text{p}K_a$ values for *N*-methylaniline, tetrahydroquinoline, and indoline are 4.9, 5.1, and 5.5,³⁸ and the open percent of the open percent of these derivatives at equilibrium in DCM goes from 11 to 19 to 31% (Figure 2b and Figure S10). Notably, by using electron-rich 5-diheptylamino indolines (S3 and 13), the donor shifts the equilibrium to nearly 100% in the open form in DCM. This demonstrates that the equilibrium of these systems can be controlled by the basicity of the donor amine, which can also be used to tune the depth of color. Finally, the equilibrium ratio plays a role in the observed rate of switching with electron-deficient anilines switching from colored-to-colorless the most readily.

Kinetics. For aniline-based DASA compounds, it was also observed that the rate of thermal relaxation varied depending

on the derivative, and as such, we sought to investigate the fundamental kinetic properties of this new photochromic system. The opening and closing rates and activation energies (E_A) of the aniline DASAs were determined by ^1H NMR spectroscopy. *N*-Methylaniline (**8**), tetrahydroquinoline (**9**), and indoline (**10**) barbituric acid-derived DASAs were dissolved in deuterated chlorobenzene in the absence of light and allowed to thermally relax to equilibrium (from triene to triene-cyclopentenone mixtures) at four different temperatures inside the NMR. Integration of protons unique to the open triene and closed cyclopentenone forms were utilized to monitor the rate of closing over time. The data obtained from the NMR experiments was fit to an isomer equilibrium model assuming first order rates of opening and closing. The model used was of the form:

$$[A]_t = \frac{k_{\text{open}} + k_{\text{close}}e^{-(k_{\text{close}} + k_{\text{open}})t}}{k_{\text{close}} + k_{\text{open}}}[A]_0$$

where k_{open} , k_{close} , and A_0 represent the rate of opening, the rate of closing, and the initial concentration, respectively. Interestingly, the rates of equilibration were found to increase from tetrahydroquinoline (**9**) < *N*-methylaniline (**8**) < indoline (**10**), with indoline being ~3.5 times faster than aniline. In addition, by plotting the rate constants relative to $1/T$, we could use the Arrhenius expression to extract activation energies (E_{open} and E_{close}) (Figure 5b and Table S1). The E_{open} and E_{close} values were similar for the three derivatives, ranging from 60 to 71 kJ/mol (Table S1). This is comparable

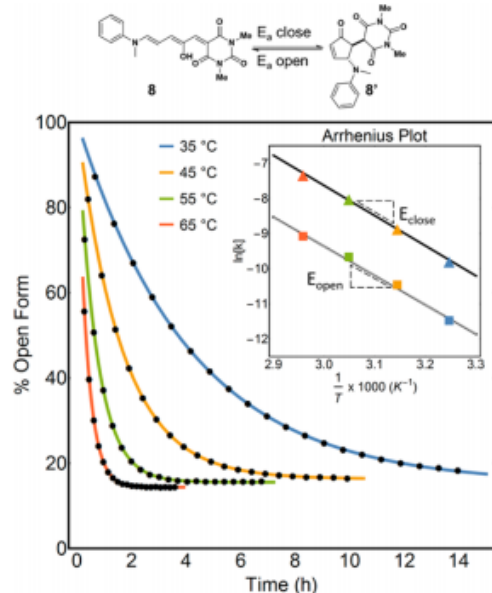


Figure 5. Open to closed equilibration kinetics for select *N*-methylaniline-based barbituric acid DASAs (**8**) determined using ^1H NMR spectroscopy in chlorobenzene- d_5 at the specified temperatures. (inset) Corresponding Arrhenius plot for determining activation energy.

to both experimental and computational results obtained by Feringa³⁹ and Jacquemin⁴⁰ for dialkyl DASAs and lower than the ~90 kJ/mol measured for reported spiropyran-based photoswitches.¹⁸

Fatigue Resistance. Reversibility and stability are further crucial performance parameters in photochromic systems, in particular for applications that rely on recyclability of the photoswitch (e.g., actuators, sensors, mechanophores, etc.) To test the robustness of these aniline-based DASA derivatives, we performed extensive cycling tests with the *p*-methoxy indoline barbituric acid derivative **11** given its fast reversible kinetics (Figure 6). Pump-probe absorption spectroscopy with a broadband white light-emitting diode (LED) for excitation and a heated stage for equilibration (50 °C in chlorobenzene, 67% open by ^1H NMR) were used for the cycling experiments under ambient atmospheric conditions (i.e., in the presence of oxygen). Figure 6a shows a detailed plot of absorption at λ_{max} (629 nm) during the first cycle, where a snapshot (100 ms exposure time) of the absorption trace was taken every 5 s over the course of 20 min with irradiation for the first 30 s and then off for the remaining time. The following cycles were recorded by taking individual measurements immediately following photoswitching and thermal equilibration (Figure 6b). Similar to the previously reported dialkyl DASAs, minimal degradation was observed after 10 cycles.³² Extending to 100 cycles then 200 cycles showed slow degradation with 80 and 60% absorbance recovery, respectively, with no observable change to the absorption profile. These in-depth cycling experiments highlight the stability of DASAs in the presence of oxygen and at elevated temperatures, making them good candidates for applications requiring a recyclable color-to-transparent photoswitch that operates under ambient conditions.

Switching Properties. A significant advantage of these second generation aniline-based DASAs is photoswitchability in a variety of solvents. Whereas the previously reported dialkyl DASAs were limited to photoswitching in nonpolar solvents (e.g., toluene, xylenes, etc.), the aniline DASAs are capable of photoswitching in polar solvents such as THF, DCM, ethyl acetate, and acetonitrile as highlighted in Figure 7 for *N*-methylaniline barbituric acid DASA **8**. In all cases, quantitative photoconversion, evident by the generation of colorless solutions and UV/vis absorption spectroscopy, was observed in a range of solvents with the exception of **12**. In this case, photoswitching was largely limited to less polar solvents such as a toluene/hexanes mixture, presumably due to the increased basicity of the aniline. It is worth noting that one unique aspect of DASA-based photoswitches, compared to azobenzene or acylhydrazones for example, is that photomediated reaction (*E*-*Z* alkene isomerization) is coupled with a thermal 4π electrocyclicization. As a consequence, this cascade process provides a pathway to leverage a potentially incomplete *E*-*Z* alkene isomerization into an efficient photoswitch. However, this also makes the evaluation of photostationary states (PSS) difficult because the *Z*-isomer can convert to the colorless cyclopentenone adduct.

The ability to efficiently activate the new aniline-derivatives in a variety of solvents is a critical breakthrough that provides the potential for DASA-based photoswitches to be used in numerous applications that require polar matrices (e.g., sensors, mechanophores, etc.).⁴¹ Additionally, alkyl-based DASAs were not readily responsive to visible light when dispersed in a solid polymer matrix irrespective of the polymer tested (e.g., polystyrene, poly(methyl methacrylate), etc.). In direct

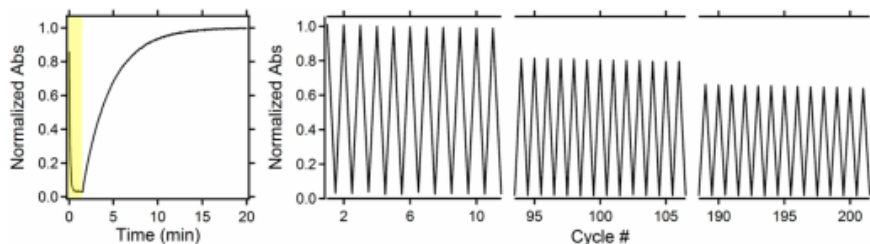


Figure 6. Pump–probe absorption spectroscopy of *p*-methoxy indoline barbituric acid DASA **11** in chlorobenzene at 50 °C, exciting with a broadband white light-emitting diode. (a) Detailed first cycle showing a rapid photoresponse (<30 s) followed by thermal equilibration over 20 min. (b) Cycling study showing approximately 20% decrease in absorption every 100 cycles.

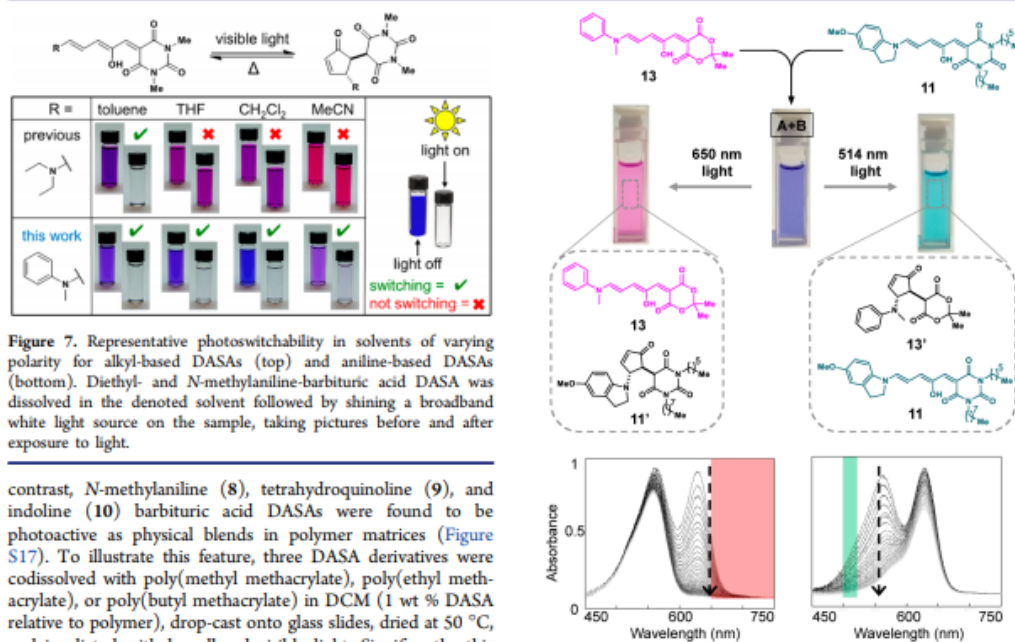


Figure 7. Representative photoswitchability in solvents of varying polarity for alkyl-based DASAs (top) and aniline-based DASAs (bottom). Diethyl- and *N*-methylaniline-barbituric acid DASA was dissolved in the denoted solvent followed by shining a broadband white light source on the sample, taking pictures before and after exposure to light.

contrast, *N*-methylaniline (**8**), tetrahydroquinoline (**9**), and indoline (**10**) barbituric acid DASAs were found to be photoactive as physical blends in polymer matrices (Figure S17). To illustrate this feature, three DASA derivatives were codissolved with poly(methyl methacrylate), poly(ethyl methacrylate), or poly(butyl methacrylate) in DCM (1 wt % DASA relative to polymer), drop-cast onto glass slides, dried at 50 °C, and irradiated with broadband visible light. Significantly, this results in photoswitching in all matrices with the initial color of the equilibrated films having different shades. This is believed to indicate varying ratios of open:closed forms in each matrix, an attribute that we are actively exploring in more detail.

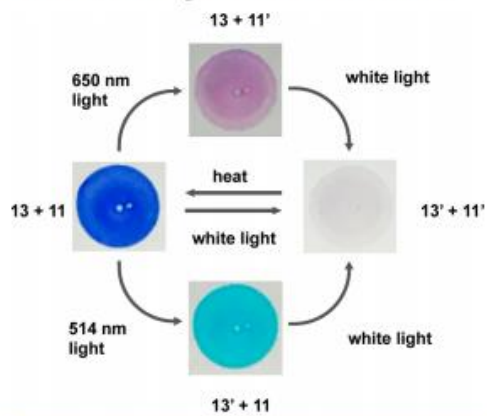
An enabling aspect of the aniline-based DASAs is addressability (the difference in absorption wavelengths between two different isomers or photoswitches), which relies on the inherent tunability of the absorption wavelength. This feature is critical for independently controlling two different photoswitches and holds great potential for various applications.⁴² Accordingly, we sought to demonstrate the selective switching of two different DASAs in solution (Figure 8).⁴³ DASA (**13**) bearing an *N*-methylaniline donor and Meldrum's acid acceptor group (λ_{max} 560 nm in PhMe) and DASA (**11**) bearing a *p*-methoxy indoline donor and barbituric acid acceptor group (λ_{max} 623 nm in PhMe) were chosen based on their minimal absorption overlap (Figure 8).⁴⁴ First, a long-pass 650 nm filter (red light) was used to selectively switch **11** at room temperature, converting the initially violet solution to

Figure 8. Selective photoswitching of two mixed DASAs, *N*-methylaniline Meldrum's acid **13** and indoline barbituric acid **11** using filtered broadband white LED. Compounds **11** and **13** were mixed in toluene followed by photoswitching through a 514 nm bandpass filter to cyclize **13** or a 650 nm long-pass filter to cyclize **11**.

pink (color of **13**). Of note, the minor decrease at 560 nm during the course of >650 nm irradiation corresponds to photoswitching of **11** (not **13**) due to partial absorption overlap of a shoulder at 560 nm. This was confirmed by running control experiments where red light irradiation of a solution containing only **13** did not lead to photoswitching (Figure S18). For the alternative case, a 514 nm bandpass filter (green light) was used to selectively switch **13** with minimal switching of **11** (Figure S21). As a result, the initial violet solution was converted to turquoise (color of **11**). Alternatively, by using a broad spectrum white LED light source, both DASAs switched to their colorless cyclized form at the same time.

Encouraged by these results, the selective switching methodology was also investigated for the same pairwise combination of DASA derivatives dispersed in a solid matrix of poly(methyl methacrylate) (PMMA). The films were prepared by drop-casting a DCM solution containing 100 mg/mL PMMA and ~1 mg/mL of **11** and **13** onto a glass slide (Scheme 1).

Scheme 1. Selective Photoswitching of Two Mixed DASAs, *N*-Methylaniline Meldrum's Acid **13, and Indoline Barbituric Acid **11** Suspended in Drop-Cast Films Containing ~1 wt % DASA in PMMA Using Filtered Broadband White LED**



Irradiation of the DASA blend in PMMA with a 650 nm LED again resulted in a distinct color change from purple to pink due to the selective photoswitching of **11**. Alternatively, **13** could be selectively switched by irradiating with a 450 nm LED to give a turquoise film. Finally, broad-spectrum white light led to the cyclization of both derivatives, leaving a transparent film, and heating the sample at 50 °C for 2 min reverted the sample back to its original colored state. This clearly demonstrates for the first time the ability to selectively and reversibly switch mixtures of DASA derivatives in both solution and the solid state.

In summary, a second generation aniline-based donor–acceptor Stenhouse adduct was developed and characterized. The new photochromic platform is highly tunable, providing a wide photoresponsive region from 500–650 nm that is not restricted to solution-state or nonpolar matrices for reversible switchability. Through careful choice of the donor moiety, the wavelength and solvent switching properties can be precisely controlled. This combined with computational modeling and equilibrium kinetics provide valuable guidelines for the development of future DASA systems. Finally, selective switching in both solutions and polymer-matrices highlights the significant potential of inverse DASA photoswitches in materials applications.

■ ASSOCIATED CONTENT

Supporting Information

The Supporting Information is available free of charge on the ACS Publications website at DOI: 10.1021/jacs.6b07434.

Experimental procedures and characterization data for all compounds (PDF)

■ AUTHOR INFORMATION

Corresponding Author

*javier@chem.ucsb.edu

Notes

The authors declare the following competing financial interest(s): A patent has been filed on the photochromic materials.

■ ACKNOWLEDGMENTS

We thank the National Science Foundation (MRSEC program, DMR 1121053) and California NanoSystems Institute (CNSI) Challenge Grant Program for support. Y.J.D. and N.T. thanks the National Science Foundation for a Graduate Research Fellowship. We thank Dr. Alexander Mikhailovsky for his help constructing the optical setup used for the cycling and selective switching experiments and also thank Dr. Jerry Hu for his help with the cryoprobe and DOSY NMR experiment measurements.

■ REFERENCES

- (1) Szymanski, W.; Beierle, J. M.; Kistemaker, H. A. V.; Velema, W. A.; Feringa, B. L. *Chem. Rev.* **2013**, *113*, 6114.
- (2) Kawata, S.; Kawata, Y. *Chem. Rev.* **2000**, *100*, 1777.
- (3) Russew, M. M.; Hecht, S. *Adv. Mater.* **2010**, *22*, 3348.
- (4) Rosario, R.; Gust, D.; Hayes, M.; Jahnke, F.; Springer, J.; Garcia, A. A. *Langmuir* **2002**, *18*, 8062.
- (5) Schöller, K.; Küpfer, S.; Baumann, L.; Hoyer, P. M.; De Courten, D.; Rossi, R. M.; Vetushka, A.; Wolf, M.; Bruns, N.; Scherer, L. J. *Adv. Funct. Mater.* **2014**, *24*, 5194.
- (6) Shirashi, Y.; Shirakawa, E.; Tanaka, K.; Sakamoto, H.; Ichikawa, S.; Hirai, T. *ACS Appl. Mater. Interfaces* **2014**, *6*, 7554.
- (7) Kundu, P. K.; Samanta, D.; Leizrowice, R.; Margulis, B.; Zhao, H.; Börner, M.; Udayabhaskararao, T.; Manna, D.; Klajn, R. *Nat. Chem.* **2015**, *7*, 646.
- (8) Dong, M.; Babalhavaeji, A.; Samanta, S.; Beharry, A. A.; Woolley, G. A. *Acc. Chem. Res.* **2015**, *48*, 2662.
- (9) Beharry, A. A.; Woolley, G. A. *Chem. Soc. Rev.* **2011**, *40*, 4422.
- (10) Velema, W. A.; Szymanski, W.; Feringa, B. L. *J. Am. Chem. Soc.* **2014**, *136*, 2178.
- (11) Beharry, A. A.; Sadovski, O.; Woolley, G. A. *J. Am. Chem. Soc.* **2011**, *133*, 19684.
- (12) Samanta, S.; Beharry, A. A.; Sadovski, O.; McCormick, T. M.; Babalhavaeji, A.; Tropepe, V.; Woolley, G. A. *J. Am. Chem. Soc.* **2013**, *135*, 9777.
- (13) Barrett, C. J.; Mamiya, J.; Yager, K. G.; Ikeda, T. *Soft Matter* **2007**, *3*, 1249.
- (14) Li, J.; Nagamani, C.; Moore, J. S. *Acc. Chem. Res.* **2015**, *48*, 2181.
- (15) Bandara, H. M. D.; Burdette, S. C. *Chem. Soc. Rev.* **2012**, *41*, 1809.
- (16) Irie, M.; Fukaminato, T.; Matsuda, K.; Kobatake, S. *Chem. Rev.* **2014**, *114*, 12174.
- (17) Broman, S. L.; Petersen, M. Å.; Tortzen, C. G.; Kadziola, A.; Kilså, K.; Nielsen, M. B. *J. Am. Chem. Soc.* **2010**, *132*, 9165.
- (18) Minkin, V. I. *Chem. Rev.* **2004**, *104*, 2751.
- (19) Yamaguchi, T.; Kobayashi, Y.; Abe, J. *J. Am. Chem. Soc.* **2016**, *138*, 906.
- (20) Tanaka, M.; Ikeda, T.; Xu, Q.; Ando, H.; Shibutani, Y.; Nakamura, M.; Sakamoto, H.; Yajima, S.; Kimura, K. *J. Org. Chem.* **2002**, *67*, 2223.
- (21) Ayub, K.; Mitchell, R. H. *J. Org. Chem.* **2014**, *79*, 664.
- (22) Minami, M.; Taguchi, N. *Chem. Lett.* **1996**, *25*, 429.
- (23) Hatano, S.; Horino, T.; Tokita, A.; Oshima, T.; Abe, J. *J. Am. Chem. Soc.* **2013**, *135*, 3164.
- (24) Yang, Y.; Hughes, R. P.; Aprahamian, I. *J. Am. Chem. Soc.* **2014**, *136*, 13190.

- (25) Yang, Y.; Hughes, R. P.; Aprahamian, I. *J. Am. Chem. Soc.* **2012**, *134*, 15221.
- (26) Bléger, D.; Schwarz, J.; Brouwer, A. M.; Hecht, S. *J. Am. Chem. Soc.* **2012**, *134*, 20597.
- (27) Siewertsen, R.; Neumann, H.; Buchheim-Stehn, B.; Herges, R.; Näther, C.; Renth, F.; Temps, F. *J. Am. Chem. Soc.* **2009**, *131*, 15594.
- (28) Mason, B. P.; Whittaker, M.; Hemmer, J.; Arora, S.; Harper, A.; Alnemrat, S.; Meechen, A.; Helmy, S.; Read de Alaniz, J.; Hooper, J. P. *Appl. Phys. Lett.* **2016**, *108*, 041906.
- (29) Li, X.; Li, J.; Wang, Y.; Matsuura, T.; Meng, J. *J. Photochem. Photobiol. A* **2004**, *161*, 201.
- (30) Radu, A.; Byrne, R.; Alhashimy, N.; Fusaro, M.; Scarmagnani, S.; Diamond, D. *J. Photochem. Photobiol. A* **2009**, *206*, 109.
- (31) Helmy, S.; Oh, S.; Leibfarth, F. A.; Hawker, C. J.; Read de Alaniz, J. *J. Org. Chem.* **2014**, *79*, 11316.
- (32) Helmy, S.; Leibfarth, F. A.; Oh, S.; Poelma, J. E.; Hawker, C. J.; Read de Alaniz, J. *J. Am. Chem. Soc.* **2014**, *136*, 8169.
- (33) Singh, S.; Friedel, K.; Himmerlich, M.; Lei, Y.; Schlingloff, G.; Schober, A. *ACS Macro Lett.* **2015**, *4*, 1273.
- (34) Balamurugan, A.; Lee, H. *Macromolecules* **2016**, *49*, 2568.
- (35) Cheng, Y.-J.; Yang, S.-H.; Hsu, C.-S. *Chem. Rev.* **2009**, *109*, 5868.
- (36) Li, Y. *Acc. Chem. Res.* **2012**, *45*, 723.
- (37) Kanzian, T.; Nigst, T. A.; Maier, A.; Pichl, S.; Mayr, H. *Eur. J. Org. Chem.* **2009**, *36*, 6379.
- (38) Yang, D.; Zuccarello, G.; Mattes, B. R. *Macromolecules* **2002**, *35*, 5304.
- (39) Lerch, M. M.; Wezenberg, S. J.; Szymanski, W.; Feringa, B. L. *J. Am. Chem. Soc.* **2016**, *138*, 6344.
- (40) Laurent, A.; Medved, M.; Jacquemin, D. *ChemPhysChem* **2016**, *17*, 1846.
- (41) Of note, the ability to photoswitch in a given solvent depends on the basicity of the amine. The N-methyl aniline DASAs readily switched in a variety of solvents, whereas the 5-diheptylamino-indole derivatives photoswitched only in nonpolar solvents such as toluene or hexanes.
- (42) Hansen, M. J.; Velema, W. A.; Lerch, M. M.; Szymanski, W.; Feringa, B. L. *Chem. Soc. Rev.* **2015**, *44*, 3358.
- (43) Lerch, M. M.; Hanson, M. J.; Velema, W. A.; Szymanski, W.; Feringa, B. L. *Nat. Commun.* **2016**, *7*, 12504.
- (44) The absorption for each DASA at equilibrium was normalized and pump-probe measurements with a filtered white LED was used to monitor changes in absorption over time.